



HAL
open science

Application of the theory of the viscosity solutions to the Shape From Shading problem

Emmanuel Prados

► **To cite this version:**

Emmanuel Prados. Application of the theory of the viscosity solutions to the Shape From Shading problem. Human-Computer Interaction [cs.HC]. Université Nice Sophia Antipolis, 2004. English. NNT: . tel-00007916

HAL Id: tel-00007916

<https://theses.hal.science/tel-00007916>

Submitted on 4 Jan 2005

HAL is a multi-disciplinary open access archive for the deposit and dissemination of scientific research documents, whether they are published or not. The documents may come from teaching and research institutions in France or abroad, or from public or private research centers.

L'archive ouverte pluridisciplinaire **HAL**, est destinée au dépôt et à la diffusion de documents scientifiques de niveau recherche, publiés ou non, émanant des établissements d'enseignement et de recherche français ou étrangers, des laboratoires publics ou privés.

PHD THESIS

prepared at the **INRIA** of Sophia Antipolis, Odyssee Lab.,

presented at the

UNIVERSITY OF NICE - SOPHIA ANTIPOLIS

Doctoral School in Sciences and Technologies of Information
and of Communication

for obtaining the title of

DOCTOR OF SCIENCE

Specialized in Automatic, Signal and Image Processing

Emmanuel Prados

October 22, 2004

Application of the theory of the viscosity
solutions to the Shape From Shading
problem

Advisor : Olivier Faugeras

Jury (Examinators)

Luis Alvarez	Professor	University of Las Palmas, Spain
Pierre Bernhard	Professor	University of Nice-Sophia Antipolis, France
Rachid Deriche	Research Director	INRIA Sophia Antipolis, France
Jean-Denis Durou	Associate Professor	University of Toulouse, France
Luc Robert	Chief Technical Officer	REALVIZ S.A., France
Christoph Schnörr	Professor	University of Mannheim, Germany

Reviewers

Luis Alvarez	Professor	University of Las Palmas, Spain
John Oliensis	Associate Professor	Stevens Institute of Technology, USA
Christoph Schnörr	Professor	University of Mannheim, Germany

THÈSE DE DOCTORAT

préparée à l'INRIA de Sophia Antipolis, projet Odysée,

présentée à l'École Doctorale STIC

(Sciences et Technologies de l'Information et de la Communication)

de l' **UNIVERSITÉ DE NICE - SOPHIA ANTIPOLIS**

pour obtenir le titre de

DOCTEUR EN SCIENCES

Mention: Automatique, Traitement du Signal et des Images

soutenue par

Auteur: Emmanuel Prados

le 22 octobre 2004

Titre

Application de la théorie des solutions
de viscosité au problème du "Shape
From Shading"

Directeur : Olivier Faugeras

Jury

Luis Alvarez	Professeur (Université de Las Palmas, Espagne)
Pierre Bernhard	Professeur (Université de Nice-Sophia Antipolis, France)
Rachid Deriche	Directeur de recherche (INRIA Sophia Antipolis, France)
Jean-Denis Durou	Matre de conférence (Université de Toulouse, France)
Luc Robert	Directeur technique (REALVIZ S.A., France)
Christoph Schnörr	Professeur (Université de Mannheim, Allemagne)

À Laetitia et Thomas.

Acknowledgments

Je voudrais tout d'abord remercier Olivier Faugeras, mon directeur de thèse, pour sa gentillesse, sa confiance et sa disponibilité. Plus qu'un soutien scientifique infailible, Olivier s'est toujours soucié d'apporter des réponses aux nombreuses questions que je pouvais lui poser; en particulier concernant mon avenir...

Je ne remercierai jamais assez tous les permanents de l'équipe Odyssee pour leur accueil chaleureux puis leur soutien constant. Merci en particulier à Nour., Maureen, Pierre pour les divers conseils précieux et pour avoir très gentiment accepté de relire régulièrement mes articles et autre documents... Un grand merci à Théo qui n'a jamais compté son temps et qui a toujours été là pour nous donner un coup de pouce face aux innombrables problèmes informatiques (WebOdyssee, biblio...). Enfin je voudrai remercier Thierry pour son soutien plus administratif mais tout aussi essentiel.

I would like also to thank warmly

- my reviewers:

Luis Alvarez, John Oliensis, and Christoph Schnörr who have accepted to read in detail my manuscript and to comment it;

- my thesis jury:

Luis Alvarez, Pierre Bernhard, Rachid Deriche, Jean-Denis Durou, Luc Robert and Christoph Schnörr for the interest they have thus attached to my work and for their enthusiasm.

- Je voudrais en particulier remercier Pierre Bernhard qui a gentiment accepté de présider ma soutenance.

Thank to Fabio Camilli for the warm and important exchanges that I could have with him.

J'aurai également toujours en mémoire les bons moments passés avec Jean Phi., Mikaël, Christophe, David, Nico., Marie-Cécile et bien d'autres. Leur bonne humeur, leur soutien, les innombrables petites astuces et les nombreux moments partagés au sein du labo (repas, pause-café, pots...) ou en mission sont très importants à mes yeux. Bien évidemment, une place importante est aussi réservée à Gerardo, Jacques et Christophe qui par de petits conseils m'ont

permis entre autre de démarrer efficacement ma thèse (YAR++ compile encore ;).

Merci à mes parents pour m'avoir soutenu chaleureusement et financièrement jusqu'à l'obtention de mon DEA: diplôme à l'origine de cette aventure...

Enfin, les mots me manquent pour remercier Laëtitia dont le soutien est quotidien et sans limite.

Pour finir, je voudrais remercier Thomas d'avoir été (d'être) un gentil bébé et qui globalement a laissé dormir son papa...

Abstract

“Shape From Shading” is considered as an ill-posed problem which is therefore difficult to solve. In order to understand the difficulty of this problem and to design reliable and relevant solutions, we propose a rigorous approach based on the notion of viscosity solutions. In particular, we systematically prove the existence and uniqueness of the solution; if necessary (when uniqueness does not hold) we characterize the solutions. We also demonstrate the convergence of our algorithms.

After having considered and fully exploited the (partial differential) equations provided by the classical modeling of the Shape From Shading problem, we propose and study some new equations arising from modelings which are more realistic than the ones considered in the Shape From Shading literature. In particular, this allows us to demonstrate that, with more realistic modelings, the Shape From Shading problem is generally well-posed. In effect, we prove that the classical version of the Shape From Shading problem is ill-posed because of an over-simplification in the modeling.

In this work, we also propose an extension of the notion of the singular viscosity solutions developed recently in [26, 27]. This extension allows to propose a new characterization of the discontinuous viscosity solutions. This new mathematical framework also allows to unify the various theoretical results that have been obtained in the Shape From Shading area.

Résumé

Le problème du “Shape From Shading” est aujourd’hui considéré comme un problème mal posé et difficile à résoudre. Afin de bien comprendre les difficultés de ce problème et d’apporter des solutions fiables et pertinentes, nous proposons une approche rigoureuse basée sur la notion de solution de viscosité. En particulier, nous prouvons systématiquement l’existence et l’unicité de la solution; le cas échéant, nous proposons des caractérisations des solutions. Nous prouvons aussi la convergence de nos algorithmes.

Après avoir considéré et exploité au maximum les équations (aux dérivées partielles) obtenues à partir de la modélisation classique du problème du “Shape From Shading”, nous proposons et étudions de nouvelles équations provenant de modélisations plus réalistes que celles qui avaient été traitées classiquement dans la littérature. Cette démarche nous permet alors de démontrer qu’avec de telles nouvelles modélisations, le problème du “Shape From Shading” est généralement un problème complètement bien posé. En d’autres termes, nous prouvons que la version classique du problème du “Shape from Shading” est devenu mal posée à cause d’une trop grande simplification de la modélisation.

Dans ce travail, nous proposons aussi une extension de la notion de solutions de viscosité singulières développée récemment dans [26, 27]. Cette extension nous permet de proposer une nouvelle caractérisation des solutions de viscosité discontinues. Ce nouveau cadre théorique nous permet aussi d’unifier les différents résultats théoriques proposés dans le domaine du “Shape From Shading”.

Contents

Abstract	10
Résumé	11
Introduction et contributions (in french)	21
1 Introduction and state of the art	35
1.1 The “Shape from Shading” problem	35
1.2 Propagation and PDEs methods	38
1.3 Optimization methods	40
1.4 Other SFS methods	43
1.4.1 Local methods	43
1.4.2 The linear methods	44
1.4.3 Other SFS methods	44
1.5 Applicability and applications of the Shape from Shading methods	45
1.5.1 Improvement of the applicability of the SFS methods . . .	45
1.5.2 Applications of Shape from Shading	46
1.6 Setup and numerical methods considered in our work	48
1.7 Contributions of this thesis	48
2 “Classical” Shape From Shading	51
2.1 Mathematical formulations of the “classical” Lambertian SFS problem	51
2.1.1 The “orthographic SFS” problem	52
2.1.2 The “perspective SFS” problem	53
2.1.3 The “perspective SFS” with a point light source located at the optical center	55
2.2 Shape from Shading and Viscosity solutions	57
2.2.1 Why using viscosity solutions to solve SFS	57
2.2.2 Viscosity solutions of Hamilton-Jacobi equations	58
2.2.3 Hamiltonians for the SFS problems and unification of the “perspective” and “orthographic SFS”	65
2.2.4 Existence of viscosity solutions of the “classical” SFS problems	71
2.2.5 Proof of proposition 2.3 claimed in section 2.2.4	74

2.2.6	Characterization of viscosity solutions of the “classical” SFS problems	76
2.2.7	Noise robustness of the viscosity solutions of SFS	86
2.2.8	SFS with discontinuous images; shadows	87
2.3	Conclusion and contributions of chapter 2	89
3	Monotonous approximation schemes and associated numerical algorithms; application to the “classical” Shape from Shading	91
3.1	Monotonous approximation schemes and associated numerical algorithms; Examples for HJB equations	91
3.1.1	Approximation schemes of the form $S(\nu, x, u(x), u) = 0$	91
3.1.2	Decentered schemes for HJB equations	94
3.1.3	Stability of the approximation schemes	100
3.1.4	Convergence of the solutions of the approximation schemes toward the viscosity solutions	112
3.1.5	Numerical algorithm for monotonous schemes of the form $S(\nu, x, u(x), u) = 0$	118
3.2	Application to the “classical” Shape from Shading problem	121
3.2.1	Decentered schemes for the “classical” SFS problem	121
3.2.2	New “generic” algorithms for the “classical” Shape from Shading	124
3.2.3	Pushing things to the limit: SFS with discontinuous images and black shadows	131
3.2.4	Experimental results	132
3.3	Conclusion and contributions of chapter 3	149
4	A viscosity method for “classical” Shape from Shading without boundary data	151
4.1	Weaknesses of the previous theoretical approaches of the SFS problem	151
4.2	Singular discontinuous viscosity solutions with Dirichlet boundary conditions and state constraints (SDVS)	154
4.2.1	Singular viscosity supersolutions of (4.2)-(4.5)	158
4.2.2	Existence of the singular solution of (4.2)-(4.5)	162
4.2.3	Uniqueness results	166
4.2.4	Stability of the singular solution	168
4.2.5	A new characterization of the discontinuous viscosity solutions by their “minimums”	170
4.3	Application to the “classical” Shape from Shading problem	172
4.3.1	Existence and uniqueness of the SDVS of the “classical” SFS equations	172

4.3.2	Applications of the stability of the SDVS to the Shape from Shading problem	173
4.4	A general framework for the “classical” Shape from Shading problem	180
4.5	Minimal and global viscosity solutions	184
4.6	Numerical approximation of the SDVS of the “classical” Shape from Shading problem	185
4.6.1	Management of the state constraints	185
4.6.2	Regularization of the generic SFS equation	187
4.6.3	Approximation schemes for the nondegenerate SFS equations	187
4.6.4	Numerical algorithms for the generic SFS problem	188
4.6.5	Examples of SFS results obtained from synthetic images	188
4.7	Toward applications of Shape from Shading	188
4.7.1	Document restoration using SFS	190
4.7.2	Face reconstruction from SFS	191
4.7.3	Potential applications to medical images	192
4.8	Conclusion and contributions of chapter 4	195
5	Toward more realistic modelizations.	
	Shape from Shading: a well-posed problem?	197
5.1	More realistic modeling of the SFS problem	200
5.2	New mathematical formulation of the SFS problem	203
5.3	Shape From Shading can be a completely well-posed problem!	205
5.3.1	Related work	205
5.3.2	Well-posedness of the SFS problem	207
5.4	A provably convergent numerical method	212
5.4.1	Control formulation of the Hamiltonian H_F	213
5.4.2	Management of the boundary conditions	215
5.4.3	Two new approximation schemes	215
5.4.4	A numerical algorithm	220
5.5	Experimental results	224
5.5.1	Experiments with synthetic images	226
5.5.2	Experimental results on real images	249
5.6	Proof of lemmas and propositions of chapter 5	258
5.7	Conclusion and contributions of chapter 5	264
6	Conclusion	267

Conclusion (in french)	270
Appendices	272
A How to transform a convex Hamiltonian into a HJB Hamiltonian; Legendre Transform	273
B The “classical” SFS Hamiltonians and the generic Hamiltonian H_g	277
B.1 The Hamiltonians H_*^{orth} and H_*^{pers} are special cases of H_g	277
B.2 HJB formulation of H_g	280
C Maxi(Mini)mization of various functions	281
C.1 Maximisation of $\delta\sqrt{1 - a ^2} + w \cdot a + c$	281
C.2 Maximisation of $\delta\sqrt{c - br - ar^2} + \mu r + \nu$	281
C.3 Minimization $\delta\sqrt{c + br + ar^2} + \mu r + \nu$	282
C.4 Solving $\sqrt{c + br + ar^2} + \mu r + \nu = 0$ with respect to r	283
D List of all hypotheses	285
E Publications of the author	289
Bibliography	292
Rapport de soutenance	308

List of Figures

1	Le problème du “Shape-from-Shading”	21
2	L’illusion du cratère	22
3	“Ambiguïté du Bas-relief”	23
1.1	The “Shape-from-Shading” problem.	35
1.2	The crater illusion	36
1.3	The “Bas-relief Ambiguity”	37
1.4	The two strategies allowing to minimize a functional numerically.	42
2.1	Images arising from an orthogonal (versus perspective) projection.	54
2.2	Perspective projection with a single point light source located at the optical center.	56
2.3	Viscosity solutions for opposite hamiltonians	59
2.4	Example of discontinuous a viscosity solution	64
2.5	A surface with a singular point at the boundary.	84
2.6	Examples of several discontinuous viscosity solutions.	85
3.1	Partition of $\bar{\Omega}$ in dimension 2.	103
3.2	Most effective path we have tested.	120
3.3	Solution computed by our and Falcone’s algorithms	132
3.4	Results for a synthetic image generated by a paraboloidal surface.	136
3.5	Results for a synthetic image generated by a sinusoidal surface.	137
3.6	Results for a synthetic image generated by a pyramidal surface.	138
3.7	Experimental results obtained with the implicit algorithm start- ing from a subsolution, for a synthetic image representing Mozart’s face	139
3.8	Experimental results obtained with the semi-implicit algorithm starting from a supersolution, for a synthetic image representing Mozart’s face	140
3.9	Experimental results obtained with the implicit algorithm start- ing from a supersolution, for a synthetic image representing Mozart’s face	141

3.10	First example of a reconstruction from an image with black shadows.	143
3.11	Second example of a reconstruction from an image with black shadows	144
3.12	Results for a noisy image generated by a sinusoidal surface . . .	145
3.13	Results for a noisy image generated by a pyramidal surface . . .	146
3.14	“Perspective SFS” results for an image generated by a smooth surface.	147
3.15	“Perspective SFS” results for an image generated by a pyramidal surface.	147
3.16	“Perspective SFS” results for an image generated by Mozart’s face.	148
3.17	“Perspective SFS” results for a noisy image of Mozart’s face . . .	148
4.1	Examples of continuous (versus discontinuous) viscosity solution of (4.1)	152
4.2	Solutions of Eikonal equation with nonsuitable kinks	153
4.3	solutions of H versus $-H$; minimal solutions	185
4.4	Reconstruction of Mozart’s face without boundary data	189
4.5	Reconstruction of Mozart’s face from a noisy image with the wrong parameters	190
4.6	Singular points of the profile of a face.	192
4.7	3D reconstruction of an inked page from a real image	193
4.8	Reduction of the geometric and photometric distortions	194
4.9	Face reconstruction from SFS	194
4.10	Reconstruction of a normal stomach	195
5.1	Concave/convex duality in the Eikonal framework	198
5.2	Consequences of the concave/convex duality with more complex surfaces	199
5.3	The surface local coordinate system (see [103, 65]).	201
5.4	Example of initial supersolution for the image of Mozart’s Face .	225
5.5	Example of results for an image of a surface with several local minima	229
5.6	Example of results for the “field of bumps” image	230
5.7	Result for the image of Mozart’s face	231
5.8	Result for an image containing discontinuities	232
5.9	Results for another image containing discontinuities	233
5.10	Evolution of the reconstructed surface in the course of iterations for the image of Mozart’s face	234
5.11	Evolution of the reconstructed surface in the course of iterations for the image of Mozart’s face, starting from the supersolution v_0	235

5.12	Evolution of the reconstructed surface in the course of iterations for the “field of bumps”	237
5.13	Results for the noisy images of Mozart’s face	241
5.14	Results for the images of Mozart face distorted by gamma distortions	242
5.15	Results for the images of Mozart’s face distorted by the corrections of the constant coefficient σ	243
5.16	Results obtained from Mozart’s face image with distorted focal length parameter	244
5.17	Results for the image Fig.5.7-b) of Mozart’s face distorted by noise, gamma and albedo distortions, and with a wrong parameter for the focal length	245
5.18	Images of Mozart’s face with the light source not located at the optical center	246
5.19	Reconstructed surfaces from images of Mozart’s face with the light source not located at the optical center	247
5.20	Reconstructed surfaces from images of Mozart’s face (side view) with the light source not located at the optical center	248
5.21	Example of reconstructions with or without eyes.	251
5.22	Surface reconstructed from the photo Fig.5.21-c) viewed from several points of view	252
5.23	Same surface as Figure 5.22 illuminated by a single point light source located at the optical center (0,0,0)	252
5.24	Influence of the error on the albedo parameter	253
5.25	A sample of our database of real images of faces	254
5.26	Surfaces reconstructed from the real images of Figure 5.25	255
5.27	Surfaces reconstructed from the images Fig.5.26-k) and Fig.5.26-l)	256
5.28	Evolution of the reconstructed surfaces in the course of the iterations (n =number of iterations)	257

We start this document by a detailed introduction written in french. Afterwards, this manuscript is written in english. The english-speaking reader is invited to start reading from the page 35.

Introduction et contributions (en français)

Le problème du “Shape From Shading” (SFS) consiste à calculer la forme tridimensionnelle d’une surface à partir de *l’intensité d’une seule* image en niveaux de gris de cette surface; voir figure 1. C’est un problème

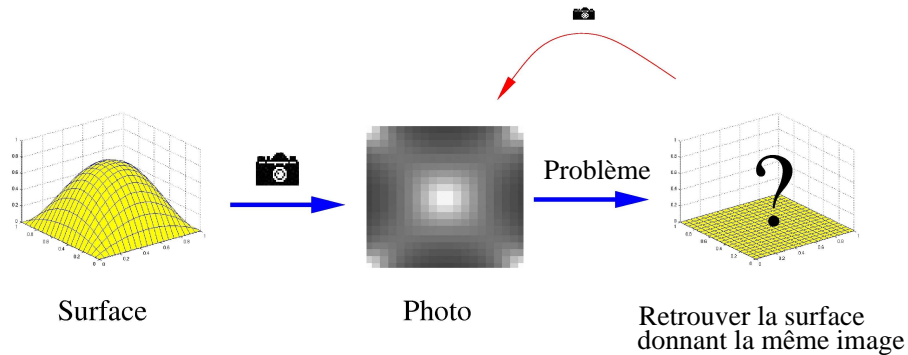


Figure 1: Le problème du “Shape-from-Shading”.

de vision *monoculaire* basé sur l’ information photométrique.

Selon Durou [49, 48], dans le début des années 50, Van Diggelen [162] fût le premier à considérer le problème de reconstruction 3D à partir d’indices photométriques. La première solution fût suggérée par Rindfleisch [131] dans les années 60. Plus tard, Horn [67] fût le premier à formuler le problème du “Shape From Shading” de manière simple et rigoureuse, sous la forme d’une Équation Différentielle Partielle (EDP) appelée l’équation d’irradiance. C’est aussi Horn qui suggéra d’appeler ce problème “Shape From Shading”. Par la suite, tous les travaux publiés jusqu’à ce jour en “Shape From Shading” reposent sur les travaux de

Horn. Dans un premier temps (dans les années 80) les auteurs se concentraient sur la partie numérique du problème. Les questions d’existence et d’unicité de la solution du problème n’étaient pas évoquées en ce temps à l’exception notable du travail de Bruss et Brooks [22, 16]. Cependant, en raison de la médiocrité des résultats obtenus, ces questions, ainsi que celles relatives à la convergence des schémas numériques, devinrent essentielles dans la dernière décennie du 20ème siècle. Suite à ces travaux théoriques, le problème du “Shape From Shading” est aujourd’hui considéré comme étant un problème mal posé. Par exemple, un grand nombre d’articles montrent qu’il n’y a pas unicité de la solution [16, 106, 107, 134, 11, 51, 127, 120]. Les difficultés rencontrées ont souvent

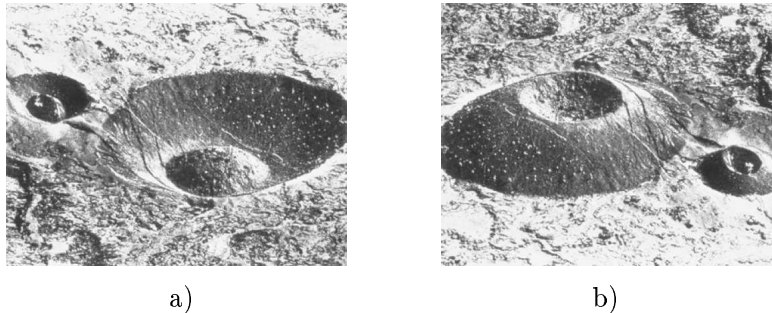


Figure 2: L’illusion du cratère [115]. Dans l’image a), nous percevons deux cratères: un petit et un grand. Mais nous pouvons transformer ces cratères en volcans (bien qu’à l’envers) si nous imaginons que la scène est illuminée par le bas plutôt que par le haut. En fait, cette image est celle d’une paire de volcans dans les îles Hawaïennes, et non pas d’une paire de cratères. L’image b) affiche la photographie dans le bon sens.

été illustrées par des ambiguïtés concaves/convexes comme celle présentée par la Figure 2. Sur cette figure, l’ambiguïté résulte d’un changement d’estimation des paramètres de l’éclairage. En fait, ce type d’ambiguïté peut être largement généralisé. En effet, dans [11], Belhumeur et ses co-auteurs démontrent que lorsque la direction de l’éclairage¹ et l’albedo d’une surface Lambertienne sont inconnus, alors la même image peut être

¹Dans le cas d’une source de lumière éloignée.

obtenue par une famille continue de surfaces (dépendant linéairement de trois paramètres). En d'autres termes, ils montrent que ni la brillance ni les ombres portées d'un objet, ne peuvent, à partir d'un unique point de vue, révéler exactement sa structure 3D. Ceci est l'“Ambiguïté du Bas-relief”, voir [11] et la Figure 3. Etant conscients de ces difficultés, nous

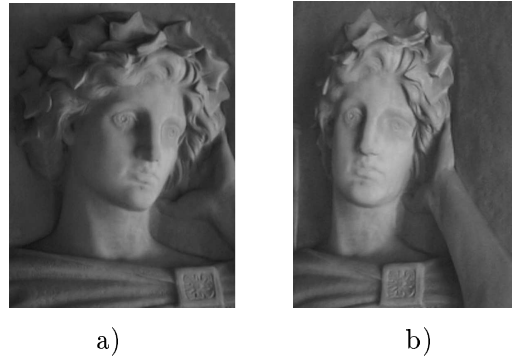


Figure 3: “Ambiguïté du Bas-relief” [11]: Vues frontale et de profil d'une sculpture en bas-relief. Bien que la profondeur réelle de cette sculpture ne dépasse pas la dizaine de centimètres, la vue frontale a) semble avoir une profondeur 3D correcte. La vue de profil b) révèle l'écrasement. Ceci prouve donc que l'image a) peut être obtenue par deux surfaces: la surface 3D que nous imaginions en regardant l'image a) et l'actuel bas-relief qui est à l'origine des deux photos a) et b). Pour plus de détails, le lecteur peut se référer à [11].

supposons donc ici que tous les paramètres de la source de lumière, de la réflectance de la surface et de l'appareil photographique sont connus.

Comme nous avons mentionné ci-dessus, la modélisation du problème du “Shape From Shading” introduite par Horn aboutit à une EDP: l'équation de brillance. Cette équation peut être grossièrement abrégée par

$$E(x_1, x_2) = R(\mathbf{n}(x_1, x_2)).$$

L'équation de brillance relie la carte de réflectance (R) à la brillance de l'image (E); voir le chapitre 5 pour plus de détails.

A notre connaissance, à l'exception des travaux présentés dans [3, 92, 130], toutes les méthodes pour résoudre le problème du “Shape From Shading” supposent que la scène est Lambertienne. Dans ce cas, la réflectance

correspond au cosinus de l'angle entre le vecteur lumière $\mathbf{L}(x_1, x_2)$ et le vecteur normal à la surface $\mathbf{n}(x_1, x_2)$:

$$R = \cos(\mathbf{L}, \mathbf{n}) = \frac{\mathbf{L}}{|\mathbf{L}|} \cdot \frac{\mathbf{n}}{|\mathbf{n}|}$$

(R , \mathbf{L} et \mathbf{n} dépendent de (x_1, x_2)).

La première EDP *explicite* déduite de l'équation de brillance et étudiée dans la littérature du "Shape From Shading" est l'*équation Eikonale*:

$$|\nabla u(x)| = \sqrt{\frac{1}{I(x)^2} - 1}, \quad \forall x = (x_1, x_2) \in \Omega$$

où $\Omega \subset \mathbb{R}^2$ représente le support de l'image et $I : \Omega \rightarrow \mathbb{R}$ représente la brillance de l'image. Cette équation est obtenue à partir de la modélisation la plus simple du problème du "Shape From Shading": projection orthographique, source de lumière frontale disposée à l'infini, réflectance Lambertienne. C'est l'équation la plus étudiée dans la littérature du "Shape From Shading". Dans la section 2.1 nous décrivons différentes modélisations du problème du "Shape From Shading" et nous détaillons plusieurs EDP associées.

Comme nous l'avons mentionné plus haut, le problème du "Shape From Shading" peut se formuler mathématiquement sous la forme d'équations aux dérivées partielles du premier ordre. Ainsi, la première catégorie de méthodes pour résoudre ce problème consiste à résoudre *directement* les équations *exactes* formulées. Ces méthodes ne font aucune linéarisation (contrairement aux méthodes présentées dans la section 1.4.2) et elles n'introduisent aucun biais. Je les nommerai "méthodes de propagation et d'EDP". La principale difficulté rencontrée par les méthodes de propagation et EDP est due au caractère mal posé du problème. Ces méthodes peuvent être divisées en deux classes. Les *méthodes "single-pass"* et les *méthodes itératives*. Les principales méthodes "single-pass" sont:

- la méthode des *bandes caractéristiques* (introduite par Horn dans [65]),
- les méthodes de *propagation des contours* (lignes de niveaux) introduites par Bruckstein [21] et améliorées par Kimmel et Bruckstein [80],

- la méthode de “*fast marching*” introduite par Sethian [138, 139] et légèrement modifiée par Kimmel et Sethian [81] pour le “Shape From Shading orthographique” avec une source de lumière oblique.

Parmi les méthodes itératives citons en particulier: l’algorithme introduit par Rouy et Tourin pour l’équation Eikonale [134], ses extensions par Prados et Faugeras [127, 120], les algorithmes de Dupuis et Oliensis [47] basés sur la théorie du contrôle et les jeux différentiels, les algorithmes de Falcone et al. [24, 55, 56] basés sur les éléments finis. Insistons sur le fait que globalement **toutes ces méthodes calculent une approximation de la même solution.**

Il est bien connu que, même si l’image est continue, l’équation d’irradiance n’a pas nécessairement de solution différentiable (solution au sens classique) [19, 18, 17, 82]. En particulier, en raison du bruit, des erreurs faites sur les paramètres (longueur focale, position de la lumière, etc) et d’une modélisation incorrecte (interréflexions, source de lumière non ponctuelle, réflectance non lambertienne...), dans la pratique avec des images réelles il n’existe presque jamais de solution au sens classique. Ainsi, les algorithmes basés sur les EDP calculent des approximations de solutions faibles. Par ailleurs, mis à part des systèmes expérimentaux qui sont physiquement instables, une surface non lisse (i.e. non différentiable) ne peut donner une image continue. Donc, il peut paraître judicieux de ne pas vouloir calculer une solution faible de l’équation d’irradiance mais de vouloir calculer une surface lisse (i.e. différentiable) qui satisfasse “approximativement” l’équation d’irradiance. Ceci nous mène à considérer un autre type d’algorithmes basés sur les méthodes d’optimisation et sur les approches variationnelles. Dans ces méthodes, deux ingrédients de base doivent être choisis: la fonctionnelle qui va être minimisée et la méthode de minimisation. Voir la section 1.3 pour plus de détails... En plus de ces deux grandes catégories (méthodes de propagation/EDP et méthodes d’optimisation), nous pouvons définir deux catégories plus petites: les méthodes locales et les méthodes linéaires. Voir la section 1.4.

D’un point de vue algorithmique, les méthodes que nous développons

dans ce manuscrit sont des “méthodes de propagation et EDP” (voir section 1.2). Nos méthodes numériques sont décrites principalement dans le chapitre 3 et la section 5.4. D’un point de vue théorique, notre travail prend place dans le cadre des solutions de viscosité. Initialement, il était basé sur les travaux de Lions, Rouy et Tourin [134, 96] qui utilisent la notion de solutions de viscosité *continues* [39, 95, 41]. Mais ici, nous exploitons également au maximum le potentiel d’autres notions de solutions de viscosité. En particulier, nous considérons les notions de solutions de viscosité *discontinues* [76, 75] et *singulières* [77, 26, 23, 27]. Enfin, en modifiant légèrement ces notions nous définissons une nouvelle notion de solutions de viscosité: la notion de “solutions de viscosité singulières discontinues” (SDVS); voir le chapitre 4. Cette nouvelle notion permet de généraliser et d’unifier les résultats théoriques démontrés par Lions et al. [96, 134], par Dupuis et Oliensis [47], par Falcone et al. [24, 55, 56] et par Prados et Faugeras [127, 120]. Plus généralement, le cadre des solutions de viscosité permet également de démontrer l’existence et l’unicité du problème du SFS; voir par exemple les sections 2.2, 4.3 et 5.3.

Insistons sur le fait que notre travail est basé sur l’interaction des trois domaines suivants:

- les mathématiques,
- l’algorithmique,
- la modélisation.

Nous apportons notre contribution tout d’abord dans le domaine des Mathématiques: nous adaptons la notion de solutions de viscosité singulières (récemment développée par Camilli et Siconolfi [26, 27]) afin d’obtenir une “nouvelle” classe de solutions de viscosité bien mieux adaptée au problème “classique” du SFS que les précédentes. Du point de vue de la vision par ordinateur, ce cadre mathématique permet d’améliorer et d’unifier tous les précédents travaux théoriques sur le “Shape From Shading” [134, 96, 47, 127, 120, 56]. Du point de vue mathématique, ce cadre original nous permet d’obtenir une nouvelle

caractérisation des solutions de viscosité discontinues classiques par leur “minima” locaux (voir le chapitre 4).

Nous apportons également notre contribution dans le domaine de l’Algorithmique. Par exemple, nous décrivons deux schémas d’approximation et leurs algorithmes associés pour les équations de Hamilton-Jacobi-Bellman. Nous démontrons plusieurs résultats généraux afin de prouver la stabilité et la convergence de nos méthodes (voir le chapitre 3). Nous démontrons également que cette méthode s’applique à d’autres équations en l’appliquant à une autre équation de “Shape From Shading” (voir le chapitre 5)...

Enfin, nous apportons notre contribution au domaine du “Shape From Shading”, en particulier dans sa modélisation. En effet, nous sommes les premiers à fournir des formulations simples et correctes et une étude théorique rigoureuse du problème du “Shape From Shading” en modélisant l’appareil photographique à l’aide d’une projection en perspective (voir le chapitre 2). Finalement, dans le chapitre 5, nous terminons cette thèse en présentant des résultats théoriques et algorithmiques révolutionnaires dans le domaine: nous démontrons que le problème du “Shape From Shading” peut être en fait un problème complètement bien posé et nous proposons un algorithme qui permet de retrouver la forme tridimensionnelle d’une surface Lambertienne à partir d’une seule image et sans utiliser aucune donnée additionnelle: nous utilisons juste l’image de départ.

Plus précisément, pour chacun des chapitres, nos contributions sont:

- pour le chapitre 2:
 - Contrairement à la plupart des méthodes de “Shape From Shading” (développées sous l’hypothèse d’une projection orthographique), dans ce chapitre, nous modélisons le problème du SFS en supposant que l’appareil photographique effectue une projection en perspective de la scène. Nous formulons les **EDP**

explicites adéquates simplement et rigoureusement (équations (2.6) et (2.8)) et des **Hamiltoniens** associés $H_{P/F}^{pers}$ et H_F^{pers} . La source de lumière peut être localisée **à l’infini** (elle peut être frontale ou oblique) ou **au centre optique**. Ces formulations explicites permettent en particulier de démontrer des résultats d’existence et d’unicité de la solution. Nous appelons problème “classique” du SFS celui qui consiste à résoudre les EDP introduites dans ce chapitre.

- Nous développons une **étude mathématique complète** des problèmes “classiques” du SFS orthographique et perspectif. Après avoir introduit et démontré l’intérêt de la notion de solutions de viscosité discontinues pour le problème du “Shape From Shading”, nous prouvons l’**existence** des solutions de viscosité des EDP associées. Par ailleurs, nous démontrons que **la caractérisation du SFS orthographique introduite par Rouy et Tourin dans [134] reste valable pour le SFS perspectif**. Plus précisément, les solutions de viscosité continues des problèmes de SFS “classiques” peuvent être caractérisées par leurs valeurs sur le bord de l’image et aux points singuliers (c’est-à-dire les points x tels que $I(x) = 1$).
 - Finalement, en introduisant un **Hamiltonien “générique”**, nous **unifions les problèmes de SFS “orthographique” et “perspectif”** et nous simplifions le formalisme. De plus, nous réécrivons l’“Hamiltonien générique du SFS” sous la forme de l’Hamiltonien d’une équation de Hamilton-Jacobi-Bellman.
- pour le chapitre 3:
 - Nous décrivons des outils et une méthode générale permettant de traiter les **schémas monotones**. En particulier, nous donnons et prouvons un théorème général assurant la **stabilité** de ces schémas. Des résultats de **convergence** pour les **algorithmes** associés s’ensuivent automatiquement. Les outils décrits sont

principalement basés sur la monotonie et sur l'existence de **sous-solutions** ou de **sur-solutions**.

Par ailleurs, nous proposons des schémas d'approximation monotones adaptés (et “consistents”) aux **équations de Hamilton-Jacobi-Bellman** et nous montrons comment appliquer nos résultats de stabilité à ces équations.

Notons que ces outils s'appliquent aux **grilles irrégulières** et qu'ils **ne nécessitent pas de régularité sur la variable d'espace**.

- Nous appliquons les outils algorithmiques au problème du “SFS classique”. Ainsi, nous proposons deux nouveaux algorithmes “génériques” de SFS (un algorithme **semi-implicite** et un **implicite**) et nous prouvons la **convergence** des solutions numériques calculées par nos algorithmes **vers la solution de viscosité** du problème de **SFS** considéré.

Insistons sur le fait que grâce à la formulation “générique” du problème de SFS, un **unique algorithme** permet de résoudre numériquement **les différentes formulations** du problème “classique” du SFS.

De plus, nous généralisons et unifions la partie algorithmique des travaux de Rouy et Tourin [134], Dupuis et Oliensis [47] et Prados et Faugeras [127, 120]. Rappelons par ailleurs que la méthode de “Fast Marching” de Sethian [138, 139] est basée sur le schéma d'approximation de Rouy et Tourin [134].

- Nous testons nos nouvelles méthodes de SFS.

En partant d'une sur-solution l'algorithme **implicite** semble être l'un des algorithmes itératifs **les plus efficaces** de la littérature du SFS.

Nos algorithmes retournent des résultats très satisfaisants avec des **images discontinues** et avec des images contenant des **ombres portées**. De plus la stabilité de nos schémas et la convergence de nos algorithmes de SFS restent valables avec de

telles images. D'autre part, nos algorithmes sont robustes au bruit.

- A ce point, le calcul de la solution numérique du problème du SFS **nécessite des données de Dirichlet sur le bord de l'image et à tous les points singuliers.**

- **pour le chapitre 4:**

- Dans la première partie de ce chapitre, nous modifions légèrement la notion de solutions de viscosité singulières développée dans [77, 26, 23, 27] de manière à obtenir une solution de viscosité **discontinue** sur le domaine Ω contenant des points singuliers et **sans nécessiter obligatoirement des données sur le bord $\partial\Omega$** . Ainsi nous définissons la notion de **SDVS**. Nous démontrons l'**existence** et l'**unicité** des SDVS pour une grande partie des équations convexes d'Hamilton-Jacobi $H(x, \nabla u) = 0$. Des **résultats de stabilité** sont démontrés. D'autre part, nous prouvons que ce nouveau cadre permet de **caractériser les solutions de viscosité discontinues classiques par leurs "minima"**.
- Dans la deuxième partie de ce chapitre, nous montrons que la notion de SDVS permet d'**unifier** les divers résultats théoriques proposés dans la littérature du "Shape From Shading". Plus précisément, elle unifie le travail de Lions et al. [96, 134], de Dupuis et Oliensis [47], de Falcone et al. [24, 55, 56] et de Prados et Faugeras [127, 120]. Notre approche permet ainsi de **généraliser** les travaux précédents à tous les Hamiltoniens "classiques" du SFS, en particulier à ceux du "SFS perspectif". Par ailleurs, la notion de SDVS que nous introduisons ici, est **beaucoup plus adaptée aux spécificités du SFS** que les autres notions de solutions faibles utilisées dans les travaux précédents [96, 134, 24, 55, 56, 127, 120]. Plus exactement, cette notion **ne nécessite pas obligatoirement de données sur le bord de l'image et à tous les points singuliers.**

Cependant, pour caractériser et calculer une solution nous avons besoin de fixer au moins un point². De plus, lorsque l'image contient **plusieurs points singuliers**, nous avons besoin de **connaître les valeurs de la solution à tous ses “minima” locaux** pour être capable de calculer véritablement une approximation de la surface originale.

Finalement, en utilisant un résultat de stabilité, nous montrons **comment approcher numériquement les SDVS** des équations “classiques” du SFS. Enfin, nous prouvons la convergence des approximations calculées vers les SDVS.

- Nous appliquons avec succès notre méthode à des **images synthétiques et des images réelles**. De plus, nous démontrons que ces outils peuvent être utiles dans un grand nombre d'**applications concrètes** (rectification de pages, reconstructions 3D de visages, traitement d'images d'endoscopie).

- **pour le chapitre 5:**

Les difficultés rencontrées dans les chapitres 2 et 4 dans lesquels nous traitons du problème “classique” du SFS, sont dues en fait à la présence (inévitable) de points singuliers. Dans le chapitre 5, nous montrons que ces difficultés disparaissent complètement lorsque nous modélisons le problème du SFS de manière plus réaliste que ce qui est habituellement fait. En particulier, la notion de points singuliers n'a plus de sens quand nous ne négligeons pas le terme d'atténuation en $1/r^2$ de l'éclairage. En d'autres termes, nous montrons que le problème du SFS “classique” est mal posé en raison d'une trop grande simplification dans la modélisation. Ainsi, nous démontrons que dans la pratique le problème du SFS est généralement bien posé. Plus précisément nous:

- détaillons des **équations et des Hamiltoniens** appropriés au problème du “SFS perspectif” pour des scènes Lambertiennes

²Depuis que la condition au bord φ doit vérifier $\varphi \neq \infty$.

illuminées par une unique source de lumière située au centre optique, dans le cas où **nous ne négligeons pas le terme d'atténuation en $1/r^2$ de l'éclairage.**

- développons une **étude mathématique complète** des équations obtenues. Nous prouvons l'**existence** et l'**unicité** de la solution de viscosité discontinue des nouvelles équations (complétées par les conditions aux limites de Dirichlet ou des contraintes d'états).
- proposons des **schémas monotones** approximant les nouvelles EDP. Nous prouvons que nos schémas sont **stables** et **cohérents** et que leurs solutions **convergent vers la solution de viscosité** (lorsque la taille de la grille tend vers zéro). Nous proposons deux **algorithmes numériques** (un implicite et un semi-implicite). De plus, nous démontrons que les solutions calculées convergent vers les solutions des schémas.
- implémentons et testons nos algorithmes.

Ainsi **en pratique**, notre méthode permet de **retrouver toute surface** qui vérifie les hypothèses (5.17) **uniquement à partir de son image**. En particulier, **nous n'avons besoin d'aucune donnée additionnelle ou d'hypothèse de régularité**. Soulignons le fait que notre méthode fonctionne même lorsque la surface possède **plusieurs minima** et maxima locaux. Il n'y a plus aucune ambiguïté. A notre connaissance aucune méthode précédente de SFS n'est capable de retourner de tels résultats. Dans ce sens, nous sommes les premiers à fournir une solution au problème du SFS qui soit vraiment satisfaisante!

Par ailleurs, insistons sur le fait que l'hypothèse (5.17) est relativement faible et qu'elle est naturellement vérifiée en pratique. Par exemple, dès que l'image à traiter contient un objet d'intérêt devant un arrière-plan, la condition est satisfaite dans un voisinage de cet objet.

Finalement, nous montrons que notre méthode est **robuste** au bruit,

aux erreurs de paramètres et aux erreurs de modélisation. Puis nous démontrons la pertinence et l'applicabilité de notre méthode en la testant sur une base de données d'images réelles. Aussi, les résultats obtenus sont très satisfaisants.

Chapter 1

Introduction and state of the art

1.1 The “Shape from Shading” problem

The “Shape from Shading” problem (SFS) is to compute the three-dimensional shape of a surface from the *brightness* of *one* black and white image of that surface; see figure 1.1. This is a *monocular* vision problem based on the photo-

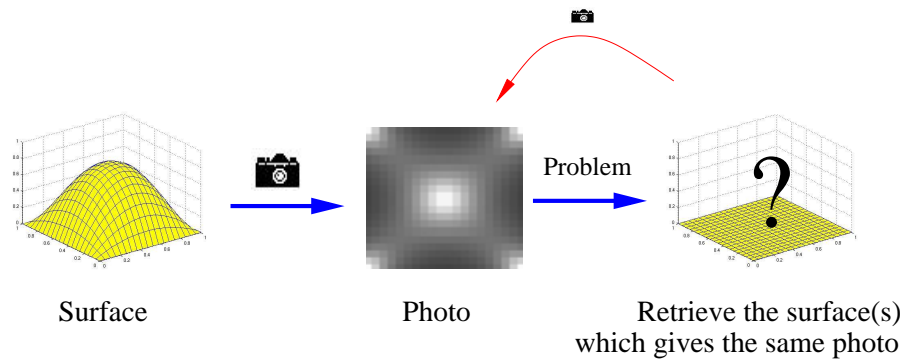


Figure 1.1: The “Shape-from-Shading” problem.

metric information.

According to Durou [49, 48], in the beginning of 50’s, Van Diggelen [162] was the first to consider the 3D reconstruction problem using photometric cues. The first resolution was suggested by Rindfleisch [131] in the 60’s. Later, Horn [67] was the first to formulate the Shape from Shading problem simply and rigorously as that of finding the solution of a nonlinear first-order Partial Differential Equation (PDE) called the brightness equation. This was also Horn

who suggested to call this problem “Shape from Shading”. Afterwards, all the Shape from Shading methods proposed to date are based on the work of Horn. In a first period (in the 80’s) the authors focus on the computational part of the problem, trying to compute directly numerical solutions. Questions about the existence and uniqueness of solutions to the problem were simply not even posed at that time with the important exception of the work of Bruss and Brooks [22, 16]. Nevertheless, due to the poor quality of the results, these questions as well as those related to the convergence of numerical schemes for computing the solutions became central in the last decade of the 20th century. Today, the Shape from Shading problem is known to be an ill-posed problem. For example, a number of articles show that the solution is not unique [16, 106, 107, 134, 11, 51, 127, 120]. The encountered difficulties have often

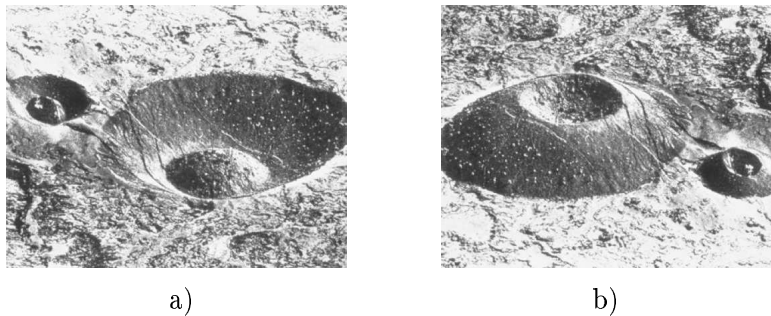


Figure 1.2: The crater illusion [115]. From picture a), we perceive two craters, a small and a big one. But we can turn these craters into volcanoes (although upside down) if we imagine the light source to be at the bottom of the picture rather than at the top. This picture is actually that of a pair of ash cones in the Hawaiian Island, not that of a pair of craters; figure b) displays the picture correctly.

been illustrated by such concave/convex ambiguities as the one displayed in Figure 1.2. In this figure, the ambiguity is due to a change of the estimation of the parameters of the lighting. In fact, this kind of ambiguity can be widely generalized. In effect, in [11], Belhumeur and colleagues prove that when the lighting direction¹ and the Lambertian reflectance (albedo) of the surface are unknown, then the same image can be obtained by a continuous family of surfaces (depending linearly of three parameters). In other words, they show that neither shading nor shadowing of an object, seen from a single viewpoint reveals its exact 3D structure. This is the “Bas-relief Ambiguity”, see [11] and Figure 1.3. Being aware of these difficulties, we therefore assume here that all the parameters of the light source, the surface reflectance and the camera are known.

¹In the case of a distant light source.

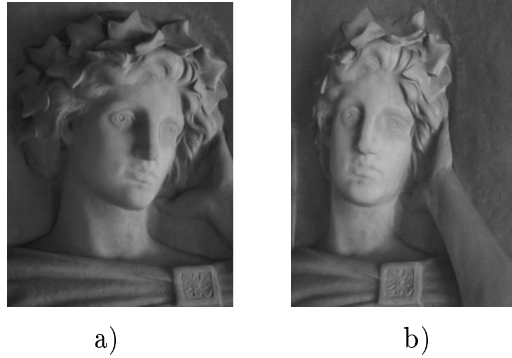


Figure 1.3: “Bas-relief Ambiguity” [11]: Frontal and side views of a marble bas-relief sculpture. Notice how the frontal views appear to have full 3-dimensional depth, while the side view reveals the flattening. This demonstrates that the image a) can be produced by two surfaces: the three-dimensional surface we imagine by visualizing image a) and the actual bas-relief which is at the origin of the two photos a) and b). For more details, the reader can refer to [11].

As we have specified above, the modeling of the Shape from Shading problem introduced by Horn yields to a PDE: the brightness equation. This equation can be roughly summarized by

$$E(x_1, x_2) = R(\mathbf{n}(x_1, x_2)).$$

The brightness equation connects the reflectance map (R) to the brightness image (E); see chapter 5 for more details. To our knowledge, at the exception of the work of [3, 92, 130], all the Shape from Shading methods assume that the scene is Lambertian. In this case, the reflectance map is the cosine of the angle between the light vector $\mathbf{L}(x_1, x_2)$ and the normal vector $\mathbf{n}(x_1, x_2)$ to the surface:

$$R = \cos(\mathbf{L}, \mathbf{n}) = \frac{\mathbf{L} \cdot \mathbf{n}}{|\mathbf{L}| |\mathbf{n}|},$$

(where R , \mathbf{L} and \mathbf{n} depend on (x_1, x_2)).

The first *explicit* PDE deduced from the brightness equation and studied in the SFS literature is the *Eikonal equation*:

$$|\nabla u(x)| = \sqrt{\frac{1}{I(x)^2} - 1}, \quad \forall x = (x_1, x_2) \in \Omega$$

where $\Omega \subset \mathbb{R}^2$ is the support of the image and $I : \Omega \rightarrow \mathbb{R}$ is the brightness of the image. This equation is obtained from the simplest modeling of the SFS problem: orthographic camera, far and frontal light source, Lambertian reflectance. It is the equation which has been considered the most in the SFS literature. In section 2.1 we describe various modelings of the SFS problem and we detail several associated PDEs.

In the sequel, we make a state of the art of the various Shape from Shading methods.

1.2 Propagation and PDEs methods

As we have mentioned above, the SFS problem can be considered as that of solving a first order PDE. Also, the first category of SFS methods consists in solving *directly* the *exact* SFS PDE. These methods we call “propagation and PDE methods” do not make any linearizations (at the opposite to the methods presented in section 1.4.2). Moreover, they do not introduce any biases in the equations contrary to the variational methods which, for example, add regularization or integrability terms (section 1.3). The main difficulty encountered by propagation and PDE methods is due to the ill-posedness of the problem. Indeed, the classical SFS equations are of the form

$$H(x, \nabla u(x)) = 0, \quad \forall x \in \Omega,$$

(see section 2.1) and, by themselves, these equations are ill-posed: *they can have several solutions* (see chapter 2). Also, to be able to compute a numerical solution, we need to add constraints to the SFS equations. In these methods, the additional constraints are boundary conditions, generally Dirichlet² boundary conditions. In other words, the computed solutions are characterized by the boundary conditions. These boundary conditions must contain enough information. Also, this information is thereby propagated “along” the solutions.

The propagation and PDEs methods can be subdivided into two classes. The “*single-pass*” methods and the *iterative methods*. The main single-pass methods are the following:

- the method of *characteristic strips* introduced in the Shape from Shading literature by Horn [65] for solving the Eikonal equation,
- the method of *propagation of the equal-height contours* introduced by Bruckstein [21] and improved by Kimmel and Bruckstein [80] (dealing with the Eikonal equation),
- the *fast marching* method introduced by Sethian [138, 139] for solving the Eikonal equation and slightly modified by Kimmel and Sethian [81] for the “orthographic Shape from Shading” with oblique light source.

Amongst the iterative methods let us cite in particular

² To impose Dirichlet boundary conditions consists of fixing the values of the solutions on the boundary...

- the algorithm introduced by Rouy and Tourin for the Eikonal equation [134] and its extension by Prados and Faugeras to the “orthographic SFS” with oblique light source [127] and to the “perspective SFS” [120],
- the algorithms of Dupuis and Oliensis [47] based on the control theory and differential games (for “orthographic SFS” with oblique light source),
- the algorithms of Falcone et al. [24, 55, 56] based on finite elements (dealing with “orthographic SFS” with oblique light source).

We prove in chapter 4 that **all these methods compute approximation of the same solution**. In particular, the initial equal-height contours method of Bruckstein [21] is a variant of the method of the characteristic strips of Horn [65]. In [21], Bruckstein assumes that the initial curve is an equal-height contour. By imposing such special Dirichlet boundary conditions, he drops the Neumann boundary conditions required by the basic method of the characteristic strips (see [82] for a nice and rigorous study of these methods). Basically both of the above methods are Lagrangian methods. Also, these methods suffer from unstability and topological problems, see for example [111]. To alleviate these problems Kimmel and Bruckstein [80] propose to upgrade Bruckstein’s method by using an Eulerian formulation of the problem. In other respects, the connection between the front propagation problems and the Hamilton Jacobi equations are well known. In particular, roughly speaking, it is proved that the viscosity solution of the Hamilton Jacobi equation associated with a front propagation corresponds with the evolution of the initial contour defined by Huygens’ principle; see for example [53]. In the same way, the other methods we cite above (Sethian’s, Rouy-Tourin’s, Dupuis-Oliensis’, Falcone’s and Prados-Faugeras’ methods) compute some approximations of the viscosity solutions of the SFS equations. In particular in [141], Sethian and Vladimirsky prove that the numerical solutions computed by the fast marching/ordered upwind methods converge toward the continuous viscosity solution (with Dirichlet boundary data on the boundary of the image). In chapter 4, we generalize and unify the results proved by Rouy and Tourin [134], by Dupuis and Oliensis [47], by Prados and Faugeras [127, 120] and by Falcone and his coworkers [24, 55, 56]. More precisely, we show that in all cases, the authors compute approximations of what we call the “singular discontinuous viscosity solutions” (SDVS) which also coincide with the value functions of the associated optimal control problems. The main difference between the previous work is based on the choice of the boundary conditions; see chapter 4 for more details.

Finally, let us remark that the approximation scheme considered by Sethian [138, 139] is the one designed by Rouy and Tourin in [134]. Moreover, we show that Prados and Faugeras’ schemes are extensions of the Rouy and Tourin’s

scheme and that their solutions coincide with those of Oliensis' scheme; see chapter 3.

Advantages and drawbacks of the propagation/PDEs methods.

- First, contrary to the variational methods for example, let us emphasize that this kind of methods does not introduce any biases and does not require additional parameters other than those directly related to the modeling of the problem.
- Except for Horn's [65] and Bruckstein and Kimmel's method [21, 80], these methods can deal with various Dirichlet/Soner³ boundary conditions. More precisely, the algorithms of Rouy and Tourin [134], Dupuis and Oliensis [47], Sethian [138, 139] and Prados and Faugeras [127, 120] can use Dirichlet and/or Soner conditions on the boundary of the image $\partial\Omega$ at all the singular points \mathcal{S} and on any other part of the image (for example, on an equal-height contour...). For instance, when we do not know the values of the solution at any points of the image, we can impose state constraints (i.e. Soner conditions) on $\partial\Omega \cup \mathcal{S}$ except for one point where we must impose a Dirichlet boundary condition. Contrary to these methods, let us note that Horn's [65] requires Dirichlet and Neumann boundary conditions and that Bruckstein's [21, 80] require the knowledge of an equal-height contour. This last constraint is a very specific Dirichlet condition and is much stronger than the previous ones. Note that implicitly, Bruckstein methods [21, 80] also impose state constraints on $\partial\Omega \cup \mathcal{S}$.
- An important drawback of iterative methods is that they require a stopping criterium. Generally, one chooses arbitrary thresholds. From this point of view, the single pass methods are clearly neater.
- Propagation/PDEs methods are the most efficient methods in the sense that they are the most accurate and the fastest.
- Finally, let us emphasize that these methods [134, 139, 47, 127, 120, 24, 56, 80] do not require regularity assumptions.

1.3 Optimization methods

It is well known that, even when the brightness image is continuous, the irradiance equation does not necessarily have a smooth solution [19, 18, 17, 82]. In

³also called state constraints.

particular, because of noise, of errors on parameters (focal length, light position, etc) and of incorrect modeling (interreflections, nonpunctual light source, nonlambertian reflectance...), in practice with real images there never exist smooth solutions. Also, except in the case of some singular experimental setups which are physically instable, a nonsmooth surface cannot yield a smooth image. Therefore, it can be justified not to compute an exact (weak) solution of the irradiance equation but instead to compute a smooth surface which satisfies “approximately” the irradiance equation. This leads to consider another type of algorithms which are based on optimization methods and on variational approaches. In this section we do not detail these numerical methods; *we just transcribe and summarize the corresponding section of the very nice paper of Durou et al. [49]*. For more details about variational approaches in Shape from Shading, we refer the reader to Horn and Brooks’ book [66] (and references therein), to the survey of Durou and his coworkers [44, 49] and to the key papers [148, 73, 69, 60, 97, 68, 87, 150, 90, 45, 42], amongst others. In the optimization methods, two basic ingredients must be chosen: the functional which has to be minimized and the minimization method.

1. Choice of the functional:

First, we must choose the unknowns. Usually, authors choose the “height” of the surface u , but they also often consider its first derivatives $\frac{\partial u}{\partial x}$ and $\frac{\partial u}{\partial y}$, noted respectively p and q . Second, the authors define the functional to minimize. In general, it is a weighted sum of various functionals corresponding to some brightness constraints, smoothness/regularity constraints, integrability constraints, intensity gradient constraints and/or unit normal constraints... For example, considering only the unknowns (p, q) , we can choose the functional \mathcal{F} :

$$\mathcal{F}(p, q) = \mathcal{F}_{data}(p, q) + \lambda_{int}\mathcal{F}_{int}(p, q) + \lambda_{smo}\mathcal{F}_{smo}(p, q)$$

where \mathcal{F}_{data} is the brightness constraint

$$\mathcal{F}_{data}(p, q) = \int_{x \in \Omega} [R(p(x), q(x)) - E(x)]^2 dx,$$

\mathcal{F}_{int} is the integrability constraint

$$\mathcal{F}_{int}(p, q) = \int_{x \in \Omega} \left[\frac{\partial p}{\partial x_2}(x) - \frac{\partial q}{\partial x_1}(x) \right]^2 dx$$

and \mathcal{F}_{smo} is the smoothness constraint

$$\mathcal{F}_{smo}(p, q) = \int_{x \in \Omega} (|\nabla p(x)|^2 + |\nabla q(x)|^2) dx.$$

The Lagrange multipliers λ_{int} and λ_{smo} are positive constants named “integrability factor” and “smoothing factor”, respectively. We call “energy” a discretization of the function \mathcal{F} . Let us denote \mathcal{E} an energy.

2. Minimization of the functional:

As explained by Durou and his coworkers [43], there exist two main strategies for finding *numerically* the minimum of a functional.

Either we minimize directly a corresponding energy \mathcal{E} ,

or we solve the system of equations produced by $\nabla\mathcal{E} = 0$ or by the discretization of the Euler equations.

These two strategies are represented in figure 1.4. Most of the methods

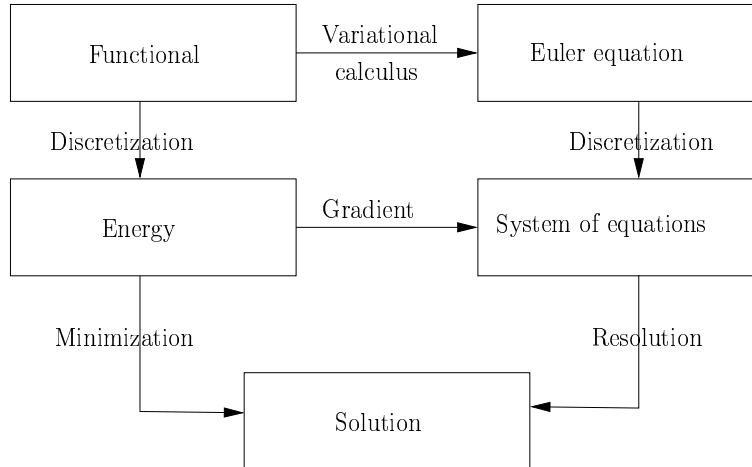


Figure 1.4: The two strategies allowing to minimize a functional numerically.

found in literature use the second way of processing although it has two important drawbacks. First, to solve $\nabla\mathcal{E} = 0$ (or Euler equations) is not equivalent to minimize globally the energy (or the functional). For $\nabla\mathcal{E} = 0$ many more configurations are solutions (local minima/maxima and others...). Second, it involves the resolution of big systems of non-linear equations, which is a difficult problem (see for example [50], but see also [89]). Concerning the first way of processing, only Szeliski [150] and Durou and his coworkers [45, 42] minimize directly the energy. Szeliski [150] uses a conjugate gradient descent. Even if the results presented in [150] are convincing, no proof of convergence is given. In [45], Daniel and Durou use a gradient descent based on line search (see [14]). Their algorithm provably converges toward a local minimum. Finally in [42], Durou and his coworkers propose a stochastic optimization method (simulated annealing) which seems to work well. They thus obtain a provably convergent algorithm toward the global minimum of the energy.

Despite these advantages optimization methods have important drawbacks:

1. They require parameters. For example λ_{int} and λ_{smo} . Most probably, these parameters could be considered as unknowns. It should be therefore necessary to minimize the functional also with respect to these new unknowns.
2. They are iterative. A stopping criterion has therefore to be chosen. In general, the authors choose arbitrary thresholds.
3. With a few exceptions [89, 45, 42], the authors cannot prove the convergence of their algorithms. Moreover the number of iterations as well as CPU times are much larger than the previous propagation methods based on PDEs. Moreover, let us note that only the method of Durou et al. described in [42] converges toward a global minimum of the energy (nevertheless, the CPU time is considerably larger than other optimization method). Also, note that in [30], Chang et al. propose to minimize their energy using graph cuts. This minimization method is able to find a local minimum “closer” to the global minimum than other (non global) minimization techniques and the computational demand is relatively small.
4. One of the most important weaknesses of the optimization methods is the loss of the “data closeness”. At the opposite of the propagation/PDEs methods, the image \tilde{I} computed from the shape reconstructed with the optimization methods is different from the initial image. It can even be completely different, see for example the experiment with the moulding of the elk in [49, 48]. In particular, the optimization methods have a tendency to over-smooth the recovered surface and so their image \tilde{I}^4 . Finally, contrary to the propagation/PDE methods, we do not understand exactly what the algorithms do in the sense that it is very difficult to predict the results they return.

1.4 Other SFS methods

Besides the two previous categories (propagation/PDEs methods and optimization methods), we can define two smaller categories: the local methods and the linear methods. Finally, a small number of methods cannot be classified easily in other categories (see section 1.4.3).

1.4.1 Local methods

The idea of the local methods is based on the assumption that locally (i.e, for example on some small patches) the surface is “almost” a plane, a sphere or a

⁴Recently, to overcome this problem, Worthington and Hancock [166] and Chang et al. [30] impose the brightness constraint as a hard constraint.

paraboloid. For example, Pentland's local approach [115] and Lee and Rosenfeld's approach [88] used the assumption that the surface is locally spherical at each point. In these methods [115, 88], the shape information is recovered from the intensity and from its first and second order derivatives. Also, in [172], Zhang et al. show that these methods suffer of instability: they are not robust to pixel noise. Recently, Tankus et al. [152] and Collings et al. [35] have proposed other methods by assuming that the surface is locally represented by quadratic functions. A limitation of these methods can be the number of iterations required for obtaining a solution. For example in [152], Tankus et al. require more than 200 000 iterations for recovering the classical vase used in the SFS literature (for example in [172]). Finally, let us indicate the original method of Robles-Kelly and Hancock [132] based on several iterations of two steps (integration and smoothing). From the surface normals, the first step splits the image in patches and estimates a surface height on each patch. The second step is a smoothing step. It consists in fitting at each pixel a local quadratic function to the height data. In such a way, the authors obtain new surface normals. Let us note that the numerical results displayed in [132] are quite good.

1.4.2 The linear methods

One of the important difficulties encountered when attempting to solve the Shape from Shading problem is the non-linearity of the equations. To get around this difficulty, several authors propose to linearize the reflectance map. Amongst linear methods, let us cite the work of Pentland [116], of Kozera and Klette [84], of Ulich [161] and of Ikeda [72]. Let us note that some theoretical results on the linear Shape from Shading problem have been demonstrated by Kozera et al. [85] (existence and uniqueness of the solution) and Ulich [161] (convergence of the algorithm). Nevertheless, even if the results obtained by these methods can be qualitatively relevant (see in particular the results returned by Tsai and Shah's method in [172] or [49]) and even if the resolution techniques are convincing (for example, Pentland proposes a numerical method based on Fourier transform, see [116]), the relevance of the linearization of the reflectance has not been proved. Also in [49], Durou et al. wonder about the legitimacy of this simplification and they support their doubts by detailing some examples.

1.4.3 Other SFS methods

Various mathematical tools have been used in order to solve the Shape from Shading problem. Bruss [22] proposes to work with some power series expansions (at a singular point). Robles-Kelly and Hancock [132] recover a solution by

using a graph spectral setting and eigenvector methods. Torreão [156] obtains excellent results with a method based on Green's Functions and inspired on the disparity-based approach to photometric stereo. Atick, Griffin and Redlich [2] propose a statistical approach for the recovery of faces from shading. Wei and Hirzinger propose a solution based on neural networks [164, 32]. Because of lack of space we do not detail these promising Shape from Shading methods.

1.5 Applicability and applications of the Shape from Shading methods

For several reasons, the interest in the Shape from Shading problem has slightly decreased in the middle of the 90s. First, due to the difficulty of the problem, progress in SFS research has been very slow. Second, until recently, the results obtained on real images have been very disappointing. For example, in [172], Zhang et al. acknowledge failure. Third, the various constraints imposed by the existing solutions to the SFS problem limit their applicability. To change this situation, we think that, from now on, it is fundamental to improve and demonstrate the applicability of the Shape from Shading methods and to point out potential applications.

1.5.1 Improvement of the applicability of the SFS methods

The first SFS methods proposed in the literature were not robust to pixel noise (for example, this was the case of the initial Horn's method [67]) and showed some instability (for example, this was the case of the local methods of Lee and Rosenfeld [88] and of Pentland [115]). Since real images contain systematically pixel noise, the SFS methods must be stable and robust to these disruptions to be applicable. The SFS methods must also be robust to errors on parameters (focal length, position of the light source) and to errors due to the coarse modeling. In particular, let us note that the SFS tools we develop in this thesis show a very high robustness to a number of errors; see sections 4.6.5 and 5.5.1. In practice the objects of the real world contain various kinds of edges and occluding contours, therefore the Shape from Shading methods must be able to deal with *discontinuous images*, *nonsmooth surfaces* and *black shadows*. Moreover to be applicable, the algorithms must require *as few parameters as possible*. Also, let us emphasize that the methods we propose here verify all these conditions. They are fast, accurate, without additional parameters⁵. They can deal with discontinuous images, black shadows, nonsmooth surfaces.

⁵internal camera parameters (focal length, size of pixels), lighting parameters and photometric calibration parameters.

One of the most (if not the most) important stages for improving the applicability of the Shape from Shading is to provide *methods based on more realistic modelings*. Indeed, despite the richness of the literature in this area, most of the SFS algorithms have been developed under the most basic modeling assumptions. Generally, the camera performs an orthographic projection of the scene, the scene is illuminated by a single point light source located at the infinity (most of the authors assume moreover that the direction of the light source coincides with one of the axes of the camera), its reflectance is assumed Lambertian and its albedo is constant and fixed to 1. Amongst the papers dealing with this setup let us cite for example the work of [67, 22, 115, 88, 21, 64, 134, 90, 47, 157, 80, 24, 81, 127, 42]. Moreover, let us note that the surveys [66, 172, 82, 49] consider only this setup. Very few authors propose algorithms adapted to more realistic modelings. Kontsevich et al. [83] and Ononye and Smith [109] reconstruct shape from shading from one color image. Recently, Yilmaz and Shah [170], Zhao and Chellappa [173, 174] and Dovgard and Basri [46] relax the common constraint of constant or piece-wise constant albedo [158] (for Lambertian surface) to arbitrary albedo. Nevertheless, to this end, they introduce an important symmetric constraint which can restrict the applicability of their method. Let us cite also the work of Samaras et al. [136] who consider surfaces with variable albedo in a general setup (for reconstructions from stereo and Shape from Shading). In other respects, Tian et al. [155, 163] describe shape recovery algorithms from shading for non-punctual and multiple light sources. Some authors take into account the perspective [114, 91, 61, 102, 165, 137, 171, 120, 152, 124, 37, 122, 154] while others deal with interreflections [101, 59, 163, 147]. Finally, Bakshi, Lee and Kuo, or Ragheb and Hancock [4, 92, 130] propose some solutions for non-Lambertian surfaces. In our work, the weakening of the modeling hypotheses is a permanent concern. In particular, we are the first to propose a rigorous perspective SFS method completely based on PDEs [120]. Our method applies with a single punctual light source located at infinity (see section 2.1.2) or close to the optical center [124, 122] (see section 2.1.3). Finally, we take into account the attenuation term of the lighting; (see chapter 5).

1.5.2 Applications of Shape from Shading

The main applications of the Shape from Shading methods can be classified into four categories:

1. Modification and improvement of images:

In [167], Worthington and Hancock use Shape from Shading for coarse view synthesis. Their aim is to generate novel object views under changing light source and/or viewer directions by using the needle-maps. In

[129], Ragheb and Hancock propose a very efficient method for removing highlights by using Shape from Shading.

2. Application to medical images:

Yamany and his coworkers [168, 100] use shape from shading techniques for recovering human jaw from intra-oral intensity images. Other potential medical applications are with endoscopic images. For example, some groups use Shape from Shading techniques in order to design an automatic endoscope navigation and advisory system [149, 86]. Other authors use Shape from Shading for correcting area measurements from images obtained through a colposcope [38]. They want to correct the errors due to the two-dimensional projection of the observed 3D object. Also, note that the computer vision community has also proposed solutions to this particular problem. Let us cite the work of Okatani and Deguchi [102, 103], of Forster and Tozzi [58] and of Tankus and Sochen [154]. In other respect, let us note that in section 4.7.3, we also show that our method produces relevant solutions to this kind of problems (see also [122]).

3. Face reconstruction:

The interest of the SFS methods for some applications dealing with faces has been demonstrated in e.g. the work of Zhao and Chellappa [173] (who use symmetric SFS for illumination-insensitive face recognition), by Smith and Hancock [143] (who use SFS needle maps for face recognition), and by Choi and coworkers [33] (who use SFS for determining the face pose). Today, one can say that face reconstruction is a classical application of Shape from Shading methods. Several authors have also proposed specific solutions: for example, Atick et al. [2], Vetter et al. [13, 133] and Dovgard and Basri [46] combine Shape from Shading techniques with statistical databases of faces. In other respect, other authors exploit the symmetry of the faces. In particular, let us cite the work of Zhao and Chellappa [173, 174], the work of Shimshoni and Moses [142], the work of Yilmaz and Shah [170] and the work of Dovgard and Basri [46]. We show in sections 4.6.2 and 5.5, that our SFS methods produce very good results from images of faces.

4. Document restoration using SFS:

Several authors [163, 31, 36, 122, 37] propose to remove the geometric and photometric distortions generated by the classical photocopy of a bulky book by using Shape from Shading techniques. For pages containing few rows of characters but a lot of graphics and pictures (separated by large white bands, this is often the case of scientific documents), the Shape from Shading methods can provide simple and efficient solutions. In section

4.7.1, we consider more precisely this application, and we propose such a solution.

1.6 Setup and numerical methods considered in our work

From the theoretical point of view, our work takes place in the setup of the viscosity solutions. Initially, it was based upon the work of Lions, Rouy and Tourin [134, 96] who use the notion of the *continuous* viscosity solutions [39, 95, 41]. But here, we also exploit at the most the potential of the other existing notions of viscosity solutions. In particular, we consider the notions of *discontinuous* [76, 75] and *singular* [77, 26, 23, 27] viscosity solutions, and finally by slightly modifying the previous notions, we define a new notion of viscosity solutions: the notion of “singular discontinuous viscosity solutions” (SDVS); see chapter 4. This new notion allows to generalize and unify the theoretical results demonstrated by Lions et al. [96, 134], by Dupuis and Oliensis [47], by Falcone et al. [24, 55, 56] and by Prados and Faugeras [127, 120]. More generally, the viscosity setup allows also to prove the existence and the uniqueness of the SFS problem; see for example sections 2.2, 4.3 and 5.3.

From the algorithmic point of view, our methods are “propagation and PDEs methods” (see section 1.2). Our numerical methods are mainly described in chapter 3 and section 5.4.

1.7 Contributions of this thesis

Almost all the material in this thesis is new. At the end of each chapter, we summarize for the reader’s convenience the main contributions therein.

Our work is based upon the interaction of the following three areas:

- Mathematics,
- Algorithmic,
- Modeling.

Our contributions are first in the area of Mathematics: we adapt the notion of singular viscosity solutions (recently developed by Camilli and Siconolfi [26, 27]) for obtaining a “new” class of viscosity solutions which is really more suitable to the “classical” SFS problem than the previous ones. From the computer vision point of view, this mathematical framework allows to improve and unify all the previous theoretical work on Shape from Shading [134, 96, 47, 127, 120, 56]. From the mathematical point of view, this original framework

allows us to obtain a new characterization of the classical discontinuous viscosity solutions by their “minima” (see chapter 4).

Our contributions are also in the area of Algorithmic. For example, we describe two approximation schemes and their associated algorithms for the Hamilton-Jacobi-Bellman equations. We prove several general results about the stability and the convergence of our methods (see chapter 3). We also prove that this methodology applies to other equations by applying it to another SFS equation (see chapter 5).

Last but not least, our contribution are in the Shape from Shading area, in particular in modeling. Indeed, we are the first to provide simple and correct formulations and a rigorous theoretical study of the Shape From Shading problem by modeling the camera as a pinhole (see chapter 2). Finally, in chapter 5, we close this thesis with some theoretical and algorithmic results which are revolutionary in the field: we prove that the Shape from Shading problem is basically a well-posed problem and we propose an algorithm which allows to recover the shape of Lambertian surfaces from shading without any additional data (we just use the input image and do not need any boundary conditions) and without additional assumptions (for example, we do not need smoothness assumptions).

Chapter 2

“Classical” Shape From Shading

In this document, we call “classical SFS problem” the problem consisting in solving the PDEs obtained by the Shape from Shading modeling we describe in the following section (section 2.1). Let us emphasize that, even though we qualify this problem of “classical”, most of the modelings and associated results we present in this chapter are contribution of our work. In particular, let us note that they are the object of several communications amongst [127, 120, 123, 124]. We choose this denomination in order to contrast the modelings and the results presented in the first parts of this thesis with the modeling and the results presented in the last chapter (chapter 5).

2.1 Mathematical formulations of the “classical” Lambertian SFS problem

The SFS problem is to retrieve the three-dimensional shape of a scene from the brightness variations in a black and white image of that scene.

The scene is represented by a surface \mathfrak{S} . Let Ω be an open set of \mathbb{R}^2 representing the domain of definition of the image; for example, Ω is the rectangular domain $]0, X[\times]0, Y[$. We assume that \mathfrak{S} can be explicitly parameterized by a function S from the closure $\overline{\Omega}$ of the set Ω into \mathbb{R}^3 by $x \mapsto S(x)$;

$$\mathfrak{S} = \{S(x); \quad x \in \overline{\Omega}\}.$$

The image intensity is modelled as a function I from $\overline{\Omega}$ into the closed interval $[0, 1]$, by

$$I : \overline{\Omega} \longrightarrow [0, 1] : x \mapsto I(x).$$

For all $x \in \overline{\Omega}$ the intensity $I(x)$ is the brightness obtained at the point $S(x)$ of the surface \mathfrak{S} .

We assume that a *single point light source* illuminates the scene. Thus with each point X in \mathbb{R}^3 we associate the unit “light vector” $\mathbf{L}(X)$ pointing to the light source.

Finally, we assume that the scene is *Lambertian*. We suppose that the albedo is constant and equal to 1.

For all $x = (x_1, x_2)$ in $\overline{\Omega}$, let us denote $\mathbf{n}(x)$, a normal vector of the surface \mathfrak{S} at the point $S(x)$ such that

$$\mathbf{n}(x) \cdot \mathbf{L}(S(x)) \geq 0.$$

With all hypotheses above, the brightness $I(x)$ of the point $S(x)$ of the surface \mathfrak{S} is the cosine of the angle $(\mathbf{n}(x), \mathbf{L}(S(x)))$. In other words:

$$I(x) = \frac{\mathbf{n}(x) \cdot \mathbf{L}(S(x))}{|\mathbf{n}(x)|}. \quad (2.1)$$

Remark 1. Through differential calculus, we can easily obtain an explicit expression for $\mathbf{n}(x)$. In effect, the two columns h_1 and h_2 of the Jacobian $DS(x)$ are two, in general different, tangent vectors to the surface \mathfrak{S} at point $S(x)$. Thus their cross product provides in general a normal vector to \mathfrak{S} .

In the remaining, we study in detail three different modelings of the SFS problem.

We deal with

1. “orthographic SFS” with a point light source at infinity,
2. “perspective SFS” with a point light source at infinity,
3. and “perspective SFS” with a point light source at the focal center.

For a more realistic modeling, the reader can see chapter 5 and [65, 82]. We also refer the reader to the papers cited in section 1.5.1.

2.1.1 The “orthographic SFS” problem

In this subsection we revisit one of the simplest versions of the shape from shading problem.

We assume that the *light source is located at infinity*. Thus, all light vectors are parallel and we can represent the light direction by a constant vector $\mathbf{L} = (\alpha, \beta, \gamma)$. We assume that the light source is above the surface, then $\gamma > 0$. We note $\mathbf{l} = (\alpha, \beta)$.

We assume that the camera performs an *orthographic projection* of the scene. With this hypothesis, it is natural to define the surface \mathfrak{S} by

$$\mathfrak{S} = \{(x_1, x_2, u(x_1, x_2)); \quad (x_1, x_2) \in \overline{\Omega}\}.$$

So, if the plane $(0, \vec{x}_1, \vec{x}_2)$ represents the retinal plane then $|u(x)|$ is the distance of the points $S(x)$ in the scene to the camera (see figure 2.1-a)).

For such a surface \mathfrak{S} , a normal vector $\mathbf{n}(x)$ is given by

$$\mathbf{n}(x) = (-\nabla u(x), 1).$$

Given these hypotheses, the brightness equation (2.1) becomes

$$\forall x \in \Omega, \quad I(x) = \frac{-\nabla u(x) \cdot \mathbf{l} + \gamma}{\sqrt{1 + |\nabla u(x)|^2}}, \quad (2.2)$$

and therefore the shape from shading problem is, given an image I and a light source direction \mathbf{L} , find a function $u : \overline{\Omega} \rightarrow \mathbb{R}$ satisfying the equation:

$$\forall x \in \Omega, \quad I(x)\sqrt{1 + |\nabla u(x)|^2} + \nabla u(x) \cdot \mathbf{l} - \gamma = 0. \quad (2.3)$$

Note that in the case where the light source is in the same direction as the direction of projection (it is the case considered by Rouy and Tourin in [134]), we have $\mathbf{L} = (0, 0, 1)$, and the PDE (2.2) can be rewritten as an Eikonal equation:

$$\forall x \in \Omega, \quad |\nabla u(x)| - \sqrt{\frac{1}{I(x)^2} - 1} = 0. \quad (2.4)$$

2.1.2 The “perspective SFS” problem

In this section, we assume that the camera performs a *perspective projection* of the scene and that the *light source is located at infinity*.

A “pinhole” camera is represented by its retinal plane and its optical center. It is characterized by its focal length $f > 0$; see figure 2.1-b).

We assume that the scene can be represented by a surface \mathfrak{S} defined by

$$\mathfrak{S} = \{u(x_1, x_2)(x_1, x_2, -f); \quad (x_1, x_2) \in \overline{\Omega}\}.$$

A normal vector of such a surface is given by:

$$\mathbf{n}(x) = \begin{pmatrix} f \nabla u(x) \\ u(x) + x \cdot \nabla u(x) \end{pmatrix}.$$

As in section 2.1.1, we represent the light by a constant unit vector $\mathbf{L} = (\alpha, \beta, \gamma)$, with $\gamma > 0$ (we suppose that the light source is above the surface \mathfrak{S}). We note

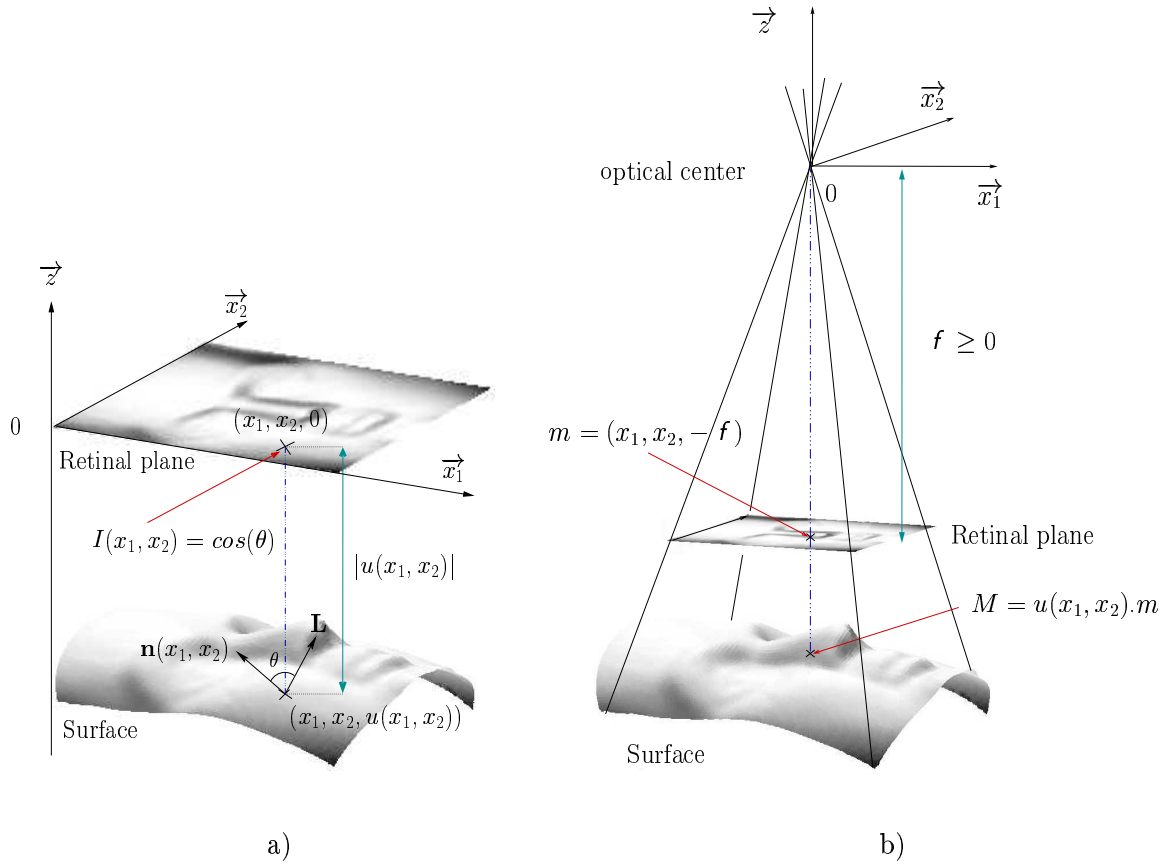


Figure 2.1:

a) Image arising from an orthogonal projection. The intensity of the “pixel” (x_1, x_2) is the intensity of the point $(x_1, x_2, u(x_1, x_2))$ on the surface \mathfrak{S} ;

b) Image arising from a perspective projection. The intensity of the “pixel” (x_1, x_2) is the intensity of the point $u(x_1, x_2)(x_1, x_2, -f)$ on the surface \mathfrak{S} ;

In both cases, we assume that the camera and the light source are above the surface.

$\mathbf{l} = (\alpha, \beta)$.

In this context, the irradiance equation becomes:

$$I(x) = \frac{f \mathbf{l} \cdot \nabla u(x) + \gamma (x \cdot \nabla u(x) + u(x))}{\sqrt{f^2 |\nabla u(x)|^2 + (x \cdot \nabla u(x) + u(x))^2}}. \quad (2.5)$$

Now, let us suppose that the surface is visible (in front of the optical center); i.e. u verifies $\forall x \in \overline{\Omega}$, $u(x) > 0$. Since equation (2.5) is homogeneous in $\nabla u(x)$ and $u(x)$, we can simplify it by the change of variables $v = \ln(u)$. Thus the “perspective SFS” problem consists in solving the original PDE.

$$I(x) \sqrt{f^2 |\nabla v|^2 + (x \cdot \nabla v + 1)^2} - (f \mathbf{l} + \gamma x) \cdot \nabla v - \gamma = 0. \quad (2.6)$$

Note that this equation has been simultaneously established by us in [118, 120] and by Tankus and his coworkers [152].

2.1.3 The “perspective SFS” with a point light source located at the optical center

In this section, we assume that the camera performs a *perspective projection* of the scene and that the scene is illuminated by a single point light source located at the optical center. This modeling is quite relevant for many applications. In effect, it nicely corresponds to the situation encountered in some medical protocols like endoscopy in which the (point) light source is located very close to the camera, because of space constraints, see section 4.7.3 for an application of SFS in this area. This modeling also corresponds approximately to the situation encountered when we use a simple camera equipped with a flash; see the sections 4.7.1 and 4.7.2 for two applications (face reconstruction and page restoration).

As in section 2.1.2, $f > 0$ represents the focal length. For mathematical convenience, we change slightly the parameterization of the scene. According to figure 2.2, we suppose that the scene is represented by a surface \mathfrak{S} defined by

$$\mathfrak{S} = \left\{ \frac{f u(x)}{\sqrt{|x|^2 + f^2}} \begin{pmatrix} x \\ -f \end{pmatrix}; x \in \overline{\Omega} \right\}.$$

For such a surface \mathfrak{S} , a normal vector $\mathbf{n}(x)$ at the point $S(x)$ is given by:

$$\mathbf{n}(x) = \begin{pmatrix} f \nabla u - \frac{f u(x)}{|x|^2 + f^2} x \\ \nabla u \cdot x + \frac{f u(x)}{|x|^2 + f^2} f \end{pmatrix}.$$

The single point light source is located at the optical center, so the unit light

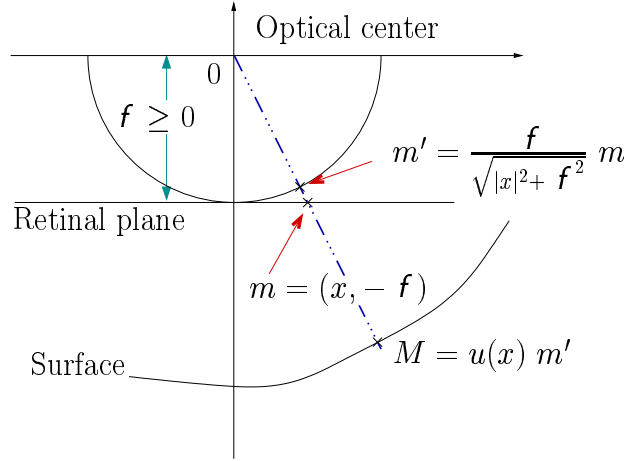


Figure 2.2: Perspective projection with a point light source located at the optical center.

The intensity of the “pixel” $(x, -f)$ is the intensity of the point $u(x)(x, -f) \frac{f}{\sqrt{|x|^2 + f^2}}$ on the surface \mathfrak{S} .

vector \mathbf{L} at point $S(x)$ is the vector

$$\mathbf{L}(S(x)) = \frac{1}{\sqrt{|x|^2 + f^2}} \begin{pmatrix} -x \\ f \end{pmatrix}.$$

The irradiance equation (2.1) then becomes:

$$I(x) \sqrt{\left(\frac{|x|^2 + f^2}{f^2}\right)} [f^2 |\nabla u(x)|^2 + (\nabla u(x) \cdot x)^2] + u(x)^2 - u(x) = 0. \quad (2.7)$$

Now, let us suppose that the surface \mathfrak{S} is visible (in front of the optical center). So u verifies

$$\forall x \in \bar{\Omega}, \quad u(x) > 0.$$

In this case, equation (2.7) being homogeneous, we can rewrite it by using the change of variables $v = \ln(u)$:

$$I(x) \sqrt{\left(\frac{|x|^2 + f^2}{f^2}\right)} [f^2 |\nabla v(x)|^2 + (\nabla v(x) \cdot x)^2] + 1 - 1 = 0.$$

It is equivalent to:

$$I(x) \sqrt{f^2 |\nabla v(x)|^2 + (\nabla v(x) \cdot x)^2} + \frac{f^2}{|x|^2 + f^2} - \frac{f}{\sqrt{|x|^2 + f^2}} = 0. \quad (2.8)$$

This explicit PDE has been established by us in [124, 119].

2.2 Shape from Shading and Viscosity solutions

2.2.1 Why using viscosity solutions to solve SFS

First, let us notice that since the beginning of the last decade of the 20th century, several authors have demonstrated the existence of images which cannot be yielded by smooth surfaces [19, 70]. Thus this suggests to consider the problem in a more weak sense.

More generally, we can remark that the SFS PDEs (2.3), (2.4), (2.6) and (2.8) do not depend on u ; so they are ill-posed¹. To characterize a solution, we need to impose some constraints. Let us impose Dirichlet boundary conditions² (DBC) for insuring uniqueness:

$$\forall x \in \partial\Omega, \quad u(x) = \varphi(x), \quad (2.9)$$

φ being continuous on $\partial\Omega$.

The SFS equations (2.3), (2.4), (2.6), and (2.8) are Hamilton-Jacobi equations. Generally, Hamilton-Jacobi equations with DBC do not have classical solutions. For example, the Rolles' theorem insures that the Eikonal equation

$$|\nabla u(x)| = 1 \text{ for all } x \text{ in }]0, 1[\quad (2.10)$$

with the DBC $u(0) = u(1) = 0$, does not have classical solutions. For solving this PDE, we need to consider a notion of weak solutions. It then appears natural to consider the notion of viscosity solutions of Hamilton-Jacobi equations. In effect, the notion of viscosity solutions is a very nice way of making quantitative and operational the intuitive idea of weak solutions of first-order³ (and for that matter, second-order) PDEs. It has been introduced by Crandall and Lions [39, 95, 41, 40] in the 80s. This theory has reached its maturity (see the book of Barles and the book of Bardi and Capuzzo-Dolcetta [7, 5]) and the numerical analysis of Hamilton-Jacobi equations has progressed considerably (see [54]).

Thus, in the Shape from shading area, the first interest of the notion of viscosity solutions of Hamilton-Jacobi equations is theoretical: it allows to characterize the SFS solutions, and so to make the problem well-posed. But let us emphasize that this notion does not only have a theoretical interest. In effect, Barles

¹For example, the solution is not unique. In effect, if u is a solution, then for all $c \in \mathbb{R}$, $u + c$ is also a solution.

²Therefore we assume that the "distance" from the camera to the scene is known on the boundary of the image. Admittedly, this hypothesis may appear a bit restrictive. We are in the process of extending our approach to remove the requirement for boundary conditions. This will be the subject of another report.

³In the context of the shape from shading problem we are only concerned with first-order PDEs.

and Souganidis [9] have proved that generally, the numerical solutions obtained by using monotonous schemes are approximations of the viscosity solutions. Thus, thanks to the notion of the viscosity solutions, we understand exactly the numerical properties of our SFS algorithms.

In the following, we recall the definitions of viscosity solutions of Hamilton-Jacobi equations and some fundamental theorems. More details about these definitions and all proofs of these theorems can be found in Barles’s, Bardi and Capuzzo Dolcetta’s or Lions’s books [7, 5, 95].

2.2.2 Viscosity solutions of Hamilton-Jacobi equations

Let us start with the notion of *continuous* viscosity solutions introduced by Crandall and Lions [39, 95, 41].

Continuous viscosity solutions

We consider a Hamilton-Jacobi equation of the form:

$$H(x, \mathbf{u}(x), \nabla \mathbf{u}(x)) = 0, \quad x \in \Omega, \quad (2.11)$$

where H is a continuous real function defined by

$$\begin{aligned} H : \Omega \times \mathbb{R} \times \mathbb{R}^N &\longrightarrow \mathbb{R} \quad , \\ (x, u, p) &\longmapsto H(x, u, p) \end{aligned}$$

and where Ω is an open subset of \mathbb{R}^N .

H is called the *Hamiltonian*. The variable associated to $\nabla \mathbf{u}(x)$ is often noted p . Let $BUC(\Omega)$ be the set of bounded and uniformly continuous functions on Ω .

Definition 2.1 (Continuous viscosity solution) $u \in BUC(\Omega)$ is a *viscosity subsolution* (respectively, a *viscosity supersolution*) of equation (2.11) if:

$$\forall \phi \in C^1(\Omega) \ , \ \forall x_0 \in \Omega \text{ local maximum of } (u - \phi), \quad H(x_0, u(x_0), \nabla \phi(x_0)) \leq 0$$

(respectively, if:

$$\forall \phi \in C^1(\Omega) \ , \ \forall x_0 \in \Omega \text{ local minimum of } (u - \phi), \ H(x_0, u(x_0), \nabla \phi(x_0)) \geq 0$$

).

u is a *continuous viscosity solution* of equation (2.11) if it is both a subsolution and a supersolution of (2.11).

Viscosity solutions are weak solutions. They are not differentiable! Nevertheless, this notion is consistent with the notion of classical solutions, as shown by the next

Theorem 2.1 *Let u be differentiable on Ω , a classical solution of (2.11). If $u \in BUC(\Omega)$, then u is a continuous viscosity solution.*

Let u be a continuous viscosity solution of equation (2.11). If u is differentiable on Ω , then u is a classical solution.

We specify for the inexperienced reader that the definition of the viscosity solutions is associated to the Hamiltonian and not to the equation. For example, it is well known that the viscosity solutions of the Hamiltonian $H(x, p)$ are different from the viscosity solutions of the Hamiltonian $-H(x, p)$. More precisely, u is a viscosity solution of $-H(x, p)$ iff $-u$ is a viscosity solution of $H(x, -p)$. Clearly, in the classical sense, the PDEs $H(x, \nabla u(x)) = 0$ and $-H(x, \nabla u(x)) = 0$ have the same solutions.

Example : When we consider $H(x, p) = |p| - 1$, the opposite two Hamiltonians on $]0, 1[$ with the DBC $u(0) = u(1) = 0$ have a unique viscosity solution shown in figure 2.3. Remember that there do not exist solutions in the classical sense. Schematically, the viscosity solutions of the Hamiltonian $H(x, p)$ allow upward kinks whereas the viscosity solutions of the Hamiltonian $-H(x, p)$ allow downward kinks.

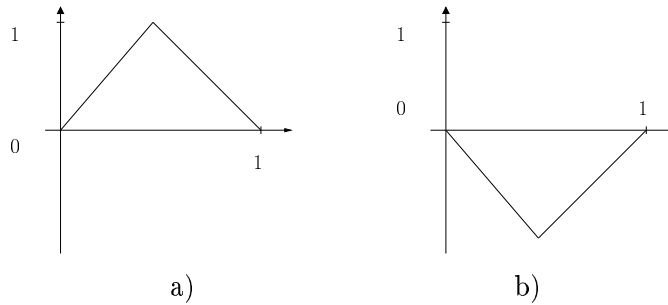


Figure 2.3: a) solution with $H(x, p) = |p| - 1$; b) solution with $H(x, p) = 1 - |p|$

Even if the viscosity solutions of a PDE depend on the Hamiltonian, the notion of viscosity solutions is consistent with strictly increasing changes of unknown (see proposition II.2.5 of [5]):

Proposition 2.1 (change of unknown) *Let $u \in C(\Omega)$ be a viscosity solution of (2.11) and $\Phi \in C^1(\mathbb{R})$ be such that $\Phi'(t) > 0$. Then $v = \Phi(u)$ is a viscosity solution of*

$$H(x, \Psi(v(x)), \Psi'(v(x))\nabla v(x)) = 0 \quad x \in \Omega,$$

where $\Psi = \Phi^{-1}$.

Thus, in order to simplify the equations, we can perform (strictly increasing) changes of variables. Therefore, even in the viscosity solutions framework, the

change of variables $v = \ln u$ used in sections 2.1.2 and 2.1.3 are completely justified.

One of the most important interests of the viscosity solutions theory is that it provides a set of general existence and uniqueness theorems which require very weak hypotheses.

Let us recall that the SFS Hamiltonians do not depend on u . Thus, to have uniqueness we must add boundary conditions. Our choice turns to Dirichlet conditions. Thus for the SFS problems we consider equations (2.12)

$$\begin{cases} H(x, \nabla u(x)) = 0 \text{ on } \Omega \\ u = \varphi \text{ on } \partial\Omega \end{cases} \quad (2.12)$$

with Ω a bounded regular and convex open set of \mathbb{R}^N , φ a real function defined on $\partial\Omega$ and H the adequate Hamiltonian.

The following theorem 2.2 applies in the special case where the Hamiltonian H appearing in equation (2.12) is convex with respect to ∇u . It ensures the *existence* of the continuous viscosity solutions of the PDE (2.12) (hence with Dirichlet boundary conditions).

We note H^* the Legendre transform⁴ of H :

$$H^*(x, q) = \sup_{p \in \mathbb{R}^N} \{p \cdot q - H(x, p)\} \leq +\infty.$$

Let us define $\forall x, y \in \overline{\Omega}$,

$$L(x, y) = \inf_{\xi \in C_{x,y}, T_0 > 0} \left\{ \int_0^{T_0} H^*(\xi(s), -\xi'(s)) ds \right\}$$

where $C_{x,y}$ is the set of $\xi : [0, T_0] \rightarrow \mathbb{R}^N$ such that

- $\xi(0) = x$,
- $\xi(T_0) = y$,
- $\forall t \in [0, T_0], \xi(t) \in \overline{\Omega}$,
- $\xi' \in L^\infty(0, T_0)$

(We denote by $L^\infty(0, T_0)$ the set of bounded real measurable functions defined on the interval $(0, T_0)$.)

Theorem 2.2 (Existence of continuous solutions) *If*

(H1) [**convexity**] H is convex with respect to p for all x in $\overline{\Omega}$,

(H2) [**uniform coercivity**]

$H(x, p) \rightarrow +\infty$ when $|p| \rightarrow +\infty$ uniformly with respect to $x \in \overline{\Omega}$,

⁴see appendix A.

(H3) [subsolution] $\inf_{p \in \mathbb{R}^N} H(x, p) \leq 0$ in $\overline{\Omega}$,

(H4) [regularity] $H \in C(\overline{\Omega} \times \mathbb{R}^N)$,

(H5) [compatibility] $\forall x, y \in \partial\Omega$, $\varphi(x) - \varphi(y) \leq L(x, y)$;

then the function u defined in $\overline{\Omega}$ by:

$$\begin{aligned} u(x) &= \inf_{y \in \partial\Omega} \{\varphi(y) + L(x, y)\} \\ &= \inf_{\xi} \left\{ \int_0^{T_0} H^*(\xi(s), -\xi'(s)) ds + \varphi(\xi(T_0)) \right\} \end{aligned} \quad (2.13)$$

is a continuous viscosity solution of equation (2.12) (in particular u verifies $u(x) = \varphi(x)$ for all x in $\partial\Omega$).

Theorem 2.2 is a special case of theorem 5.3 in [95]. It can be interpreted as giving compatibility constraints for the boundary conditions.

Remarks 2.

R2.1 - Under hypotheses (H1)-(H4), we have then the following necessary and sufficient condition:

*u defined by (2.13) is a viscosity solution of (2.12)
iff the hypothesis (H5) is true.*

We will say that φ verifies the *compatibility condition* if (H5) is verified.

R2.2 - An other interest of the viscosity theory is its link with control theory. For example, theorem 2.2 gives the solutions as value functions.

Theorem 2.2 allows to prove the existence of continuous viscosity solutions of our SFS problems (see section 2.2.4). Nevertheless, let us point out that the existence of such a solution requires a constraint on the variation of φ (the compatibility condition).

Example : Let us consider again the PDE

$$|\nabla u(x)| - 1 = 0.$$

The reader can verify easily that $H^*(x, \cdot)$ is defined on the ball $B(0, 1)$ and that for all x in Ω and for all q in $B(0, 1)$, $H^*(x, q) = 1$. So

$$L(x, y) = \inf_{\xi \in \mathfrak{X}} T_0 = y - x$$

(where

$$\mathfrak{X} = \{ \xi \mid \xi(0) = x, \xi(T_0) = y, \xi' \in L^\infty(0, T_0) \text{ s.t. } \forall s \in [0, T_0], |\xi'(s)| \leq 1 \} \quad).$$

Therefore for the Hamiltonian $H(x, p) = |p| - 1$ with DBC on $\{0, 1\}$, the compatibility condition is:

$$\begin{cases} \varphi(0) - \varphi(1) \leq L(0, 1) = 1 - 0, \\ \varphi(1) - \varphi(0) \leq L(1, 0) = 0 - 1, \end{cases}$$

that is to say

$$|\varphi(0) - \varphi(1)| \leq 1.$$

Consequently, theorem 2.2 does not apply with equation

$$\begin{cases} |\nabla u| - 1 = 0, \\ u(0) = 0 \text{ and } u(1) = 1.5. \end{cases} \quad (2.14)$$

So, we cannot prove that the PDE (2.14) has a continuous viscosity solution. In effect, it is possible to prove that this PDE does not have continuous viscosity solutions.

Come back to the SFS problem. Let us suppose that we make a large error on the function φ^5 when we compute a numerical solution of the SFS problems. If this error is too large then there do not exist continuous viscosity solutions. So what do the numerical algorithms compute? In other words, how do interpret the numerical results obtained by the algorithms?

So as soon as there do not exist continuous viscosity solutions, we need to introduce a notion of solution weaker than this notion. Also, the notion of discontinuous viscosity solutions provides an answer to these problems. The notion of discontinuous viscosity solutions is due mostly to Ishii [76, 75] and is covered in detail in the book of Barles [7]. The recent book of Bardi and Capuzzo Dolcetta [5] synthesizes some recent results.

Discontinuous viscosity solutions

Let us consider the following equation on the closed subset $\overline{\Omega}$:

$$F(x, u(x), \nabla u(x)) = 0, \text{ for } x \in \overline{\Omega}, \quad (2.15)$$

where F , defined on $\overline{\Omega} \times \mathbb{R} \times \mathbb{R}^N$, is only locally bounded (F is not supposed to be continuous). The idea is to consider both the equation and the boundary condition. Generally F is defined by:

$$F(x, u, p) = \begin{cases} H(x, u, p) & \text{for } x \text{ in } \Omega, \\ G(x, u, p) & \text{for } x \text{ in } \partial\Omega, \end{cases} \quad (2.16)$$

⁵Let us remember that we assume that we know this function φ , but in practice we only can have an approximation of it.

where H is a continuous function on $\overline{\Omega} \times \mathbb{R} \times \mathbb{R}^N$ and G is a continuous function on $\partial\Omega \times \mathbb{R} \times \mathbb{R}^N$. For example, in the case of the Dirichlet condition, we can take:

$$F(x, u, p) = \begin{cases} H(x, u, p) & \text{for } x \text{ in } \Omega, \\ u - \varphi(x) & \text{for } x \text{ in } \partial\Omega, \end{cases} \quad (2.17)$$

with φ continuous on $\partial\Omega$.

Definition 2.2 Let u be a locally bounded function on a set E .

$\forall x \in E$, let us note:

$$u^*(x) = \limsup_{y \rightarrow x} u(y)$$

$$u_*(x) = \liminf_{y \rightarrow x} u(y)$$

u^* et u_* are respectively call the upper semicontinuous envelope and lower semicontinuous envelope of u .

We recall also that $u : E \rightarrow \mathbb{R}$ is upper (respectively, lower) semicontinuous (u.s.c, resp. l.s.c) if for any $x \in E$ and $\varepsilon > 0$ there exists a δ such that for all $y \in E \cap B(x, \delta)$, $u(y) < u(x) + \varepsilon$ (respectively, $u(y) > u(x) - \varepsilon$). To familiarize oneself with these notions, the reader can refer to the sections V-1 and V-2.1 of [5].

Definition 2.3 (Discontinuous viscosity solutions) A locally bounded function, u.s.c (respectively, l.s.c) on $\overline{\Omega}$, v is a discontinuous viscosity subsolution (respectively, supersolution) of equation (2.15) if:

$$\forall \phi \in C^1(\overline{\Omega}), \forall x_0 \in \overline{\Omega} \text{ local maximum of } (v - \phi), \quad F_*(x_0, v(x_0), \nabla \phi(x_0)) \leq 0.$$

(respectively, if:

$$\forall \phi \in C^1(\overline{\Omega}), \forall x_0 \in \overline{\Omega} \text{ local minimum of } (v - \phi), \quad F^*(x_0, v(x_0), \nabla \phi(x_0)) \geq 0.$$

).

A locally bounded function, u is a discontinuous viscosity solution of (2.15) if u^* is a subsolution and u_* is a supersolution of (2.15).

For the Dirichlet problem (2.17) with H and φ continuous, it is easy to calculate the functions F^* and F_* . We have:

$$\begin{aligned} F^*(x) &= F_*(x) = H(x) && \text{if } x \in \Omega, \\ F^*(x) &= \max(H(x, u, \nabla u), u(x) - \varphi(x)) && \text{if } x \in \partial\Omega, \\ F_*(x) &= \min(H(x, u, \nabla u), u(x) - \varphi(x)) && \text{if } x \in \partial\Omega. \end{aligned}$$

For more details, we advise the reader to read chapter 4 of Barles' book [7].

Let us emphasize that the notion of discontinuous viscosity solutions extends the notion of continuous viscosity solutions. In particular a continuous viscosity

solution is a discontinuous viscosity solution. Also, the notion of discontinuous viscosity solutions allows to define solutions when there do not exist continuous viscosity solutions. For example, the reader will verify easily that the function represented in figure 2.4 is a discontinuous viscosity solution of equation (2.14)

$$\begin{cases} |\nabla u| - 1 = 0, \\ u(0) = 0 \text{ and } u(1) = 1.5. \end{cases}$$

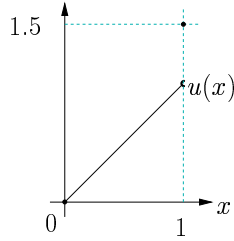


Figure 2.4: Example of a discontinuous viscosity solution of (2.14).

There exist many existence theorems for discontinuous viscosity solutions. We only give here the one we need for our applications. The reader can find the following theorem in Bardi and Capuzzo Dolcetta’s book [5] (theorem V.4.13), it deals with Hamilton-Jacobi-Bellman equations.

Definition 2.4 Let Ω be an open subset of \mathbb{R}^N and A be a set. We call *Hamilton-Jacobi-Bellman (HJB) the PDE defined as follows:*

$$\lambda u(x) + \sup_{a \in A} \{-f(x, a) \cdot \nabla u(x) - l(x, a)\} = 0 \quad \forall x \in \Omega. \quad (2.18)$$

where f is a function from $\Omega \times A$ into \mathbb{R}^N and l is a function defined from $\Omega \times A$ into \mathbb{R} .

According to the optimal control theory (see theorem 2.3 and more generally the book [5]), a is called the control, l is called the running cost, f is called the dynamics and $\lambda \geq 0$ is called the interest rate.

We associate with the HJB equations (2.18), the convex Hamiltonian

$$H(x, u, p) = \lambda u + \sup_{a \in A} \{-f(x, a) \cdot p - l(x, a)\},$$

which we call “HJB Hamiltonian”.

Before giving the theorem, let us state the assumptions we need:

- (H6) A is a compact topological space and Ω is a bounded open subset of \mathbb{R}^N ;

(H7) $f : \overline{\Omega} \times A \rightarrow \mathbb{R}^N$ is continuous;
 $l : \overline{\Omega} \times A \rightarrow \mathbb{R}$ is continuous and bounded.

(H8) f and l are Lipschitz continuous in $x \in \overline{\Omega}$ uniformly in $a \in A$.

Theorem 2.3 Let $H(x, p) = \sup_{a \in A} \{-f(x, a) \cdot p - l(x, a)\}$; assume the hypotheses (H6)-(H8) are satisfied and let $\varphi \in BC(\partial\Omega)$, then u defined by

$$u(x) = \inf_{\xi: \mathbb{R}^+ \rightarrow A} \int_0^{t_x(\xi)} l(y_x(s), \xi(s)) e^{-\lambda s} ds + e^{-\lambda t_x(\xi)} \varphi(y_x(t_x(\xi))),$$

(where y_x is the solution of the differential equation

$$\begin{cases} y'(t) = f(y(t), \xi(t)), & t > 0, \\ y(0) = x, \end{cases}$$

and $t_x(\xi)$ is the first time the trajectory $y_x(\cdot, \xi)$ goes out of $\overline{\Omega}$)
 is a viscosity solution in the discontinuous sense of

$$\begin{cases} \lambda u + H(x, \nabla u) = 0 & \text{in } \Omega, \\ u = \varphi & \text{on } \partial\Omega. \end{cases} \quad (2.19)$$

Remarks 3.

R3.1 - In other words, this theorem states that the value function of the classical optimal control problem is the viscosity solution of the adequate HJB equation.

R3.2 - We emphasize the fact that the theorem is true even if $\lambda = 0$.

The HJB equations are useful for the SFS problems. As we will see below, we can rewrite the SFS equations as HJB equations. The reader unfamiliar with control theory can read appendix A in which we detail the tools allowing to make this transformation.

2.2.3 Hamiltonians for the SFS problems and unification of the “perspective” and “orthographic SFS”

Note: In this section, and more generally when we deal with the SFS problem, we fix $N = 2$. In particular, Ω is an open subset of \mathbb{R}^2 .

2.2.3.1 Basic Hamiltonians for SFS

In section 2.1, we have presented several PDEs arising from various mathematical formulations of the SFS problem. Let us recall that the definition of the viscosity solutions is associated with the Hamiltonians and not with the equations. So for each SFS equation we have to specify an Hamiltonian.

1. In the case where $\mathbf{L} = \begin{pmatrix} 0 \\ 0 \\ 1 \end{pmatrix}$, we associate the “Eikonal” Hamiltonian H_{Eiko}^{orth} with the Eikonal equation (2.4):

$$H_{Eiko}^{orth}(x, p) = |p| - \sqrt{\frac{1}{I(x)^2} - 1}. \quad (2.20)$$

- In the case where $\mathbf{L} = \begin{pmatrix} 0 \\ 0 \\ 1 \end{pmatrix}$, we can also consider the Hamiltonian $H_{(0,0,1)}^{orth}$:

$$H_{(0,0,1)}^{orth}(x, p) = I(x)\sqrt{1 + |p|^2} - 1; \quad (2.21)$$

$H_{(0,0,1)}^{orth}$ is a particular case of $H_{R/T}^{orth}$, see below.

2. With equation (2.3) of the general “orthographic SFS” ($\mathbf{L} = (1, \gamma)$), we associate the Hamiltonian⁶ $H_{R/T}^{orth}$:

$$H_{R/T}^{orth}(x, p) = I(x)\sqrt{1 + |p|^2} + p \cdot \mathbf{l} - \gamma; \quad (2.22)$$

3. With equation (2.6) of the “perspective SFS” with a constant light source vector $\mathbf{L} = (1, \gamma)$, we associate the Hamiltonian⁷ $H_{P/F}^{pers}$:

$$H_{P/F}^{pers}(x, p) = I(x)\sqrt{f^2|p|^2 + (x \cdot p + 1)^2} - (f \mathbf{l} + \gamma x) \cdot p - \gamma; \quad (2.23)$$

4. With the “perspective SFS” with $\mathbf{L} = (0, 0, 1)$ (the light direction corresponds to the optical axis of the camera) we associate

$$H_{(0,0,1)}^{pers}(x, p) = I(x)\sqrt{f^2|p|^2 + (x \cdot p + 1)^2} - x \cdot p - 1; \quad (2.24)$$

5. And with the “perspective SFS” with a single point light source located at the optical center, we associate the Hamiltonian⁸ H_F^{pers} ;

$$H_F^{pers}(x, p) = I(x)\sqrt{f^2|p|^2 + (p \cdot x)^2 + Q(x)^2} - Q(x), \quad (2.25)$$

where $Q(x) = \frac{f}{\sqrt{|x|^2 + f^2}}$.

Let us remind the reader that in (2.22) and (2.23), we assume $\gamma > 0$.

⁶This Hamiltonian has been introduced by Rouy and Tourin [134].

⁷This Hamiltonian has been established by Prados and Faugeras in [118, 120].

⁸This Hamiltonian has been introduced by Prados and Faugeras in [119, 124].

2.2.3.2 A “generic” Hamiltonian for SFS

As we have seen in the previous section, the SFS problem leads to several Hamiltonians; nevertheless we show that all these SFS Hamiltonians are special cases of a general one, thereby simplifying the formalization of the problem.

Explicit formulation of H_g

In appendix B.1, we show that all the Hamiltonians H_*^{orth} and H_*^{pers} are special cases of the following “generic” Hamiltonian H_g

$$H_g(x, p) = \tilde{H}_g(x, A_x p + \mathbf{v}_x) + \mathbf{w}_x \cdot p + c_x,$$

with $\tilde{H}_g(x, q) = \kappa_x \sqrt{|q|^2 + K_x^2}$,

- $\kappa_x \geq 0$ and $K_x \geq 0$,
- $A_x = D_x R_x$, where
 - $D_x = \begin{pmatrix} \mu_x & 0 \\ 0 & \nu_x \end{pmatrix}$, $\mu_x, \nu_x \neq 0$,
 - if $x \neq 0$, R_x is the rotation matrix $R_x = \begin{pmatrix} \cos \theta & \sin \theta \\ -\sin \theta & \cos \theta \end{pmatrix}$;
 - where $\cos \theta = \frac{x_2}{|x|}$ and $\sin \theta = -\frac{x_1}{|x|}$,
 - if $x = 0$, $R_x = Id_{2 \times 2}$;
- $\mathbf{v}_x, \mathbf{w}_x \in \mathbb{R}^2$,
- $c_x \in \mathbb{R}$.

In appendix B.1, we detail the associated functions $\mathbf{v}_x, \mathbf{w}_x, c_x, \mu_x, \nu_x, \kappa_x$ and K_x , for all the Hamiltonians H_*^{orth} and H_*^{pers} .

Control formulation of H_g

Let us remind the reader that we call “HJB Hamiltonian”, a Hamiltonian which has the following form (see definition 2.4):

$$H(x, u, p) = \lambda u + \sup_{a \in A} \{-f(x, a) \cdot p - l(x, a)\}$$

From a theoretical point of view as well as from a practical one, it is very interesting to formulate the SFS Hamiltonians as HJB Hamiltonians. For example, such a formulation allows to apply the existence theorem 2.3. Also, in chapter 3, we show that the HJB formulation allows to design approximations schemes (section 3.1) and numerical algorithms (section 3.1). Therefore it allows to compute numerical approximations of the viscosity solutions of SFS PDEs.

We now give a HJB formulation of the “generic” Hamiltonian H_g . By using the Legendre transform⁹ of \tilde{H}_g , we can rewrite the Hamiltonian H_g as a supremum¹⁰:

$$H_g(x, p) = \sup_{a \in \text{Dom} \tilde{H}_g^*(x, \cdot)} \{ [{}^t A_x a + \mathbf{w}_x] \cdot p - [\tilde{H}_g^*(x, a) - \mathbf{v}_x \cdot a - c_x] \}.$$

Now, let us write

$$Dil_x = \kappa_x {}^t R_x D_x R_x. \quad (2.26)$$

By using the change of variables¹¹ $b = \kappa_x^{-1} {}^t R_x a$ ($a = \kappa_x R_x b$), we have:

$$H_g(x, p) = \sup_{a \in \overline{B}(0,1)} \{ [Dil_x a + \mathbf{w}_x] \cdot p - [\tilde{H}_g^*(x, \kappa_x R_x a) - \kappa_x ({}^t R_x \mathbf{v}_x) \cdot a - c_x] \}.$$

Through differential calculus¹², we obtain

$$\tilde{H}_g^*(x, a) = -K_x \sqrt{\kappa_x^2 - |a|^2},$$

so that

$$\tilde{H}_g^*(x, \kappa_x R_x a) = -\kappa_x K_x \sqrt{1 - |a|^2}.$$

Then we have

$$H_g(x, p) = \sup_{a \in \overline{B}_2(0,1)} \{ -f_g(x, a) \cdot p - l_g(x, a) \}, \quad (2.27)$$

with

$$\begin{aligned} f_g(x, a) &= - [Dil_x a + \mathbf{w}_x], \\ l_g(x, a) &= - [K_x \kappa_x \sqrt{1 - |a|^2} + \kappa_x ({}^t R_x \mathbf{v}_x) \cdot a + c_x]. \end{aligned} \quad (2.28)$$

In order to apply the theory of the viscosity solutions on HJB equations, it is important that the supremum is on a set which does not depend on x . In the control formulation (2.27) of H_g , the supremum is on the closed ball $\overline{B}_2(0, 1)$.

Remark 4. This formulation is still valid at the points x such that $\kappa_x = 0$. For most of the SFS Hamiltonians, these points correspond to pixels in *shadows*. At these points we have

$$H_g(x, p) = \mathbf{w}_x \cdot p + c_x = \sup_{a \in \overline{B}_2(0,1)} \{ \mathbf{w}_x \cdot p + c_x \}.$$

⁹See appendix A.

¹⁰See appendix B.2.

¹¹This change of variables is justified only if $\kappa_x \neq 0$. Nevertheless, the reader will verify easily that the following series of identities hold even if $\kappa_x = 0$.

¹²Using the method described in appendix A.

So

$$\begin{aligned} f_g(x, a) &= -\mathbf{w}_x, \\ l_g(x, a) &= -c_x. \end{aligned}$$

Thus, the approximation schemes based on this formulation and presented in section 3.1.2 provide numerical algorithms allowing to compute solutions of SFS for images including shadows.

2.2.3.3 SFS Hamiltonians nonnegative running cost

We start this subsection by recalling the

Definition 2.5 *Let $\psi \in C^1(\Omega)$. We say that ψ is a subsolution of $H(x, \nabla u) = 0$ if*

$$\forall x \in \Omega, \quad H(x, \nabla \psi(x)) \leq 0.$$

So by definition, the null function 0 is a subsolution of the Hamiltonian H iff $\forall x \in \Omega, \quad H(x, 0) \leq 0$. Also, for a convex Hamiltonian H , we can verify:

Proposition 2.2 *0 is a subsolution of the convex Hamiltonian H iff*

$$\forall x \in \Omega, \quad \forall q \in \mathbb{R}^N, \quad H^*(x, q) \geq 0$$

(where H^* is the Legendre transform of H , see appendix A). Also, if H is an HJB Hamiltonian (with a null interest rate), 0 is a subsolution iff the running cost is nonnegative.

Proof.

$$\begin{aligned} H(x, 0) \leq 0 &\iff \sup_{q \in \text{Dom}H^*(x, \cdot)} \{ 0 \cdot q - H^*(x, q) \} \leq 0 \\ &\iff -\inf_{q \in \text{Dom}H^*(x, \cdot)} \{ H^*(x, q) \} \leq 0 \\ &\iff \inf_{q \in \text{Dom}H^*(x, \cdot)} \{ H^*(x, q) \} \geq 0 \\ &\iff \forall q \in \text{Dom}H^*(x, \cdot), \quad H^*(x, q) \geq 0. \end{aligned}$$

In the same way, we prove the equivalent with the nonnegativity of the running cost of an HJB Hamiltonian.

□

Moreover, let us note that the running cost l_g associated with the generic Hamiltonian H_g verifies $H_g^*(x, q) = l_g(x, \text{Dil}_x^{-1}(q - \mathbf{w}_x))$.

At this stage, several reasons can suggest us to deal with such Hamiltonians:

1. It allows to apply the theory developed by Camilli and its coworkers in [26, 25, 23].
2. A large part of the results presented by Dupuis and Oliensis in [47] are demonstrated by using widely the positivity of the running cost (more precisely, they used the positivity of the Legendre transform).
3. Generally, the proofs of the existence and uniqueness of the viscosity solutions are easier with these Hamiltonians than with other Hamiltonians. For example, hypothesis (H3) becomes obvious. This is also true when we consider schemes. The proof of the stability of the schemes and the proof of the convergence of their solutions toward the viscosity solution (of the associated equations) are simpler; see for example proposition 3.2. Nevertheless, let us note that, as we show in chapter 4 (see in particular section 4.4), the work of Camilli et.al [26, 25, 23], and the work of Dupuis and Oliensis [47] can be extended to Hamiltonians with any running cost. We donot require anymore the nonnegativity of H^* .

Since the intensity image I verifies $I(x) \leq 1$, the SFS Hamiltonians $H_{Eik\sigma}^{orth}$, $H_{(0,0,1)}^{orth}$, H_F^{pers} and $H_{(0,0,1)}^{pers}$ have positive running cost (they verify $H(x, 0) \leq 0$). For the Hamiltonians $H_{R/T}^{orth}$ and $H_{P/F}^{pers}$, the associated running costs are not positive. Nevertheless, by performing some changes of variables, we can design other Hamiltonians which verify this property.

“Orthographic Hamiltonian” with nonnegative running cost

By using the change of variables¹³

$$v(x) = \mathbf{1} \cdot x + \gamma u(x), \quad (2.29)$$

the PDE (2.3) can be rewritten as

$$\forall x \in \Omega, \quad I(x) \sqrt{|\nabla u(x) - \mathbf{1}|^2 + \gamma^2} + \nabla u(x) \cdot \mathbf{1} - 1 = 0. \quad (2.30)$$

Let us note that the “change of unknown” proposition 2.1 does not apply to the change of variables (2.29).

With equation (2.30), we associate the Hamiltonian $H_{D/O}^{orth}$:

$$H_{D/O}^{orth}(x, p) = I(x) \sqrt{|p - \mathbf{1}|^2 + \gamma^2} + p \cdot \mathbf{1} - 1. \quad (2.31)$$

Since $H_{D/O}^{orth}(x, 0) = I(x) - 1$ and $I(x) \leq 1$, $H_{D/O}^{orth}$ verifies:

$$\forall x \in \overline{\Omega}, \quad H_{D/O}^{orth}(x, 0) \leq 0.$$

¹³Proposed by Dupuis and Oliensis [47].

“Perspective Hamiltonian” with nonnegative running cost

By using the change of variable

$$v(x) = \frac{\gamma}{f} [\gamma f - 1 \cdot x] u(x), \quad (2.32)$$

before the change of variables $v = \ln(u)$, the PDE (2.5) can be rewritten as a PDE which the associated Hamiltonian H_2^{pers} verifies

$$\forall x \in \bar{\Omega}, \quad H_2^{pers}(x, 0) \leq 0.$$

Since the interest of this formulation is essentially theoretic, we do not give more details about this Hamiltonian.

Remark:

Let us note that the two Hamiltonians $H_{D/O}^{orth}$ and H_2^{pers} are some particular cases of the generic SFS Hamiltonian H_g described above.

2.2.4 Existence of viscosity solutions of the “classical” SFS problems

2.2.4.1 Existence of continuous viscosity solutions of the “classical” SFS problems

In this section, we apply theorem 2.2 (page 60) for proving the existence of continuous viscosity solutions of the SFS Hamiltonians.

Let us remind the reader that the SFS Hamiltonians are special cases of the generic Hamiltonian H_g . Therefore all the properties proved for the generic Hamiltonian are also available for all the SFS Hamiltonians.

- At first, the generic Hamiltonian H_g is convex with respect to p : (H1) is true.
- About the uniform coercivity, we have the following proposition:

Proposition 2.3 *Let us consider a Hamiltonian H_g defined as in section 2.2.3.2 such that the functions κ_x , c_x , A_x^{-1} , \mathbf{w}_x , \mathbf{v}_x (or κ_x , $c_x, ({}^t R_x A_x)^{-1}$, \mathbf{w}_x , ${}^t R_x \mathbf{v}_x$) are continuous and bounded on the compact set $\bar{\Omega}$. We assume that $\mathbf{w}_x \neq 0$ for all x in $\bar{\Omega}$.*

If $\forall x \in \bar{\Omega}$, $|{}^t A_x^{-1} \mathbf{w}_x| < \kappa_x$ then $H_g(x, \cdot)$ is coercive uniformly with respect to x in $\bar{\Omega}$.

Proof. See subsection 2.2.5. □

We can remark that if $\mathbf{w}_x = 0$ and $\kappa_x \neq 0$ therefore $H_g(x, \cdot)$ is coercive

uniformly with respect to x in $\overline{\Omega}$ (by using the compacity of $S(0, 1) \times \overline{\Omega}$, we have: $\exists \delta > 0 \mid \forall p \in S(0, 1)$ and $\forall x \in \overline{\Omega}$, $|A_x p| > \delta$; therefore $\forall \lambda > 0$, $|A_x(\lambda p)| > \lambda \delta$; the conclusion follows).

Using the results of the appendix B.1 and applying proposition 2.3 to the corresponding SFS Hamiltonians, we obtain the following statements:

- H_{Eiko}^{orth} , $H_{(0,0,1)}^{orth}$, H_F^{pers} are uniformly coercive as soon as $I(x) > 0$.
- $H_{R/T}^{orth}$, $H_{D/O}^{orth}$ are uniformly coercive as soon as $I(x) > |1|$.
- $H_{(0,0,1)}^{pers}$ is uniformly coercive if $I(x) > \frac{|x|}{\sqrt{f^2 + |x|^2}}$.
- $H_{P/F}^{pers}$, H_2^{pers} are coercive as soon as

$$I(x)^2 > \frac{1}{f^2 + |x|^2} [|\gamma x + f1|^2 + (|x|^2|1|^2 - (x \cdot 1)^2)].$$

Hence, subject to the adequate conditions, all SFS Hamiltonians verify hypothesis (H2).

- Concerning hypothesis (H3), we verify that:

- for the Hamiltonians H_{Eiko}^{orth} , $H_{(0,0,1)}^{orth}$, H_F^{pers} , $H_{D/O}^{orth}$, $H_{(0,0,1)}^{pers}$ and H_2^{pers} we have

$$\inf_{p \in \mathbb{R}^2} H(x, p) \leq H(x, 0) \leq 0.$$

- for the Hamiltonian $H_{R/T}^{orth}$ (taking the derivative):

$$\inf_{p \in \mathbb{R}^2} H(x, p) = \begin{cases} \sqrt{I^2(x) - |1|^2} - \gamma & \text{if } I(x) \geq |1|. \\ -\infty & \text{otherwise.} \end{cases}$$

Since $I^2 \leq \alpha^2 + \beta^2 + \gamma^2 = 1$, we have $\inf_{p \in \mathbb{R}^2} H(x, p) \leq 0$.

- for the Hamiltonian $H_{P/F}^{pers}$, we can consider the subsolution ψ described at the page 78. We have

$$\inf_{p \in \mathbb{R}^2} H_{P/F}^{pers}(x, p) \leq H_{P/F}^{pers}(x, \nabla \psi(x)) \leq 0.$$

- If κ_x , K_x , \mathbf{w}_x , c_x are continuous and if A_x and \mathbf{v}_x (or ${}^t R_x A_x$ and ${}^t R_x \mathbf{v}_x$) are continuous then H_g is continuous in $\overline{\Omega} \times \mathbb{R}^2$. Therefore as soon as the intensity image I is continuous, all SFS Hamiltonians H_*^{pers} and H_*^{orth} are continuous in $\overline{\Omega} \times \mathbb{R}^2$ (for the Hamiltonian H_{Eiko}^{orth} , I must also verify $I > 0$ on $\overline{\Omega}$). So (H4) holds.

Therefore, if the *compatibility condition* (H5) is satisfied on $\partial\Omega$ (and if the above conditions are verified), *then all the SFS problems* (PDEs with DBC) *have continuous viscosity solutions.*

2.2.4.2 Existence of discontinuous viscosity solutions of the “classical” SFS problems

In section 2.2.3.2 at the page 67, we have shown that the “generic” Hamiltonian H_g is a HJB Hamiltonian. Precisely we have shown that:

$$H_g(x, p) = \sup_{a \in \overline{B}_2(0,1)} \{-f_g(x, a) \cdot p - l_g(x, a)\},$$

with

$$\begin{aligned} f_g(x, a) &= - [Dil_x a + \mathbf{w}_x], \\ l_g(x, a) &= - [K_x \kappa_x \sqrt{1 - |a|^2} + \kappa_x ({}^t R_x \mathbf{v}_x) \cdot a + c_x]. \end{aligned} \quad (2.33)$$

Also we have:

- If κ_x , μ_x and ν_x are continuous on $\overline{\Omega}$, then Dil_x is continuous on $\overline{\Omega}$. If furthermore \mathbf{w}_x is continuous then f_g is continuous on $\overline{\Omega} \times \overline{B}_2(0, 1)$.
- If μ_x and ν_x are bounded (which is true as soon as $\overline{\Omega}$ is bounded and μ_x and ν_x are continuous on $\overline{\Omega}$) and if κ_x is Lipschitz continuous, then Dil_x is Lipschitz continuous. If furthermore \mathbf{w}_x is Lipschitz continuous then f_g is Lipschitz continuous with respect to x with a Lipschitz constant which does not depend on $a \in \overline{B}_2(0, 1)$.
- If K_x and \mathbf{v}_x are bounded and if κ_x and c_x are Lipschitz continuous then l_g is Lipschitz continuous with respect to x (with a Lipschitz constant which does not depend on $a \in \overline{B}_2(0, 1)$) and continuous on $\overline{\Omega} \times \overline{B}_2(0, 1)$.
- If κ_x , μ_x , ν_x , \mathbf{w}_x , \mathbf{v}_x , μ_x , K_x and c_x are bounded on $\overline{\Omega}$ then f_g and l_g are bounded on $\overline{\Omega} \times \overline{B}_2(0, 1)$.

Therefore,

- if $\overline{\Omega}$ is bounded,
- if μ_x and ν_x are continuous on $\overline{\Omega}$,
- if K_x and \mathbf{v}_x are bounded and
- if κ_x , \mathbf{w}_x and c_x are Lipschitz continuous

then all hypotheses (H6)-(H8) of theorem 2.3 (at the page 65) are verified for the “generic” Hamiltonian H_g .

Consequently, using appendix B.1, we verify easily that as soon as the *intensity image I is Lipschitz continuous*, the hypotheses (H6)-(H8) hold for *all*

*SFS Hamiltonians*¹⁴. Therefore, theorem 2.3 applies for each modeling of the SFS problem.

Thus, if $\varphi \in BC(\partial\Omega)$ then for all our SFS problems (PDEs with DBC), *there exists a discontinuous viscosity solution*. Let us emphasize that the compatibility conditions are no more required.

2.2.5 Proof of proposition 2.3 claimed in section 2.2.4

Let us remind proposition 2.3.

Proposition 2.3 *Let us consider a Hamiltonian H_g defined as in section 2.2.3. such that the functions $\kappa_x, c_x, A_x^{-1}, \mathbf{w}_x, \mathbf{v}_x$ (or $\kappa_x, c_x, ({}^tR_x A_x)^{-1}, \mathbf{w}_x, {}^tR_x \mathbf{v}_x$) are continuous and bounded on the compact set $\overline{\Omega}$. We assume that $\mathbf{w}_x \neq 0$ for all x in $\overline{\Omega}$.*

If $\forall x \in \overline{\Omega}, |{}^tA_x^{-1} \mathbf{w}_x| < \kappa_x$ then $H_g(x, \cdot)$ is coercive uniformly with respect to x in $\overline{\Omega}$.

The proof of proposition 2.3 is based on the following lemma:

Lemma 2.1 *Let Q be a function defined by:*

$$\begin{aligned} Q : E \times \mathbb{R}^N &\longrightarrow \mathbb{R} \\ (x, q) &\longmapsto Q(x, q) := |q| + W(x) \cdot q + C(x), \end{aligned}$$

where E is any set, $C : E \rightarrow \mathbb{R} : x \mapsto C(x)$ is a function bounded below by $c \in \mathbb{R}$, and W is a function defined by: $W : E \rightarrow \mathbb{R}^N : x \mapsto W(x)$.

If there exists $\varepsilon > 0$ such that $\forall x \in E, |W(x)| \leq 1 - \varepsilon$ then $Q(x, \cdot) : q \mapsto Q(x, q)$ is coercive uniformly with respect to x in E .

Proof of lemma 2.1. By the Cauchy-Schwarz’s inequality we have:

$$W(x) \cdot q \geq -|W(x)||q|.$$

Therefore, $\forall x \in E, \forall q \in \mathbb{R}^N$,

$$|q| + W(x) \cdot q \geq |q|(1 - |W(x)|) \geq |q|\varepsilon.$$

Hence $Q(x, q) \geq |q|\varepsilon + c$, and the conclusion follows. \square

Proof of proposition 2.3.

¹⁴For the Hamiltonian H_{Eiko}^{orth} , we also need to impose $I > 0$ on $\overline{\Omega}$.

- Let us define

$$\hat{H}(x, p) := \kappa_x |A_x p + \mathbf{v}_x| + \mathbf{w}_x \cdot p + c_x.$$

We have

$$\forall x \in \bar{\Omega}, \forall p \in \mathbb{R}^2, \quad H_g(x, p) \geq \hat{H}(x, p),$$

So if $\hat{H}(x, \cdot) : p \mapsto \hat{H}(x, p)$ is coercive uniformly with respect to x then $H_g(x, \cdot)$ is also coercive uniformly with respect to x .

- We now consider

$$\begin{aligned} Q : \bar{\Omega} \times \mathbb{R}^2 &\longrightarrow \mathbb{R} \\ (x, q) &\longmapsto |q| + \underbrace{\frac{1}{\kappa_x} [{}^t A_x^{-1} \mathbf{w}_x] \cdot q}_{W(x)} + \underbrace{c_x - [{}^t A_x^{-1} \mathbf{w}_x] \cdot \mathbf{v}_x}_{C(x)}. \end{aligned}$$

Since we have assumed that

i) $c_x, A_x^{-1}, \mathbf{w}_x, \mathbf{v}_x$ were bounded

and that

ii) $|{}^t A_x^{-1} \mathbf{w}_x| < \kappa_x$, (so that, by continuity, there exists $\varepsilon > 0$ such that for all x in the compact set $\bar{\Omega}$, $\frac{1}{\kappa_x} |{}^t A_x^{-1} \mathbf{w}_x| \leq 1 - \varepsilon$).

Therefore by lemma 2.1, $Q(x, \cdot)$ is coercive uniformly with respect to x in $\bar{\Omega}$.

- Now, let us rewrite the uniform coercivity of $Q(x, \cdot)$ as follows:

$$\forall A \in \mathbb{R}, \exists M \in \mathbb{R} / \forall q \in \mathbb{R}^2, \forall x \in \bar{\Omega}, \quad |q| \geq M \text{ implies } Q(x, q) \geq A.$$

Let us fix A and $M_1 \in \mathbb{R}$ such that the above implication is true (with $M = M_1$). We can consider $M_2 \in \mathbb{R}$ such that for all x on $\bar{\Omega}$,

$$M_2 \geq \frac{1}{\kappa_x} |A_x^{-1}| (|M_1| + \kappa_x |\mathbf{v}_x|)$$

(we have assumed that \mathbf{v}_x and A_x^{-1} were bounded; moreover, since $|{}^t A_x^{-1} \mathbf{w}_x| > 0$ and $|{}^t A_x^{-1} \mathbf{w}_x|$ is continuous on the compact set $\bar{\Omega}$, κ_x^{-1} is also bounded).

Then for all p in \mathbb{R}^2 , $|p| \geq M_2$ implies:

$$\begin{aligned} \kappa_x |A_x p + \mathbf{v}_x| &\geq \kappa_x (|A_x p| - |\mathbf{v}_x|) \\ &\geq \kappa_x \left(\frac{1}{|A_x^{-1}|} |p| - |\mathbf{v}_x| \right) \\ &\geq \kappa_x \left(\frac{1}{|A_x^{-1}|} |M_2| - |\mathbf{v}_x| \right) \\ &\geq \kappa_x \left(\frac{1}{\kappa_x} (|M_1| + \kappa_x |\mathbf{v}_x|) - |\mathbf{v}_x| \right) \\ &\geq M_1. \end{aligned}$$

Then:

$$\forall A \in \mathbb{R}, \exists M_2 \in \mathbb{R} / \forall p \in \mathbb{R}^2, \forall x \in \bar{\Omega},$$

$$|p| \geq M_2 \quad \text{implies} \quad \hat{H}(x, p) = Q(x, \kappa_x (A_x p + \mathbf{v}_x)) \geq A.$$

In other words, $\hat{H}(x, \cdot)$ is coercive uniformly with respect to x in $\bar{\Omega}$.
The conclusion follows. □

2.2.6 Characterization of viscosity solutions of the “classical” SFS problems

In the previous section we have proved the existence of viscosity solutions of the “classical” Lambertian SFS problems. Nevertheless, as we will show in this section, *the “classical” Lambertian SFS problems with DBC (on the boundary of the image) do not have a unique viscosity solution.* For computing a numerical solution of the SFS problems, we need to choose one solution among all. To make this choice, we must characterize the solutions. Also, as Rouy and Tourin have proposed in [134], we satisfy this requirement by enlarging the DBC to the set $\partial\Omega \cup \{x \mid I(x) = 1\}$.

2.2.6.1 Uniqueness results for continuous viscosity solutions

Let us recall the following standard definition:

Definition 2.6 *We say that there is a maximum principle for the Hamilton-Jacobi equation*

$$H(x, u(x), \nabla u(x)) = 0 \text{ in an open set } \Omega, \quad (2.34)$$

when we have: “for all subsolution u and supersolution v defined on $\bar{\Omega}$, $u \leq v$ on $\partial\Omega$ involves $u \leq v$ on $\bar{\Omega}$ ”.

Let $\varphi : \partial\Omega \rightarrow \mathbb{R}$ be a continuous function.

In the case of the *continuous* viscosity solutions, the maximum principle involves the uniqueness on $\bar{\Omega}$ of the solution of the Dirichlet problem

$$\begin{cases} H(x, u(x), \nabla u(x)) = 0 \text{ on } \Omega, \\ u = \varphi \text{ on } \partial\Omega. \end{cases} \quad (2.35)$$

In other words, the maximum principle ensures that there exists at most one continuous viscosity solution of equation (2.34) verifying $u = \varphi$ in $\partial\Omega$.

Proof. Let u_1, u_2 be two continuous viscosity solutions to the Dirichlet problem (2.35). Since for all x in $\partial\Omega$, $u_1(x) = u_2(x)$ (Dirichlet condition) and u_1, u_2 are both subsolution and supersolution, the maximum principle implies

that $u_1 \leq u_2$ and $u_2 \leq u_1$ on $\overline{\Omega}$. The conclusion follows. \square

Essentially, there exists two classical uniqueness theorems for the *continuous* viscosity solutions. The first deals with the PDE(s) of the form $\lambda u(x) + H(x, \nabla u(x)) = 0$ with $\lambda > 0$. The second deals with equations of the form $H(x, \nabla u(x)) = 0$ with $H(x, p)$ convex with respect to p . The first theorem is proved in [5] (theorem II.3.1 and remark II.3.3).

Theorem 2.4 (uniqueness result (1)) *Let Ω be a bounded open subset of \mathbb{R}^N . Let us consider the Hamilton-Jacobi equation*

$$\lambda u(x) + H(x, \nabla u(x)) = 0, \quad x \in \Omega \quad (\lambda > 0).$$

We assume that H satisfies

(H9) [space variable regularity]

There exists a nondecreasing function ω which goes to zero at zero, such that

$$\forall x, y \in \Omega, \forall p \in \mathbb{R}^N, \quad |H(x, p) - H(y, p)| \leq \omega(|x - y|(1 + |p|)).$$

Then there is a maximum principle for this equation.

The second uniqueness result is due to Ishii [74] and has been proved later in a different manner by Lions [95]. For the SFS problems, this theorem is important. In effect as we have seen above, the equations provided by the “classical” formulations of the SFS problems, involve Hamiltonians which do not depend on u .

Theorem 2.5 (uniqueness result (2)) *Let Ω be a bounded open subset of \mathbb{R}^N . Let us consider the Hamilton-Jacobi equation*

$$H(x, \nabla u(x)) = 0 \quad \forall x \in \Omega. \quad (2.36)$$

If the hypotheses (H1), (H9) and the following hypothesis are verified:

(H10) [strict subsolution]

there exists a strict subsolution $\underline{u} \in C^1(\Omega) \cap C(\overline{\Omega})$ of (2.36) (i.e. such that $H(x, \nabla \underline{u}(x)) < 0$ for all x in Ω);

then there is a maximum principle for this equation.

For more general conditions, see [96]. A proof can be found in section II.5.3 of Bardi and Capuzzo-Dolcetta’s book [5].

These theorems apply to the SFS. In particular, by theorem 2.5, we can characterize the continuous viscosity solutions of the “classical” SFS problems. Let us consider the generic Hamiltonian H_g defined in section 2.2.3.2 (at the page 67). We have:

1. H_g is convex with respect to p and therefore the hypothesis (H1) is verified for all our SFS Hamiltonians.
2. If we assume that κ_x , \mathbf{w}_x and c_x are Lipschitz continuous and that K_x , D_x and \mathbf{v}_x are bounded, then the Hamiltonian H_g verifies the regularity hypothesis (H9). In particular, for all the SFS Hamiltonians H_*^{orth} and H_*^{pers} , these conditions are true as soon as the intensity image I is Lipschitz continuous¹⁵ (see appendix B).
3. About the existence of strict subsolutions:
 - The generic Hamiltonian H_g does not have a generic strict subsolution. Nevertheless, all SFS Hamiltonians H_*^{orth} and H_*^{pers} have one.
 - Let us assume that

$$\text{for all } x \text{ in } \Omega, \quad I(x) < 1.$$

Then, we have:

- all constant functions are strict subsolutions of the Hamiltonians H_{Eiko}^{orth} , $H_{D/O}^{orth}$, H_F^{pers} and H_2^{pers} .
In effect, all these Hamiltonians verify $H(x, 0) < 0$.
- it is easy to verify that the function

$$\psi : \overline{\Omega} \longrightarrow \mathbb{R} : x \longmapsto -\frac{1}{\gamma} \mathbf{1} \cdot x$$

is a strict subsolution of the Rouy-Tourin Hamiltonian $H_{R/T}^{orth}$.

- the reader can verify that the function

$$\psi : \overline{\Omega} \longrightarrow \mathbb{R} : x \longmapsto -\ln \frac{\gamma}{f} - \ln(\gamma f - \mathbf{1} \cdot x)$$

is a strict subsolution of the perspective Hamiltonian $H_{P/F}^{pers}$ (we need to impose $\gamma f - \mathbf{1} \cdot x > 0$, ie. $\mathbf{L} \cdot (x, -f) < 0$).

Thus, for all SFS Hamiltonians, as soon as the intensity image I is Lipschitz continuous and verifies

$$\forall x \in \Omega, \quad I(x) < 1,$$

all the hypotheses of theorem 2.5 are verified. Therefore, under these conditions, the SFS Hamiltonians H_*^{orth} and H_*^{pers} have a unique continuous viscosity solution.

Remark 5. To apply theorem 2.5, a difficulty lies in the search of

¹⁵for the Eikonal Hamiltonian H_{Eiko}^{orth} , we also need to impose $\forall x \in \overline{\Omega}, I(x) > 0$.

a strict subsolution. To get around this difficulty, we can make a change of variables for obtaining a new Hamiltonian with $\lambda \neq 0$ and we can try to apply theorem 2.4. For example, we can consider the Eikonal equation (2.37) with f strictly positive and Lipschitz. By using the Kruzkov change of variable $v(x) = 1 - e^{-u(x)}$ (therefore $\nabla u(x) = \frac{1}{1-v(x)} \nabla v(x)$, $v(x) < 1$), we rewrite the Eikonal equation

$$|\nabla u(x)| = f(x) \quad (2.37)$$

as

$$v(x) + \frac{1}{f(x)} |\nabla v(x)| - 1 = 0, \quad (2.38)$$

and theorem 2.4 applies to (2.38). This kind of tricks has been widely used by Falcone et.al in [24, 55, 56].

2.2.6.2 Uniqueness results for discontinuous viscosity solutions

The uniqueness results for the discontinuous viscosity solutions are almost the same as the uniqueness results for the continuous viscosity solutions. Nevertheless, they need stronger hypotheses; which is reasonable because discontinuous viscosity solutions are weaker solutions than continuous viscosity solutions (the set of the discontinuous viscosity solutions of a HJB equation contains the set of the continuous viscosity solutions). Also, the consequences on the SFS problem are almost the same.

In the continuous case, the maximum principle involves the uniqueness of the solution of the Dirichlet problem. Nevertheless in the discontinuous case, to have uniqueness we need a stronger property (see section 2.2.3 of [128]):

Definition 2.7 *Let Ω be an open subset of \mathbb{R}^N , let $E \subset \overline{\Omega}$ and let F be a real function defined on $\overline{\Omega} \times \mathbb{R} \times \mathbb{R}^N$.*

We say that the strong uniqueness property holds on the set E for the equation

$$F(x, u(x), \nabla u(x)) = 0 \quad (2.39)$$

when we have:

“for all subsolution u , for all supersolution v and for all x in E , $u(x) \leq v(x)$ ”.

We have the following strong uniqueness result:

Theorem 2.6 *Let Ω be an open subset of \mathbb{R}^N verifying (H11). Let H be a continuous real function defined on $\overline{\Omega} \times \mathbb{R}^N$ and let φ be a real continuous function defined on $\partial\Omega$. If H satisfies the hypotheses (H1), (H9) and (H10') and if H satisfies the boundary hypotheses (H12), (H13) and (H14) (described*

below) which impose properties of H on $\partial\Omega$ then the strong uniqueness property holds on the set Ω for the equation

$$F(x, u(x), \nabla u(x)) = 0 \quad \text{for } x \in \bar{\Omega}, \quad (2.40)$$

which defines the following Dirichlet problem (in the discontinuous sense)

$$F(x, u, p) = \begin{cases} H(x, p) & \text{for } x \text{ in } \Omega, \\ u - \varphi(x) & \text{for } x \text{ in } \partial\Omega. \end{cases} \quad (2.41)$$

The hypothesis (H10') is a hypothesis slightly stronger than hypothesis (H10) of the theorem 2.5:

(H10') [strict subsolution]

there exist $\underline{u} \in C^1(\Omega) \cap C(\bar{\Omega})$ and $\delta < 0$ such that for all x in Ω ,

$$H(x, \nabla \underline{u}(x)) < \delta.$$

The hypothesis (H11) deals with the regularity of the set Ω :

(H11) [regularity of Ω]

Ω is a bounded open subset of \mathbb{R}^N of class $W^{2,\infty}$.

The hypotheses (H12), (H13) and (H14) are the following:

There exist a constant $C > 0$ and a neighborhood Γ of $\partial\Omega$ (ie. Γ is an open subset of \mathbb{R}^N such that $\partial\Omega \subset \Gamma$) such that

(H12) [p - regularity on $\partial\Omega$]

There exists a function ω which goes to zero at zero, such that

$$\forall x \in \Gamma, \forall p, q \in \mathbb{R}^N, |H(x, p) - H(x, q)| \leq \omega(|p - q|);$$

(H13) $\forall x \in \Gamma, \forall p \in \mathbb{R}^N, \quad H(x, p + \lambda\eta(x)) \leq 0 \implies \lambda \leq C(1 + |p|);$

(H14) [directional coercivity on $\partial\Omega$]

$\forall p \in \mathbb{R}^N, \quad H(x, p - \lambda\eta(x)) \rightarrow +\infty$ uniformly with respect to x in Γ , when $\lambda \rightarrow +\infty$;

(where $\eta(x)$ is the unit outward pointing normal vector to $\partial\Omega$).

Proof of theorem 2.6. See theorem 4.5 and more exactly of its corollary 4.1, of Barles'book [7] in the particular case where the Hamiltonian H does not depend on u . \square

Remarks 6.

r6.1 - Clearly, the strong uniqueness property involves the uniqueness of the discontinuous viscosity solution. Therefore, thanks to theorem 2.6, we can prove the uniqueness of discontinuous viscosity solutions of (2.40) in Ω . Nevertheless, generally we do not have the uniqueness in $\bar{\Omega}$! So if u_1 and u_2 are two solutions, then for all x in Ω , $u_1(x) = u_2(x)$; but for all x in $\partial\Omega$, $u_1(x)$ can be different from $u_2(x)$.

r6.2 - The strong uniqueness property involves the continuity of the solution (see proposition 2 of [128]).

r6.3 - Theorem 2.6 deals with a Hamiltonian H which does not depend of u ; More general results can be found in [7].

Proposition 2.4 *A sufficient condition for the hypotheses (H13) and (H14) to be satisfied is: $H(x, p)$ coercive in p uniformly with respect to x in Γ , a neighborhood of $\partial\Omega$.*

Proof. See proposition 3 of [128]. □

As theorem 2.5 (uniqueness of the continuous viscosity solution), theorem 2.6 applies to the SFS problem. The three hypotheses (H1), (H9), and (H10') are (almost) the hypotheses of theorem 2.5. As in the previous section, we prove that they are verified for the SFS Hamiltonians H_*^{orth} and H_*^{pers} as soon as the intensity image is Lipschitz continuous and verifies $I < 1$ on $\bar{\Omega}$. Concerning the hypothesis (H12), we can easily prove (by computing the gradient of $H_g(x, \cdot) : p \mapsto H_g(x, p)$) that if κ_x and \mathbf{w}_x are bounded then $H_g(x, \cdot)$ is Lipschitz continuous (with a Lipschitz constant which does not depend on x). Therefore (H12) is true for all SFS Hamiltonians H_*^{orth} and H_*^{pers} . Then, thanks to proposition 2.4, the strong uniqueness theorem applies as soon as the considered Hamiltonian $H(x, p)$ is coercive with respect to p uniformly with respect to x in a neighborhood of $\partial\Omega$. In section 2.2.4 (when we apply the existence theorem 2.2 to the Hamiltonian H_g and later to the SFS Hamiltonians), we have described in detail the conditions for the coercivity property for the SFS Hamiltonians H_*^{pers} and H_*^{orth} .

Conclusion: If the intensity image I is Lipschitz continuous, if I verifies $I < 1$ on $\bar{\Omega}$ and if the values of I on the *boundary of the image* are such that the coercivity hypothesis holds, then there exists at most one discontinuous viscosity solution on Ω .

2.2.6.3 Characterization of the viscosity solutions of the “classical” SFS problem when the set $\{x \mid I(x) = 1\}$ is not empty

In practice, I can reach the value 1 in an arbitrary compact set in $\bar{\Omega}$. This implies that there does not exist a strict subsolution and *we lose uniqueness*. Let us denote

$$\mathcal{S} = \{ x \in \bar{\Omega} \mid I(x) = 1 \}.$$

The points of \mathcal{S} are called the *singular points*. These points are the pixels of the image corresponding to points of the surface such that the surface normal coincides with the light direction. These points have maximal brightness. Sometimes, they are also called “critical points”.

In [134], Rouy and Tourin characterize the loss of uniqueness of the continuous viscosity solution of the equation (2.12)

$$\begin{cases} H(x, \nabla u(x)) = 0 & \forall x \in \Omega \\ u = \varphi & \forall x \in \partial\Omega, \end{cases}$$

in the case where H is the Hamiltonian $H_{R/T}^{orth}$ and where the set \mathcal{S} is a set of isolated points. In their paper [96], Lions, Rouy and Tourin characterize completely the continuous viscosity solutions, in the case where the set \mathcal{S} is a finite union $\cup_{i=1}^n K_i$ of disjoint connected compact sets. Nevertheless, they only consider the particular case of the Eikonal Hamiltonian H_{Eiko}^{orth} . In this chapter, we generalize their result: we characterize the continuous viscosity solutions of all our SFS Hamiltonians (H_*^{orth} and H_*^{pers}); in particular we extend their work to the “perspective SFS” problem. As in [134], in this section we assume that $\mathcal{S} = \{x_1, \dots, x_n\}$ (let us note that in chapter 4, we relax this assumption). Also, we deal with the characterization of the discontinuous viscosity solutions of all SFS Hamiltonians.

Case of the continuous viscosity solutions

To begin with, we generalize [134, 96] (concerning the continuous viscosity solutions) to all the SFS Hamiltonians H_*^{orth} and H_*^{pers} .

Let us fix n real constants $(C_i)_{i=1..n}$. For all SFS equations with Dirichlet boundary conditions,

$$\begin{cases} H(x, \nabla u(x)) = 0 & \forall x \in \Omega \\ u = \varphi & \forall x \in \partial\Omega, \end{cases}$$

there exists at most one continuous viscosity solution u such that for all $i = 1..n$, $u(x_i) = C_i$ (the various constants C_i have just to verify the compatibility conditions¹⁶). To prove this last assertion, we just have to enlarge the

¹⁶See page 61

DBC to the set $\partial\Omega \cup \mathcal{S}$ and to apply theorems 2.2¹⁷ and 2.5¹⁸, and the results presented in section 2.2.6.1. Thus, we just have to fix the constants C_i , for characterizing a viscosity solution of the SFS problems.

In other words, globally, for characterizing a SFS (viscosity) solution, we can ignore the set \mathcal{S} and work in the open set $\Omega' = \Omega - \mathcal{S}$. Therefore, we consider the problem

$$\begin{cases} H(x, \nabla u(x)) = 0 & \forall x \in \Omega' \\ u(x) = \varphi(x) & \forall x \in \partial\Omega', \end{cases} \quad (2.42)$$

rather than (2.12). Thus, as soon as the intensity image I is Lipschitz continuous, the problem (2.42) associated to any SFS Hamiltonian has at most one continuous viscosity solution. All the continuous viscosity solutions of (2.12) are then obtained from these by choosing almost arbitrarily¹⁹ the constants C_i .

Remarks 7.

R7.1 - In practice, for computing a numerical solution of the SFS problem, we must characterize the solution we want to compute, first. The characterization we propose here is somewhat disappointing. In effect, it assumes that we know the values of the solution at all the singular points and on the boundary of the image. But the input data to a SFS problem consists only in general of an image. We do not have at our disposal the values of the solution at the singular points or on the boundary of the image. Nevertheless, in a first time we will assume that we know these ‘‘boundary’’ data. In chapter 4, we will describe how to remove partly this constraint.

R7.2 - Another possibility is to choose among all solutions one which possesses an extra property, as in the work of M. Falcone et al. [24, 55, 56] where the uniqueness is obtained by choosing the maximal solution. This method has been developed by F. Camilli et al. in [26, 25]. Let us emphasize that M. Falcone assumes (as we do in this chapter) that the solution is known on the boundary $\partial\Omega$. Let us note that in chapter 4, we define a new mathematical framework which generalizes the tools used by Falcone et.al and which unifies the various viscosity approaches.

¹⁷Theorem 2.2 ensures the existence of the continuous viscosity solution; see at page 60.

¹⁸Theorem 2.5 ensures the uniqueness of the continuous viscosity solution; see at page 77.

¹⁹Let us recall that for ensuring the existence of a continuous viscosity solution, the compatibility condition must be verified.

Case of the discontinuous viscosity solutions

The above result does not apply directly to the discontinuous viscosity solutions of the “classical” SFS problem. The reason of this difficulty lies on the difference between the hypotheses (H10) and (H10') (hypotheses dealing with the strict subsolutions) we recall them here:

(H10) *there exists $\underline{u} \in C^1(\Omega) \cap C(\overline{\Omega})$ such that*

$$\forall x \in \Omega, \quad H(x, \nabla \underline{u}(x)) < 0;$$

(H10') *there exist $\underline{u} \in C^1(\Omega) \cap C(\overline{\Omega})$ and $\delta < 0$ such that*

$$\forall x \in \Omega, \quad H(x, \nabla \underline{u}(x)) < \delta.$$

The uniqueness of the continuous viscosity solution only requires the hypothesis (H10) (theorem 2.5), when the uniqueness of the discontinuous viscosity solution requires the stronger hypothesis (H10') (theorem 2.6). In the first case, the hypothesis (H10) holds even if there are singular points on the boundary of Ω , whereas in the second case, the hypothesis (H10') imposes that $\forall x \in \overline{\Omega}$, $I(x) < 1$; and so there are not singular points on $\partial\Omega$.

Remark 8. It is important to notice that the hypothesis (H10') is optimal for obtaining the uniqueness of the *discontinuous* viscosity solution (the hypothesis (H10) is not sufficient). In effect, for example, although the following SFS equation verifies the hypothesis (H10) (therefore it has a unique continuous viscosity solution), it has several discontinuous viscosity solutions.

Example : Let us consider the orthographic SFS problem, in dimension 1, with a vertical light direction. Let I be the intensity image obtained from the C^1 surface v represented in figure 2.5. Let us note that v and I are defined on

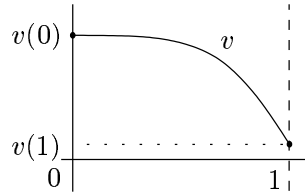


Figure 2.5: A surface with a singular point at the boundary.

$[0, 1]$, that for all x in $]0, 1]$, we have $0 < I(x) < 1$, and that 0 is a singular

point ($I(0) = 1$). Clearly, v is the unique continuous viscosity solution of

$$\begin{cases} H_{Eiko}^{orth}(x, \nabla u) = 0, & \forall x \in]0, 1[, \\ u(0) = v(0) & \text{and} \quad u(1) = v(1); \end{cases} \quad (2.43)$$

but there exist several discontinuous viscosity solutions. In effect, the continuous viscosity solutions of all the equations

$$\begin{cases} H_{Eiko}^{orth}(x, \nabla u) = 0, & \forall x \in]0, 1[, \\ u(0) = u_0 & \text{and} \quad u(1) = v(1), \end{cases}$$

where $u_0 \leq v(0)$, are discontinuous viscosity solutions of (2.43). Some examples of discontinuous viscosity solutions of (2.43) are shown in figure 2.6.

Proof.

For all x in $]0, 1]$, there are not difficulties.

For $x = 0$:

- $u(0)$ is always inferior to $v(0)$ then the subsolution property²⁰ always holds;
- since $I(0) = 1$, then for all test functions ϕ , we have $H_{Eiko}^{orth}(0, \nabla\phi(0)) \geq 0$.
Therefore the supersolution property holds at the point 0.

□

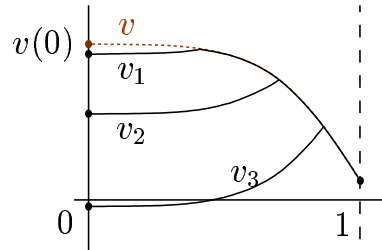


Figure 2.6: Examples of some discontinuous viscosity solutions when there exists a singular point on the boundary.

²⁰In the discontinuous sense, the subsolution property at a point x_0 in $\partial\Omega$ is:

◦ $H(x_0, \nabla\phi(x_0)) \leq 0$, where ϕ is an adequate test function;

or ◦ $u(x_0) \leq \varphi(x_0)$, where φ is the boundary condition.

As a matter of fact, this limitation is not really a problem. In effect, before we have assumed that we know the values of the solution at all the singular points of the image. Also it is not more absurd to assume that we know the values of the solution on an extremely small neighbourhood of the set the singular points. Thus for characterizing a discontinuous viscosity solution, we can specify the values of this solution on the boundary of the image and in a neighbourhood of its singular points. Let us emphasize on the fact that, as for the continuous case, this characterization is not satisfying in practice. Also, in chapter 4, we will provide a better answer.

2.2.7 Noise robustness of the viscosity solutions of SFS

Viscosity solutions also enjoy important stability properties.

Let $(v_\varepsilon)_{\varepsilon>0}$ be a sequence of uniformly locally bounded functions defined on $\overline{\Omega}$. Let us define the two functions \overline{v} and \underline{v} :

Definition 2.8 $\forall x \in \overline{\Omega}$,

$$\overline{v}(x) = \limsup_{\substack{\varepsilon \rightarrow 0, \\ y \rightarrow x}} v_\varepsilon(y)$$

$$\underline{v}(x) = \liminf_{\substack{\varepsilon \rightarrow 0, \\ y \rightarrow x}} v_\varepsilon(y)$$

We have the theorem (see Barles' book [7]):

Theorem 2.7 (Stability of viscosity solutions) *Let F_ε be a sequence of uniformly locally bounded functions on $\overline{\Omega} \times \mathbb{R} \times \mathbb{R}^N$ (Ω being a open set of \mathbb{R}^N). Let us suppose that for all $\varepsilon > 0$, v_ε is a subsolution (respectively a supersolution) of F_ε on $\overline{\Omega}$ and that the functions v_ε are uniformly locally bounded on $\overline{\Omega}$.*

Then

$$\overline{v}(x) = \limsup_{\substack{\varepsilon \rightarrow 0, \\ y \rightarrow x}} v_\varepsilon(y) \quad (\text{respectively } \underline{v}(x) = \liminf_{\substack{\varepsilon \rightarrow 0, \\ y \rightarrow x}} v_\varepsilon(y))$$

is a subsolution (a supersolution, respectively) of the equation

$$\underline{F}(x, u(x), \nabla u(x)) = 0 \text{ on } \overline{\Omega} \quad (\text{respectively } \overline{F}(x, u(x), \nabla u(x)) = 0 \text{ on } \overline{\Omega});$$

where $\underline{F}(X) = \liminf_{\substack{\varepsilon \rightarrow 0, \\ Y \rightarrow X}} F_\varepsilon(Y)$ ($X, Y \in \overline{\Omega} \times \mathbb{R} \times \mathbb{R}^N$)
 $(\overline{F}(X) = \limsup_{\substack{\varepsilon \rightarrow 0, \\ Y \rightarrow X}} F_\varepsilon(Y), \text{ respectively}).$

When the strong uniqueness property is true the previous result yields:

Corollary 2.1 *Let $F : \overline{\Omega} \times \mathbb{R} \times \mathbb{R}^N \rightarrow \mathbb{R}$ be a locally bounded function verifying the strong uniqueness property on Ω (see definition 2.7). Let $(F_\varepsilon)_{\varepsilon > 0}$ be a sequence of functions such that*

$$\begin{array}{ccc} F_\varepsilon & \longrightarrow & F \\ \varepsilon \rightarrow 0 & & \end{array}$$

locally uniformly with respect to the other variables. Let u_ε be uniformly locally bounded functions such that for all $\varepsilon > 0$, u_ε is a solution (in the discontinuous sense) of

$$F_\varepsilon(x, u, \nabla u) = 0 \text{ on } \overline{\Omega}.$$

Then, when ε vanishes to zero, the sequence u_ε converges on Ω toward a function u which is equal to the discontinuous viscosity solution of $F(x, u, \nabla u) = 0$ on Ω .

In computer vision or more generally in image processing, the images are always corrupted by noise. So, it is very important to design schemes and algorithms *robust* to noise. That is to say we would like that the result obtained by the algorithm from a noisy image be close to the ideal result obtained from the perfect image. This robustness is mathematically expressed by the continuity of the application which, given an image I , returns the associated surface u .

In the research report [128], section 4.1.3, we have applied corollary 2.1 to the Hamiltonian $H_{R/T}^{orth}$ associated to the orthographic SFS problem. Thus, we have proved that if the intensity image I verifies $I(x) < 1$ for all x in $\overline{\Omega}$, then the viscosity solutions (of this SFS problem) are robust to noise. This also applies to the other SFS Hamiltonians H_*^{orth} and H_*^{pers} .

In chapter 4, section 4.3.2, we consider in details this fundamental point. In particular, we deal with the case where the intensity image I reaches the value 1. Moreover, we also show the robustness of the Shape from Shading solutions to errors on parameters.

2.2.8 SFS with discontinuous images; shadows

The reader has most probably noticed that the existence theorems 2.2 and 2.3, and the uniqueness theorems 2.4 and 2.5 require regularity of the Hamiltonians

with respect to the space variable x . For the SFS Hamiltonians, these regularity hypotheses impose to take intensity functions I which are (*Lipschitz*) *continuous*.

Let us emphasize that this limitation is very constraining; in effect, generally, edges, black shadows and occluding boundaries involve discontinuities. Therefore the *theoretical part* of our method (based on the notion of the viscosity solutions) cannot deal with such singularities, yet. Most probably, ongoing work will shortly allow to extend the theory to discontinuous Hamiltonians in the space variables. See the work of Ostrov [78, 112], the work of Soravia [146] or the work of Camilli and Siconolfi [28] which only deals with the Eikonal case.

Nevertheless, as we will see in the following chapter, the *numerical method* we propose does not require such a regularity of the intensity function I . In effect, we prove that our schemes are stable (see remark at the end of section 3.1.3.1 at the page 105, the last remark at the page 107 and remark at page 108) and the associated algorithms converge (see remark at page 120) without such hypotheses. Also, that holds for our *Shape From Shading* method (see section 3.2.3). In particular *in practice*, our algorithms produce suitable numerical solutions even when the input image has some black shadows and some discontinuities (see section 3.2.4).

2.3 Conclusion and contributions of chapter 2

- Contrary to most of the SFS methods (which have been developed under the assumption of orthographic projection), in this chapter, we model the SFS problem by assuming that the camera is a **pinhole** (i.e. performs a perspective projection of the scene). We have rigorously derived the corresponding **explicit PDEs** (equations (2.6) and (2.8)) and the associated **Hamiltonians** $H_{P/F}^{pers}$ and H_F^{pers} . The light source can be located **at infinity** (in any direction) or **at the optical center**. These explicit formulations allow in particular to prove existence and uniqueness results. We call “classical SFS” the problem consisting in solving the PDEs introduced in this chapter.
- We have developed a **complete mathematical study** of the “classical” orthographic and perspective SFS problems. After having introduced and shown the interest of the notion of discontinuous viscosity solutions in the Shape from Shading problem, we have proved the **existence** of the viscosity solutions of the associated PDEs. We have demonstrated that **the characterization introduced by Rouy and Tourin in [134] for the orthographic SFS is still relevant for the perspective SFS**. More precisely, the continuous viscosity solutions of the “classical” SFS problems can be characterized by their values on the boundary of the image and at the singular points (i.e. the points x such that $I(x) = 1$). This is one of the reasons which led us to qualify as “classical” the models and the PDEs we have described in this chapter.
- Finally, by introducing a “**generic**” **Hamiltonian**, we have **unified the “orthographic” and “perspective SFS”** problems and we have simplified the formalism. Moreover, we have rewritten the “generic SFS Hamiltonian” as a Hamilton-Jacobi-Bellman Hamiltonian.
- **Note:** several articles stem from this chapter. A first publication has been accepted to ECCV’02 [127], a second to ICCV’03 [120]. An article has been submitted to the International Journal of Computer Vision [123]. Another has been accepted to RFIA’04 [121]...

Chapter 3

Monotonous approximation schemes and associated numerical algorithms; application to the “classical” Shape from Shading

In this chapter, in a first time, we describe a general method for solving Hamilton Jacobi equation. We also detail various tools and theoretical results allowing to demonstrate the relevance and the applicability of this method in practice. In a second time, we apply this method to the “classical” SFS problem.

3.1 Monotonous approximation schemes and associated numerical algorithms; Examples for HJB equations

3.1.1 Approximation schemes of the form $S(\nu, x, u(x), u) = 0$

First, let us define the notion of approximation schemes, we use in this thesis.

Let Ω a open subset of \mathbb{R}^N ($N \in \mathbb{N}$; $N \geq 1$). We call “continuous *mesh*” (or “mesh”) a map

$$\nu : \overline{\Omega} \rightarrow \mathcal{P}_F(\mathbb{R}^N),$$

where $\mathcal{P}_F(\mathbb{R}^N)$ is the set of the finite subsets of \mathbb{R}^N . For a point $x \in \overline{\Omega}$, we denote $\mathcal{V}_x := \nu(x)$. \mathcal{V}_x is the set of the “neighborhoods” of x . We denote

\mathcal{M} the set of all the continuous meshes. An important example of meshes is the case of the “regular meshes”. We say that a mesh ν is a regular mesh when there exists a vectorial base (V_1, \dots, V_N) of \mathbb{R}^N such that for all $x \in \overline{\Omega}$, $\mathcal{V}_x = \{x \pm V_i; i = 1..N\}$. For all $i = 1..N$, we denote $h_i = |V_i|$, $\rho = (h_1, \dots, h_N)$ and $h = \max_i h_i$. This defines the size of the mesh. For lots of applications, it is relevant to consider the canonical base:

$$\forall i = [1..N], V_i = h_i \vec{e}_i.$$

In this case, we say that the mesh is “canonical”. For example, the canonical mesh is generally used in the “basic” Shape from Shading problem¹ and in the computation of the Connectivity Mapping of the White Matter using TDI [93, 94]. In this particular case, the mesh is completely characterized by ρ . If $h_1 = h_2 = \dots = h_N$, we let $\rho = h_i \in \mathbb{R}^+$. Also, we (mis)use the notation “ $\forall \rho > 0$ ” which stands for “ $\forall \rho \in \mathbb{R}^N$ such that $\forall i \in 1, \dots, N, h_i > 0$ ”.

An approximation scheme is a functional equation of the form

$$T(\nu, x, u) = 0 \quad \forall x \in \overline{\Omega};$$

where $T : \mathcal{M} \times \overline{\Omega} \times B(\overline{\Omega}) \rightarrow \mathbb{R}$, and $B(D)$ is the space of bounded functions defined on a set D . $\nu \in \mathcal{M}$ corresponds to the mesh that is used in the corresponding numerical algorithms, see section 3.1.5. u^ν is a solution of the scheme T , for a fixed mesh ν .

Following [9], we introduce the representations S of a scheme T as

$$S(\nu, x, u(x), u) = 0 \quad \forall x \in \overline{\Omega},$$

where

$$\begin{aligned} S : \mathcal{M} \times \overline{\Omega} \times \mathbb{R} \times B(\overline{\Omega}) &\longrightarrow \mathbb{R} \\ (\nu, x, t, u) &\longmapsto S(\nu, x, t, u). \end{aligned}$$

Note that a representation of a scheme is also a scheme. It is in effect a way to simplify computations, see below. For example, suppose we want to approximate a function u such that its directional derivative in the direction \vec{v} at point x is equal to $\lambda(x)$. We can use the following scheme $S(\rho, x, u(x), u) = 0$ in \mathbb{R}^N (case of a canonical mesh of size $\rho = h_1 = h_2 = \dots = h_N$):

$$S(\rho, x, t, u) = \frac{u(x + \rho \vec{v}) - t}{\rho} - \lambda(x).$$

¹Until now, except for a very few number of papers (for example [135]), all the Shape from Shading methods are based on “canonical” meshes. This restriction is due to the structure of data: the pixels of the image define explicitly a regular mesh.

Remark 9. For a scheme $T(\nu, x, u) = 0$, we can come up with various representations

$$S : \mathcal{M} \times \overline{\Omega} \times \mathbb{R} \times B(\overline{\Omega}) \longrightarrow \mathbb{R}$$

such that $S(\nu, x, u(x), u) = T(\nu, x, u)$.

For example, we can take

$$S_1(\nu, x, t, u) = T(\nu, x, u),$$

or

$$S_2(\nu, x, t, u) = u(x) + T(\nu, x, u) - t, \text{ etc.}$$

In the sequel, we will see that the choice of the representation S implies some important differences in the corresponding numerical algorithm (see section 3.1.5). It also influences greatly the complexity of the proofs of stability and convergence, see sections 3.1.3 and 3.1.4.

Here, we consider *finite difference* schemes. So for all schemes $S(\nu, x, u(x), u) = 0$, we assume the hypothesis (H15).

(H15) *Let ν be a fixed mesh. For all (x, t) in $\overline{\Omega} \times \mathbb{R}$, the value of $S_{\nu, x, t}(u) := S(\nu, x, t, u)$ does not depend on all the values of the function u but only on the values that u takes on the neighborhood \mathcal{V}_x of x (i.e. at points $y \in \mathcal{V}_x$). In other words, we can rewrite $S(\nu, x, t, u)$ as $\check{S}(\nu, x, t, (u(y))_{y \in \mathcal{V}_x})$.*

As we have remarked in the previous chapter, the Hamilton-Jacobi equations are generally ill-posed and require boundary conditions. In our applications, we impose *Dirichlet boundary conditions*. Also, here we consider “schemes with Dirichlet conditions”. These schemes are defined by $S(\nu, x, u(x), u) = 0$, where S is defined by

$$S(\nu, x, t, u) = \begin{cases} \check{S}(\nu, x, t, u) & \text{if } x \in \Omega_{\nu}, \\ t - \varphi(x) & \text{if } x \in \text{b}\Omega_{\nu}, \end{cases} \quad (3.1)$$

where

$$\Omega_{\nu} = \{x \in \Omega \mid \forall y \in \mathcal{V}_x, \text{ we have } y \in \overline{\Omega}\} = \{x \in \Omega \mid \mathcal{V}_x \subset \overline{\Omega}\},$$

and $\text{b}\Omega_{\nu} = \overline{\Omega} - \Omega_{\nu}$. Since φ is defined only on $\partial\Omega$, we assume in (3.1) that we have extended it continuously to Ω_{ν} . Let us note that this choice of boundary conditions (Dirichlet conditions) can be modified. For example, the methods presented here can be easily adapted to some Neumann conditions.

We now introduce the

Definition 3.1 (monotonicity) *The scheme $S(\nu, x, u(x), u) = 0$ defined on $\overline{\Omega}$, is monotonous if $\forall \nu \in \mathcal{M}, \forall x \in \overline{\Omega}, \forall t \in \mathbb{R}$ and $\forall u, v \in B(\overline{\Omega})$,*

$$u \leq v \implies S(\nu, x, t, u) \geq S(\nu, x, t, v)$$

(that is to say: the scheme is nonincreasing with respect to u)

There exists essentially only one method for proving the convergence of the solutions of schemes toward viscosity solutions, i.e. the one presented by Barles and Souganidis in [9]. This method requires the monotonicity of the scheme; this is why we design monotonous schemes in the sequel.

Remark 10. The representation of a scheme $T(\nu, x, u) = 0$ by a scheme of the form $S(\nu, x, u(x), u) = 0$ is not innocent. In particular, this formulation suggests an iterative algorithm for computing a numerical approximation of the solution of the scheme. Given u^n (the approximation of u^ν at step n), and a point x of Ω_ν , the associated algorithm consists in solving the equation

$$S(\nu, x, t, u^n) = 0 \tag{3.2}$$

with respect to t . A solution of (3.2) is the updated value of u^n at x (see section 3.1.5). In other words, it is $u^{n+1}(x)$. When this solution can be obtained explicetely we talk about explicit schemes, when it cannot, we talk about implicit schemes, see next section.

3.1.2 Decentered schemes for HJB equations

In the previous chapter, we have shown that the “classical” modeling of the Shape from Shading problem leads to solving HJB equations. Let us remind that these equations are of the form

$$\lambda u(x) + \sup_{a \in A} \{-f(x, a) \cdot \nabla u(x) - l(x, a)\} = 0 \quad \forall x \in \Omega. \tag{2.18}$$

Also throughout this chapter we will consider in particular the HJB equations. To start, we present some schemes allowing to approximate these equations. Thereby this allows to solve numerically the SFS equations. Despite the fact that for SFS problems we only need the two-dimensional case, we consider the general case.

In a first time, we design an “implicit” scheme and a “semi-implicit” scheme on a canonical mesh. In a second time, we deal with irregular meshes.

3.1.2.1 An “implicit” decentered scheme

We consider here a canonical mesh \mathcal{M} defined by $\rho = (h_1, \dots, h_N)$. Since for the canonical meshes, the meshes are characterized by $\rho = (h_1, \dots, h_N)$, we denote the solution of the scheme u^ρ instead of u^ν . We need the following notations:

Notation. Given a function $g : B \rightarrow \mathbb{R}$, we denote

$$g_+ : B \rightarrow \mathbb{R} \quad g_- : B \rightarrow \mathbb{R}$$

$$x \mapsto \begin{cases} g(x) & \text{if } g(x) > 0, \\ 0 & \text{otherwise;} \end{cases} \quad x \mapsto \begin{cases} -g(x) & \text{if } g(x) < 0, \\ 0 & \text{otherwise;} \end{cases}$$

Remark 11. The functions g_+ and g_- are positive.

We want to design an approximation scheme of (2.18) by using only the backward and forward approximations of the partial derivatives. Thus in order to guarantee the monotonicity of the scheme, it appears natural to substitute $\partial_{\vec{e}_i} u(x)$ with $\left(\frac{t-u(x-h_i\vec{e}_i)}{h_i}\right)$ when $-f_i(x, a) \geq 0$ and by $\left(\frac{u(x+h_i\vec{e}_i)-t}{h_i}\right)$ when $-f_i(x, a) \leq 0$.

We therefore consider the scheme S with \tilde{S} (see equation (3.1)) defined as

$$\tilde{S}(\rho, x, t, u) = \lambda t + \sup_{a \in A} \left\{ \sum_{i=1}^N (f_i(x, a))_- \frac{t - u(x - h_i \vec{e}_i)}{h_i} + \sum_{i=1}^N (f_i(x, a))_+ \frac{t - u(x + h_i \vec{e}_i)}{h_i} - l(x, a) \right\}, \quad (3.3)$$

which can be rewritten as

$$\tilde{S}(\rho, x, t, u) = \lambda t + \sup_{a \in A} \left\{ t \sum_{i=1}^N \frac{|f_i(x, a)|}{h_i} - \sum_{i=1}^N \left(\frac{(f_i(x, a))_-}{h_i} u(x - h_i \vec{e}_i) + \frac{(f_i(x, a))_+}{h_i} u(x + h_i \vec{e}_i) \right) - l(x, a) \right\}. \quad (3.4)$$

We note $s_i(x, a)$ the sign of $f_i(x, a)$ and obtain

$$\begin{aligned} \tilde{S}(\rho, x, t, u) &= \lambda t + \sup_{a \in A} \left\{ \sum_{i=1}^N f_i(x, a) \frac{t - u(x + s_i(x, a) h_i \vec{e}_i)}{s_i(x, a) h_i} - l(x, a) \right\} \\ &= \lambda t + \sup_{a \in A} \left\{ \sum_{i=1}^N (-f_i(x, a)) \frac{t - u(x + s_i(x, a) h_i \vec{e}_i)}{-s_i(x, a) h_i} - l(x, a) \right\}. \end{aligned} \quad (3.5)$$

The scheme (3.3) is clearly nondecreasing with respect to t and nonincreasing with respect to u . Let us emphasize the fact that the scheme S with \tilde{S} defined by (3.3) is monotonous. Also in section 3.1.3, we prove that this scheme is stable under some mild conditions. Since the variable t appears inside the sup operator, the scheme is implicit (see remark 10).

3.1.2.2 A “Semi implicit” decentered scheme

A classical method to deal with the implicit scheme (3.3) consists in transforming the scheme into a fixed point problem. We multiply \tilde{S} by a fictitious time increment $-\Delta\tau$ (with $\Delta\tau > 0$) and we add $u(x)$ to both sides of the equation $\tilde{S} = 0$. In other words, instead of considering the scheme defined by $\tilde{S}(\rho, x, t, u)$, we consider the one defined by the function

$$\hat{S}(\rho, x, t, u) = t - u(x) + \Delta\tau \tilde{S}(\rho, x, u(x), u).$$

For the sake of simplicity, we write s_i for $s_i(x, a)$ in the sequel. Thus we obtain a new formulation of the scheme $S(\rho, x, u(x), u) = 0$ by defining

$$\begin{aligned} \tilde{S}_2(\rho, x, t, u) = & t(1 + \lambda\Delta\tau) - u(x) \\ & + \Delta\tau \sup_{a \in A} \left\{ \sum_{i=1}^N -f_i(x, a) \frac{u(x) - u(x + s_i h_i \vec{e}_i)}{-s_i h_i} - l(x, a) \right\}, \end{aligned} \quad (3.6)$$

or, equivalently,

$$\begin{aligned} \tilde{S}_3(\rho, x, t, u) = & t + \frac{1}{1 + \lambda\Delta\tau} \\ \sup_{a \in A} \left\{ - \left(1 - \Delta\tau \sum_{i=1}^N \frac{|f_i(x, a)|}{h_i} \right) u(x) - \Delta\tau \sum_{i=1}^N \frac{|f_i(x, a)|}{h_i} u(x + s_i h_i \vec{e}_i) - \Delta\tau l(x, a) \right\}. \end{aligned} \quad (3.7)$$

Note that $\hat{S}(\rho, x, t, u)$ is nondecreasing with respect to t and nonincreasing with respect to u as soon as the function $q \mapsto -q + \Delta\tau \tilde{S}(\rho, x, q, u)$ is nonincreasing. Also, we can verify easily that the scheme associated to (3.6) and (3.7) is monotonous iff $\Delta\tau$ is small enough ($\Delta\tau \leq \left(\sum_{i=1}^N \frac{|f_i(x, a)|}{h_i} \right)^{-1}$, for all a in A and for all x such that $f(x, a) \neq 0$; if $f(x, a) = 0$, then no constraints are required). In other words, this formulation of the decentered schemes requires that some conditions be satisfied in order to be monotonous. Despite this disadvantage, the formulation (3.6) or (3.7) is interesting because it yields *semi implicit* algorithms whereas the formulation (3.3) provides *totally implicit* algorithms. We use the expression “semi implicit” because the value of the sup has to be evaluated at each point x , but it does not involve t . Nevertheless in

SFS problems, we will see that the algorithms resulting from the formulation (3.3) can be made explicit through the use of calculus.

Remarks 12.

R12.1 - Let us mention that the larger the “parameter” $\Delta\tau$, the faster the convergence. Therefore, if $f(x, a_0) \neq 0$ (where a_0 is the optimal control of (3.6)), we can choose an optimal $\Delta\tau$:

$$\Delta\tau_{opt} = \left(\sum_{i=1}^N \frac{|f_i(x, a_0)|}{h_i} \right)^{-1},$$

where a_0 is the optimal control of (3.6).

Let us remark that a_0 and the optimal $\Delta\tau_{opt}$ depend on x , but that a_0 does not depend on $\Delta\tau$.

Thus, for all x such that $f(x, a_0) \neq 0$, if we choose $\Delta\tau = \Delta\tau_{opt}$, the scheme (3.6) becomes:

$$\begin{aligned} \tilde{S}_2^{opt}(\rho, x, t, u) &= \left(1 + \frac{\lambda}{\sum_{j=1}^N |f_j(x, a_0)|/h_j} \right) t \\ &- \sum_{i=1}^N \frac{|f_i(x, a_0)|/h_i}{\sum_{j=1}^N |f_j(x, a_0)|/h_j} u(x + s_i h_i \vec{e}_i) - \frac{1}{\sum_{j=1}^N |f_j(x, a_0)|/h_j} l(x, a_0), \end{aligned}$$

where a_0 is the optimal control of (3.6).

For x such that $f(x, a_0) = 0$,

$$\tilde{S}_2(\rho, x, t, u) = t - \frac{u(x)}{1 + \lambda\Delta\tau} - \frac{\Delta\tau}{1 + \lambda\Delta\tau} l(x, a_0).$$

Therefore, for such an x , if $\lambda \neq 0$ then the optimal (semi-implicit) scheme is

$$\tilde{S}_2^{opt}(\rho, x, t, u) = t - \frac{1}{\lambda} l(x, a_0).$$

If $\lambda = 0$ and $f(x, a_0) = 0$, there no exist optimal $\Delta\tau$. In this case the scheme is

$$\tilde{S}_2(\rho, x, t, u) = t - u(x) - \Delta\tau l(x, a_0).$$

R12.2 - Let us emphasize that the schemes defined with (3.6) have exactly the same solutions as the schemes defined with (3.3).

3.1.2.3 Decentered schemes for irregular meshes

In this section, we extend the implicit decentered scheme (designed in section 3.1.2.1) to irregular meshes. Of course the extension to the semi-implicit scheme follows trivially.

First, let us recall that for a function $u \in C^1(\Omega, \mathbb{R})$ we have:

$$\forall v \in \mathbb{R}^N, \quad \forall x \in \Omega, \quad \nabla u(x) \cdot v = \partial_v u(x),$$

where $\partial_v u(x)$ is the directional derivative of u in the direction v :

$$\partial_v u(x) = \lim_{h \rightarrow 0} \frac{u(x + hv) - u(x)}{h}.$$

So, if $\mathbf{v} = (v_1, \dots, v_N)$ is a vectorial basis of \mathbb{R}^N , we have:

$$\begin{pmatrix} t_{v_1} \\ \vdots \\ t_{v_N} \end{pmatrix} \nabla u(x) = \begin{pmatrix} \partial_{v_1} u(x) \\ \vdots \\ \partial_{v_N} u(x) \end{pmatrix}.$$

If we denote $B_{\mathbf{v}} = \begin{pmatrix} t_{v_1} \\ \vdots \\ t_{v_N} \end{pmatrix}$, we have:

$$\nabla u(x) = B_{\mathbf{v}}^{-1} \begin{pmatrix} \partial_{v_1} u(x) \\ \vdots \\ \partial_{v_N} u(x) \end{pmatrix}.$$

Thus, if we know the values of u at the points $x, x + v_1, \dots, x + v_N$, it is natural to approximate $\nabla u(x)$ by:

$$\nabla u(x) \cong B_{\mathbf{v}}^{-1} \begin{pmatrix} u(x + v_1) - u(x) \\ \vdots \\ u(x + v_N) - u(x) \end{pmatrix}.$$

So, if we replace $u(x)$ by t , it is natural to approximate $-f(x, a) \cdot \nabla u - l(x, a)$ by

$$[{}^t B_{\mathbf{v}}^{-1} f(x, a)] \cdot \begin{pmatrix} t - u(x + v_1) \\ \vdots \\ t - u(x + v_N) \end{pmatrix} - l(x, a).$$

Second, for a fixed basis of \mathbb{R}^N $\mathbf{v} = (v_1, \dots, v_N)$, let us denote

$$S_{\mathbf{v}} = \{\lambda_1 v_1 + \dots + \lambda_N v_N; (\lambda_1, \dots, \lambda_N) \in (\mathbb{R}^+)^N\}.$$

We remark that²

$$[\forall k = 1, \dots, N, [{}^t B_{\mathbf{v}}^{-1} f(x, a)]_k \geq 0] \iff [f(x, a) \in S_{\mathbf{v}}].$$

²Let us remind that if $V \in \mathbb{R}^N$ and $k \in [1, \dots, N]$ we denote $[V]_k$ the k^{th} component of V . In other words, $[V]_k = V \cdot e_k$, where e_k is the k^{th} vector of the canonical basis.

In other words, $f(x, a) \in S_{\mathbf{v}}$ iff all the components of ${}^t B_{\mathbf{v}}^{-1} f(x, a)$ are nonnegative.

Proof. $\forall i = 1, \dots, N$, let $f_{v_i} \in \mathbb{R}$ be such that

$$f(x, a) = \sum_{i=1}^N f_{v_i} v_i.$$

Let $k \in [1, \dots, N]$, we have:

$$[{}^t B_{\mathbf{v}}^{-1} f(x, a)]_k = \sum_{i=1}^N f_{v_i} [{}^t B_{\mathbf{v}}^{-1} v_i]_k.$$

Since $\forall i = 1, \dots, N$ ${}^t B_{\mathbf{v}}^{-1} v_i = e_i$, it follows:

$$[{}^t B_{\mathbf{v}}^{-1} f(x, a)]_k = f_{v_k}.$$

□

Now, let us complete the hypotheses on the mesh ν .

For all $x \in \overline{\Omega}$, let V_x be the finite set of vectors $\{\overrightarrow{x\tilde{y}}; y \in \mathcal{V}_x\}$. We assume here that for all $x \in \overline{\Omega}$, there exists a finite family $(\mathbf{v}_i)_{i=1\dots q}$ of bases $\mathbf{v}_i = (v_1^i, \dots, v_N^i)$ where $\forall i \in [1\dots q]$ and $\forall j \in [1\dots N]$, $v_j^i \in V_x$ and such that

$$\bigcup_{i=1\dots q} S_{\mathbf{v}_i} = \mathbb{R}^N$$

and

$$S_{\mathbf{v}_i}^\circ \cap S_{\mathbf{v}_j}^\circ = \emptyset, \quad \forall i \neq j.$$

Roughly speaking, the family of the sets $S_{\mathbf{v}_i}$ defines a partition of \mathbb{R}^N . Also, we can define:

$$A_i = \{a \in A \mid f(x, a) \in S_{\mathbf{v}_i}\}.$$

Of course, we have:

$$A = \bigcup_{i=1\dots q} A_i.$$

These notations in hand, we can easily design a monotonous approximation scheme for equation (2.18). For that, we can approximate

$$\sup_{a \in A} \{-f(x, a) \cdot \nabla u(x) - l(x, a)\}$$

by

$$\max_{i=1\dots q} \sup_{a \in A_i} \left\{ [{}^t B_{\mathbf{v}_i}^{-1} f(x, a)] \cdot \begin{pmatrix} t - u(x + v_1^i) \\ \vdots \\ t - u(x + v_N^i) \end{pmatrix} - l(x, a) \right\}. \quad (3.8)$$

In other words, we approximate ∇u by one of the vectors

$$B_{\mathbf{v}_i}^{-1} \begin{pmatrix} u(x + v_1^i) - u(x) \\ \vdots \\ u(x + v_N^i) - u(x) \end{pmatrix}, \quad i \in [1\dots q].$$

The choice of the relevant basis \mathbf{v}_i (the good simplex) depends on the dynamic of the optimal control. In other words, this scheme is an “upwind scheme”.

To conclude, let us remark that for all i in $[1\dots q]$, the supremum of (3.8) is restricted to the controls a in A_i . Therefore

$$f(x, a) \in S_{\mathbf{v}_i}$$

and so

$$\forall k = 1, \dots, N, \quad [{}^t B_{\mathbf{v}_i}^{-1} f(x, a)]_k \geq 0.$$

The monotonicity of the scheme follows.

3.1.3 Stability of the approximation schemes

Definition 3.2 (stability) *The scheme $T(\nu, x, u) = 0$ defined on $\overline{\Omega}$, is stable if for all $\nu \in \mathcal{M}$, it has a solution $u^\nu \in B(\overline{\Omega})$.*

Remark 13. The stability of a scheme requires the existence of a solution but not its uniqueness.

Definition 3.3 (uniform stability) *The scheme $T(\nu, x, u) = 0$ defined on $\overline{\Omega}$, is uniformly stable if it is stable and if its solutions u^ν are bounded independently of ν .*

Remark 14. Note that a scheme (3.6) is (uniformly) stable iff the associated scheme (3.3) is (uniformly) stable.

There exists only two main methods for proving the stability of a scheme, they use

1. the monotonicity,
2. fixed point theorems.

Here, we use the monotonicity.

3.1.3.1 Stability of monotonous schemes

We need the definition of a subsolution of a scheme.

Definition 3.4 (subsolution of an approximation scheme)

For a fixed mesh $\nu \in \mathcal{M}$, $v : \overline{\Omega} \rightarrow \mathbb{R}$ is a subsolution of the scheme

$$S(\nu, x, u(x), u) = 0 \text{ if } \forall x \in \overline{\Omega}, S(\nu, x, v(x), v) \leq 0.$$

The stability theorem 3.1 is based on the monotonicity.

Theorem 3.1 (Stability of monotonous schemes) *Let us consider a finite difference scheme*

$$S(\nu, x, u(x), u) = 0, \quad \forall x \in \overline{\Omega}. \tag{3.9}$$

We suppose that the scheme (3.9) verifies (H15) and the following hypotheses:

(H16) $\forall \nu \in \mathcal{M}, x \in \overline{\Omega}, u \in B(\overline{\Omega})$, the function $S_{\nu, x, u} : t \mapsto S(\nu, x, t, u)$ is continuous, nondecreasing and $\lim_{t \rightarrow +\infty} S_{\nu, x, u}(t) \geq 0$.

(H17) The scheme is monotonous (see definition 3.1).

(H18) $\forall \nu \in \mathcal{M}, x \in \overline{\Omega}$, the function $\check{S}_{\nu, x}$ is continuous with respect to $(t, (u(y))_{y \in \mathcal{V}_x})$ (we denote $\check{S}_{\nu, x}(\cdot, \cdot) := \check{S}(\nu, x, \cdot, \cdot)$ where \check{S} is defined in the hypothesis (H15)).

(H19) $\forall \nu \in \mathcal{M}$, there exists a subsolution of the scheme (3.9).

(H20) $\forall \nu \in \mathcal{M}$, there exists $M^\nu \in \mathbb{R}$ such that for all subsolutions v^ν of (3.9), $\forall x \in \overline{\Omega}, v^\nu(x) \leq M^\nu$.

Then the scheme (3.9) is stable.

Proof of Theorem 3.1. The idea of the proof is the following:

ν being fixed, we construct a nondecreasing sequence of functions u_n such that for all x of $\overline{\Omega}$,

$$S(\nu, x, u_n(x), u_n) \leq 0.$$

In other words, we construct a nondecreasing sequence of subsolutions of the scheme (3.9). By the hypothesis (H20), this sequence is upper bounded therefore convergent. We note u^ν its limit. For all x in $\overline{\Omega}$, the sequence u_n is constructed such that $S(\nu, x, u_n(x), u_{n-1})$ is zero. Thus by an argument of continuity, we prove that the limit u^ν of the sequence u_n is a solution of the scheme (3.9).

Let us now fix $\nu \in \mathcal{M}$.

1. Recursive construction of the sequence of functions $(u_n)_{n \in \mathbb{N}}$:

- (a) Let u_0 be a subsolution of the scheme (3.9) (see hypothesis (H19)).
- (b) Let us suppose that we have constructed the first n elements $(u_k)_{k=0..n-1}$ of our sequence such that:

$$\forall k \in [0..n-2], \quad u_{k+1} \geq u_k,$$

and $\forall k \in [0..n-1]$,

$$\forall x \in \overline{\Omega}, \quad S(\rho, x, u_k(x), u_k) \leq 0.$$

◦ We now construct u_n :

$\forall x \in \overline{\Omega}$, $u_n(x)$ is chosen in such a way that

$$S(\nu, x, u_n(x), u_{n-1}) = 0. \tag{3.10}$$

Note that this is always possible, by hypothesis (H16). In effect, we know that

$$S(\nu, x, u_{n-1}(x), u_{n-1}) \leq 0;$$

and

$$\lim_{t \rightarrow +\infty} S(\nu, x, t, u_{n-1}) \geq 0.$$

So the “intermediate values” theorem applied to the continuous function $t \mapsto S(\nu, x, t, u_{n-1})$ allows us to conclude.

◦ By (H16), the function $t \mapsto S(\nu, x, t, u_{n-1})$ is nondecreasing. Then $\forall x \in \overline{\Omega}$, $u_n(x) \geq u_{n-1}(x)$. Therefore

$$u_n \geq u_{n-1} \text{ on } \overline{\Omega}.$$

◦ Finally, u_n is a subsolution of the scheme (3.9):

By the monotonicity of the scheme (hypothesis (H17)), we have $S(\nu, x, u_n(x), u_n) \leq S(\nu, x, u_n(x), u_{n-1})$. The property (3.10) allows to conclude that

$$\forall x \in \overline{\Omega}, \quad S(\nu, x, u_n(x), u_n) \leq 0.$$

Thus we have constructed a nondecreasing sequence $(u_n)_{n \geq 0}$ of subsolutions of the scheme (3.9).

2. Convergence and properties of the limit:

The functions u_n are subsolutions of the scheme; then the hypothesis (H20) implies that they are upper bounded. Being nondecreasing and upper bounded, the sequence $(u_n)_{n \geq 0}$ converges toward a limit. We note this limit u^ν .

Let us fix x in $\bar{\Omega}$. Obviously, $\forall y \in \mathcal{V}_x, u_n(y) \xrightarrow{n \rightarrow +\infty} u^\nu(y)$. Since \mathcal{V}_x is finite, then we have clearly by hypothesis (H18):

$$\lim_{n \rightarrow +\infty} S(\nu, x, u_n(x), u_{n-1}) = S(\nu, x, u^\nu(x), u^\nu).$$

Moreover, for all $n > 0$, we have $S(\nu, x, u_n(x), u_{n-1}) = 0$. Therefore, $S(\nu, x, u^\nu(x), u^\nu) = 0$. u^ν is a solution of the scheme (3.9). Also, we have clearly $u^\nu \leq M^\nu$.

□

Remarks 15.

R15.1 - By replacing the hypothesis (H20) by (H21)

(H21) *There exists $M \in \mathbb{R}$ such that for all $\nu \in \mathcal{M}$, all subsolutions of (3.9) are upper bounded by M ,*

we have the uniform stability of the scheme.

R15.2 - *Jacobi and Gauss-Seidel methods:*

In the proof of theorem 3.1, we construct a sequence $(u_n)_{n \geq 0}$ of subsolutions by using an *update at all points x of $\bar{\Omega}$* : i.e., $\forall x \in \bar{\Omega}, u_n(x)$ is chosen in such a way that $S(\nu, x, u_n(x), u_{n-1}) = 0$. As an alternative, we can update the sequence only on part of $\bar{\Omega}$.

For simplicity we assume here that ν is a canonical mesh and that $\bar{\Omega}$ is a bounded set. Of course, this remark can be easily extended to the irregular meshes. Let us pave the set $\bar{\Omega}$ with $h_1 \times \dots \times h_N$ boxes (or subsets thereof), see figure 3.1. We order the boxes lexicographically as P^1, \dots, P^q ; since $\bar{\Omega}$

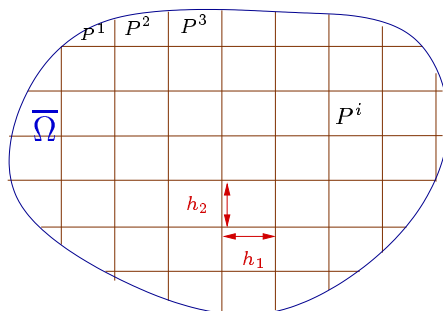


Figure 3.1: Partition of $\bar{\Omega}$ in dimension 2.

is bounded this is possible with a finite number of boxes. Also, we can

impose that the subsets P^1, \dots, P^q form a partition of $\bar{\Omega}$ (the partition is non unique). Now, let us define the infinite periodic sequence $(P_n)_{n \in \mathbb{N}}$ by $P_n = P^i$, where $i \equiv n [q]$.

For updating the sequel $(u_n)_{n \geq 0}$, we can use the subset P_n :

$$\begin{cases} \forall x \in \bar{\Omega} - P_n, & \text{let } u_n(x) = u_{n-1}(x) \\ \forall x \in P_n, & u_n(x) \text{ is chosen in such a way that } S(\nu, x, u_n(x), u_{n-1}) = 0. \end{cases}$$

As above, we prove that the sequence $(u_n)_{n \geq 0}$ is a nondecreasing sequence of subsolutions of the scheme (3.9). Let us fix $x \in \bar{\Omega}$ and denote n_x the integer such that $n_x \in [1..q]$ and $x \in P^{n_x}$. For all n in \mathbb{N} such that $n \equiv n_x (q)$, we have $S(\rho, x, u_n(x), u_{n-1}) = 0$. Thus, as above, by (H18), the sequence $(u_n)_{n \geq 0}$ converges toward a solution of the considered scheme.

From a theoretical point of view we gain nothing. Nevertheless, from an algorithmic point of view, this remark is very interesting. In effect, numerically, for approximating the solution of the scheme (3.9), we compute the sequence u_n . More precisely, for a fixed ν , we consider a mesh \mathcal{Z}_ν

$$\mathcal{Z}_\nu := \bar{\Omega} \cap \left\{ x_k = \sum_{i=1..N} k_i h_i \vec{e}_i; k \in \mathbb{Z}^N \right\}$$

and we approximate $u^\nu(x_k)$ by $u_n(x_k)$. Thus, the sequence u_n designed in the proof of theorem 3.1 yields *Jacobi*-type algorithms. The sequence u_n constructed in this remark yields *Gauss-Seidel*-type algorithms. In both cases, we prove the convergence of the algorithms. Finally, let us emphasize that if, mathematically, the “Jacobi method” is “better” than the “Gauss-Seidel method” in the sense that it is more elegant, nevertheless numerically, the opposite is true. In effect, numerically, we call “iteration”, an update of all the pixels. An iteration of the “numerical Jacobi method” allows to compute the approximations $\{u_{n+1}(x_k)\}_k$ from the approximations $\{u_n(x_k)\}_k$. For the “numerical Gauss-Seidel method”, an iteration allows to compute the approximations $\{u_{n+|\mathcal{Z}_\rho|}(x_k)\}_k$ from the approximations $\{u_n(x_k)\}_k$ (where $|\mathcal{Z}_\rho|$ is the cardinal number of the set \mathcal{Z}_ρ). Also, unlike the “numerical Gauss-Seidel method”, during one iteration of the “numerical Jacobi method”, the update of the approximation of u at the pixel x_k does not use the update of the approximation of u at the previous pixels (of the same iteration). Therefore, one iteration of the “numerical Gauss-Seidel method” is more effective than one iteration of the “numerical Jacobi method”.

R15.3 - In theorem 3.1, we can replace hypotheses (H16),(H19) and (H20) by hypotheses (H16’), (H19’) and (H20’)

(H16') $\forall \nu \in \mathcal{M}, x \in \overline{\Omega}, u \in B(\overline{\Omega})$, the function $S_{\nu,x,u} : t \mapsto S(\nu, x, t, u)$ is continuous, nondecreasing and $\lim_{t \rightarrow -\infty} S_{\nu,x,u}(t) \leq 0$.

(H19') $\forall \nu \in \mathcal{M}$, there exists a supersolution of the scheme (3.9) (v is a supersolution of the scheme $S(\nu, x, u(x), u) = 0$ if $\forall x \in \overline{\Omega}, S(\nu, x, v(x), v) \geq 0$).

(H20') $\forall \nu \in \mathcal{M}$, there exists $M^\nu \in \mathbb{R}$ such that for all supersolutions v^ν of (3.9), $\forall x \in \overline{\Omega}, v^\nu(x) \geq M^\nu$.

In this case, the sequence u_n we design is a nonincreasing sequence of supersolutions of the scheme (3.9).

The interest of this remark appears in practice. In effect it allows to prove the convergence of the algorithms with initial surfaces U_0 which are supersolutions. Also, the number of iterations required to obtain the convergence is much smaller when U_0 is a supersolution than when U_0 is a subsolution; see section 3.2.2.

r15.4 - Let us emphasize that theorem 3.1 does not impose regularity hypotheses with respect to the space variable x .

3.1.3.2 Stability of the implicit schemes (3.3) associated with HJB equations

In this section, we assume that the mesh ν is canonical. Also, since in this case ν is characterized by ρ , we identify the both notations. Let us note that the results presented here can be easily generalized to irregular meshes. We prove the stability of the “scheme with Dirichlet conditions”

$$S(\rho, x, u(x), u) = 0$$

with S defined by

$$S(\rho, x, t, u) = \begin{cases} \tilde{S}(\rho, x, t, u) & \text{if } x \in \Omega_\rho, \\ t - \varphi(x) & \text{if } x \in \text{b}\Omega_\rho. \end{cases} \quad (3.11)$$

and \tilde{S} defined by (see section 3.1.2)

$$\tilde{S}(\rho, x, t, u) = \lambda t + \sup_{a \in A} \left\{ \sum_{i=1}^N (f_i(x, a))_- \frac{t - u(x - h_i \vec{e}_i)}{h_i} + \sum_{i=1}^N (f_i(x, a))_+ \frac{t - u(x + h_i \vec{e}_i)}{h_i} - l(x, a) \right\}, \quad (3.12)$$

which can be rewritten as $\tilde{S}(\rho, x, t, u) = \lambda t +$

$$\sup_{a \in A} \left\{ t \sum_{i=1}^N \frac{|f_i(x, a)|}{h_i} - \sum_{i=1}^N \left(\frac{(f_i(x, a))_-}{h_i} u(x - h_i \vec{e}_i) + \frac{(f_i(x, a))_+}{h_i} u(x + h_i \vec{e}_i) \right) - l(x, a) \right\}. \quad (3.13)$$

A stability result based on subsolutions

Proposition 3.1 *Consider the scheme S described in (3.11) with \tilde{S} defined by (3.12). Suppose that for all x in $\overline{\Omega}$, the functions $f(x, \cdot) : a \mapsto f(x, a)$ and $l(x, \cdot) : a \mapsto l(x, a)$ verify the hypotheses (H6’), (H7’) and (H22) (described below). Suppose also that $\forall \rho > 0$, there exists a subsolution of the scheme S and that there exists $M^\rho \in \mathbb{R}$ such that for all subsolutions v^ρ of S , $\forall x \in \overline{\Omega}$, $v^\rho(x) \leq M^\rho$. Then the scheme S is stable.*

Also, if $M^\rho \equiv M \in \mathbb{R}$ does not depend on ρ then the stability is uniform.

(H6’) *A is a compact topological space;*

(H7’) *$f : A \rightarrow \mathbb{R}^N$ is continuous;
 $l : A \rightarrow \mathbb{R}$ is continuous and bounded.*

(H22) *For all $x \in \Omega$, we have:
 there exists $a_x \in A$ such that $f(x, a_x) \neq 0$.*

Proof of proposition 3.1. See section 3.1.3.3. □

Remarks 16.

r16.1 - Let us remind the reader that the (uniform) stability of an implicit decentered scheme given by (3.11) implies the (uniform) stability of the associated semi implicit scheme (3.6).

r16.2 - The difficulty for proving the stability of an implicit decentered scheme given by (3.11) lies in the proof of the existence of subsolutions and in the proof that the subsolutions are bounded. In the next subsection, we present some results for dealing with the HJB equation with null interest rate ($\lambda = 0$).

r16.3 - Proposition 3.1 holds for $\lambda \neq 0$ and $\lambda = 0$.

r16.4 - The hypotheses (H6') and (H7') do not impose regularity of f and l with respect to the space variable x . Therefore, proposition 3.1 does not require the regularity with respect to x , to be applied.

The difficulty in applying proposition 3.1 lies in the proof of the existence of subsolutions. In the case $\lambda = 0$ which is true for the SFS problems, things turn out to be simpler, as shown next.

Particular case of the HJB equations with null interest rate ($\lambda = 0$)

In this section we consider an HJB equation with null interest rate. Concerning the existence of the subsolutions of the decentered schemes for Hamiltonians H with nonnegative running cost (or equivalently such that $H(x, 0) \leq 0$), we have the following result:

Proposition 3.2 *Let H be an HJB Hamiltonian with null interest rate ($\lambda = 0$), defined on $\overline{\Omega} \times \mathbb{R}^N$. Let φ be a bounded function defined on a neighbourhood of $\partial\Omega$. If H has a nonnegative running cost l then all constant functions u on $\overline{\Omega}$ such that $u \leq \min_x \varphi(x)$, are subsolutions of the associated decentered scheme S defined by (3.11).*

Proof. See section 3.1.3.3. □

In order to apply proposition 3.1, we also need to prove that all the subsolutions of the scheme S are upper bounded.

Notation. For $K > 0$, we denote by \mathcal{M}_K the set of canonical meshes ρ such that

$$\max_{i=1..N} h_i \leq K \min_{i=1..N} h_i.$$

In particular, if we choose ρ such that $h_1 = \dots = h_N$, then $\rho \in \mathcal{M}_1$.

Proposition 3.3 *Consider an implicit decentered scheme S defined by (3.11) with $\lambda = 0$. Assume that Ω is a bounded open subset of \mathbb{R}^N .*

We suppose that for all x in $\overline{\Omega}$, there exists a control $a_x \in A$ such that for all $i = 1..N$, the sign of $f_i(x, a_x)$ does not depend on x . For $i = 1..N$, we denote by s_i the sign of $f_i(x, a_x)$. Also, let us suppose that there exists $\varepsilon > 0$ and j in $[1..N]$ such that $\forall x \in \overline{\Omega}$, $s_j f_j(x, a_x) \geq \varepsilon$.

If l and φ are upper bounded (on $\overline{\Omega} \times A$ and on a neighbourhood of $\partial\Omega$) then all the subsolutions of S are upper bounded.

Also, for all $K > 0$, there exists $B_K > 0$ such that $\forall \rho \in \mathcal{M}_K, \forall v_\rho$ subsolution of S , we have $v_\rho \leq B_K$.

Proof. See section 3.1.3.3. □

Remark 17. Let us emphasize that all the results described in this section (section 3.1.3) do not require regularity of the Hamiltonian with respect to the space variable x .

3.1.3.3 Proofs of propositions 3.1, 3.2 and 3.3

The proof of proposition 3.1 requires the following notations and lemmas:

Notation. Let B be a set. For a function

$$\begin{aligned} g : B &\rightarrow \mathbb{R}^N \\ x &\mapsto (g_1(x), \dots, g_i(x), \dots, g_N(x)) \end{aligned}$$

we define

$$\begin{aligned} g_+ : B &\rightarrow \mathbb{R}^N & \text{and } g_- : B &\rightarrow \mathbb{R}^N \\ x &\mapsto (g_{1+}(x), \dots, g_{N+}(x)) & x &\mapsto (g_{1-}(x), \dots, g_{N-}(x)) \end{aligned} .$$

Lemma 3.1 *Let $f : A \rightarrow \mathbb{R}^N$ and $l : A \rightarrow \mathbb{R}$ be such that the hypotheses (H6') and (H7') are verified. Then the function*

$$H(p) = \sup_{a \in A} \{-f(a) \cdot p - l(a)\}$$

is continuous.

Proof. See lemma III.2.11 of Bardi and Capuzzo-Dolcetta 's book [5]. □

Lemma 3.2 *Let $f : A \rightarrow \mathbb{R}^N$ and $l : A \rightarrow \mathbb{R}$ be such that the hypotheses (H6') and (H7') are verified. Let*

$$\begin{aligned} \bar{f} : A &\rightarrow \mathbb{R}^{2N} \\ a &\mapsto \begin{pmatrix} f(a)_+ \\ f(a)_- \end{pmatrix} \end{aligned}$$

and

$$\begin{aligned} \bar{H} : \mathbb{R}^N \times \mathbb{R}^N &\rightarrow \mathbb{R} \\ (p, q) &\mapsto \sup_{a \in A} \left\{ -\bar{f}(a) \cdot \begin{pmatrix} p \\ q \end{pmatrix} - l(a) \right\} \end{aligned}$$

Then \bar{H} is continuous.

Proof. Since the hypotheses (H6') and (H7') hold for f , they also hold for \bar{f} , and lemma 3.1 applies to \bar{H} . \square

Lemma 3.3 *Let S be defined by (3.11) with \tilde{S} defined by (3.12). For all $\rho > 0$, $x \in \bar{\Omega}$ and $u : \bar{\Omega} \rightarrow \mathbb{R}$, the function $S_{\rho, x, u} : \mathbb{R} \rightarrow \mathbb{R} : t \mapsto S(\rho, x, t, u)$ is nondecreasing. If the hypothesis (H22) holds, then $\lim_{t \rightarrow +\infty} S_{\rho, x, u}(t) \geq 0$. Moreover if for all x in $\bar{\Omega}$, the functions $f(x, \cdot) : a \mapsto f(x, a)$ and $l(x, \cdot) : a \mapsto l(x, a)$ verify the hypotheses (H6') and (H7'), then the functions $S_{\rho, x, u}$ and $\tilde{S}_{\rho, x}$ are continuous.*

Proof. For $x \in \text{b}\Omega_\rho$, the result is obvious.

Let us fix x in Ω_ρ . We have $S_{\rho, x, u} = \tilde{S}_{\rho, x, u}$.

Since λ and $\sum_{i=1}^N \frac{|f_i(x, a)|}{h_i}$ are positive, the formulation (3.13) implies that $\tilde{S}_{\rho, x, u}$ is nondecreasing. Because of hypothesis (H22) there exists $a_x \in A$ such that $f(x, a_x) \neq 0$, therefore $\sum_{i=1}^N \frac{|f_i(x, a_x)|}{h_i} > 0$. By using the formulation (3.13), we have

$$\tilde{S}_{\rho, x, u}(t) \geq \left(\lambda + \sum_{i=1}^N \frac{|f_i(x, a_x)|}{h_i} \right) t + F(x, a_x)$$

where

$$F(x, a_x) = - \sum_{i=1}^N \left(\frac{(f_i(x, a_x))_-}{h_i} u(x - h_i \vec{e}_i) + \frac{(f_i(x, a_x))_+}{h_i} u(x + h_i \vec{e}_i) \right) - l(x, a_x).$$

Therefore $\lim_{t \rightarrow +\infty} \tilde{S}_{\rho, x, u}(t) = +\infty$.

By lemma 3.2, \bar{H} is continuous. Let us fix $\rho > 0$ and $u : \bar{\Omega} \rightarrow \mathbb{R}$. The functions

p and q

$$\begin{aligned}
 p: \mathbb{R} &\rightarrow \mathbb{R}^N & q: \mathbb{R} &\rightarrow \mathbb{R}^N \\
 t &\mapsto \begin{pmatrix} \frac{t-u(x+h_1\vec{e}_1)}{h_1} \\ \vdots \\ \frac{t-u(x+h_N\vec{e}_N)}{h_N} \end{pmatrix} & t &\mapsto \begin{pmatrix} \frac{t-u(x-h_1\vec{e}_1)}{h_1} \\ \vdots \\ \frac{t-u(x-h_N\vec{e}_N)}{h_N} \end{pmatrix}
 \end{aligned}$$

are continuous. Since $\check{S}_{\rho,x,u}(t) = \lambda t + \overline{H}(x, p(t), q(t))$, the function $\check{S}_{\rho,x,u}$ is a composition of continuous functions, hence continuous. Therefore $S_{\rho,x,u}$ is continuous.

In the same way, we prove the continuity of $\check{S}_{\rho,x}$. □

Proof of Proposition 3.1. We apply theorem 3.1.

Clearly the hypothesis (H15) is true ($\mathcal{V}_x = \{x \pm h_i \vec{e}_i, i = 1..N\}$). The hypotheses (H16) and (H18) are true by lemma 3.3. Clearly (H17) is true.

Remark R15.1 allows us to deal with the uniform stability case. □

Proof of proposition 3.2. If u is a constant function, we have

- $\forall x \in \Omega_\rho,$

$$\begin{aligned}
 S(\rho, x, u(x), u) &= \check{S}(\rho, x, u, u) \\
 &= \sup_{a \in A} \{-l(x, a)\} \\
 &= H(x, 0) \\
 &\leq 0.
 \end{aligned}$$

- $\forall x \in b\Omega_\rho,$

$$S(\rho, x, u(x), u) = u - \varphi(x) \leq 0.$$

□

Proof of proposition 3.3. Let v be a subsolution of the scheme S . By definition, for all $x \in \overline{\Omega}$,

$$S(\rho, x, v(x), v) \leq 0. \tag{3.14}$$

For all x in $\mathring{b}\Omega_\rho$, (3.14) implies $v(x) \leq \varphi(x)$. Thus for all x in $\mathring{b}\Omega_\rho$, $v(x) \leq \max \varphi$.
 For all x in Ω_ρ , (3.14) implies

$$\sup_{a \in A} \left\{ \sum_{i=1}^N \text{sign}(f_i(x, a)) f_i(x, a) \frac{v(x) - v(x + \text{sign}(f_i(x, a)) h_i \vec{e}_i)}{h_i} - l(x, a) \right\} \leq 0.$$

In particular,

$$\sum_{i=1}^N s_i f_i(x, a_x) \frac{v(x) - v(x + s_i h_i \vec{e}_i)}{h_i} - l(x, a_x) \leq 0.$$

Let us note $w_i(x)$ the quantity $\frac{s_i f_i(x, a_x)}{h_i}$. We have

$$v(x) \sum_{i=1}^N w_i(x) \leq l(x, a_x) + \sum_{i=1}^N w_i(x) v(x + s_i h_i \vec{e}_i).$$

Therefore, by considering L , an upper bound of l , we have:

$$v(x) \leq \frac{L}{\sum_{k=1}^N w_k(x)} + \sum_{i=1}^N \frac{w_i(x)}{\sum_{k=1}^N w_k(x)} v(x + s_i h_i \vec{e}_i);$$

Since $\sum_{k=1}^N w_k(x) \geq w_j(x) \geq \frac{\varepsilon}{h_j}$, then

$$v(x) \leq \frac{L h_j}{\varepsilon} + \sum_{i=1}^N \frac{w_i(x)}{\sum_{k=1}^N w_k(x)} v(x + s_i h_i \vec{e}_i).$$

We notice that $\sum_{i=1}^N \frac{w_i(x)}{\sum_{k=1}^N w_k(x)} v(x + s_i h_i \vec{e}_i)$ is a barycentric combination of the $\{v(x + s_i h_i \vec{e}_i)\}_{i=1..N}$, therefore

$$v(x) \leq \frac{L}{\varepsilon} h_j + \max_{i=1..N} v(x + s_i h_i \vec{e}_i).$$

Since $\bar{\Omega}$ is bounded and since $\forall i = 1..N$, s_i does not depend on x , then by recursivity

$$v(x) \leq \left(\frac{L}{\varepsilon} h_j\right) \left(\sum_{i=1}^N \frac{X}{h_i}\right) + \max_{y \in \mathring{b}\Omega_\rho} \varphi(y)$$

where $\bar{\Omega}$ is a subset of the box $[-\frac{X}{2}, \frac{X}{2}]^N$, and therefore v is bounded above.

We continue with

$$v(x) \leq \left(\frac{L}{\varepsilon} h_j\right) N X \frac{1}{\min h_i} + \max \varphi,$$

$$v(x) \leq \frac{L}{\varepsilon} N X \frac{\max_i h_i}{\min_i h_i} + \max \varphi,$$

If $\rho \in \mathcal{M}_K$ (we can suppose that $K = \frac{\max_i h_i}{\min_i h_i}$), we have

$$v(x) \leq \frac{L K N X}{\varepsilon} + \max \varphi.$$

Let us denote $B_K := \frac{LKNX}{\varepsilon} + \max \varphi$.

We have $v \leq B_K$. □

3.1.4 Convergence of the solutions of the approximation schemes toward the viscosity solutions

The main method for proving the convergence of the solutions of an approximation scheme toward the viscosity solution of an Hamilton-Jacobi equation is due to Barles and Souganidis [9] and is based on the notion of weak limits.

In this section, we consider a canonical mesh. As in the previous sections, we denote it ρ . In the sequel, we suppose that $\rho \in \mathbb{R}$. In other words we suppose that $\rho = h_1 = \dots = h_N$.

3.1.4.1 Consistency of a scheme (with an equation) and convergence of its solutions towards discontinuous viscosity solutions

We now give the definition of the *consistency* of an approximation scheme according to Barles and Souganidis [9].

Remember that in the framework of discontinuous viscosity solutions, the PDE with Dirichlet boundary conditions must be rewritten as:

$$F(x, u(x), \nabla u(x)) = 0, \quad \forall x \in \bar{\Omega}; \tag{3.15}$$

where F is defined on $\bar{\Omega} \times \mathbb{R} \times \mathbb{R}^N$ by

$$F(x, u, p) = \begin{cases} H(x, u, p) & \text{for } x \text{ in } \Omega, \\ u(x) - \varphi(x) & \text{for } x \text{ on } \partial\Omega. \end{cases} \tag{3.16}$$

Definition 3.5 (consistency) *The scheme $S(\rho, x, u(x), u) = 0$ defined on $\bar{\Omega}$, is consistent with equation (3.15) if :*

$\forall x \in \bar{\Omega}$ and $\forall \phi \in C_b^\infty(\bar{\Omega})$

$$\limsup_{\rho \rightarrow 0, y \rightarrow x, \xi \rightarrow 0} \frac{S(\rho, y, \phi(y) + \xi, \phi + \xi)}{\rho} \leq F^*(x, \phi(x), \nabla \phi(x)),$$

and

$$\liminf_{\rho \rightarrow 0, y \rightarrow x, \xi \rightarrow 0} \frac{S(\rho, y, \phi(y) + \xi, \phi + \xi)}{\rho} \geq F_*(x, \phi(x), \nabla \phi(x)).$$

F^* and F_* are defined on page 63.

Let us recall the definitions of the functions \bar{u} and \underline{u} :

Definition 3.6 $\forall x \in \overline{\Omega}$,

$$\overline{u}(x) = \limsup_{\substack{\rho \rightarrow 0, \\ y \rightarrow x, y \text{ in } \overline{\Omega}}} u^\rho(y)$$

$$\underline{u}(x) = \liminf_{\substack{\rho \rightarrow 0, \\ y \rightarrow x, y \text{ in } \overline{\Omega}}} u^\rho(y)$$

With these definitions in hand we can now formulate the following theorem:

Theorem 3.2 *If an approximation scheme S is monotonous, uniformly stable and consistent with equation (3.15) then \overline{u} and \underline{u} are respectively viscosity subsolution and supersolution of this equation.*

Proof. See theorem 2.1 of [9]. □

Thus, as soon as we have a strong uniqueness property (definition 2.7 on page 79), a proof of the convergence follows:

Theorem 3.3 (convergence toward the viscosity solution) *Let S be a monotonous, uniformly stable and consistent (with equation (3.15)) approximation scheme. Let us suppose that the strong uniqueness property is verified on a subset D of $\overline{\Omega}$. Then the solutions u^ρ of the scheme S converge on D toward the viscosity solution of (3.15) when $\rho \rightarrow 0$.*

Proof. By theorem 3.2, the functions \overline{u} and \underline{u} are respectively viscosity subsolution and supersolution of the PDE (3.15). The strong uniqueness property involves $\overline{u} \leq \underline{u}$ on D . By definition, we have $\underline{u} \leq \overline{u}$, and hence:

$$\overline{u} = \underline{u} \quad (\text{on } D).$$

For all $x \in D$, we now know that the limit $\lim_{\rho \rightarrow 0} u^\rho(x)$ exists and is equal to $u(x) := \overline{u}(x)$ (which is also equal to $\underline{u}(x)$). Finally, let v be a viscosity solution of (3.15). By definition 2.3, v^* and v_* is a subsolution and a supersolution, respectively; so the strong uniqueness property involves:

$$\forall x \in D, \quad \overline{u}(x) \leq v_*(x) \leq v^*(x) \leq \underline{u}(x)$$

Therefore $u = v_* = v^* = v$ on D and $\lim_{\rho \rightarrow 0} u^\rho(x) = v(x)$. □

Remark 18. Note that despite the fact that we do not have uniqueness of the viscosity solution on $\overline{\Omega}$, we have it within D . Hence all viscosity solutions coincide on D .

Another important interpretation of the result presented in theorem 3.3 is the following:

Theorem 3.4 (existence result of a discontinuous viscosity solution)

If the hypotheses of theorem 3.3 are verified then equation (3.15) has a discontinuous viscosity solution.

In other words, the existence of a solution of a HJ PDE can be obtained directly by designing a monotonous scheme and by using the strong uniqueness result.

3.1.4.2 Application to the decentered schemes for the HJB equations

Theorem 3.3 applies to the implicit decentered schemes S (presented in section 3.1.2)

$$S(\rho, x, t, u) = \begin{cases} \tilde{S}(\rho, x, t, u) & \text{if } x \in \Omega_\rho, \\ t - \varphi(x) & \text{if } x \in \mathfrak{b}\Omega_\rho, \end{cases} \quad (3.17)$$

where \tilde{S} is defined by

$$\tilde{S}(\rho, x, t, u) = \lambda t + \sup_{a \in A} \left\{ \sum_{i=1}^N (f_i(x, a))_- \frac{t - u(x - \rho \vec{e}_i)}{\rho} + \sum_{i=1}^N (f_i(x, a))_+ \frac{t - u(x + \rho \vec{e}_i)}{\rho} - l(x, a) \right\}.$$

It also applies to HJB equations, $\forall x \in \overline{\Omega}$, $F(x, u(x), \nabla u(x)) = 0$, where F is defined by

$$F(x, u, p) = \begin{cases} \lambda u + \sup_{a \in A} \{-f(x, a) \cdot p - l(x, a)\} & \text{if } x \in \Omega, \\ u - \varphi(x) & \text{if } x \in \partial\Omega. \end{cases} \quad (3.18)$$

In effect, we have following proposition:

Proposition 3.4 (consistency of the decentered schemes with HJB equations)

Let $f : \bar{\Omega} \times A \rightarrow \mathbb{R}^N$ and $l : \bar{\Omega} \times A \rightarrow \mathbb{R}$ be two functions such that the hypotheses (H6)-(H8) are verified. Then the scheme $S(\rho, x, u^\rho(x), u^\rho) = 0$ with

$$S(\rho, x, t, u) = \begin{cases} \tilde{S}(\rho, x, t, u) & \text{if } x \in \Omega_\rho, \\ t - \varphi(x) & \text{if } x \in \partial\Omega_\rho. \end{cases}$$

\tilde{S} , defined by (3.3):

$$\tilde{S}(\rho, x, t, u) = \lambda t + \sup_{a \in A} \left\{ \sum_{i=1}^N (f_i(x, a))_- \frac{t - u(x - h_i \vec{e}_i)}{h_i} + \sum_{i=1}^N (f_i(x, a))_+ \frac{t - u(x + h_i \vec{e}_i)}{h_i} - l(x, a) \right\},$$

is consistent with the HJB equation

$$\forall x \in \bar{\Omega}, \quad F(x, u(x), \nabla u(x)) = 0, \quad (3.19)$$

where F is defined by

$$F(x, u, p) = \begin{cases} \lambda u + \sup_{a \in A} \{-f(x, a) \cdot p - l(x, a)\} & \text{if } x \in \Omega, \\ u - \varphi(x) & \text{if } x \in \partial\Omega. \end{cases}$$

Proof. See section 3.1.4.3. □

We can now state the main result of this section.

Proposition 3.5 (convergence for the decentered schemes and the HJB equations)

Consider the decentered scheme S defined by (3.17) and the associated HJB equation (3.18). Suppose that f and l verify the hypotheses (H6)-(H8).

Suppose that there exist subsolutions of the scheme S and $M \in \mathbb{R}$ such that $\forall \rho > 0, \forall v^\rho$ subsolution of $S, \forall x \in \bar{\Omega}, v^\rho(x) \leq M$. Suppose also that the strong uniqueness property is verified on a subset D of $\bar{\Omega}$.

Then the solutions u^ρ of the scheme S converge on D toward the unique restriction to D of the viscosity solutions of the HJB equation when ρ vanishes to zero.

Proof. The monotonicity of the scheme S is clear. The uniform stability is given by proposition 3.1. The consistency of S with the HJB equation is given by proposition 3.4. Theorem 3.3 allows to conclude. □

Remark 19. Since the solutions of the semi-implicit scheme (3.6) are the same as the solutions of the implicit scheme (3.11), the conclusion of proposition 3.5 applies also to the semi-implicit scheme.

3.1.4.3 Proof of proposition 3.4

The proof of proposition 3.4 needs the following lemmas:

Lemma 3.4 *Let $f : \bar{\Omega} \times A \rightarrow \mathbb{R}^N$ and $l : \bar{\Omega} \times A \rightarrow \mathbb{R}$ be such that the hypotheses (H6)-(H8) are verified. Then the function*

$$H(x, p) = \sup_{a \in A} \{-f(x, a) \cdot p - l(x, a)\}$$

is continuous.

Proof. See lemma III.2.11 of Bardi and Capuzzo-Dolcetta 's book [5]. □

Lemma 3.5 *Let $f : \bar{\Omega} \times A \rightarrow \mathbb{R}^N$ and $l : \bar{\Omega} \times A \rightarrow \mathbb{R}$ be such that the hypotheses (H6)-(H8) are verified. Let*

$$\begin{aligned} \bar{f} : \bar{\Omega} \times A &\rightarrow \mathbb{R}^{2N} \\ (x, a) &\mapsto \begin{pmatrix} f(x, a)_+ \\ f(x, a)_- \end{pmatrix} \end{aligned}$$

and

$$\begin{aligned} \bar{H} : \bar{\Omega} \times \mathbb{R}^N \times \mathbb{R}^N &\rightarrow \mathbb{R} \\ (x, p, q) &\mapsto \sup_{a \in A} \left\{ -\bar{f}(x, a) \cdot \begin{pmatrix} p \\ q \end{pmatrix} - l(x, a) \right\} \end{aligned}$$

Then \bar{H} is continuous.

Proof. See proof of lemma 3.2. □

Proof of proposition 3.4. Instead of considering the scheme

$$S(\rho, x, u^\rho(x), u^\rho) = 0 \quad \text{in } \bar{\Omega},$$

we consider the scheme

$$S'(\rho, x, u^\rho(x), u^\rho) = 0 \quad \text{in } \overline{\Omega},$$

such that

$$S'(\rho, x, t, u) = \rho S(\rho, x, t, u).$$

Monotonicity, stability and solutions are exactly the same for both schemes.

We prove that S' is consistent with equation (3.19), i.e.:

$$\forall x \in \overline{\Omega} \text{ et } \forall \phi \in C_b^\infty(\overline{\Omega})$$

$$\text{i) } \limsup_{\rho \rightarrow 0, y \rightarrow x, \xi \rightarrow 0} \frac{S'(\rho, y, \phi(y) + \xi, \phi + \xi)}{\rho} \leq F^*(x, \phi(x), \nabla \phi(x)),$$

$$\text{ii) } \liminf_{\rho \rightarrow 0, y \rightarrow x, \xi \rightarrow 0} \frac{S'(\rho, y, \phi(y) + \xi, \phi + \xi)}{\rho} \geq F_*(x, \phi(x), \nabla \phi(x)).$$

We only prove i), the proof of ii) being identical. We consider two cases.

1. $x \in \Omega$:

For ρ sufficiently small and y sufficiently close to x , we have $y \in \Omega_\rho$, and

$$\begin{aligned} \frac{S'(\rho, y, \phi(y) + \xi, \phi + \xi)}{\rho} &= \tilde{S}(\rho, y, \phi(y) + \xi, \phi + \xi) \\ &= \lambda(\phi(y) + \xi) + \\ \sup_{a \in A} \left\{ \sum_{i=1}^N (f_i(y, a))_- \frac{\phi(y) - \phi(y - \rho \vec{e}_i)}{\rho} + \sum_{i=1}^N (f_i(y, a))_+ \frac{\phi(y) - \phi(y + \rho \vec{e}_i)}{\rho} - l(y, a) \right\}. \end{aligned}$$

Since $\phi \in C^2$, we have

$$\lim_{\rho \rightarrow 0, y \rightarrow x} \frac{\phi(y) - \phi(y - \rho \vec{e}_i)}{\rho} = \partial_{\vec{e}_i} \phi(x),$$

$$\lim_{\rho \rightarrow 0, y \rightarrow x} \frac{\phi(y) - \phi(y + \rho \vec{e}_i)}{\rho} = -\partial_{\vec{e}_i} \phi(x),$$

and the function K

$$K : (\rho, y) \mapsto \left(y, \left(\frac{\phi(y) - \phi(y - \rho \vec{e}_i)}{\rho} \right)_{i=1..N}, \left(\frac{\phi(y) - \phi(y + \rho \vec{e}_i)}{\rho} \right)_{i=1..N} \right)$$

is continuous on $\mathcal{M} \times \Omega$ and

$$\lim_{\rho \rightarrow 0, y \rightarrow x} K(\rho, y) = (x, (\partial_{\vec{e}_i} \phi(x))_{i=1..N}, (-\partial_{\vec{e}_i} \phi(x))_{i=1..N}).$$

Since f and l verify the hypotheses (H6)-(H8), lemma 3.5 involves:

$$\begin{aligned}
 & \limsup_{\rho \rightarrow 0, y \rightarrow x, \xi \rightarrow 0} \tilde{S}(\rho, y, \phi(y) + \xi, \phi + \xi) \\
 = & \lambda\phi(x) + \sup_{a \in A} \left\{ \sum_{i=1}^N (f_i(x, a))_- \partial_{\bar{e}_i} \phi(x) + \sum_{i=1}^N (f_i(x, a))_+ (-\partial_{\bar{e}_i} \phi(x)) - l(x, a) \right\} \\
 = & \lambda\phi(x) + \sup_{a \in A} \left\{ \sum_{i=1}^N -f_i(x, a) \partial_{\bar{e}_i} \phi(x) - l(x, a) \right\} \\
 = & \lambda\phi(x) + \sup_{a \in A} \{-f(x, a) \cdot \nabla \phi(x) - l(x, a)\} \\
 & \hspace{15em} = H(x, \phi(x), \nabla \phi(x))
 \end{aligned}$$

where $H(x, u, p) = \lambda u + \sup_{a \in A} \{-f(x, a) \cdot p - l(x, a)\}$.

Since x is in Ω , for all y sufficiently close to x , $F(y, u, p) = H(y, u, p)$.

By continuity of H (by lemma 3.4), we have $F^*(x, u, p) = F(x, u, p) = H(x, u, p)$. Thus

$$\limsup_{\rho \rightarrow 0, y \rightarrow x, \xi \rightarrow 0} \frac{S'(\rho, y, \phi(y) + \xi, \phi + \xi)}{\rho} = F^*(x, u, p).$$

2. $x \in \partial\Omega$:

In the same way, by continuity of the involved functions, we have:

$$\begin{aligned}
 & \limsup_{\rho \rightarrow 0, y \rightarrow x, \xi \rightarrow 0} S(\rho, y, \phi(y) + \xi, \phi(y) + \xi) \\
 & \hspace{10em} = \max(H(x, \phi(x), \nabla \phi(x)), \phi(x) - \varphi(x)) \\
 & \hspace{15em} = F^*(x, \phi(x), \nabla \phi(x)).
 \end{aligned}$$

We deal the same way with point ii), comparing the inferior limit and F_* . Thus, the scheme S' is consistent with the equation (3.19); This ends the proof of proposition 3.4. □

3.1.5 Numerical algorithm for monotonous schemes of the form

$$S(\nu, x, u(x), u) = 0$$

In section 3.1.1, we have described the monotonous schemes of the form $S(\nu, x, u(x), u) = 0$. In section 3.1.2, theorem 3.1 provides sufficient conditions ensuring the stability of such schemes. Later, theorem 3.3 establishes that the strong uniqueness property involves the convergence of the solutions u^ν toward the unique viscosity solution of the associated equation (section 3.1.4). For a fixed continuous mesh $\nu \in \mathcal{M}$, we are now going to describe an algorithm that

computes an approximation of u^ν , on a finite discret mesh \mathcal{X} compatible with ν (see below). We also prove the convergence of our algorithm. It is important to keep in mind that this algorithm converges toward u^ν but not toward the viscosity solution.

Let us fix $\nu \in \mathcal{M}$.

Definition 3.7 *We say that a set $\mathcal{X} \subset \bar{\Omega}$ is a “finite discret mesh compatible with ν ” if \mathcal{X} is finite and if $\forall x \in \mathcal{X}, \mathcal{V}_x \subset \mathcal{X}$.*

Example : Let us consider a canonical mesh ν characterized by

$$\rho = (h_1, \dots, h_N). \text{ Let us denote } x_k = \begin{pmatrix} k_1 h_1 \\ \vdots \\ k_N h_N \end{pmatrix} \text{ for } k \text{ in } \mathbb{Z}^N. \text{ Now, let}$$

us denote $\mathcal{X} = \{x_k; k \in \mathbb{Z}^N\} \cap \bar{\Omega}$. If $\bar{\Omega}$ is bounded, then \mathcal{X} is a finite mesh compatible with the canonical mesh ν .

The following algorithm computes for all $x \in \mathcal{X}$ a sequence of approximations U_x^n of $u^\rho(x)$ (let us emphasize that \mathcal{X} is a finite set):

Algorithm 3.1 *1. Initialisation ($n = 0$):*

$$\forall x \in \mathcal{X}, \quad U_x^0 = u_0(x),$$

where u_0 is a subsolution of the considered scheme.

2. Choice of a point x in the discret mesh \mathcal{X} and modification (step $n + 1$) of U_x^n : We choose

$$U^{n+1} = \sup \{V = (V_y)_{y \in \mathcal{X}} \text{ such that } \forall y \neq x, \quad V_y = U_y^n \text{ and } S(\rho, x, V_x, V) = 0\}.$$

In other words, we choose U^{n+1} such that

$$\begin{cases} U_y^{n+1} = U_y^n & \text{if } y \neq x, \\ U_x^{n+1} = \max \{ t \mid S(\rho, x, t, U^n) = 0 \}. \end{cases}$$

3. Choose the next pixel x in such a way that all points of the discret mesh \mathcal{X} are regularly visited and go back to 2.

Definition 3.8 *The algorithm 3.1 is well-defined if for all steps, the set of V 's defined at step (2) of the algorithm, is not empty and bounded; in other words, if for all steps we can compute the next approximation.*

We have the following theorem:

Theorem 3.5 *If the hypotheses of theorem 3.1 are satisfied, algorithm 3.1 is well-defined and the constructed sequence U^n is increasing and converges when $n \rightarrow +\infty$ towards the solution u^ν of the considered scheme.*

Proof. The elements of the sequence U^n are the restrictions to \mathcal{X} of the functions u_n introduced in the proof of the remark R15.2 (page 103). □

Remarks 20.

R20.1 - The algorithm we propose here is a Gauss-Seidel algorithm. The associated Jacobi algorithm also converges (see the proof of theorem 3.1), nevertheless it is less effective.

R20.2 - Let us emphasize the fact that in practice, the limit does not depend on the particular path used to traverse the pixels. Nevertheless, the convergence velocity strongly depends on this choice. For example, the strategy which consists in following back and forth the path indicated in figure 3.2 is the most effective one we have tested so far³.

R20.3 - If hypotheses (H16’), (H19’) and (H20’) described in the remark R15.3 (page 104) are verified then the conclusion of theorem 3.5 holds even if the initial function u_0 (used at step 1 of algorithm 3.1) is a supersolution.

R20.4 - Since the theorem 3.1 does not impose regularity hypotheses with respect to the space variable x , therefore such hypotheses are also not required for ensuring the convergence of the computed solutions toward the solutions of the schemes; see remark R15.4 at page 105.

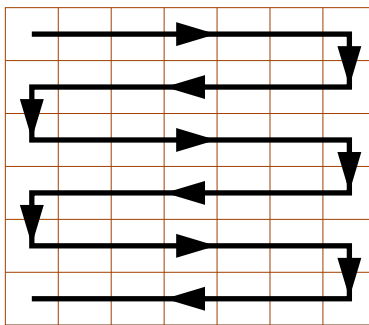


Figure 3.2: Most effective path we have tested.

³Path described by Dupuis and Oliensis in [47].

3.2 Application to the “classical” Shape from Shading problem

As in sections 3.1.3.2 and 3.1.4, for simplicity we assume that the mesh is canonical and we identify ν and ρ .

3.2.1 Decentered schemes for the “classical” SFS problem

In the previous section, we have described schemes allowing to approximate the HJB equations. In sections 3.1.3 and 3.1.4, we proved theorems and propositions which ensure the stability and the convergence (toward the viscosity solution) of these schemes.

In this section, we show that these results apply to the “classical” Shape from Shading problem.

3.2.1.1 Stability of the Decentered schemes for the “classical” SFS problem

In sections 2.1 and 2.2, we show that the classical modelings of the SFS problem lead to solving PDEs and that the associated Hamiltonians are special cases of a “generic” Hamiltonian H_g . In section 2.2.3 we proved that the “generic” Hamiltonian H_g is a HJB Hamiltonian. Therefore the implicit (and semi implicit) schemes we described in section 3.1.2 allow to approximate SFS PDEs. Following the notations introduced in Definition 2.4 (page 64), we have $\lambda = 0$, $N = 2$, and Ω is bounded.

By using proposition 3.1 stated on page 106, we can prove the stability of the decentered schemes with SFS Hamiltonians.

- First, it is easy to verify that the functions $f_g(x, \cdot)$ and $l_g(x, \cdot)$ associated with the generic Hamiltonian H_g (see at the page 68) verify the hypotheses (H6') and (H7'). Also, x being fixed, we have for the generic Hamiltonian H_g ,

$$\forall a \in A, f_g(x, a) = 0 \iff \mathbf{w}_x = 0 \text{ and } \kappa_x = 0$$

(since $f_g(x, 0) = 0$ involves⁴ $\mathbf{w}_x = 0$; we conclude by using the definition of Dil_x , equation (2.26) on page 68, the fact that $\mu_x \neq 0$ and $\nu_x \neq 0$).

Therefore the hypothesis (H22) is true iff for all x in $\overline{\Omega}$, $\kappa_x \neq 0$ or $\mathbf{w}_x \neq 0$. Also, we have

- For $H_{R/T}^{orth}$ and $H_{D/O}^{orth}$, we have $\mathbf{w}_x = \mathbf{l}$, therefore, if $\mathbf{l} \neq 0$ then the hypothesis (H22) holds ($I(x)$ can be null). In the case where $\mathbf{l} = 0$, the hypothesis (H22) holds iff $I(x) \neq 0$.

⁴See equation (2.33) on page 73.

- For H_{Eiko}^{orth} and H_F^{pers} , the hypothesis (H22) holds iff $I(x) \neq 0$.
- For $H_{P/F}^{pers}$, $\mathbf{w}_x = 0$ iff $x = -\frac{f}{\gamma}\mathbf{1}$. Therefore the hypothesis (H22) holds iff $I(-\frac{f}{\gamma}\mathbf{1}) \neq 0$.

Remark 21. In practice, for H_{Eiko}^{orth} and H_F^{pers} , and for $H_{P/F}^{pers}$, H_2^{pers} , $H_{R/T}^{orth}$ and $H_{D/O}^{orth}$ with $\mathbf{1} = 0$, there are no shadows, therefore, $I(x)$ is never null.

• Second,

- since the intensity image I verifies $I(x) \leq 1$, proposition 3.2 (page 107) applies to the SFS Hamiltonians H_{Eiko}^{orth} , $H_{(0,0,1)}^{orth}$, H_F^{pers} , $H_{(0,0,1)}^{pers}$, $H_{D/O}^{orth}$ and H_2^{pers} . Thus for these SFS Hamiltonians, the associated decentered schemes (3.11) have subsolutions.
- Concerning the Hamiltonian $H_{R/T}^{orth}$, we prove that $u_0(x) := -\frac{1}{\gamma}\mathbf{1} \cdot x + C$ (where C is chosen such that $\forall x \in \bar{\Omega}$, $u_0(x) \leq \min_y \varphi(y)$) is a subsolution of the associated decentered scheme (3.11).

Proof.

◊ $\forall x \in \Omega_\rho$, we have $S(\rho, x, u_0(x), u_0) = \tilde{S}(\rho, x, u_0(x), u_0)$.

Since

$$\begin{aligned} \frac{u_0(x) - u_0(x - h_1 \vec{e}_1)}{h_1} &= -\frac{\alpha}{\gamma}, & \frac{u_0(x) - u_0(x + h_1 \vec{e}_1)}{h_1} &= \frac{\alpha}{\gamma}, \\ \frac{u_0(x) - u_0(x - h_2 \vec{e}_2)}{h_2} &= -\frac{\beta}{\gamma}, & \frac{u_0(x) - u_0(x + h_2 \vec{e}_2)}{h_2} &= \frac{\beta}{\gamma}, \end{aligned}$$

then

$$\begin{aligned} S(\rho, x, u_0(x), u_0) &= \sup_{a \in A} \{[-f(x, a)_- + f(x, a)_+] \cdot \frac{1}{\gamma}\mathbf{1} - l(x, a)\} \\ &= \sup_{a \in A} \{f(x, a) \cdot \frac{1}{\gamma}\mathbf{1} - l(x, a)\} \\ &= H(x, -\frac{1}{\gamma}\mathbf{1}) \\ &\leq 0. \end{aligned}$$

◊ $\forall x \in \mathfrak{b}\Omega_\rho$,

$$S(\rho, x, u_0(x), u_0) = u_0(x) - \varphi(x) \leq 0.$$

□

3.2 Application to the “classical” Shape from Shading problem 123

- We have not found subsolutions of the decentered scheme (3.11) associated with the Hamiltonian $H_{P/F}^{pers}$. The subsolution (of the Hamiltonian $H_{P/F}^{pers}$) proposed in section 2.2.6 (at the page 78) is not a subsolution the decentered scheme (3.11). This shows the interest of the Hamiltonian H_2^{pers} , and more generally the interest of the Hamiltonians which verify $H(x, 0) \leq 0$.

- Third, since

$$l_g(x, a) = - [K_x \kappa_x \sqrt{1 - |a|^2} + \kappa_x ({}^t R_x \mathbf{v}_x) \cdot a + c_x],$$

we have: if κ_x , K_x , \mathbf{v}_x and c_x are bounded then the running cost l_g of H_g is bounded. Moreover, since

$$f_g(x, a) = - [Dil_x a + \mathbf{w}_x],$$

we have: if for all x in $\bar{\Omega}$ we denote⁵ $a_x = Dil_x^{-1} \left[\begin{pmatrix} 1 \\ 1 \end{pmatrix} - \mathbf{w}_x \right]$, then we

have $f_g(x, a_x) = - \begin{pmatrix} 1 \\ 1 \end{pmatrix}$. Therefore proposition 3.3 (page 107) applies with the generic Hamiltonian H_g . Hence the subsolutions are bounded by a same constant (uniformly for ρ in \mathcal{M}_K). Obviously, as a consequence, this result holds with all⁵ SFS Hamiltonians H_*^{orth} and H_*^{pers} .

Consequently, proposition 3.1 applies with all SFS Hamiltonians⁶. Therefore, for all SFS Hamiltonians, the implicit (and therefore semi-implicit) decentered schemes are stable (uniformly for ρ in \mathcal{M}_K).

Remark 22. Let us emphasize that the continuity of the intensity image I is not required for obtaining the stability of our SFS schemes. Therefore our numerical SFS method is still relevant when the intensity image is discontinuous and when there are shadows.

3.2.1.2 Convergence toward the viscosity solutions of SFS

In the previous subsection we have described some sufficient conditions ensuring the stability of the implicit schemes (and therefore of the semi-implicit schemes)

⁵ We assume that $\forall x \in \bar{\Omega} \kappa_x \neq 0$. If there exist some x such that $\kappa_x = 0$ and if for example \mathbf{w}_x is a nonnull constant function (this holds for example with $H_{R/T}^{orth}$ and $H_{D/O}^{orth}$ when $\mathbf{1} \neq 0$), then we can choose $a_x = 0$.

⁶Except for $H_{P/F}^{pers}$, because we have not found subsolutions of the associated scheme.

associated with the “classical” SFS Hamiltonians. In other words, the SFS schemes we propose have uniformly bounded solutions. Now, we claim that (with some weak hypotheses) these solutions converge towards the viscosity solutions of the SFS PDEs when the size of the mesh vanishes to zero. This assertion can be proved easily by using proposition 3.5 (stated on page 115):

1. If the intensity image I is Lipschitz continuous then hypotheses (H6)-(H8) are verified for all the SFS Hamiltonians⁷: see section 2.2.4.2 in which we detail the conditions for which the generic Hamiltonian H_g verifies the hypotheses (H6)-(H8).
2. Questions about subsolutions have also been studied in the previous subsection.
3. Some conditions involving the strong uniqueness property for the SFS equations are described at the end of section 2.2.6.

The reader will conclude without difficulty.

3.2.2 New “generic” algorithms for the “classical” Shape from Shading

3.2.2.1 Two new “generic” algorithms for the “classical” Shape from Shading problem

In section 3.1.2 we have described two approximation schemes of the form $S(\rho, x, u(x), u) = 0$ (an implicit scheme and a semi-implicit one) allowing to approximate the solutions of HJB PDEs. Since the various models of the “classical” SFS problem we present all led to HJB equations, we have at our disposal two new approximation schemes, hence *two new algorithms* for computing numerical solutions of each formulation of the SFS problem.

We have *implemented* the algorithms associated with the implicit scheme and with the semi-implicit scheme, for the “*generic SFS*” Hamiltonian. Thus the code applies to all the “classical” SFS Hamiltonians. Let us emphasize the interest of the “generic” formulation of the SFS problems. In effect, instead of implementing an algorithm for each formulation of the SFS problem, we implement only one algorithm. In particular, a single algorithm allows to compute numerical solutions of the “perspective SFS” problem and of the “orthographic SFS” problem.

In return, our code is clearly not optimal for a particular formulation of the SFS problem. Nevertheless, it is very easy to optimize the code for a specific algorithm.

⁷For the Hamiltonian H_{Eiko}^{orth} , we also need to impose $I > 0$ on $\bar{\Omega}$. In practice, this is not a problem; see the remark below.

3.2 Application to the “classical” Shape from Shading problem 125

In other respects, let us remark that the implementation of the implicit algorithm is more difficult than that of the semi-implicit algorithm. Also, the cost of one iteration of the implicit scheme is greater than the cost of one iteration of the semi-implicit scheme. Nevertheless, the number of iterations required for reaching the convergence is much smaller for the implicit scheme than for the semi-implicit scheme. For a quantitative comparison see section 3.2.4.

Remark 23. The algorithm proposed by Rouy and Tourin in [134] is a particular case of the implicit algorithm with the Eikonal Hamiltonian.

The first algorithm proposed by Dupuis and Oliensis in [47] is a particular case of the semi-implicit algorithm with the Hamiltonian $H_{D/O}^{orth}$ ⁸.

Therefore, from an algorithmic point of view, here, we generalize and unify the work of Rouy and Tourin [134] and the work of Dupuis and Oliensis [47]. Let us remind the reader that the implicit scheme and the semi-implicit scheme have the same solutions; see remark R12.2 in section 3.1.2.

3.2.2.2 Comments about initialisation

The algorithms we propose here are *iterative*. Also, the behaviour of the sequence of approximations U^n strongly depends on the choice of the initial surface u_0 . Nevertheless, in this section, we prove that in all cases (when u_0 is a subsolution and when u_0 is a supersolution) the sequence of approximations (computed with the implicit or the semi-implicit algorithm) converges toward the solutions of the scheme. Finally, we remark that the convergence velocity strongly depends on the choice of u_0 .

1. If u_0 is a subsolution :

- By using theorem 3.5 (stated on page 120), proposition 3.1 (stated on page 106) and the previous subsection, the reader will verify easily that, if u_0 is a subsolution⁹, then the numerical approximations computed with the associated *implicit* SFS algorithms converge toward the solutions of the scheme associated with the SFS Hamiltonians.

⁸In [47], Dupuis and Oliensis describe two schemes and algorithms for computing numerical solutions of the “classical” SFS problem. The first algorithm corresponds with the one associated with the semi-implicit scheme; the second algorithm is an other semi-implicit scheme based on the differential games instead of the control theory. Let us note that the both schemes of Dupuis and Oliensis have exactly the same solutions. Therefore they have also the same solutions as our implicit scheme.

⁹The semi-implicit schemes and the implicit schemes have exactly the same supersolutions, the same subsolutions and the same solutions

- Concerning the algorithms provided by the *optimal semi-implicit scheme* (described in the remark R12.1 at page 97) the reader will verify without difficulty that the hypotheses of theorem 3.1 are satisfied with all SFS Hamiltonians:
 - the hypotheses (H16) and (H17) are always true,
 - the hypothesis (H18) is true if for all x in $\overline{\Omega}$, the functions $f(x, \cdot) : a \mapsto f(x, a)$ and $l(x, \cdot) : a \mapsto l(x, a)$ verify the hypotheses (H6') and (H7'),
 - the subsolutions of the semi-implicit schemes are exactly the same as the subsolutions of the implicit schemes. Therefore, the study of the hypotheses (H19) and (H20) has been done previously.

Thereby, if u_0 is a subsolution of the scheme, then the numerical approximations computed with the SFS *semi-implicit* algorithms converge toward the solutions of the associated scheme.

Nevertheless, let us emphasize that in practice, the semi-implicit algorithms starting from a subsolution are really not effective.

Remark 24. Let us note that in [134], Rouy and Tourin start the algorithm from subsolutions.

2. If u_0 is a supersolution:

We prove easily that the hypotheses (H19') and (H20') described in the remark R15.3 (page 104) are verified with the SFS implicit schemes and the SFS semi-implicit schemes. Therefore, if the hypothesis (H16') holds, we can conclude that:

if the initial function u_0 is a supersolution, then the numerical approximations computed with the SFS implicit / semi-implicit algorithms converge toward the solutions of the associated schemes.

Clearly, the hypothesis (H16') holds with the semi-implicit schemes. Nevertheless, (H16') is not always true with the implicit schemes. For proving that (H16') holds with a specific implicit scheme, we can use the following proposition:

Proposition 3.6 *Let us consider an implicit scheme S as presented in section 3.1.2. We assume that A is a compact subset of \mathbb{R}^N , that for all $x \in \overline{\Omega}$, the function $f(x, \cdot) : a \mapsto f(x, a)$ is a homeomorphism (we*

3.2 Application to the “classical” Shape from Shading problem 127

denote $f^{-1}(x, \cdot)$ its inverse), and that the function $l(x, \cdot) : a \mapsto l(x, a)$ is continuous on A .

Therefore: If $\lambda \neq 0$, then

$$\lim_{t \rightarrow -\infty} S_{\rho, x, u}(t) \leq 0,$$

else, if there does not exist $a \in A$ such that $f(x, a) = 0$ or if

$$l(x, f^{-1}(x, 0)) \geq 0,$$

then we have the same conclusion.

Remark 25.

Since for the “generic” Hamiltonian, we have $H_g^*(x, q) = l_g(x, [-f_g]^{-1}(x, q))$ and $f_g^{-1}(x, 0) = [-f_g]^{-1}(x, 0)$ (we note $[-f_g]$ the opposite of the function f_g), then the condition $l_g(x, f_g^{-1}(x, 0)) \geq 0$ is equivalent to $H^*(x, 0) \geq 0$.

By the previous proposition and the remark 25, for all SFS Hamiltonians with nonnegative running cost, (H_{Eiko}^{orth} , $H_{(0,0,1)}^{orth}$, H_F^{pers} , $H_{(0,0,1)}^{pers}$, H_2^{pers} and $H_{D/O}^{orth}$), the numerical approximations computed with an implicit algorithm converge toward the solution of the adequate scheme, when u_0 is a supersolution.

The reader will verify easily that this is also true for the Hamiltonian $H_{R/T}^{orth}$. Indeed, we have,

$$f_{R/T}^{-1}(x, 0) = -\frac{1}{I(x)} \mathbf{1}$$

and

$$l_{R/T}(x, f_{R/T}^{-1}(x, 0)) = -\left[\sqrt{I(x)^2 - |\mathbf{1}|^2} - \sqrt{1 - |\mathbf{1}|^2}\right] \geq 0$$

(because $I(x) \leq 1$).

Remarks 26.

r26.1 - By considering for example the Hamiltonian $H_{R/T}^{orth}$, one can verify that, when x converges toward a singular point x_0 , then

$$\lim_{x \rightarrow x_0} l_g(x, f_g^{-1}(x, 0)) = 0.$$

Thus, in a neighbourhood of such a point, the equation in t

$$S(\rho, x_{ij}, t, U) = 0 \tag{3.20}$$

is almost degenerate. In particular, if we do not implement carefully the resolving of the equation (3.20), it is possible that *numerically*, we do not obtain solutions of the equation (3.20) (even if theoretically there exists a solution). In this case, instead of solving the equation (3.20), we can compute the value t which minimizes $S(\rho, x_{ij}, t, U)$. Another alternative consists in corrupting slightly the values of the intensity image, considering the image I_ε instead of I ; where I_ε is the image: $I_\varepsilon(x) = I(x)$ if $I(x) < 1 - \varepsilon$, else $I_\varepsilon(x) = 1 - \varepsilon$; for a small $\varepsilon > 0$ (see section 4.6; in particular section 4.6.2).

R26.2 - In some cases, it is easy to compute supersolutions. For example, one can verify that

$$u_0(x) = \frac{\gamma}{|\mathbf{1}|^2} \mathbf{1} \cdot x + c$$

(where $c = -\min_{y \in b\Omega_\rho} \frac{\gamma}{|\mathbf{1}|^2} \mathbf{1} \cdot y + \max_{y \in b\Omega_\rho} \varphi(y)$) is a supersolution of the schemes (with DBC) associated with the Hamiltonian $H_{R/T}$. Nevertheless, let us note that, in practice, we do not compute the supersolution u_0 required for starting the algorithm. In effect a large constant function u_0 with the appropriated boundary data does the trick!

R26.3 - Let us note that in [47], Dupuis and Oliensis start the algorithm from supersolutions.

About the convergence velocity

Finally, let us remark that *in practice, the speed of convergence strongly depends on the initial surface u_0 used at step one of the algorithm. For an optimal velocity, we can start from a supersolution*; a quantitative comparison can be found in chapter 3.2.4.

Proof of proposition 3.6

Let us remind the reader the

Proposition 3.6 *Let us consider an implicit scheme S as presented in section 3.1.2. We assume that A is a compact subset of \mathbb{R}^N , that for all $x \in \overline{\Omega}$, the function $f(x, \cdot) : a \mapsto f(x, a)$ is a homeomorphism (we denote $f^{-1}(x, \cdot)$ its inverse), and that the function $l(x, \cdot) : a \mapsto l(x, a)$ is continuous on A .*

Therefore: If $\lambda \neq 0$, then

$$\lim_{t \rightarrow -\infty} S_{\rho, x, u}(t) \leq 0,$$

3.2 Application to the “classical” Shape from Shading problem 129

else, if there does not exist $a \in A$ such that $f(x, a) = 0$ or if

$$l(x, f^{-1}(x, 0)) \geq 0,$$

then we have the same conclusion.

Proof. We consider the case where $\lambda = 0$ (the case where $\lambda \neq 0$ is easier to prove). By contradiction, let us assume that

$$\lim_{t \rightarrow -\infty} S_{\rho, x, u}(t) > 0,$$

that is to say

$$\lim_{t \rightarrow -\infty} \sup_{a \in A} \left\{ \sum_{i=1}^N (-f_i(x, a)) \frac{t - u(x + s_i(x, a) h_i \vec{e}_i)}{-s_i(x, a) h_i} - l(x, a) \right\} > 0, \quad (3.21)$$

where $s_i(x, a)$ is the sign of $f_i(x, a)$.

For all $(s_1, \dots, s_N) \in \{\pm 1\}^N$, we denote

$$A_{s_1, \dots, s_N} := \{a \in A \mid \forall i = 1..N, s_i f_i(x, a) \geq 0\}.$$

By (3.21) there exists $(s_1, \dots, s_N) \in \{\pm 1\}^N$, such that

$$\lim_{t \rightarrow -\infty} \sup_{a \in A_{s_1, \dots, s_N}} \left\{ \sum_{i=1}^N (-f_i(x, a)) \frac{t - u(x + s_i h_i \vec{e}_i)}{-s_i h_i} - l(x, a) \right\} > 0. \quad (3.22)$$

Since $f(x, \cdot)$ and $l(x, \cdot)$ are continuous, there exists a control a_t maximizing the supremum of (3.22). Therefore, we have

$$\lim_{t \rightarrow -\infty} \sum_{i=1}^N \frac{f_i(x, a_t)}{s_i h_i} (t - u(x + s_i h_i \vec{e}_i)) - l(x, a_t) > 0. \quad (3.23)$$

We now proceed in two steps.

◦ Now, let us assume that

$$\text{there does not exist } a \text{ in } A \text{ such that } f(x, a) = 0. \quad (3.24)$$

Therefore, by compactness of A_{s_1, \dots, s_N} , there exists $\varepsilon > 0$ such that

$$\forall a \in A_{s_1, \dots, s_N}, \quad \sum_{i=1}^N \frac{f_i(x, a)}{s_i h_i} \geq \varepsilon.$$

Therefore, for all t sufficiently small ($t \leq \min_i u(x + s_i h_i \vec{e}_i)$),

$$\sum_{i=1}^N \frac{f_i(x, a_t)}{s_i h_i} (t - u(x + s_i h_i \vec{e}_i)) \leq \varepsilon \left(t - \min_i u(x + s_i h_i \vec{e}_i) \right).$$

Since $l(x, \cdot)$ is bounded¹⁰,

$$\lim_{t \rightarrow -\infty} \sum_{i=1}^N \frac{f_i(x, a_t)}{s_i h_i} (t - u(x + s_i h_i \vec{e}_i)) - l(x, a_t) = -\infty.$$

We obtain a contradiction with (3.23). Therefore (3.24) does not hold.

◦ Henceforth, we assume that there exists a in A such that $f(x, a) = 0$. Now, we claim that

$$\lim_{t \rightarrow -\infty} f(x, a_t) = 0.$$

Proof. By contradiction, let us assume that there exist $\varepsilon_1 > 0$ and a sequence $t_n \rightarrow -\infty$ such that $\forall n$

$$|f(x, a_{t_n})| \geq \varepsilon_1.$$

So, there exists $\varepsilon_2 > 0$ such that

$$\forall n \in \mathbb{N}, \quad \sum_{i=1}^N \frac{f_i(x, a_{t_n})}{s_i h_i} \geq \varepsilon_2.$$

Since $l(x, \cdot)$ is bounded, we obtain as above that

$$\lim_{n \rightarrow +\infty} \sum_{i=1}^N \frac{f_i(x, a_{t_n})}{s_i h_i} (t_n - u(x + s_i h_i \vec{e}_i)) - l(x, a_{t_n}) = -\infty.$$

This contradicts equation (3.23). □

So $\lim_{t \rightarrow -\infty} f(x, a_t) = 0$. Also, $f(x, \cdot)$ being a homeomorphism, we obtain

$$\lim_{t \rightarrow -\infty} a_t = f^{-1}(x, 0).$$

In other respects, since

$$\lim_{t \rightarrow -\infty} \sum_{i=1}^N \frac{f_i(x, a_t)}{s_i h_i} (t - u(x + s_i h_i \vec{e}_i)) - l(x, a_t) > 0,$$

and since for all t sufficiently small ($t \leq \min_i u(x + s_i h_i \vec{e}_i)$), we have

$$\sum_{i=1}^N \frac{f_i(x, a_t)}{s_i h_i} (t - u(x + s_i h_i \vec{e}_i)) \leq 0,$$

then

$$\lim_{t \rightarrow -\infty} -l(x, a_t) > 0.$$

By continuity of $l(x, \cdot)$, we conclude that

$$l(x, f^{-1}(x, 0)) < 0.$$

¹⁰Because $l(x, \cdot)$ is continuous on the compact set A .

□

3.2.3 Pushing things to the limit: SFS with discontinuous images and black shadows

Among the difficulties encountered when attempting to solve the SFS problem, the intensity discontinuities such as those caused by black shadows are among the most difficult to deal with. Despite the fact that the notion of viscosity solutions provides a natural framework for dealing with non smooth surfaces¹¹ (with edges) *this theory does not yet apply to discontinuous images*¹² (and hence to black shadows). Technically, when the Hamiltonian is discontinuous with respect to the space variable x (which is the case in SFS when the intensity image is discontinuous), the main difficulty is the loss of uniqueness of the viscosity solution. Note that, in the particular case of the black shadows, this difficulty is increased by the loss of coercivity of the Hamiltonian.

In order to deal with black shadows, Lions et al. [96] do not “recover” surfaces in the areas of 0 intensity and pose the problem in terms of boundary conditions. This is not necessary since, as noted in [56], in the black shadows areas the surface formed by the rays of light grazing the solution surface, verify the irradiance equation, see figure 3.3. Thus, for recovering a solution, we do not need, as in [96], to separate the “shading areas” and the “shadow areas” and in general¹³ our generic algorithm graciously computes approximations of the exact solutions in shading areas and the grazing rays of light in the black shadows areas (as does the algorithm proposed by Falcone [56] for the “orthographic SFS”), see figures 3.3 and 3.11.

Finally all the results presented in section 3.2.1.1 and section 3.2.2 (the stability of our approximation schemes and the convergence of the numerical solutions computed by our algorithms) *hold even when the image contains discontinuities and black shadows*, even though the theory of viscosity solutions does not yet apply to this case, see for example the remark 17 at the page 108 and the remark 22 at the page 123. As an illustration of this, the pyramid example displayed in figures 3.6, 3.13 and 3.15 shows the ability of our numerical algorithms to deal with discontinuous images while figure 3.11 shows their ability to deal with black shadows.

¹¹Viscosity solutions are weak (i.e. non differentiable) solutions.

¹²Most probably, some recent work [112, 78, 146, 28] on the Eikonal equation will shortly remove this limitation.

¹³If we assume that the critical points and the boundary of the image are not covered by the shadows.

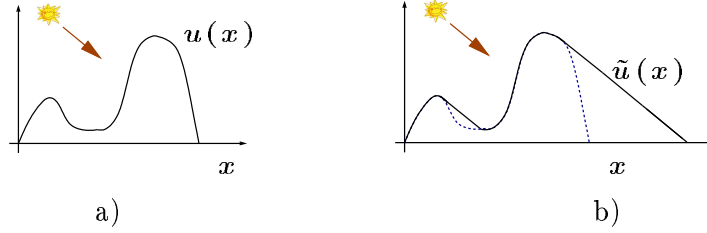


Figure 3.3: a) Original surface u ; b) Solution computed by our and Falcone’s algorithms [56].

3.2.4 Experimental results

We have implemented for the “**generic Hamiltonian**” H_g the algorithms described in the previous sections for approximating the solutions of the “schemes with Dirichlet conditions”

$$S(\rho, x, t, u) = \begin{cases} \tilde{S}(\rho, x, t, u) & \text{if } x \in \Omega_\rho, \\ t - \varphi(x) & \text{if } x \in \text{b}\Omega_\rho, \end{cases}$$

for the **implicit** decentered scheme defined by

$$\tilde{S}(\rho, x, t, u) = \sup_{a \in A} \left\{ \sum_{i=1}^N (f_i(x, a))_- \frac{t - u(x - h_i \vec{e}_i)}{h_i} + \sum_{i=1}^N (f_i(x, a))_+ \frac{t - u(x + h_i \vec{e}_i)}{h_i} - l(x, a) \right\},$$

and for the (optimal) **semi-implicit** decentered scheme defined by

$$\tilde{S}(\rho, x, t, u) = \left(1 + \frac{\lambda}{\sum_{j=1}^N |f_j(x, a_0)|/h_j} \right) t - \sum_{i=1}^N \frac{|f_i(x, a_0)|/h_i}{\sum_{j=1}^N |f_j(x, a_0)|/h_j} u(x + s_i h_i \vec{e}_i) - \frac{1}{\sum_{j=1}^N |f_j(x, a_0)|/h_j} l(x, a_0),$$

where a_0 is the optimal control of (3.6); see remark 12 at page 97.

Remark 27.

- In [127] and [128], we have implemented and tested the algorithm associated with the implicit decentered scheme for the “orthographic SFS” problem (with the Hamiltonian $H_{R/T}^{orth}$) in the case where $\mathbf{l} = (\alpha, 0)$.
- In [120], we have implemented and tested the algorithm associated with the implicit decentered scheme for the “perspective SFS” problem.

3.2 Application to the “classical” Shape from Shading problem 133

- In [127, 128, 120] we start the algorithms from subsolutions.

Let us emphasize that in this chapter **we assume that we have the exact knowledge of the Dirichlet boundary data on $\partial\Omega' = \partial\Omega \cup \{x \mid I(x) = 1\}$** . This is required for characterizing a solution (see section 2.2.6). In other words, in order to compute the correct solution (i.e. the original surface used for creating the image; remember that there exist several viscosity solution), **we must provide the “height” of the solution at the boundary of the image and at all singular points** (the pixels x_{ij} such that $I(x_{ij}) = 1$).

In the following subsections, we compare the results obtained with all our algorithms. This comparison is based on the speed of convergence and the reconstruction error (the groundtruth data is available since in these experiments, we deal with synthetic images).

We start with the algorithms associated with the orthographic SFS problem. In this context, we emphasize the comparison of the implicit and semi-implicit algorithms, and the influence of the initial surface u_0 on the speed of convergence. We have tested our algorithms with synthetic images generated by shapes with several degrees of regularity e.g. C^∞ (a paraboloid, a sinusoid and a smoothed vase, see figures 3.4, 3.5, 3.14), or C^0 (a pyramid, see figures 3.6, 3.15), to demonstrate the ability of our method to work with smooth and nonsmooth objects. Next, we deal with the perspective SFS algorithms.

In all the examples, the parameters are n , the number of iterations, ε_1 , ε_2 and ε_∞ the mean absolute errors between the reference and reconstructed surfaces measured according to the L_1 , L_2 and L_∞ norms, respectively, θ the angle of the direction of illumination with the z -axis. We denote $\mathbf{L} = (\mathbf{l}, \gamma)$ the light vector and f the focal length.

3.2.4.1 Experimental results for the “classical orthographic SFS”

Comparison of the implicit algorithm and the semi-implicit algorithm

We tested the orthographic SFS algorithms (i.e. the algorithms associated with the Hamiltonians H_*^{orth}) with synthetic images generated by an orthographic projection.

In all cases, we show the original object, the input image and the reconstructed surface.

First we show that the accuracy of the implicit algorithm is approximately the same as that of the semi-implicit algorithm. This confirms the prediction of the theory which states that an implicit scheme and its associated semi-implicit

scheme have the same solutions, and that the computed numerical approximations converge towards the solution of these schemes. Figures 3.4 and 3.5 show the reconstructions of smooth surfaces obtained by the implicit algorithm (associated with the Hamiltonian $H_{R/T}^{orth}$) and by the semi-implicit algorithm, starting from a subsolution and from a supersolution. Since, in practice, the combination of the semi-implicit algorithms with the subsolutions is really not effective, we only return the results obtained with the three other combinations. Also, in these three other cases, we recover almost exactly the same surface. Contrariwise, the numbers of iterations required for converging are very different. Globally, the number of iterations required for converging with a semi-implicit algorithm is very larger than with an implicit algorithm. For example, when u_0 is a supersolution, approximately 100 iterations are required for obtaining the sinusoidal surface with the semi-implicit algorithm (figure 3.5-d), when only 20 iterations are sufficient with the implicit algorithm (figure 3.5-e). Furthermore, the number of iterations required when the approximation sequence starts from a subsolution is very larger than when it starts from a supersolution. For the example of the sinusoidal surface displayed in figure 3.5, the implicit algorithm requires approximately 600 iterations for converging when u_0 is a subsolution; when only $\simeq 20$ iterations are required when u_0 is a supersolution.

Clearly, the optimal algorithm is the implicit algorithm starting from a supersolution.

To demonstrate the ability of our method to deal with nonsmooth objects, we have tested our algorithms with a pyramidal surface; see figure 3.6. The previous remarks about accuracy and speed of convergence are still true for nonsmooth surfaces.

Remarks 28.

r28.1 - In [47], Dupuis and Oliensis propose two numerical algorithms for the orthographic SFS. The scheme associated with their first algorithm corresponds with our semi-implicit scheme. Their second algorithm, based on the differential games, is faster than their first one because the control dependency is quadratic¹⁴. The scheme associated with this original algorithm is still semi-implicit; therefore, it is “theoretically” less effective than our implicit algorithm.

r28.2 - In figures 3.4, 3.5 and 3.6, we show results obtained by applying the Gauss-Seidel method. Convergence using the Jacobi updating is much slower. As explained by Dupuis and Oliensis [47] the expected convergence

¹⁴see [47], for more details...

3.2 Application to the “classical” Shape from Shading problem 135

iteration	ε_1 error	ε_2 error	ε_∞ error
30	0.0182615	0.0379	0.112334
60	0.0100561	0.0244	0.0664543
90	0.00679089	0.0178	0.050051
120	0.0049317	0.0128	0.0391274
150	0.0035902	0.0086	0.0336975
200	0.00202838	0.0032	0.0336975

Table 3.1: Errors associated to figure 3.7 (implicit algorithm starting from a subsolution).

iteration	ε_1 error	ε_2 error	ε_∞ error
8	0.0215886	0.0358	0.0881951
16	0.00840164	0.0157	0.056211
24	0.00420738	0.0086	0.0389878
32	0.00288298	0.0058	0.0335179
40	0.00234463	0.0042	0.0335179
48	0.00206178	0.0033	0.0335179

Table 3.2: Errors associated to figure 3.8 (semi-implicit algorithm starting from a supersolution).

time for the Jacobi method is on the order of the maximum length of the optimal path. In effect, when we perform an iteration (i.e. we once scan of all pixels) of the Jacobi method, the information is only able to propagate by “one pixel” along the optimal path. For a Gauss-Seidel method, the information is able to propagate all along the optimal path in only one iteration. Note that for obtaining convergences as fast as those we obtain, we need to use the path indicated in the remark 3.1.5. In effect, this path provides a homogeneous propagation¹⁵ of the information.

Figures 3.7-3.9 show the speed of convergence of the two algorithms for two different initial conditions, i.e. a subsolution (except for the semi-implicit scheme, as mentioned above) and a supersolution. Clearly, as shown in tables 3.1-3.3, the combination (implicit, supersolution) is the best.

Robustness to noise

We also show the stability of our method with respect to pixel noise. Uniformly distributed white noise has been added to all pixels of the input images and the corresponding reconstructed surfaces are shown, see figure 3.12

¹⁵i.e in all directions and in all senses

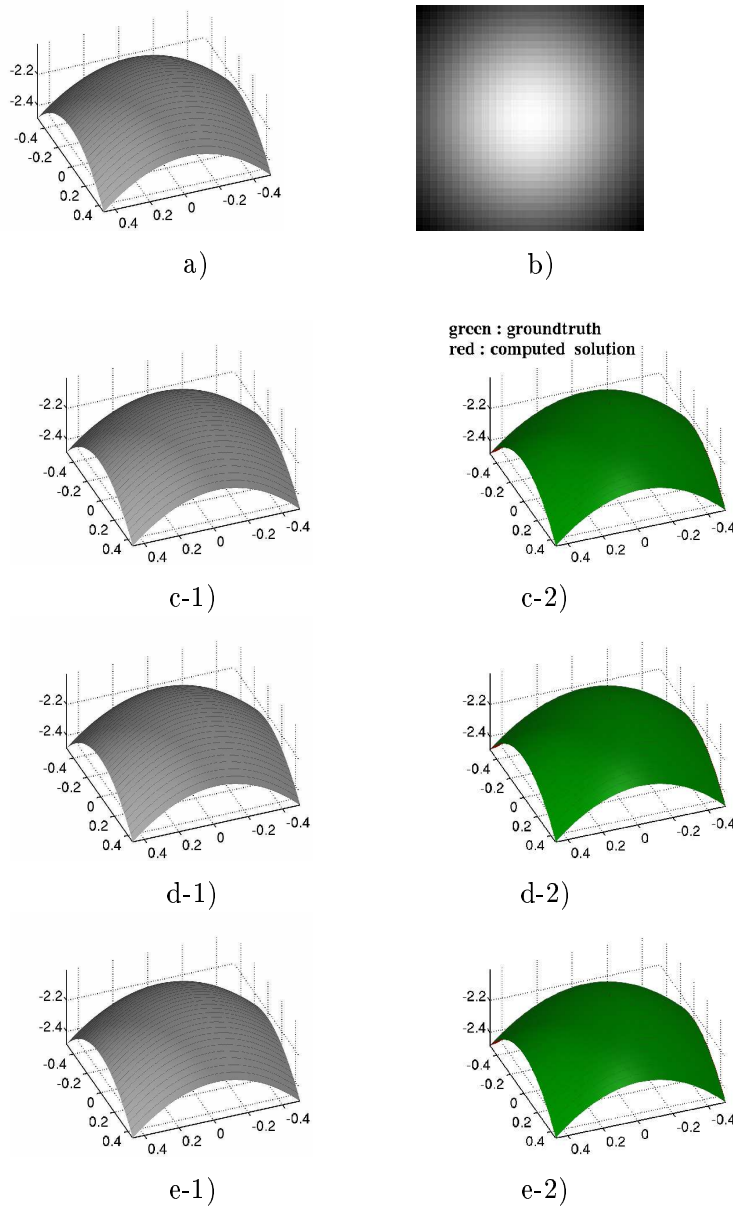


Figure 3.4: Results for a synthetic image generated by a paraboloidal surface sampled on a grid of size 32×32 with $\mathbf{l} = (0, 0)$ ($\theta \simeq 0^\circ$):

- a) original surface (groundtruth), b) original image,
- c) surface reconstructed from b) with the implicit algorithm starting from a subsolution: $n = 18, \varepsilon_1 = 0.0015, \varepsilon_2 = 0.0018, \varepsilon_\infty = 0.0021$;
- d) surface reconstructed from b) with the semi-implicit algorithm starting from a supersolution: $n = 15, \varepsilon_1 = 0.0014, \varepsilon_2 = 0.0016, \varepsilon_\infty = 0.0020$;
- e) surface reconstructed from b) with the implicit algorithm starting from a supersolution: $n = 5, \varepsilon_1 = 0.0015, \varepsilon_2 = 0.0018, \varepsilon_\infty = 0.0020$;

3.2 Application to the “classical” Shape from Shading problem 137

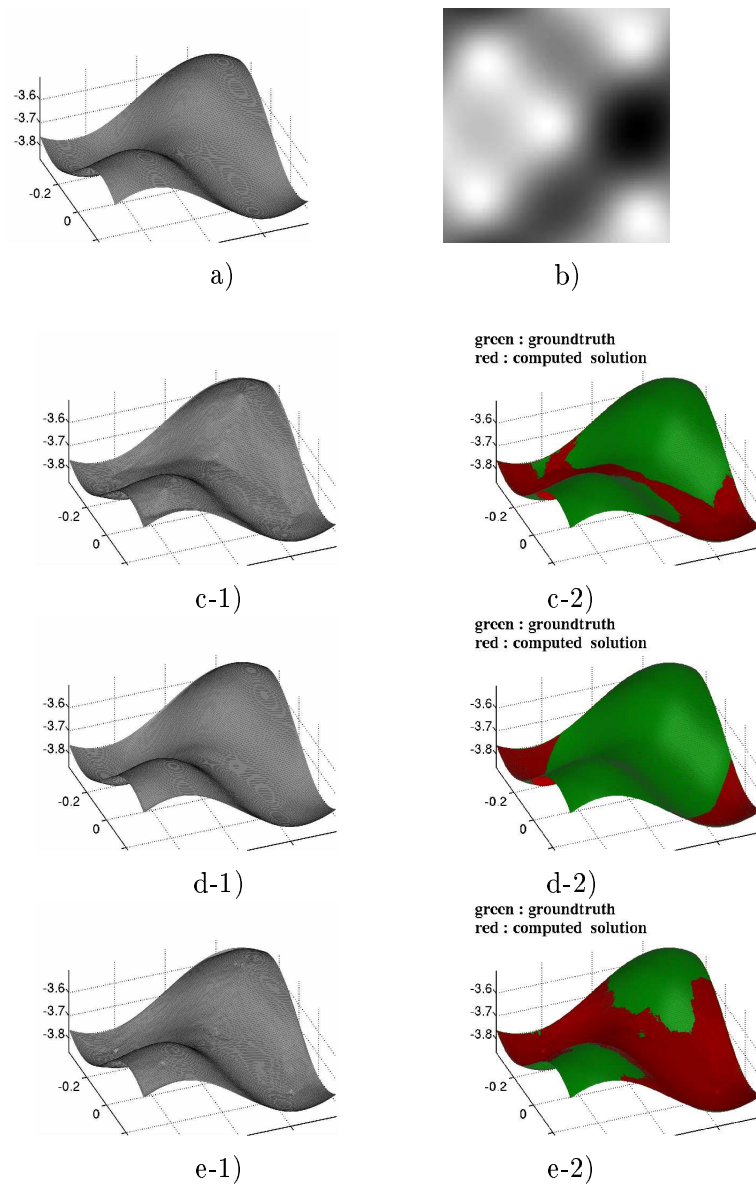


Figure 3.5: Results for a synthetic image generated by a sinusoidal surface sampled on a grid of size 200×200 with $\mathbf{l} = (0.1, 0.3)$ ($\theta \simeq 18.5^\circ$):

a) original surface, b) original image,

c) surface reconstructed from b) with the implicit algorithm starting from a subsolution: $n \simeq 700$, $\varepsilon_1 = 0.003902$, $\varepsilon_2 = 0.005762$, $\varepsilon_\infty = 0.00740$;

d) surface reconstructed from b) with the semi-implicit algorithm starting from a supersolution: $n \simeq 120$, $\varepsilon_1 = 0.003900$, $\varepsilon_2 = 0.005762$, $\varepsilon_\infty = 0.00747$;

e) surface reconstructed from b) with the implicit algorithm starting from a supersolution: $n \simeq 25$, $\varepsilon_1 = 0.003905$, $\varepsilon_2 = 0.005768$, $\varepsilon_\infty = 0.00747$;

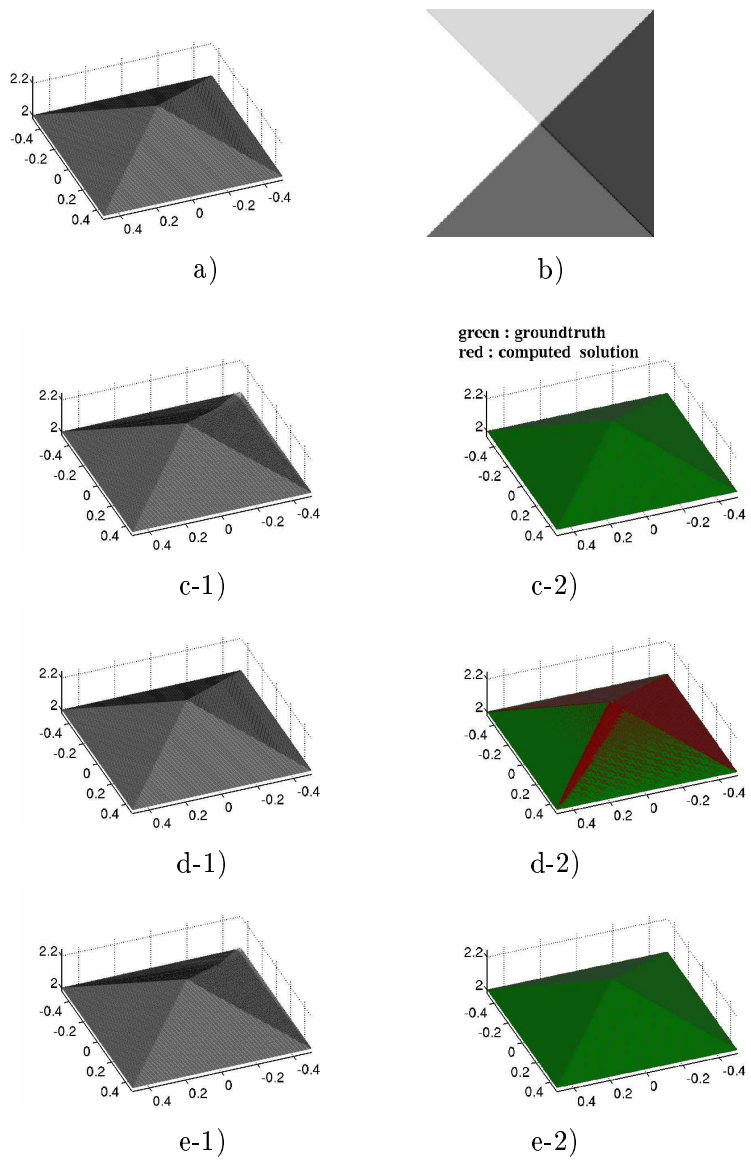


Figure 3.6: Results for a synthetic image generated by a pyramidal surface sampled on a grid of size 200×200 with $\mathbf{l} = (0.5, 0.3)$ ($\theta \simeq 35.6^\circ$):

- a) original surface, b) original image,
- c) surface reconstructed from b) with the implicit algorithm starting from a subsolution: $n \simeq 1000$, $\varepsilon_1 = 8.461e-05$, $\varepsilon_2 = 1.6116e-04$, $\varepsilon_\infty = 9.40e-04$;
- d) surface reconstructed from b) with the semi-implicit algorithm starting from a supersolution: $n \simeq 110$, $\varepsilon_1 = 8.461e-05$, $\varepsilon_2 = 1.6116e-04$, $\varepsilon_\infty = 9.40e-04$;
- e) surface reconstructed from b) with the implicit algorithm starting from a supersolution: $n \simeq 50$, $\varepsilon_1 = 8.461e-05$, $\varepsilon_2 = 1.6116e-04$, $\varepsilon_\infty = 9.40e-04$;

3.2 Application to the “classical” Shape from Shading problem 139

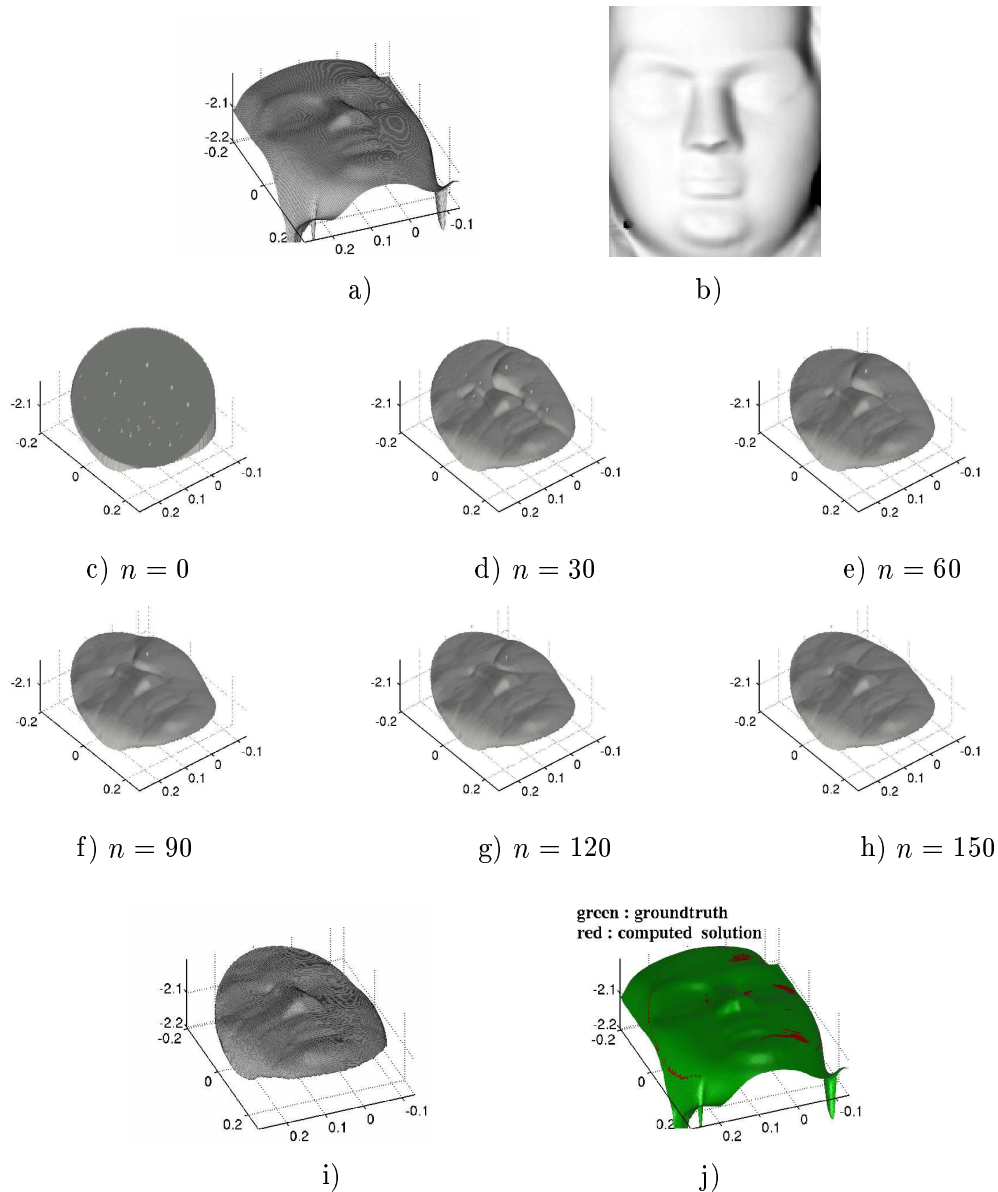


Figure 3.7: Experimental results obtained with the *implicit algorithm* starting from a *subsolution*, for a synthetic image representing Mozart’s face.

- a) Original surface of size $\simeq 150 \times 150$,
- b) synthetic image generated from the original surface a) with $\mathbf{l} = (0.2, 0.1)$ ($\theta \simeq 13^\circ$),
- c) to h) surface U^n at the n^{th} iteration for $n = 0, n = 30, n = 60, n = 90, n = 120$ and $n = 150$, respectively.
- i) Final result : $n = 200$
- j) visual comparison of the final result i) with the original surface a).

Error : $\varepsilon_1 \simeq 0.002, \varepsilon_2 \simeq 0.0032, \varepsilon_\infty \simeq 0.034$;

The errors of each iteration are given in the table 3.1.

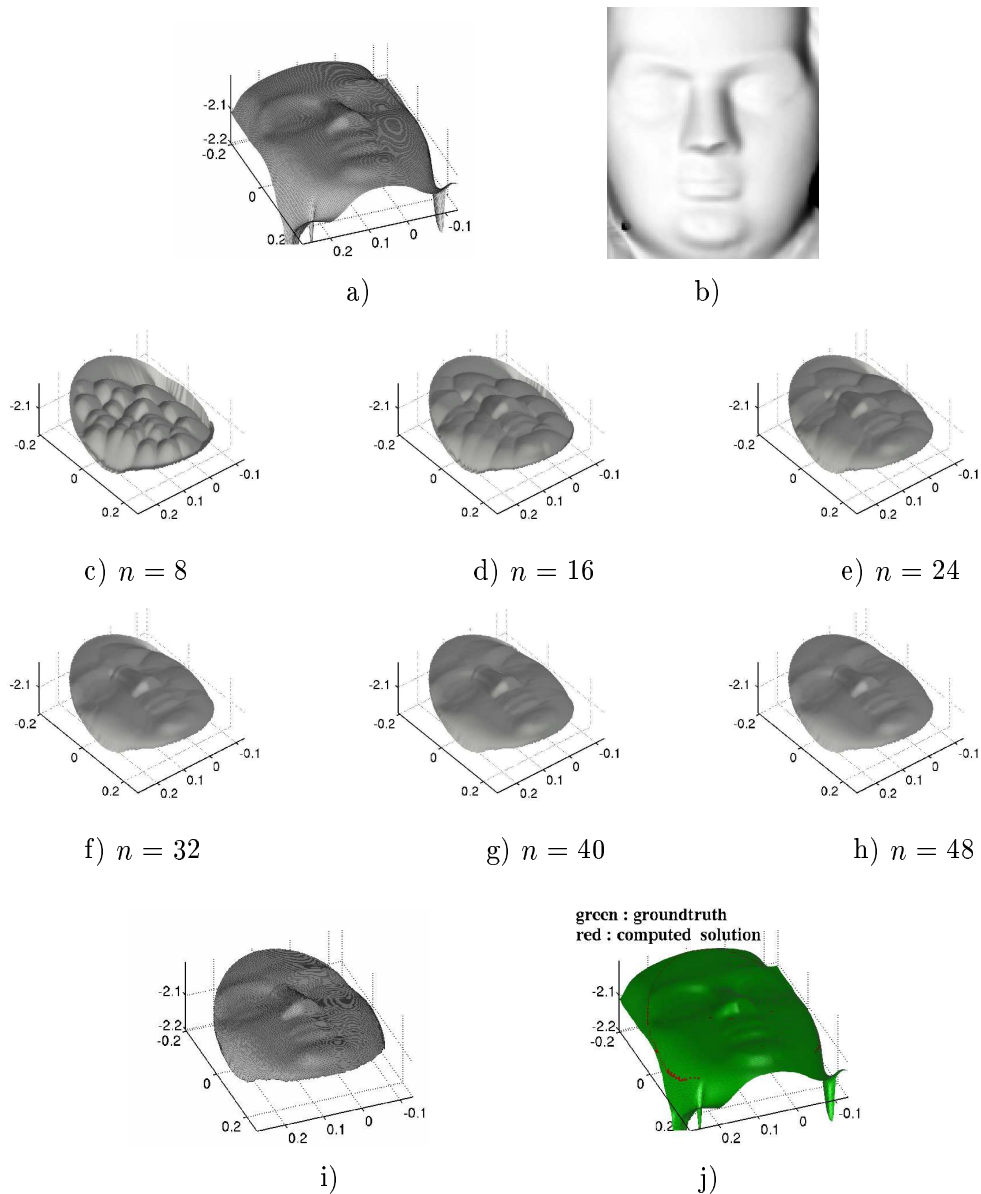


Figure 3.8: Experimental results obtained with the *semi-implicit algorithm* starting from a *supersolution*, for a synthetic image representing Mozart’s face.

- a) Original surface of size $\simeq 150 \times 150$,
 b) synthetic image generated from the original surface a) with $\mathbf{l} = (0.2, 0.1)$ ($\theta \simeq 13^\circ$),
 c) to h) surface U^n at the n^{th} iteration for $n = 8$, $n = 16$, $n = 24$, $n = 32$, $n = 40$ and $n = 48$, respectively.
 i) Final result : $n \leq 50$;
 j) visual comparison of the final result i) with the original surface a).

Error : $\varepsilon_1 \cong 0.002$, $\varepsilon_2 \cong 0.0033$, $\varepsilon_\infty \cong 0.0335$;

The errors of each iteration are given in the table 3.2.

3.2 Application to the “classical” Shape from Shading problem 141

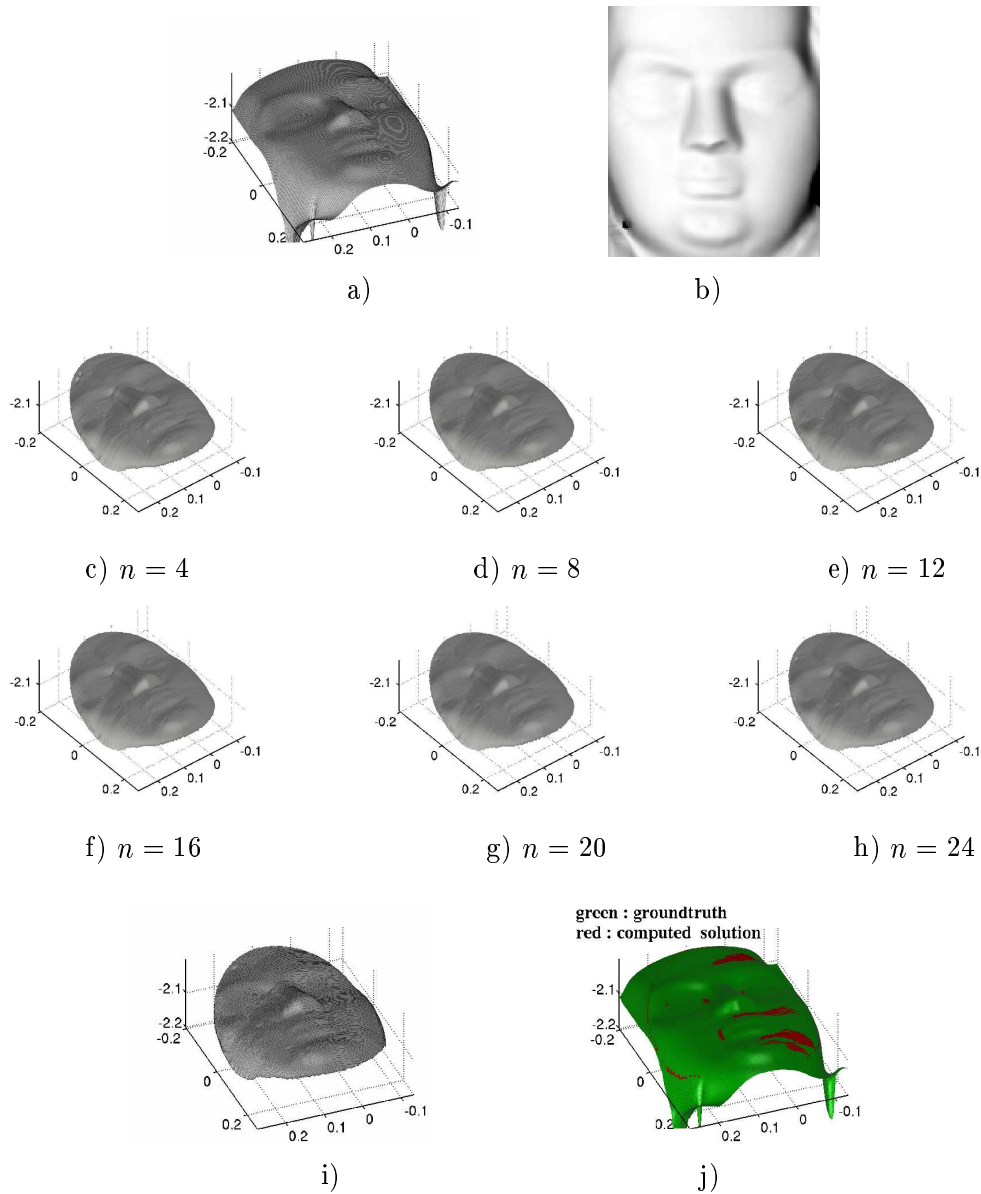


Figure 3.9: Experimental results obtained with the *implicit algorithm* starting from a *supersolution*, for a synthetic image representing Mozart's face.

a) Original surface of size $\simeq 150 \times 150$,

b) synthetic image generated from the original surface a) with $\mathbf{l} = (0.2, 0.1)$ ($\theta \simeq 13^\circ$),

c) to h) surface U^n at the n^{th} iteration for $n = 4, n = 8, n = 12, n = 16, n = 20$ and $n = 24$, respectively.

i) Final result : $n = 30$;

j) visual comparison of the final result i) with the original surface a).

Error : $\varepsilon_1 \simeq 0.002, \varepsilon_2 \simeq 0.0032, \varepsilon_\infty \simeq 0.0336$;

The errors of each iteration are given in the table 3.3.

iteration	ε_1 error	ε_2 error	ε_∞ error
4	0.00281226	0.0046	0.0432186
8	0.00217095	0.0034	0.0333782
12	0.00203401	0.0032	0.0335754
16	0.00199646	0.0032	0.033603
20	0.00199058	0.0032	0.03361
24	0.00198982	0.0032	0.03361
28	0.00198976	0.0032	0.03361

Table 3.3: Errors associated to figure 3.9 (implicit algorithm starting from a supersolution).

for the sinusoidal surface and 3.13 for the pyramidal surface. The Signal to Noise Ratio (SNR) is equal to 3.2 in figure 3.12 and to 2.7 in figure 3.13. As seen from these figures, our algorithms are very robust to intensity noise, as also observed in [134, 47].

Remarks 29.

R29.1 - The pyramid example shows the remarkable ability of the numerical algorithms to deal with *surfaces which are only continuous* as well as with *discontinuous images*.

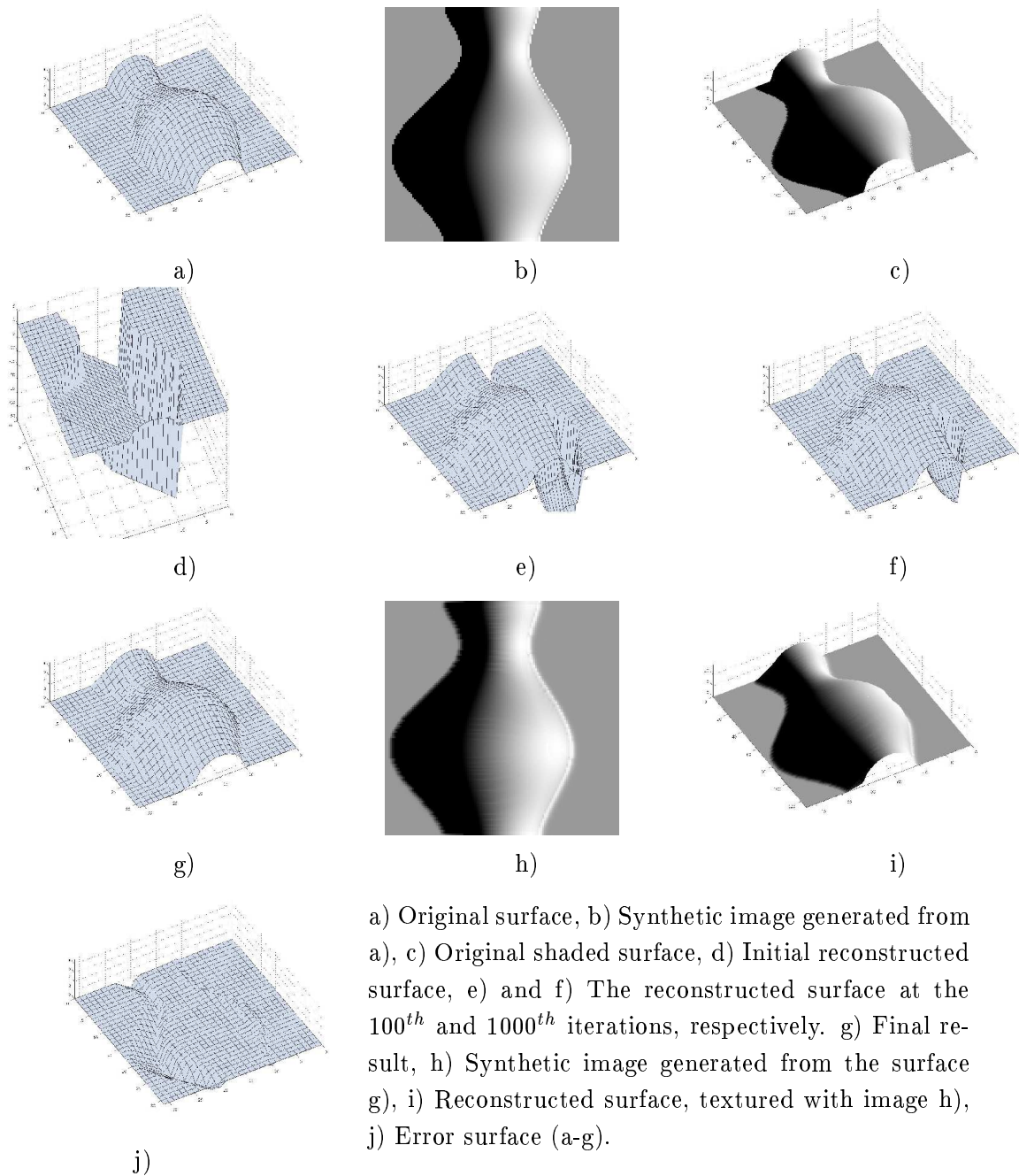
R29.2 - Figures 3.10 and 3.11 show the ability of the numerical algorithms to deal with *shadows*, as predicted by the theory and pointed out in section 3.2.3.

R29.3 - The synthetic surfaces of the vase and of Mozart’s face, as well as other surfaces are available by anonymous ftp under the pub/tech_paper/survey directory at eustis.cs.ucf.edu (132.170.108.42). They are associated to the paper by Zhang et al. [172].

3.2.4.2 Experimental results for “perspective SFS”

We have tested the “perspective” algorithms (i.e. the algorithms associated with the Hamiltonians H_*^{pers}) with synthetic images generated by using a “perspective” projection. The previous remarks about the speed of convergence of the orthographic SFS algorithms still hold for the perspective SFS algorithms. In the following results, the solutions are computed with the implicit algorithm associated with the Hamiltonian $H_{P/F}^{pers}$ starting from subsolutions (figures 3.14, 3.15 and 3.16) or from a supersolutions (figure 3.17).

3.2 Application to the “classical” Shape from Shading problem 143

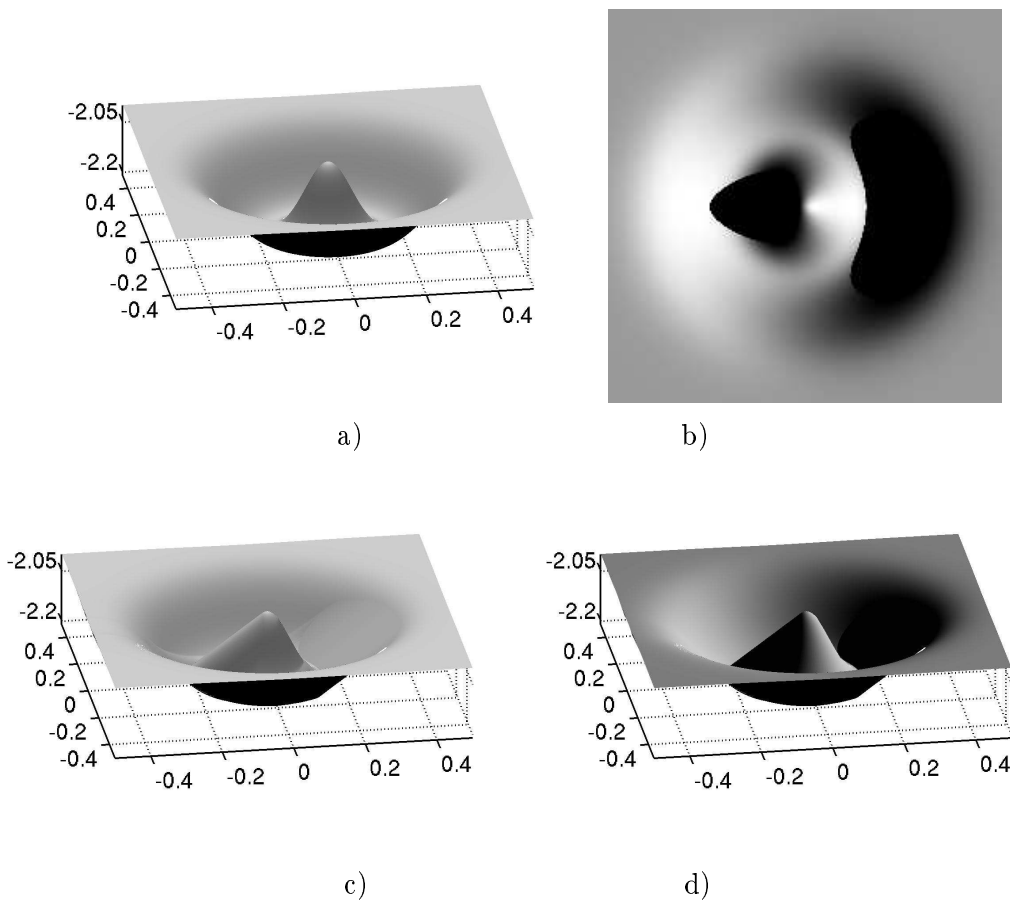


Size of the image = 256×256 .

Algorithm: implicit algorithm starting from a subsolution: $n < 2500$.

$\mathbf{L} = (\alpha, \beta, \gamma) = (0.8, 0.0, 0.6)$ i.e. $\theta = 53^\circ$.

Figure 3.10: First example of a reconstruction from an image with black shadows: the case of the vase.



Size of the image $\simeq 1000 \times 1000$.

Algorithm: implicit algorithm starting from a supersolution:

$n < 90$.

Figure 3.11: Second example of a reconstruction from an image with black shadows: the case of the Mexican hat. a) Original surface (the direction of the visualisation light is $(0, 0, 1)$), different from \mathbf{L} ; b) Synthetic image computed from the surface a) with $\mathbf{L} = (0.8, 0.0, 0.6)$ (the angle between the light direction \mathbf{L} and the camera axis is around 53°); c) Solution recovered by our algorithm from the image b) (the direction of the visualisation light is $(0, 0, 1)$); d) Surface c) illuminated by a light of direction $(0.8, 0.0, 0.6)$.

3.2 Application to the “classical” Shape from Shading problem 145

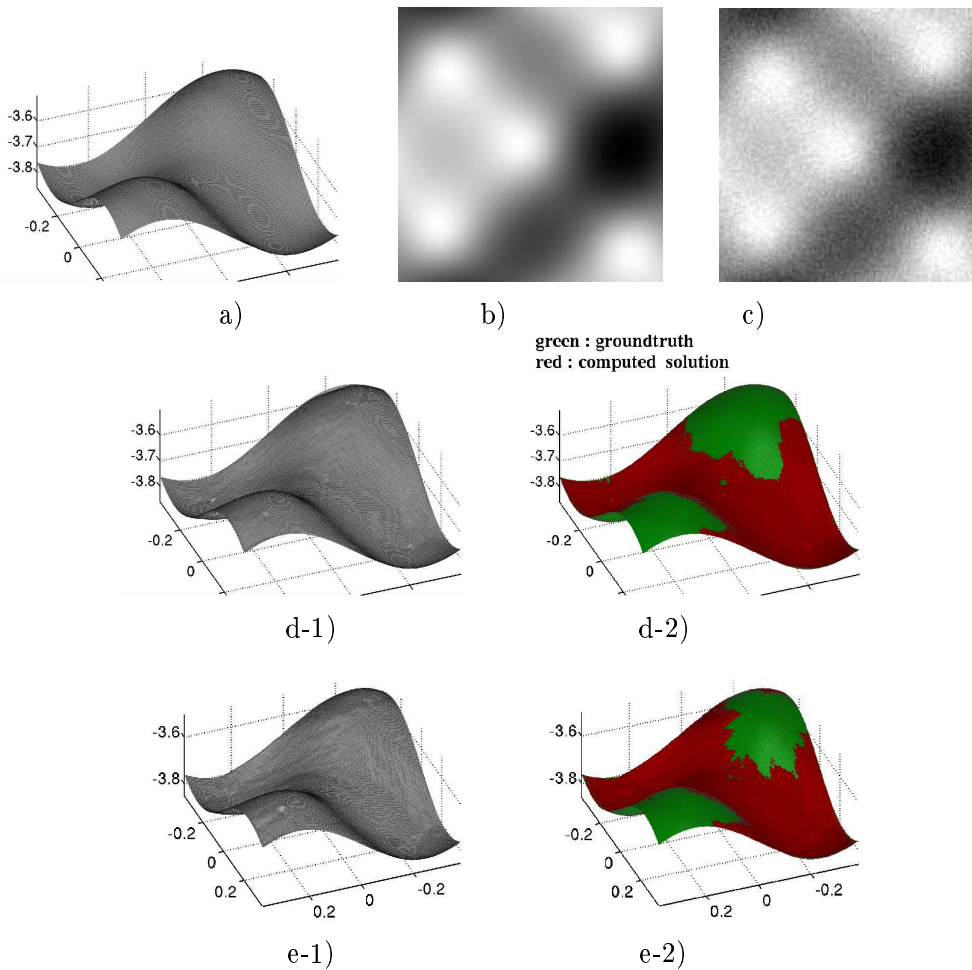


Figure 3.12: Results for a *noisy* image generated by a sinusoidal surface sampled on a grid of size 200×200 with $\mathbf{l} = (0.1, 0.3)$ ($\theta = 18.5^\circ$).

a) Original surface, b) Original image, c) Noisy image;

d) Reconstructed surface from b): $n \simeq 25$, $\varepsilon_1 = 0.003905$, $\varepsilon_2 = 0.005768$, $\varepsilon_\infty = 0.00747$;

e) Reconstructed surface from c): $n \simeq 30$, $\varepsilon_1 = 0.003905$, $\varepsilon_2 = 0.005766$, $\varepsilon_\infty = 0.00748$

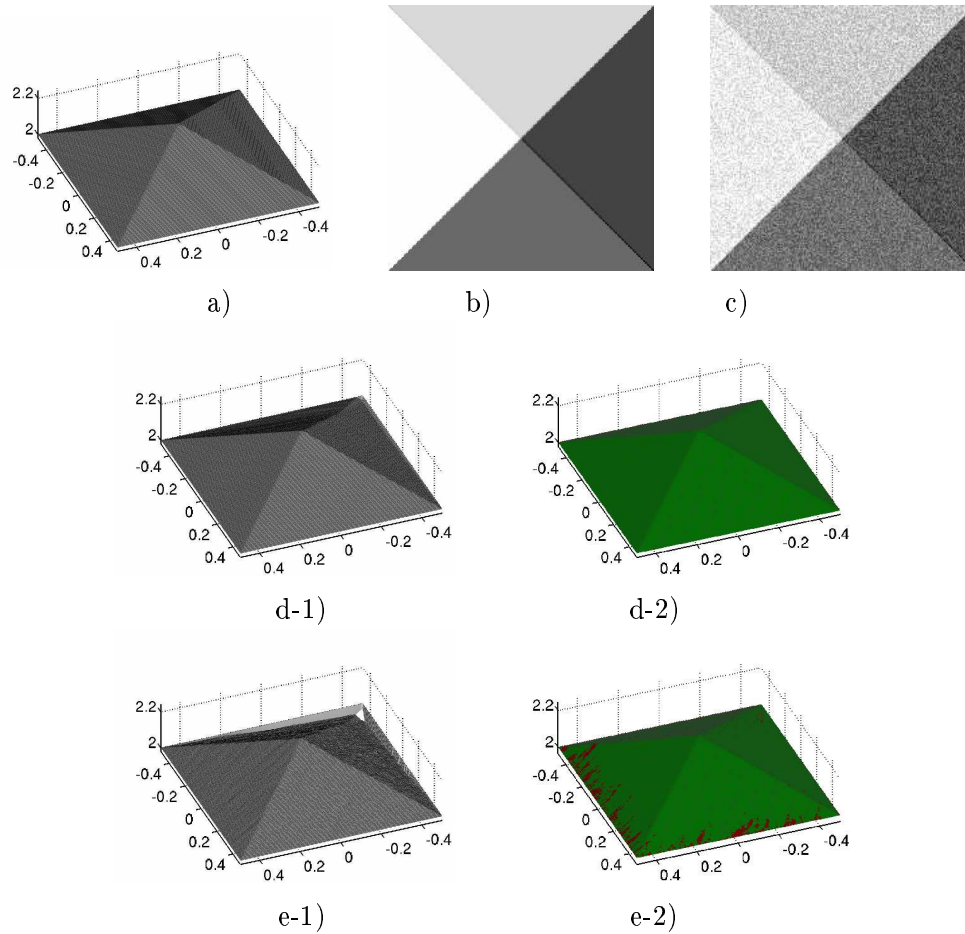


Figure 3.13: Results for a *noisy* image generated by a pyramidal surface sampled on a grid of size 200×200 with $\mathbf{l} = (0.5, 0.3)$ ($\theta = 35.6^\circ$).

a) original surface, b) original image, c) noisy image;

d) surface reconstructed from b): $n \simeq 50$, $\varepsilon_1 = 8.461e-05$, $\varepsilon_2 = 1.6116e-04$, $\varepsilon_\infty = 0.000940$;

e) surface reconstructed from c): $n \simeq 50$, $\varepsilon_1 = 0.00467$, $\varepsilon_2 = 0.00916$, $\varepsilon_\infty = 0.044$.

3.2 Application to the “classical” Shape from Shading problem 147

In all cases we show the original object, the input image and the surface reconstructed by the new “perspective algorithm” (see figures 3.14, 3.15 and 3.16). As for the orthographic algorithms, we demonstrate the stability of the perspective SFS algorithms with respect to image intensity errors due to noise (see figure 3.17, $\text{SNR} \simeq 3.7$). As seen from these figures, the algorithms are quite robust to intensity noise.

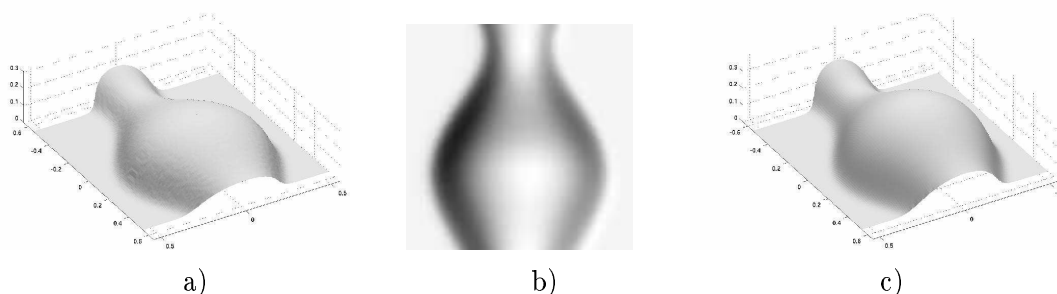


Figure 3.14: “Perspective SFS” results for an image generated by a smooth surface (computed by the implicit algorithm starting from a subsolution):

a) original surface, b) original image

($\mathbf{l} = (0.2, 0.2)$, $r = 2.5$, $\text{size} = 128 \times 128$),

c) surface reconstructed from b) by the “perspective algorithm”:

$n \simeq 1000$, $\varepsilon_1 = 0.0041$, $\varepsilon_2 = 0.00485$, $\varepsilon_\infty = 0.00814$;

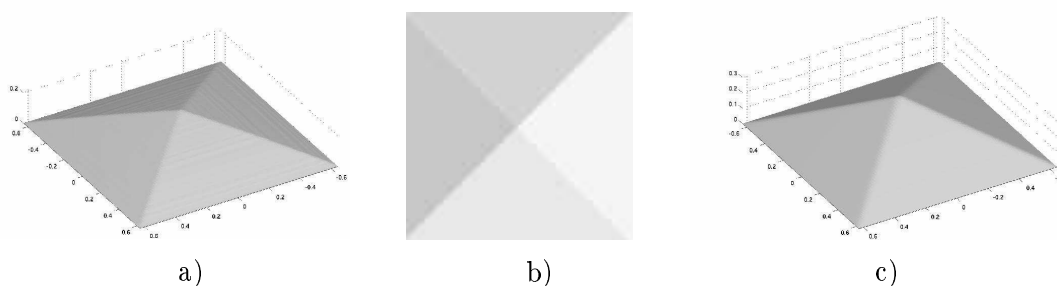


Figure 3.15: “Perspective SFS” results for an image generated by a pyramidal surface (computed by the implicit algorithm starting from a subsolution):

a) original surface, b) original image ($\mathbf{l} = (0.2, 0.2)$, $r = 2.1$, $\text{size} = 100 \times 100$),

c) surface reconstructed from b) by the “perspective algorithm”:

$n \simeq 76$, $\varepsilon_1 \simeq 0.00015$, $\varepsilon_2 \simeq 0.0005$, $\varepsilon_\infty \simeq 0.00110$;

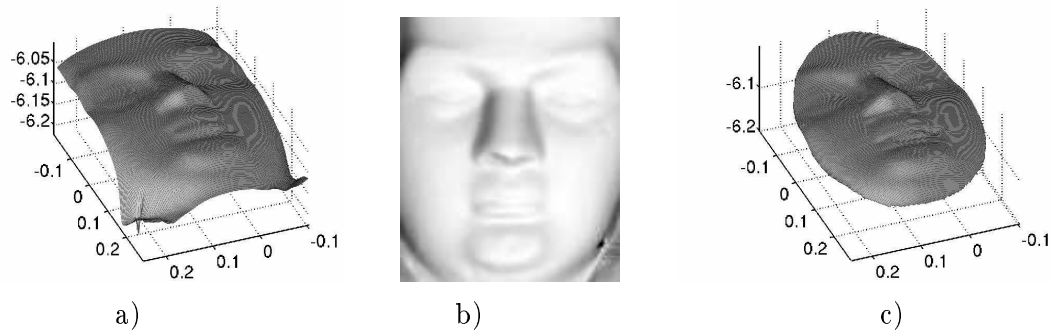


Figure 3.16: “Perspective SFS” results for an image generated by Mozart’s face (computed by the implicit algorithm starting from a supersolution):

a) original surface, b) original image ($\mathbf{l} = (0.1, 0.3)$, $\text{size} \approx 200 \times 200$, $f = 4$),
 c) surface reconstructed from b) by the “perspective algorithm”,

$$n \simeq 5, \quad \varepsilon_1 = 0.00197, \quad \varepsilon_2 = 0.00338, \quad \varepsilon_\infty = 0.00721;$$

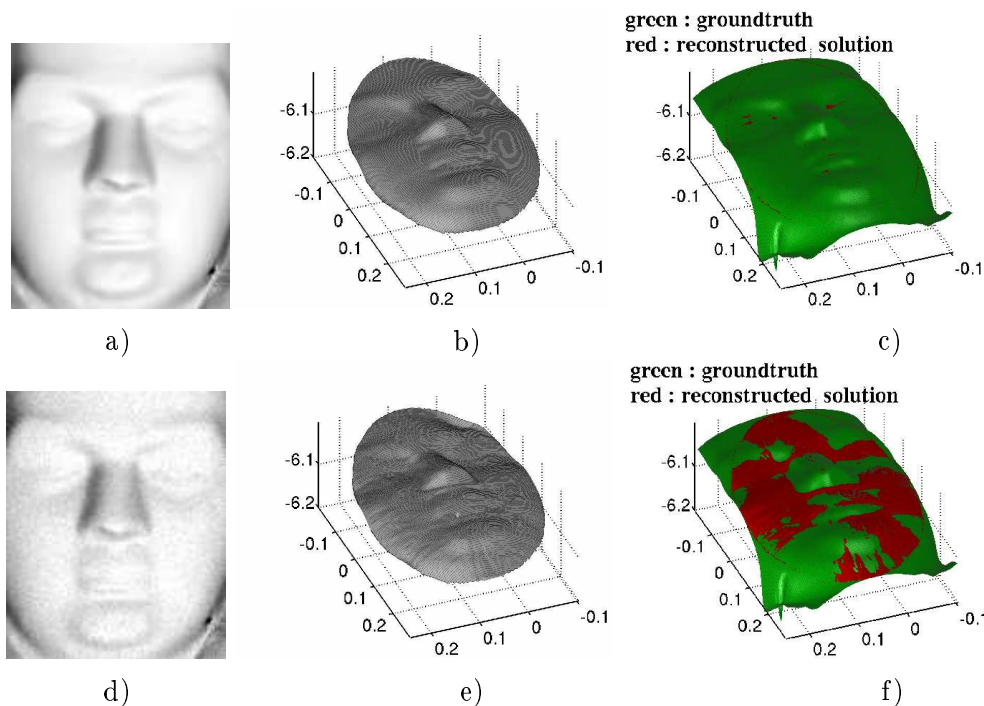


Figure 3.17: “Perspective SFS” results for an image of Mozart’s face corrupted by a uniformly distributed noise.

light parameter: $\mathbf{l} = (0.1, 0.3)$ ($\theta = 18.4^\circ$); focal length: $f = 4$.

a) original image, b) and c) surface reconstructed from a):

$$n \simeq 5, \quad \varepsilon_1 = 0.00197, \quad \varepsilon_2 = 0.00338, \quad \varepsilon_\infty = 0.00721;$$

d) noisy image, e) and f) surface reconstructed from d):

$$n \simeq 7, \quad \varepsilon_1 = 0.00247, \quad \varepsilon_2 = 0.0045, \quad \varepsilon_\infty = 0.0116.$$

3.3 Conclusion and contributions of chapter 3

- We have described some tools and a general method allowing to deal with **monotonous schemes**. In particular, we have stated and proved a general theorem ensuring the **stability** of these schemes. Some **convergence** results for the associated **algorithms** follow automatically. The described tools are mainly based on the monotonicity and on the existence of **solutions** or **supersolutions**.

In other respects, we have designed some monotonous approximation schemes adapted to (and consistent with) the **Hamilton-Jacobi-Bellman equations**. We have applied our stability results to them.

Let us note that the method applies to **irregular meshes** and it **does not require regularity with respect to the space variable**.

- We have demonstrated the practicality of our tools by applying them to the “classical SFS” problem. We have proposed two new “generic” SFS algorithms: a **semi-implicit** algorithm and an **implicit** one. We have proved the **convergence** of the numerical solutions computed by our algorithms **toward the viscosity solution** of the considered **SFS** problem.

Let us emphasize the fact that the “**generic**” formulation of the SFS problem allows to design a **unique SFS algorithm** which can be used to solve numerically **the various formulations** of the “classical” SFS problem.

Moreover, we have generalized and unified the algorithmic part of the work of Rouy and Tourin [134], Dupuis and Oliensis [47] and Prados and Faugeras [127, 120]. Let us recall that the basic fast marching method of Sethian [138, 139] is based on the approximation scheme of Rouy and Tourin [134].

- We have tested our new SFS methods.

Our algorithms are robust to pixel noise. **When starting from a supersolution** the **implicit** algorithm is **one of the most efficient** iterative algorithms of the SFS literature.

In other respects, our algorithms can deal with **discontinuous images** and with **black shadows**; let us recall that the stability of our SFS schemes and the convergence of our SFS algorithms hold for such images.
- At this stage, the computation of a numerical solution of the SFS problem **requires Dirichlet data on the boundary of the image and at all the singular points**.
- **Note:** the algorithmic and numerical parts of our articles [120, 123, 121] are based on the content of this chapter.

Chapter 4

A viscosity method for “classical” Shape from Shading without boundary data

This chapter is the result of a friendly and profitable collaboration with Fabio Camilli¹. I would like to thank Fabio Camilli for the warm and important exchanges that I could have with him.

The main weakness of the theoretical results presented in the previous chapters is due to the fact that we need to provide data (height of the solution) on the boundary of the image and at all the singular points. Also, in practice with real images, we rarely have such data. In this chapter, we weaken this constraint. In particular, we design a viscosity framework allowing to characterize solutions without requiring data on the boundary of the image.

4.1 Weaknesses of the previous theoretical approaches of the SFS problem

The theory of viscosity solutions was first used to solve SFS problems by Lions, Rouy and Tourin [134, 96] in the 90s. Their work was based upon the notion of *continuous* viscosity solution. Let us remind that the viscosity solutions

¹Pure and Applied Mathematics Department of the University of L'Aquila, Italy (camilli@ing.univaq.it).

are PDE solutions in a weak sense. In particular, they are not necessarily differentiable and can have edges. Let us emphasize that continuous viscosity solutions are continuous (on the closure of the set where they are defined) and that a solution in the classical sense is a viscosity solution; see chapter 2. As we explain in section 2.2.2, a drawback of this notion is due to the compatibility condition necessary to the existence of a solution (constraint on the variation of the boundary conditions [95]). For example, the equation

$$|\nabla u(x)| = 1 \text{ for all } x \text{ in }]0, 1[\tag{4.1}$$

with $u(0) = u(1) = 0$, does not have classical solutions but has a continuous viscosity solution (see figure 4.1-a)). The same equation (4.1) with $u(0) = 0$, $u(1) = 1.5$ does not have continuous viscosity solutions (see section 2.2.2). Also,

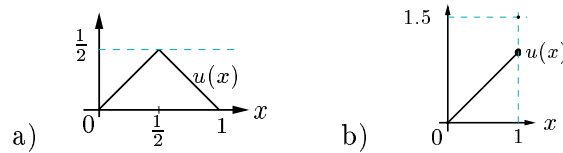


Figure 4.1: a) Continuous viscosity solution of (4.1) with $u(0) = u(1) = 0$; b) discontinuous viscosity solution of (4.1) with $u(0) = 0$ and $u(1) = 1.5$.

let us suppose that we make a large error on the boundary condition, when we compute a numerical solution of the SFS problems. If this error is too large then there do not exist continuous viscosity solutions. In this case one may wonder what the numerical algorithm of [134, 96] computes. In chapter 2, we answer this question by proposing to use the more general idea of *discontinuous* viscosity solutions. For example, equation (4.1) with $u(0) = 0$, $u(1) = 1.5$ has a discontinuous viscosity solution; (see figure 4.1-b)). Let us remind that a “discontinuous viscosity solution” *can* have discontinuities and that a continuous viscosity solution is a discontinuous viscosity solution.

In sections 2.2.4 and 2.2.6, we show that the classical theory of viscosity solutions offers simple and general theorems of existence and uniqueness of solutions for exactly the type of PDEs that arise in the context of SFS. In particular the theory allows to characterize exactly all possible continuous viscosity solutions: given a particular Dirichlet condition on the image boundary (verifying the compatibility condition), if the set of *singular points* (points of maximal intensity, i.e. $I(x) = 1$) is empty, then there exists a unique continuous viscosity solution satisfying the boundary conditions. If the set of singular points is not empty there exists an infinity of continuous viscosity solutions which are characterized by their values at the singular points. Note that this result is general and applies equally to all the SFS models described in section 2.1. As a consequence, the SFS problem is ill-posed and, in section 3.2, to compute a

numerical approximation of a solution, we must assume that the values of the solutions are given at the image boundary and at the singular points (see in particular section 3.2.4). This is quite unsatisfactory, even more so since small errors on these values create undesirable crests, see figure 4.2-b) or [127] for an example with a real image.

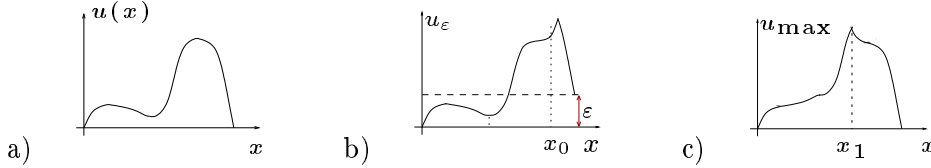


Figure 4.2: a) original surface u ; b) solution u_ϵ associated to corrupted boundary conditions and to the image obtained from the original surface a) with the Eikonal equation; c) maximal solution u_{\max} (in Falcone’s sense [24, 55, 56]) associated to the same image. u_ϵ and u_{\max} present a kink at x_0 and x_1 .

Falcone [24, 55, 56] proposes to not specify anymore the values of the solution at the singular points (he still requires to specify the values at the image boundary though). In order to achieve this, he uses the notion of “maximal” viscosity solutions developed by Camilli and Siconolfi [24, 26, 23]. Despite its advantages, this approach is not really adapted to the SFS problem, see for example figure 4.2-c). In this figure, the maximal solution u_{\max} associated to the image obtained from the original surface u shows a highly visible crest where the surface should be smooth. Even with the correct boundary conditions, Falcone’s method does not allow to recover the original surface, but only the maximal surface with the same brightness $I(x)$.

To summarize the work of Rouy et al. [134], Prados et al. [127, 120] and Falcone et al. [24, 55, 56] suggests theories and numerical methods based on the concept of viscosity solutions and requiring data on the boundary of the image. At the opposite, Dupuis and Oliensis [47] consider C^1 solutions and value functions. They characterize a C^1 solution by specifying only its values at the singular points which are local minima. In particular, they do not specify the values of the solution on the boundary of the image. Also, they provide algorithms for approximating these solutions. Nevertheless, in practice, because of noise, of incorrect modeling, errors on parameters or on the depth values enforced at the singular points, there do not exist C^1 solutions to the SFS equations; also the notion of value functions is not always very intuitive. Considering the drawbacks and the advantages of all these methods, it seems important to consider an other class of weak solutions such that the characterization of Dupuis and Oliensis holds, which provides a (theoretical and numerical) solution when there do not exist smooth solutions, and which unifies all this previous work.

As we show in the second part of section 2.2.6.3, the notion of discontinuous viscosity solutions does not allow to impose the values of the solution at the singular points (this does not allow to characterize the discontinuous viscosity solutions). Therefore, this notion cannot provide an extension of the Dupuis and Oliensis work. Moreover, the notion of singular viscosity solutions developed by Camilli and Siconolfi in [26, 23, 27] uses Dirichlet conditions all around the boundary of the image. Thus, it does not also provide a direct extension of the Dupuis and Oliensis work. For such an extension, we must slightly modify these notions and we must consider a “new” type of boundary conditions (called “state constraints” [145]). It turns out that the correct notion of viscosity solution for the “classical” SFS problem is the “singular discontinuous viscosity solution with Dirichlet boundary conditions and state constraints”. These solutions can be interpreted as maximal solutions and have the great advantage of not necessarily requiring boundary or singular points conditions. Moreover, this notion provides a mathematical framework unifying the work of Rouy et al. [96, 134], Prados et al. [127, 120], Falcone et al. [24, 55, 56] and Dupuis and Oliensis [47].

4.2 Singular discontinuous viscosity solutions with Dirichlet boundary conditions and state constraints (SDVS)

The notion of singular viscosity solutions was pioneered by Ishii and Ramaswamy [77] and has been recently upgraded by Camilli and Siconolfi [26, 23, 27]. In this section, we slightly modify the tools developed in these papers introducing the notion of “singular viscosity solution with Dirichlet boundary conditions and state constraints” (SDVS), and we prove the existence and uniqueness of the SDVS. Some stability results are proved. Moreover, we show that this framework allows to characterize the classical discontinuous viscosity solutions by their “minimums”.

Let Ω be a bounded open subset of \mathbb{R}^N with smooth boundary (say $W^{2,\infty}$). In the SFS problem $N = 2$. So Ω is a smooth part of rectangular domain $]0, X[\times]0, Y[$ which typically represents the domain of definition of the image. We consider the partial differential equation (PDE):

$$H(x, \nabla u) = 0, \quad \forall x \in \Omega, \tag{4.2}$$

where $H : \overline{\Omega} \times \mathbb{R}^N \rightarrow \mathbb{R}$ is a continuous (hypothesis (H4)), *convex* (with respect to p) Hamiltonian (hypothesis (H1)), and satisfies the coercivity condition

$$(H2') \quad \liminf_{|p| \rightarrow +\infty} H(x, p) = +\infty, \quad \text{for any } x \in \overline{\Omega}.$$

Moreover we assume that

(H3') *there exists a subsolution $\psi \in C^1(\Omega) \cap W^{1,\infty}(\Omega)$ of (4.2) (i.e. $\forall x \in \Omega, H(x, \nabla\psi(x)) \leq 0$)*

and

(H23) *for any $\lambda \in (0, 1), p \in \mathbb{R}^N$ s.t $H(x, p) \leq 0$ then*

$$H(x, \lambda p + (1 - \lambda)\nabla\psi(x)) < 0.$$

Note that the previous hypotheses hold for all the “classical” SFS Hamiltonians considered in section 2.1 as soon as the intensity image I is continuous and verifies $I(x) > 0$ for any $x \in \overline{\Omega}$.

We say that ψ is a strict subsolution of (4.2) at x when $H(x, \nabla\psi(x)) < 0$. We denote by \mathcal{S} the set of *singular points* of H respect to ψ :

$$\mathcal{S} = \{x \in \overline{\Omega} \mid H(x, \nabla\psi(x)) = 0\},$$

i.e. the set where ψ fails to be a strict subsolution of (4.2). \mathcal{S} is closed by the continuity of $\nabla\psi$ and H .

We also assume that

$$\mathcal{S} \cap \partial\Omega = \emptyset. \tag{4.3}$$

Remarks 30.

R30.1 - In the case where H is an Hamilton-Jacobi-Bellman (HJB) Hamiltonian

$$H(x, p) = \sup_{a \in A} \{-f(x, a) \cdot p - l(x, a)\} \tag{4.4}$$

with $f : \overline{\Omega} \times A \rightarrow \mathbb{R}^N, l : \overline{\Omega} \times A \rightarrow \mathbb{R}$ and the running cost l is nonnegative, \mathcal{S} corresponds to the set

$$\{x \in \overline{\Omega} \mid l(x, a) = 0 \text{ for some } a \in A\}.$$

In this case $\psi \equiv 0$ is a subsolution of the equation. Yet, at the opposite to [23], here we do not assume that l is a nonnegative function. As it was shown in chapter 2, the Rouy/Tourin Hamiltonian $H_{R/T}^{orth}$ (where, $l_{R/T}(x, a) = I(x)\sqrt{1 + |a|^2} - \gamma$) and the perspective Hamiltonian $H_{P/F}^{pers}$, which fit in the class of Hamiltonians given by (4.4) but with a cost of arbitrary sign, admit a regular subsolution. Therefore, in this chapter, to each “classical” SFS Hamiltonian we systematically associate the corresponding subsolution ψ defined in section 2.2.6.1 (at the page 78).

R30.2 - In section 2.2.6, we prove that for all the “classical” SFS equations presented in section 2.1 the set of singular points \mathcal{S} corresponds to the set $\{x \in \overline{\Omega} \mid I(x) = 1\}$ where I is the intensity image. Note that in the SFS problem, even if we do not make this assumption, it may appear natural to assume that $\mathcal{S} = \{x_1, \dots, x_k\}$, since the situation where $\overset{\circ}{\mathcal{S}}$ (the interior of the set \mathcal{S}) is not empty, is non generic². Nevertheless, in practice, due to some saturation or discretisation effects, several connected points can have an intensity equal to the maximal intensity (i.e $I(x) = 1$).

R30.3 - As we have shown in subsection 2.2.4.1, the coercivity hypothesis (H2') is not systematically verified for all the SFS Hamiltonians. Globally, it does not hold for the pixels of the image with a low brightness, i.e. $I(x)$ close to 0, when the direction of the distant light source is very different to the one of the camera. In this work, we do not weaken this hypothesis explaining in various remarks some difficulties involved by the non coercivity.

Definition 4.1 *Let u be a locally bounded function on a set E . For any $x \in E$, we set:*

$$u^*(x) = \limsup_{y \rightarrow x} u(y) = \sup\{\limsup_{n \rightarrow \infty} u(x_n) : x_n \rightarrow x\},$$

$$u_*(x) = \liminf_{y \rightarrow x} u(y) = \inf\{\liminf_{n \rightarrow \infty} u(x_n) : x_n \rightarrow x\}.$$

u^* and u_* are respectively called the upper semicontinuous envelope and lower semicontinuous envelope of u .

Recall that, if u is a locally bounded function, then u^* is u.s.c and u_* is l.s.c. (see sections V-1 and V-2.1 of [5] for more details).

We now give the definition of viscosity subsolution. The definition of viscosity supersolution, which is modified respect to the standard one to solve the uniqueness issue, is postponed to the next subsection.

Definition 4.2 (Viscosity subsolution of (4.2)) *A locally bounded function u , u.s.c in Ω , is said a viscosity subsolution of equation (4.2) if*

$$\forall \phi \in C^1(\Omega), \forall x_0 \in \Omega \quad \text{local maximum of } (u - \phi), \quad H(x_0, \nabla \phi(x_0)) \leq 0.$$

The regularity of $\partial\Omega$ and the hypothesis on H imply that a viscosity subsolution of (4.2) is Lipschitz continuous in Ω . Moreover we have (see Prop. 4.3 in [26])

Proposition 4.1 *The following three properties are equivalent*

²In effect, for a given experimental setup (surface, light, camera) such that $\overset{\circ}{\mathcal{S}} \neq \emptyset$, an arbitrarily small change in the experimental parameters (for example, when the light moves) will make $\overset{\circ}{\mathcal{S}} = \emptyset$. An image such that $\overset{\circ}{\mathcal{S}} \neq \emptyset$ is highly unlikely.

- u is a viscosity subsolution of (4.2) in Ω ;
- u is a Lipschitz continuous a.e. subsolution of (4.2) in Ω ;
- u is Lipschitz continuous and, defined the (Clarke) generalized gradient [34] by

$$\partial u(x) = \overline{\text{co}}\{p \in \mathbb{R}^N : p = \lim_n \nabla u(x_n),$$

for a sequence $x_n \in \text{Dom}(\nabla u)$ converging to $x\}$,

then the inequality

$$H(x, p) \leq 0$$

holds for any $x \in \Omega$, $p \in \partial u(x)$.

Remark 31. If the Hamiltonian is noncoercive then the subsolutions are not necessarily Lipschitz continuous. Moreover, subsolutions can yield discontinuities at the points x where $p \mapsto H(x, p)$ is non coercive. Nevertheless, note that, if \mathcal{S} is empty, only the coercivity on a *neighborhood* of $\partial\Omega$ is sufficient for ensuring the strong uniqueness, and so the continuity of the discontinuous viscosity solution on Ω . For a proof of this fact, see for example theorem 4.5 of [7] and more especially its Corollary 4.1. In this corollary, the “HNCL” hypotheses of [7] is implied by convexity, existence of a strict subsolution and regularity of the Hamiltonian. The coercivity hypotheses (H18) and (H20) of [7] are only required on a neighborhood of $\partial\Omega$. The reader can also refer to [8].

With equation (4.2), we associate the Dirichlet boundary conditions (DBC)

$$u(x) = \varphi(x), \quad \forall x \in \partial\Omega \cup \mathcal{S} \tag{4.5}$$

where φ is defined on $\partial\Omega \cup \mathcal{S}$ into $\mathbb{R} \cup \{+\infty\}$, l.s.c., bounded from below and continuous in $\{x \in \partial\Omega \cup \mathcal{S} : \varphi(x) < +\infty\}$, with $\varphi \not\equiv +\infty$. At points x where $\varphi(x) = +\infty$, we say that we impose a *state constraint* boundary condition (see [145, 29]).

Definition 4.3 (Viscosity subsolution of (4.2)-(4.5)) *A locally bounded function u , u.s.c on $\overline{\Omega}$, is said a viscosity subsolution of (4.2)-(4.5) if u is a viscosity subsolution of (4.2) and if:*

- $\forall x_0 \in \mathcal{S}, \quad u(x_0) \leq \varphi(x_0)$.
- $\forall x_0 \in \partial\Omega,$

- $u(x_0) \leq \varphi(x_0)$
- or $\forall \phi \in C^1(\overline{\Omega})$ s.t. x_0 is a local maximum of $(u - \phi)$,
 $H(x_0, \nabla \phi(x_0)) \leq 0$.

Note that points $x \in \partial\Omega$ where $\varphi(x) = +\infty$, the boundary condition is automatically satisfied.

4.2.1 Singular viscosity supersolutions of (4.2)-(4.5)

Before giving the definition of the singular viscosity supersolution of (4.2)-(4.5), we need to detail various assumptions and definitions.

The multivalued map

Let $\mathcal{Z}(x)$ be the multivalued map on Ω defined as:

$$\mathcal{Z}(x) = \{p \in \mathbb{R}^N : H(x, p) \leq 0\}. \quad (4.6)$$

For all the “classical” SFS Hamiltonians, it is easy to see that:

$$(H24) \quad \forall x \in \mathcal{S}, \quad \mathcal{Z}(x) = \{\nabla \psi(x)\}.$$

Therefore, in the sequel, we assume that hypothesis (H24) holds.

Remarks 32.

r32.1 - Under the hypothesis (H24), the continuity of H provides a new characterization of \mathcal{S} :

$$x \in \mathcal{S} \iff \mathcal{Z}(x) = \{\nabla \psi(x)\}.$$

r32.2 - Assumption (H24) and proposition 4.1 imply that for a subsolution u , $\partial u(x) = \{\nabla \psi(x)\}$ for $x \in \mathcal{S}$. Therefore a subsolution u is strictly differentiable (see [34]) on the singular set.

By hypotheses (H2') and (H23), the set-valued map $\mathcal{Z}(x)$ is continuous in $\overline{\Omega}$ respect to the Hausdorff metric. Moreover, for any $x \in \overline{\Omega}$, the set $\mathcal{Z}(x)$ is compact, convex and strictly star-shaped respect to $\nabla \psi(x)$ and

$$\partial \mathcal{Z}(x) = \{p \in \mathbb{R}^N \mid H(x, p) = 0\}. \quad (4.7)$$

As explained in [27], (4.7) is a geometric property which allows us to study the equation $H(x, \nabla u) = 0$ through the level sets $\mathcal{Z}(x)$. Let W an open subset of Ω . If $F(x, p)$ is any continuous function representing $\mathcal{Z}(x)$ in the sense that for all $x \in W$,

$$F(x, p) < 0 \quad \text{if and only if} \quad p \in \overset{\circ}{\mathcal{Z}(x)},$$

$$F(x, p) = 0 \quad \text{if and only if} \quad p \in \partial\mathcal{Z}(x),$$

then the equation

$$F(x, \nabla u) = 0, \quad \forall x \in W$$

is equivalent to $H(x, \nabla u) = 0$ in W from a viscosity point of view. Moreover the definition of subsolution could be equivalently expressed by the condition $\nabla u(x) \in \mathcal{Z}(x)$ in viscosity sense for any $x \in \Omega$.

Let us remark that, the assumptions imposed in this section are properties satisfied by the map $\mathcal{Z}(x)$. They are not directly about the Hamiltonian H .

A new Hamiltonian with the same multivalued map

Now, let us introduce the gauge function $\rho(x, p)$ of $\mathcal{Z}(x)$. We set for any $x \in \overline{\Omega}$, $p \in \mathbb{R}^N$,

$$\rho(x, p) = \inf\{\lambda > 0 : \lambda^{-1}p + (1 - \lambda^{-1})\nabla\psi(x) \in \mathcal{Z}(x)\}. \quad (4.8)$$

As in [7, 6], (see also proposition 5.1 of [27]), we can prove that the function ρ is l.s.c in $\overline{\Omega} \times \mathbb{R}^N$ (continuous in $(\overline{\Omega} - \mathcal{S}) \times \mathbb{R}^N$) and verifies the homogeneity condition:

$$\forall \mu > 0 \quad \text{and} \quad \forall (x, p) \in \overline{\Omega} \times \mathbb{R}^N, \quad \rho(x, \mu p + (1 - \mu)\nabla\psi(x)) = \mu\rho(x, p). \quad (4.9)$$

Moreover, $p \in \mathcal{Z}(x)$ if and only if $\rho(x, p) \leq 1$. If $x \in \mathcal{S}$, we have $\rho(x, \nabla\psi(x)) = 0$ and $\rho(x, p)$ is infinite for $p \neq \nabla\psi(x)$. Then the equation

$$\rho(x, \nabla u) = 1, \quad \forall x \in \Omega$$

defines an equation equivalent to (4.2) in $\Omega - \mathcal{S}$ and singular for $x \in \mathcal{S}$.

Adaptation of the topology

Now, let us set, $\forall x \in \overline{\Omega}$,

$$r(x) = \sup\{r > 0 \mid B(\nabla\psi(x), r) \subset \mathcal{Z}(x)\}.$$

In [27], Lemma 3.1 it is proved that $r(x)$ is continuous in $\overline{\Omega}$, $r(x)$ is nonnegative and $r(x) = 0$ if and only if $x \in \mathcal{S}$.

Remark 33. For the SFS Hamiltonians $H_{R/T}^{orth}, H_{D/O}^{orth}, H_{Eiko}^{orth}, H_F^{pers}$, it is possible to prove that $\forall x \in \overline{\Omega}$, $r(x)$ is finite and that $r(\cdot)$ is bounded on $\overline{\Omega}$ (even when these Hamiltonians are not coercive)³. The proof of Lemma 3.1 of [27] is essentially based on the fact that $r(\cdot)$ is bounded. Thus, this result

³For the coercitivity of H_{Eiko}^{orth} and H_F^{pers} , we must assume that $I > 0$ on the compact set $\overline{\Omega}$.

applies to the previous SFS Hamiltonians, even at the points x where they are not coercive.

Note that by definition of $r(\cdot)$ and (H24) we have

- $x \in \mathcal{S} \iff \mathcal{Z}(x) = \{\nabla\psi(x)\} \iff r(x) = 0$,
- $x \notin \mathcal{S} \iff \exists r > 0 \text{ s.t. } B(\nabla\psi(x), r) \subset \mathcal{Z}(x) \iff r(x) > 0$.

As in [26, 27], we proceed defining a semidistance on $\overline{\Omega}$. We set for any $x, y \in \overline{\Omega}$,

$$S(x, y) = \inf \left\{ \int_0^1 r(\xi(t)) |\xi'(t)| dt : \xi(t) \in W^{1,\infty}([0, 1], \overline{\Omega}) \right. \\ \left. \text{s.t. } \xi(0) = x \text{ and } \xi(1) = y \right\}. \quad (4.10)$$

It is easy to verify that S satisfies:

$$S(x, y) \leq S(x, z) + S(z, y) \quad x, y, z \in \overline{\Omega}, \\ S(x, y) = S(y, x) \quad x, y \in \overline{\Omega}, \\ S(x, x) = 0 \quad x \in \overline{\Omega}$$

and

$$0 \leq S(x, y) \leq \|r\|_\infty d_E(x, y) \quad x, y \in \overline{\Omega}$$

where $d_E(x, y)$ is the Euclidean geodesic distance in Ω (i.e. the distance defined as in (4.10) with $r(x) \equiv 1$).

So S is a semidistance on $\overline{\Omega}$, but in general not a distance since, if $x_0 \in \mathcal{S}$, the set of points which have 0 S -distance from x_0 is in general a subset of \mathcal{S} containing elements different from x_0 . The family of balls:

$$B_S(x_0, R) = \{x \in \Omega \mid S(x_0, x) \leq R\}$$

induces a topology τ_S in Ω . Note that on a neighborhood of a point $x \in \Omega - \mathcal{S}$ the topology τ_S is equivalent to the Euclidean topology. At a point $x \in \mathcal{S}$, it is a weaker topology.

We denote by $B_S(x_0)$ the subset

$$B_S(x_0) = \{x \in \overline{\Omega} \mid S(x_0, x) = 0\}.$$

Definition of singular viscosity supersolutions and solutions

Definition 4.4 (Strict subsolution of (4.2)) *A function v is said to be a strict subsolution of (4.2) in an open subset A of Ω if v is a viscosity subsolution of*

$$\rho(x, \nabla v) \leq \theta \quad x \in A$$

for some $\theta \in]0, 1[$.

Definition 4.5 ((Strict) Subtangent) For a l.s.c. function v , a Lipschitz continuous function ϕ is called S -subtangent to v at $x_0 \in \Omega$ if x_0 is a minimizer of $v - \phi$ in a τ_S -neighborhood of x_0 (or equivalently, in a neighborhood A of $B_S(x_0)$). The S -subtangent is called strict if the inequality

$$(v - \phi)(x) > (v - \phi)(x_0)$$

holds for $x \in A - B_S(x_0)$.

Definition 4.6 (Singular viscosity supersolution of (4.2) at $x_0 \in \Omega$) A l.s.c. function $v : \Omega \rightarrow \mathbb{R}$ is said singular viscosity supersolution of (4.2) at $x_0 \in \Omega$, if it does not admit a S -subtangent at x_0 which is a strict subsolution of (4.2) in a neighborhood of $B_S(x_0)$.

Note: It is worth noting that if $x_0 \notin \mathcal{S}$, the previous definition coincides with the standard notion of discontinuous discontinuous viscosity supersolution of equation (4.2), i.e. a locally bounded function v , l.s.c in Ω , is said a viscosity supersolution if

$$\forall \phi \in C^1(\Omega), \forall x_0 \in \Omega \quad \text{local minimum of } (u - \phi), H(x_0, \nabla \phi(x_0)) \geq 0.$$

Definition 4.7 (Singular viscosity supersolution of (4.2)-(4.5)) A locally bounded function $v : \overline{\Omega} \rightarrow \mathbb{R}$, l.s.c. on $\overline{\Omega}$, is said singular viscosity supersolution of (4.2)-(4.5) if:

- $\forall x_0 \in \Omega - \mathcal{S}$, v is a singular viscosity supersolution of (4.2) at x_0 .
- $\forall x_0 \in \partial\Omega \cup \mathcal{S}$,
 - v is a singular viscosity supersolution of (4.2) at x_0
 - or there exists $x \in B_S(x_0)$ such that $v(x_0) \geq \varphi(x) + \psi(x_0) - \psi(x)$.

Let us emphasize that, if the set of singular points \mathcal{S} is empty, then the singular supersolutions of (4.2)-(4.5) coincide with the standard discontinuous viscosity supersolutions of (4.2)-(4.5). Let us also recall that, at the points x_0 where $\varphi(x_0) = +\infty$, the Dirichlet boundary condition corresponds to a state constraint condition [145, 29].

Note that if $x_0 \in \mathcal{S}$, then $B_S(x_0)$ can be larger than $\{x_0\}$. As the definition of supersolution, also the boundary condition on \mathcal{S} is adapted to the weak topology induced by S .

Now, we can give the definition of the singular viscosity solution of (4.2)-(4.5).

Definition 4.8 (Singular viscosity solution of (4.2)-(4.5))

A locally bounded function $u : \overline{\Omega} \rightarrow \mathbb{R}$ is said singular viscosity solution of (4.2)-(4.5) if u^* is a subsolution of (4.2)-(4.5) and if u_* is a singular supersolution of (4.2)-(4.5).

We will call “singular discontinuous viscosity solutions with Dirichlet boundary conditions and state constraints” (SDVS), the singular solution of (4.2)-(4.5).

4.2.2 Existence of the singular solution of (4.2)-(4.5)

In this section, we prove the existence of SDVS by giving an explicit representation formula of it.

Let $\delta : \Omega \times \mathbb{R}^N \rightarrow \mathbb{R}$ be the support function of the set $\tilde{\mathcal{Z}}(x) = \mathcal{Z}(x) - \nabla\psi(x)$, i.e.:

$$\delta(x, p) = \max\{pq : q \in \tilde{\mathcal{Z}}(x)\}. \tag{4.11}$$

$\delta(x, p)$ is continuous in $\Omega \times \mathbb{R}^N$, convex and positively homogeneous in p and there exists R such that

$$0 \leq \delta(x, p) \leq R|p| \quad \forall x \in \overline{\Omega}, p \in \mathbb{R}^N \tag{4.12}$$

(see [27]).

For $A \subset \overline{\Omega}$, we denote: $\forall x, y \in \overline{A}$,

$$L_A(x, y) = \inf \left\{ \int_0^1 \delta(\xi(t), -\xi'(t))dt \mid \xi(t) \in W^{1,\infty}([0, 1], \overline{A}) \right. \\ \left. s.t. \quad \xi(0) = x \text{ and } \xi(1) = y \right\}$$

and we set $L(x, y) := L_\Omega(x, y)$. From (4.12) it follows that $0 \leq L(x, y) \leq Rd_E(x, y)$ and therefore $y \mapsto L(x, y)$ is Lipschitz continuous in $\overline{\Omega}$ for any fixed $x \in \overline{\Omega}$ (with a Lipschitz constant which does not depend on x).

Remark 34. If $x \in \mathcal{S}$, then $\tilde{\mathcal{Z}}(x) = \{0\}$ and therefore $\delta(x, p) = 0$ for any $p \in \mathbb{R}^N$. Also, the inverse statement holds. Hence

$$\delta(x, p) = 0, \forall p \in \mathbb{R}^N \iff x \in \mathcal{S} \iff r(x) = 0.$$

So $\forall x, y \in \overline{\Omega}$,

$$L(x, y) = 0 \iff S(x, y) = 0.$$

In other words,

$$\forall x_0 \in \overline{\Omega}, \quad B_S(x_0) = \{x \in \Omega : L(x_0, x) = 0\}. \tag{4.13}$$

Remark 35. When the Hamiltonian is not coercive, there can exist $x \in \overline{\Omega}$ such that $\mathcal{Z}(x)$ is unbounded. Hence for some $p \in \mathbb{R}^N$, we can have $\rho(x, p) = 0$ and $\delta(x, p) = +\infty$. So, for some $(x, y) \in \overline{\Omega} \times \overline{\Omega}$, we can have $L(x, y) = +\infty$. Note that, since L is in general nonsymmetric, it can result $L(y, x) < +\infty$.

Let us consider the function V :

$$V(x) = \psi(x) + \min\{ L(x, y) + \varphi(y) - \psi(y) \mid y \in \partial\Omega \cup \mathcal{S} \}. \quad (4.14)$$

Theorem 4.1 *The function V is a singular solution of (4.2)-(4.5).*

It is standard to prove that V is a viscosity subsolution of (4.2) (see [95, 29]). To show that V is a singular supersolution of (4.2)-(4.5), we need some preliminary results.

Proposition 4.2 *u is a subsolution of (4.2) in Ω if and only if*

$$u(x) \leq \psi(x) + u(y) - \psi(y) + L(x, y) \quad \text{for any } x, y \in \Omega \quad (4.15)$$

Proof. See proposition 4.7 in [28]. □

Proposition 4.3 *Set*

$$\Gamma_V = \{x \in \mathcal{S} \mid V(x) \geq \varphi(y) + \psi(x) - \psi(y) \text{ for some } y \in B_S(x)\}.$$

If $x_0 \in \Omega - \Gamma_V$, then $B_S(x_0) \cap \Gamma_V = \emptyset$.

Proof. Assume by contradiction that there exists $x_1 \in B_S(x_0) \cap \Gamma_V$. Hence there exists $y \in B_S(x_1)$ such that $V(x_1) \geq \varphi(y) + \psi(x_1) - \psi(y)$. Since $S(x_0, y) \leq S(x_0, x_1) + S(x_1, y) = 0$, $y \in B_S(x_0)$. By (4.13), (4.15) and $x_0 \notin \Gamma_V$ we have

$$V(x_1) \leq V(x_0) + \psi(x_1) - \psi(x_0) < \varphi(y) + \psi(x_0) - \psi(y) + \psi(x_1) - \psi(x_0)$$

and so

$$V(x_1) < \varphi(y) + \psi(x_1) - \psi(y)$$

hence a contradiction. □

Proposition 4.4 (Dynamic programming principle) *For all $x \in \Omega - \Gamma_V$ and all τ_S -neighborhood A of x s.t. $A \cap (\Gamma_V \cup \partial\Omega) = \emptyset$,*

$$V(x) = \psi(x) + \min_{y \in \partial A} \{L(x, y) + V(y) - \psi(y)\}. \quad (4.16)$$

Proof. Classic; see for example [5]. □

Proposition 4.5 *Let u be a l.s.c. function, ϕ_0 a S -subtangent to u at a point x_0 and a strict subsolution of (4.2) in a τ_S -neighborhood of x_0 . Then there exists a function ϕ which is strict S -subtangent to u at x_0 and a strict subsolution of (4.2) in a τ_S -neighborhood of x_0 and such that for any $x \in \Omega$, $q \in \partial\phi(x)$, one can select $p \in \partial\phi_0(x)$ verifying*

$$\rho(x, q) \leq \rho(x, p) + L(x_0, x) \quad (4.17)$$

Proof. See the proofs of proposition 6.1 of [27] and of proposition 5.1 of [26].
 □

Proof of Theorem 4.1. We argue by contradiction.

1. Let $x_0 \in \Omega - \Gamma_V$. Let us assume that there exists a function ϕ_0 , a neighborhood A of $B_S(x_0)$ and $\theta \in]0, 1[$ s.t. ϕ_0 is a S -subtangent to V at x_0 with $\phi_0(x_0) = V(x_0)$ and

$$\rho(x, \nabla\phi_0) \leq \theta, \quad x \in A \quad (4.18)$$

in the viscosity sense.

Let ϕ be a strict S -subtangent to V at x_0 verifying the statement of proposition 4.5. By continuity of the function $x \mapsto L(x_0, x)$ and (4.13), we can select a neighborhood A' of $B_S(x_0)$ and with $\overline{A'} \subset A$ satisfying

$$\sup_{x \in A'} L(x_0, x) < 1 - \theta, \quad (4.19)$$

$$\phi < V \quad \text{on} \quad \partial A' \quad (4.20)$$

and

$$A' \cap (\Gamma_V \cup \partial\Omega) = \emptyset. \quad (4.21)$$

Since $x_0 \in \Omega - \Gamma_V$, we can assume the dynamic programming principle (4.16) holds on A' , so there exists $y_0 \in \partial A'$ such that

$$V(x_0) = \psi(x_0) + L_{A'}(x_0, y_0) + V(y_0) - \psi(y_0).$$

By

$$V(x_0) = \phi(x_0) \quad \text{and} \quad V(y_0) > \phi(y_0)$$

we get

$$L_{A'}(x_0, y_0) + [\phi(y_0) - \psi(y_0)] - [\phi(x_0) - \psi(x_0)] < 0.$$

So we can select a path $\xi \in W^{1,\infty}([0, 1], \overline{A'})$ joining x_0 to y_0 satisfying

$$\int_0^1 \left[\delta(\xi(t), -\dot{\xi}(t)) + \frac{d}{dt}(\phi(\xi(t)) - \psi(\xi(t))) \right] dt < 0.$$

Hence there exists $t_0 \in [0, 1]$ such that the functions $\phi(\xi(t))$ and $\xi(t)$ are differentiable at t_0 and

$$\delta(\xi(t_0), -\dot{\xi}(t_0)) - \dot{\xi}(t_0) \nabla \psi(\xi(t_0)) + \frac{d}{dt} \phi(\xi(t_0)) < 0. \quad (4.22)$$

Using the chain rule for the generalized gradient (see [34]), we derive from (4.22)

$$\delta(\xi(t_0), -\dot{\xi}(t_0)) < -\dot{\xi}(t_0)(q_0 - \nabla \psi(\xi(t_0)))$$

for some $q_0 \in \partial \phi(\xi(t_0))$. Hence

$$\rho(\xi(t_0), q_0) > 1.$$

Therefore by (4.17) and (4.19) the inequality

$$\rho(\xi(t_0), p_0) > \theta$$

holds for a suitable $p_0 \in \partial \phi_0(\xi(t_0))$. This contradicts (4.18) and proposition 4.1 .

2. Let $x_0 \in \Gamma_V$. By definition of Γ_V , we have $V(x_0) \geq \varphi(x) + \psi(x_0) - \psi(x)$ for some $x \in B_S(x_0)$.
3. If $x_0 \in \partial \Omega$, assumption (4.3) implies that $B_S(x_0) = \{x_0\}$. If $V(x_0) > \varphi(x_0)$ and the conditions of viscosity supersolution does not hold. We can obtain a contradiction by adapting the proof of theorem V.4.13 of [5].

□

Remarks 36.

R36.1 - Γ_V is the set where V takes the boundary datum φ in the sense of the topology τ_S .

R36.2 - In the case where the Hamiltonian is not coercive, we can have $V(x) = +\infty$, for some x in $\overline{\Omega}$. Nevertheless, note that this difficulty is mainly due to the state constraints. In effect if we assume that there exists $p_0 \in \mathbb{R}^N$ such that $\forall x \in \overline{\Omega}$, $\delta(x, p_0) \leq R < +\infty$ for some R not depending on x (this hypothesis holds for all the “classical” SFS Hamiltonians) and if we enforce Dirichlet boundary conditions on $\partial\Omega$ (with Ω bounded), therefore

$$\forall x \in \overline{\Omega}, \quad V(x) < +\infty.$$

4.2.3 Uniqueness results

In this section we prove the uniqueness of the SDVS. This result applies for all the “classical” Shape from Shading equations described in section 2.1. We start this section with a maximum principle:

Theorem 4.2 (Maximum principle) *Let $u, v : \Omega \rightarrow \mathbb{R}$ be respectively an u.s.c. subsolution of (4.2) and a l.s.c. singular supersolution of (4.2)-(4.5). Let us denote*

$$\Gamma_v = \{x \in \mathcal{S} \mid v(x) \geq \varphi(y) + \psi(x) - \psi(y) \text{ for some } y \in B_S(x)\}.$$

Then

$$\min_{\overline{\Omega}} \{v - u\} = \min_{\partial\Omega \cup \Gamma_v} \{v - u\}.$$

Proof. Given $\theta \in]0,1[$, the function $u_\theta = \theta u + (1 - \theta)\psi(x)$ is a strict subsolution of (4.2) in Ω by the homogeneity of ρ (see (4.9)). Let us assume that $x_0 \in \Omega - \Gamma_v$ is a minimizer of $(v - u_\theta)$ in $\overline{\Omega}$. Therefore u_θ is a S -subtangent of v at x_0 which is also a strict subsolution of (4.2) in Ω . This contradicts that v is a singular supersolution at x_0 . So the minimizers of $(v - u_\theta)$ are in $\partial\Omega \cup \Gamma_v$. The assertion is obtained by letting θ go to 1. \square

In the sequel, we assume that there exists a neighborhood A of $\partial\Omega$ and $\lambda > 0$ such that:

$$(H12'') \quad |H(x, p) - H(x, q)| \leq \lambda|p - q| \quad \forall x \in A, \quad \forall p, q \in \mathbb{R}^N.$$

In other words, we impose that H is Lipschitz continuous in p (with a Lipschitz constant which does not depend on $x \in A$) on a neighbourhood of $\partial\Omega$. Note that the “classical” SFS Hamiltonians H_{pers}^* and H_{orth}^* verify the hypothesis

(H12'') (see section 2.2.6.2).

Using the maximum principle, we deduce the following strong uniqueness result:

Theorem 4.3 (Strong uniqueness of the SDVS with $\varphi = +\infty$ on $\partial\Omega$)

Let $u, v : \Omega \rightarrow \mathbb{R}$ be respectively an u.s.c. subsolution of (4.2)-(4.5), and a l.s.c. singular supersolution of (4.2)-(4.5), with φ verifying $\forall x \in \partial\Omega, \varphi(x) = +\infty$. If H verifies (H12'') then

$$\forall x \in \Omega, \quad u(x) \leq v(x). \quad (4.23)$$

Proof. We consider $M = \max_{\overline{\Omega}}(u(x) - v(x))$. We argue by contradiction and assume that $M > 0$. By the maximum principle (theorem 4.2), we have:

$$M = \max_{x \in \overline{\Omega}}(u(x) - v(x)) = \max_{x \in \partial\Omega \cup \Gamma_v}(u(x) - v(x)).$$

Let $x \in \Gamma_v$ and $y \in B_S(x)$ be such that $v(x) \geq \varphi(y) + \psi(x) - \psi(y)$. By (4.15) and because $\Gamma_v \subset \mathcal{S}$

$$v(x) \geq \varphi(y) + \psi(x) - \psi(y) \geq u(y) + \psi(x) - \psi(y) \geq u(x).$$

So, $\forall x \in \Gamma_v, u(x) - v(x) \leq 0$ and therefore

$$M = \max_{x \in \overline{\Omega}}(u(x) - v(x)) = \max_{x \in \partial\Omega}(u(x) - v(x)).$$

In other words, M is reached at a point $x_0 \in \partial\Omega$. Henceforth, we can work on a neighborhood A of the boundary $\partial\Omega$ where hypothesis (H12'') holds. We can assume that $A \cap \mathcal{S} = \emptyset$. So in this neighborhood A , the notion of singular viscosity solution coincides with the classical notion of discontinuous viscosity solutions. Therefore, we can obtain a contradiction exactly as in the proof of theorem 4.6 of [7] (let us recall that we have assumed that H is coercive in p uniformly with respect to x). \square

More generally, we have the theorem:

Theorem 4.4 (Strong uniqueness of the SDVS) Let $u, v : \Omega \rightarrow \mathbb{R}$ be respectively an u.s.c. subsolution of (4.2)-(4.5), and a l.s.c. singular supersolution of (4.2)-(4.5). Then

$$\forall x \in \Omega, \quad u(x) \leq v(x).$$

Proof. The statement can be proved combining the proofs of the previous theorem and of theorem 4.5 (and of its Corollary 4.1) of Barles' book [7]. \square

Let us note that clearly the strong uniqueness involves the uniqueness on Ω of

the singular viscosity solution of (4.2)-(4.5): i.e, if u_1 and u_2 are two singular viscosity solutions of (4.2)-(4.5), then $\forall x \in \Omega$, $u_1(x) = u_2(x)$. Moreover, it proves that this solution is continuous on Ω ($u = u^* = u_*$), therefore it is Lipschitz continuous on Ω (because subsolutions are Lipschitz continuous).

4.2.4 Stability of the singular solution

In this section, we show that the notion of SDVS enjoys some significative stability properties. This stability has important and appreciable consequences for the Shape from Shading problem.

A general stability result

We consider for $n \in \mathbb{N}$ the equations:

$$H_n(x, \nabla u) = 0, \quad \forall x \in \Omega \quad (4.24)$$

with continuous, convex and coercive Hamiltonians H_N satisfying the hypotheses (H2'),(H3') and (H23).

We set for any $x \in \overline{\Omega}$:

$$\begin{aligned} \mathcal{Z}_n(x) &= \{p \in \mathbb{R}^N \mid H_n(x, p) \leq 0\}, \\ \mathcal{S}_n(x) &= \{x \in \overline{\Omega} \mid H_n(x, \nabla \psi(x)) = 0\}. \end{aligned}$$

We require the following conditions:

$$\text{there exists } M > 0 \text{ s.t. } \mathcal{Z}_n(x) \subset B(0, M) \text{ for any } x \in \overline{\Omega}, n \in \mathbb{N} \quad (4.25)$$

$$\theta_n \mathcal{Z}(x) + (1 - \theta_n) \nabla \psi(x) \subset \mathcal{Z}_n(x) \quad \text{for any } x \in \overline{\Omega}, n \in \mathbb{N} \quad (4.26)$$

$$H(x, p) \leq \liminf_{n \rightarrow +\infty} {}_*H_n(x, p) \quad \text{for any } (x, p) \in \overline{\Omega} \times B(0, M) \quad (4.27)$$

where θ_n is a sequence converging to 1.

Remarks 37.

R37.1 - Assumption (4.25) implies that the SDVSs u_n of (4.24)-(4.5) verify $\|\nabla u_n\|_\infty \leq M$, for any n . So the functions u_n are uniformly Lipschitz continuous and also uniformly bounded on $\overline{\Omega}$.

R37.2 - By (H24) and remark 32, (4.26) involves

$$\mathcal{S}_n \subset \mathcal{S}$$

and

$$\theta_n \mathcal{S}(x, y) \leq \mathcal{S}_n(x, y), \quad \forall x, y \in \overline{\Omega},$$

where \mathcal{S}_n is the distance defined as in (4.10) with $r_n(x) = \sup\{r > 0 \mid B(\nabla \psi(x), r) \subset \mathcal{Z}_n(x)\}$ in place of $r(\cdot)$. In particular, the topology τ_n is stronger than the topology τ .

We have the following stability result:

Theorem 4.5 (stability) *Let $u_n : \overline{\Omega} \rightarrow \mathbb{R}$ be a sequence of SDVS of (4.24)-(4.5) (with \mathcal{S}_n in place of \mathcal{S}) on $\overline{\Omega}$. Assume that (4.25)-(4.27) are satisfied. If u is the SDVS of (4.2)-(4.5), then*

$$u(x) = \lim_{n \rightarrow \infty} u_n(x)$$

uniformly in $\overline{\Omega}$.

Proof. By (4.25) the sequence u_n is uniformly bounded and uniformly Lipschitz continuous in $\overline{\Omega}$. Hence, all the subsequences of $(u_n)_{n \in \mathbb{N}}$ converging toward $\limsup^* u_n$ and $\liminf_* u_n$ converge uniformly and $\limsup^* u_n$ and $\liminf_* u_n$ are bounded and Lipschitz continuous on $\overline{\Omega}$. By (4.27) it follows that $\limsup^* u_n$ is a viscosity subsolution of (4.2)-(4.5) (see for example [5], [6]).

If $\liminf_* u_n$ is a singular supersolution of (4.2)-(4.5), then by theorem 4.4, we get

$$\limsup^* u_n \leq \liminf_* u_n.$$

Since the reverse inequality is true by definition we get that $\limsup^* u_n = \liminf_* u_n$ and therefore the sequence u_n converges uniformly toward the SDVS of (4.2)-(4.5). So, to conclude, it is sufficient to prove that all the limits u of subsequences of u_n uniformly convergent are singular supersolutions of (4.2)-(4.5):

1. Let $x_0 \in \mathcal{S}$ be such that $u(x_0) < \varphi(y) + \psi(x_0) - \psi(y)$ for any $y \in B_S(x_0)$, otherwise the conclusion is obvious. Note that, by continuity of u, φ and ψ , this inequality holds on a neighborhood of $B_S(x_0)$.

- By (4.26), we have

$$\rho_n(x, p) \leq \theta_n \rho(x, p) \tag{4.28}$$

for any $n \in \mathbb{N}$, $x \in \Omega$ and $p \in \mathbb{R}^N$.

- Assume for purpose of contradiction that there is a strict S -subtangent ϕ to u at x_0 which is also a strict viscosity subsolution of (4.2) in a neighborhood A of $B_S(x_0)$, i.e.

$$(u - \phi)(y) > (u - \phi)(x_0), \text{ for any } y \in A - B_S(x_0),$$

$$\rho(y, \nabla \phi(y)) \leq \eta \tag{4.29}$$

in A in the viscosity sense, for some $\eta \in]0, 1[$.

- A standard argument in viscosity solution theory gives the existence of a sequence x_n of minimizer of $u_n - \phi$ verifying $S(x_0, x_n) \rightarrow 0$ (see [7], Lemma 4.2). By the uniform convergence of $(u_n)_{n \in \mathbb{N}}$, we have that $u_n(x_n) < \varphi(y) + \psi(x_n) - \psi(y)$ for any $y \in B_{S_n}(x_n) \subset B_S(x_n) \subset A$ for n sufficiently large. Hence, even if $x_n \in \mathcal{S}_n$, for n sufficiently large, u_n verifies at x_n the singular supersolution property. Since A is a neighborhood of $B_{S_n}(x_n)$, ϕ is S_n -subtangent to u_n at x_n .
- (4.28) and (4.29) involve:

$$\rho_n(y, \nabla \phi(y)) \leq \theta_n \eta, \quad \forall y \in A,$$

in viscosity sense. Hence ϕ is a strict subsolution of (4.24) for n large enough. This contradicts u_n being a singular supersolution of (4.24) at x_n .

2. If $x_0 \in \overline{\Omega} - \mathcal{S}$ then $\rho(x, p) \geq 1$ if and only if $H(x, p) \geq 0$ and singular and discontinuous viscosity supersolution coincide. Hence the previous argument can be adapted to show that u is a viscosity supersolution also in this case.

□

4.2.5 A new characterization of the discontinuous viscosity solutions by their “minimums”

Let us denote by Π_u the set of points in Ω such that a constant function cannot be S -subtangent to $u - \psi$ at x . If $x \notin \mathcal{S}$ or $B_S(x) = \{x\}$, this means that x cannot be a local minimum point for $u - \psi$. For this reason we call Π_u the set of minimum points of $u - \psi$. We also set

$$\Gamma_u = \{x \in \Omega \mid \exists y \in B_S(x) \text{ verifying } u(x) \geq \varphi(y) + \psi(x) - \psi(y)\}.$$

Theorem 4.6 *Let u be a (discontinuous) viscosity solution of (4.2)-(4.5) such that $u(x) \leq \varphi(x)$ for any $x \in \mathcal{S}$. If $\Pi_u \subset \Gamma_u$ then u is the SDVS of (4.2)-(4.5).*

In other words, the SDVS is the unique (discontinuous) viscosity solution u of (4.2)-(4.5) (verifying $\forall x \in \mathcal{S}, u(x) \leq \varphi(x)$) without local minima on $\Omega - \Gamma_u$. Of course, the reciprocal statement of theorem 4.6 holds. That is to say that the SDVS cannot have points of local minimum (in Ω) outside of Γ_u . In effect, by contradiction, if $u - \psi$ admits a constant function S -subtangent to $x_0 \notin \Gamma_u$, then the function ψ is a S -subtangent to u at x_0 . Since by the definition of

\mathcal{S} , ψ is a strict subsolution of (4.2) it follows that u cannot be a (singular) supersolution at x_0 .

An important interpretation and consequence of theorem 4.6 is the following:

The (discontinuous) viscosity solutions of (4.2)-(4.5) can be characterized only by their minima.

That is to say, if u is a (discontinuous) viscosity solutions of (4.2)-(4.5) then u is the (unique) SDVS of

$$\begin{cases} H(x, \nabla u) = 0, & \forall x \in \Omega, \\ u(x) = \hat{\varphi}(x), & \forall x \in \partial\Omega \cup \mathcal{S}, \end{cases}$$

where

$$\begin{aligned} \hat{\varphi}(x) &= \varphi(x), & \forall x \in \Pi_u \cup \partial\Omega, \\ \text{and } \hat{\varphi}(x) &= +\infty, & \forall x \in \mathcal{S} - \Pi_u. \end{aligned}$$

Proof of Theorem 4.6. We have just to prove that the solution u is a singular supersolution at all the singular points which are not in Γ_u . We assume for simplicity that $B_S(x_0) = \{x_0\}$ but it is straightforward to extend the argument to the general case.

We argue by contradiction assuming that there exists a function ϕ , a neighborhood $A \subset \Omega - \Gamma_u$ of x_0 and $\theta \in]0, 1[$ such that ϕ is a S -subtangent to u at x_0 with

$$\begin{aligned} \phi(x_0) &= u(x_0), \\ \phi(x) &\leq u(x), & x \in A, \\ \phi(x) &\leq u(x) - \eta, & x \in \partial A \end{aligned}$$

for some $\eta > 0$ and

$$\rho(x, \nabla \phi) \leq \theta \quad x \in A$$

in the viscosity sense. Since u is a solution of (4.2) in A we have (see [95, 5])

$$u(x) = \psi(x) + \min\{u(y) - \psi(y) + L_A(x, y) : y \in \partial A\} \wedge \{u(x_0) - \psi(x_0) + L(x, x_0)\}. \quad (4.30)$$

Since x_0 is not a minimum point of $u - \psi$, we can find x_n such that $L(x_n, x_0) \rightarrow 0$ for $n \rightarrow \infty$ and $u(x_n) - \psi(x_n) \leq u(x_0) - \psi(x_0)$. It follows that $u(x_0) - \psi(x_0) + L(x_n, x_0) > u(x_n) - \psi(x_n)$ (since $L(x_n, x_0) > 0$). By (4.30), we can find $y_n \in \partial A$ such that $u(x_n) = \psi(x_n) + u(y_n) - \psi(y_n) + L(x_n, y_n)$. Hence

$$\begin{aligned} 0 &\geq u(y_n) - \psi(y_n) - u(x_0) + \psi(x_0) + L(x_n, y_n) - L(x_n, x_0) \geq \\ &\phi(y_n) + \eta - \psi(y_n) - \phi(x_0) + \psi(x_0) + L(x_n, y_n) - L(x_n, x_0). \end{aligned} \quad (4.31)$$

Passing to a subsequence we can assume that $y_n \rightarrow y_0$ with $y_0 \in \partial A$. Since $L(x_n, y_n)$ and $L(x_0, y_n)$ converge to $L(x_0, y_0)$ and $L(x_n, x_0)$ converges to 0, we can find n large such that

$$L(x_n, y_n) - L(x_n, x_0) + \eta > L(x_0, y_n).$$

Substituting the previous inequality in (4.31) we get

$$0 > \phi(y_n) - \psi(y_n) - \phi(x_0) + \psi(x_0) + L(x_0, y_n).$$

Fixed such n , we can find $\xi \in W^{1,\infty}([0, 1], \bar{A})$ joining x_0 to y_n satisfying

$$\int_0^1 \left(\delta(\xi(t), -\dot{\xi}(t)) + \frac{d}{dt}(\phi(\xi(t)) - \psi(\xi(t))) \right) dt < 0.$$

From the previous inequality we get a contradiction to the definition of singular viscosity supersolution as in the proof of theorem 4.1. \square

4.3 Application to the “classical” Shape from Shading problem

4.3.1 Existence and uniqueness of the SDVS of the “classical” SFS equations

The hypotheses required for applying the theory developed in section 4.2 are

(H1) H is convex with respect to p for all x in $\bar{\Omega}$.

(H4) $H \in C(\bar{\Omega} \times \mathbb{R}^N)$.

(H3') There exists a subsolution $\psi \in C^1(\Omega) \cap W^{1,\infty}(\Omega)$ of (4.2) (i.e: $\forall x \in \Omega, H(x, \nabla\psi(x)) \leq 0$).

(H23) For any $\lambda \in (0, 1)$, $p \in \mathbb{R}^N$ s.t $H(x, p) \leq 0$ then

$$H(x, \lambda p + (1 - \lambda)\nabla\psi(x)) < 0.$$

By using chapter 2, one can verify easily that these hypotheses hold for all the “classical” SFS Hamiltonians (considered in section 2.1) as soon as the intensity image I is continuous and verifies $I(x) > 0$ for any $x \in \bar{\Omega}$.

It is also required that the following coercitivity condition holds:

(H2') $\liminf_{|p| \rightarrow +\infty} H(x, p) = +\infty$, for any $x \in \bar{\Omega}$.

4.3 Application to the “classical” Shape from Shading problem 173

This coercivity hypothesis is not systematically verified for all the SFS Hamiltonians (see subsection 2.2.4.1). Globally, it does not hold for the pixels of the image with a low brightness (i.e. $I(x)$ close to 0) when the direction of the distant light source is very different to the one of the camera.

Moreover, one can verify easily that the hypotheses

$$(H24) \quad \forall x \in \mathcal{S}, \quad \mathcal{Z}(x) = \{\nabla\psi(x)\}$$

and

$$(H12'') \quad |H(x, p) - H(x, q)| \leq \lambda|p - q| \quad \forall x \in A, \quad \forall p, q \in \mathbb{R}^N$$

hold for all the “classical” SFS Hamiltonians. So theorems 4.1 and 4.4 ensure⁴ the existence and the uniqueness of the SDVS of all the “classical” SFS equations.

4.3.2 Applications of the stability of the SDVS to the Shape from Shading problem

In this subsection we apply theorem 4.5 to the “classical” SFS problem.

1. Approximation of the degenerated equations by non-degenerated equations:

The lack of uniqueness of the solution to (4.2) is a noteworthy problem for numerical computations of a solution to the Shape from Shading problem, since it causes numerical instability and sometimes fail of convergence of standard approximation schemes. It is therefore usual to regularize (4.2) by cutting the image intensity at a certain level strictly less than 1 before applying the approximation procedure. As a first application of Theorem 4.5, we show that the notion of SDVS is stable respect to this type of regularization.

Given a continuous image I and $\varepsilon > 0$, we set⁵

$$I_\varepsilon(x) = \min(I(x), 1 - \varepsilon), \quad \forall x \in \overline{\Omega}.$$

For a SFS Hamiltonian H , we denote by H_ε the new Hamiltonian obtained replacing $I(x)$ by $I_\varepsilon(x)$ in H . Since $I_\varepsilon \leq I$, the reader will verify easily that for all the “classical” SFS Hamiltonians,

$$\forall x \in \overline{\Omega}, \quad \forall p \in \mathbb{R}^N, \quad H_\varepsilon(x, p) \leq H(x, p).$$

Therefore,

$$\forall x \in \overline{\Omega}, \quad \mathcal{Z}(x) \subset \mathcal{Z}_\varepsilon(x).$$

⁴Under the condition that the coercivity hypothesis (H2') holds.

⁵Let us remind the reader that we assume that the intensity is between 0 and 1.

So the condition (4.26) holds for $\theta_\varepsilon = 1$. Moreover, it is easy to prove that H_ε converge toward H (when $\varepsilon \rightarrow 0$) uniformly with respect to $(x, p) \in \overline{\Omega} \times K$ for all compact set $K \subset \mathbb{R}^N$. Therefore, theorem 4.5 applies and the singular viscosity solutions of (4.24)-(4.5) converge toward the unique singular viscosity solution of (4.2)-(4.5).

Now, let us remark that, $\forall \varepsilon > 0$, the SFS Hamiltonian H_ε (associated with I_ε) is not degenerate anymore (i.e $\mathcal{S} = \emptyset$). So, its (unique) singular viscosity solution is the (unique) classical discontinuous viscosity solution. Thus, for approximating its solution, we can use the classical tools we have developed in chapter 2.

2. Robustness of the Shape from Shading solutions to the image regularization:

In computer vision or more generally in image processing, the images are always corrupted by noise. To remove this noise, the images are often regularized [159]. In other respects, most of CCD sensors slightly smooth the images and defocus effects can strongly diffuse the brightness information [57]. Since, we do not have taken into account these regularization effects in the modeling, it seems important to guarantee the robustness of our SFS methods to them.

We consider a sequence of noisy (or denoised) images I_n converging uniformly to I and we set $\omega_n = \|I - I_n\|_{L^\infty(\Omega)}$.

Unfortunately, in this general situation, stability does not hold. It is possible to design counter examples for which I_n converges uniformly toward I but the corresponding SDVSs do not converge uniformly (see for example [10]). Here we show that if the images I_n are appropriately regularized, we recover again the stability of SDVSs.

Let ε_n be a sequence such that $\omega_n/\varepsilon_n \rightarrow 0$ for $n \rightarrow +\infty$. Set

$$I_{n\varepsilon_n} = \min(I_n(x), 1 - \varepsilon_n), \quad \forall x \in \overline{\Omega},$$

let $H_n(x, p)$ be the SFS Hamiltonians corresponding to the intensity $I_{n\varepsilon_n}$ and $Z_n = \{p \in \mathbb{R}^N : H_n(x, p) \leq 0\}$. For simplicity we assume that both the limit equation (4.2) and the regularized equations corresponding to the Hamiltonians H_n admit $\psi \equiv 0$ as a subsolution⁶. We want to show that assumption (4.26), with $\psi \equiv 0$, holds (the other assumptions of the stability theorem being obvious).

Set $\mathcal{S}^n = \{x \in \Omega : I(x) \geq 1 - \varepsilon_n\}$. We distinguish two cases

⁶Let us recall that by an appropriate change of variables, the SFS Hamiltonians $H_{P/F}^{pers}$ and $H_{R/T}^{orth}$ can be reduced to this case.

4.3 Application to the “classical” Shape from Shading problem 175

(a) If $x \in \mathcal{S}^n$, then $I_{n\varepsilon_n}(x) \leq 1 - \varepsilon_n \leq I(x)$, hence, recalling that the SFS Hamiltonians are increasing in I , we get $Z(x) \subset Z_n(x)$.

(b) If $x \notin \mathcal{S}^n$, then

$$I(x) \geq I_n(x) - \omega_n \geq I_{n\varepsilon_n}(x) - \omega_n = I_{n\varepsilon_n}(x) - \frac{\omega_n}{\varepsilon_n} \varepsilon_n \geq I_{n\varepsilon_n}(x) - \frac{\omega_n}{\varepsilon_n} (I_{n\varepsilon_n}(x) - 1) \geq (1 - \frac{\omega_n}{\varepsilon_n}) I_{n\varepsilon_n}(x).$$

Therefore, recalling that $\omega_n/\varepsilon_n \rightarrow 0$, we find that hypothesis (4.26) is satisfied with $\theta_n = (1 - \frac{\omega_n}{\varepsilon_n})^{-1}$.

Example : A typical example of a denoised sequence of images is given by $I_n(x) = (I * \eta_n)(x)$, where η_n is a standard mollifier, i.e. $\eta_n(x) = n^N \eta(nx)$ with $\eta : \mathbb{R}^N \rightarrow \mathbb{R}$ a smooth, nonnegative function such that the support of η is contained in the unit ball and $\int_{\mathbb{R}^N} \eta(z) dz = 1$ (we assume for simplicity that I is defined in a neighborhood of $\overline{\Omega}$, so I_n can be defined in $\overline{\Omega}$ for n sufficiently large). I_n is a smooth function and $0 \leq I_n(x) \leq 1$. Moreover $I_n(x) = 1$ if and only if $I(y) = 1$ for any $y \in B(x, 1/n)$. Hence $\mathcal{S}_n = \{x \in \Omega : I_n = 1\}$ is a proper subset of \mathcal{S} . If \mathcal{S} reduces for example to a finite number of points, the regularized problem is not singular. Note that H_n satisfies the same hypothesis of H , i.e. it is continuous, convex and, since $I \geq m > 0$ implies $I_n \geq m > 0$, also coercive in p .

3. Robustness of the Shape from Shading solutions to pixel noise and errors on parameters:

As we have pointed out previously, in computer vision, the images are always corrupted by noise. It is therefore very important to design schemes and algorithms *robust* to noise. That is to say we would like that the result obtained by the algorithm from a noisy image be close to the ideal result obtained from the perfect image. Moreover, the computer vision algorithms use frequently various parameters. In this work, we assume that the camera is calibrated and that the position of the light source is known. So, for applying our algorithms, the user must input (as parameters) the focal length, the size of the pixels (width, height) and a vector representing the light source direction (following the chosen modeling). In practice, these additional data can be not known precisely and the inputs provided by the user can contain important errors. Consequently, to be applicable, the algorithms must be robust to these unavoidable errors

on parameters. In other words, the returned results by the algorithms with corrupted parameters must be close to the results returned with the perfect theoretical parameters.

Mathematically, the robustness is expressed by the continuity of the application which from an image I (a focal length f or a light source direction \mathbf{L}, \dots , respectively), returns the solution u of the associated PDE. In other words, we would like that, for all sequences of noisy images I_n (of focal lengths f_n or of light source directions \mathbf{L}_n, \dots , respectively) converging toward an image I (f or \mathbf{L}, \dots , respectively), the sequence of recovered solutions u_n converges toward the solution u associated to I (f or \mathbf{L} , respectively). In other words, if we denote H_n the Hamiltonian obtained by replacing the parameters \mathbf{L} , f and I by \mathbf{L}_n , f_n and I_n in H , then the desired stability property corresponds with the convergence of the SDVSs of (4.24)-(4.5) towards the SDVS of (4.2)-(4.5) when $n \rightarrow +\infty$. Theorem 4.5 allows to demonstrate that this property is satisfied.

Below, we *sketch* an example of steps for proving that theorem 4.5 applies to SFS problem. We consider the case, where \mathbf{L}_n and f_n converge toward \mathbf{L} and f (here, we fix $I_n = I$). Up to a change of variables, we assume that $\psi = 0$. For a maximum of generality, we deal with the generic SFS Hamiltonian.

- (a) Let us recall that the “classical” SFS Hamiltonians are special cases of the generic SFS Hamiltonian

$$H_g(x, p) = \kappa_x \sqrt{|A_x p + \mathbf{v}_x|^2 + K_x^2} + \mathbf{w}_x \cdot p + c_x$$

where $\kappa_x, A_x, \mathbf{v}_x, K_x, \mathbf{w}_x$ and c_x are completely described in chapter 2. For all the “classical” SFS Hamiltonians, the functions $\kappa_x, A_x, \mathbf{v}_x, K_x, \mathbf{w}_x$ and c_x depend continuously on x, \mathbf{L} and f (see appendix B for details). Let us denote \mathbf{L}_n and f_n the approximations of \mathbf{L} and f . $\kappa_x^n, A_x^n, \mathbf{v}_x^n, K_x^n, \mathbf{w}_x^n, c_x^n$ the approximations of $\kappa_x, A_x, \mathbf{v}_x, K_x, \mathbf{w}_x, c_x$ obtained by replacing \mathbf{L} and f by \mathbf{L}_n, f_n . H_n is the approximation of H_g .

- (b) Let us remind that the notion of SDVS requires the coercivity of the Hamiltonians. So we assume that there exists $\delta > 0$ such that

$$\forall x \in \overline{\Omega}, \quad \kappa_x - |{}^t A_x^{-1} \mathbf{w}_x| > \delta$$

(see proposition 2.3 at page 71). If we assume that $\mathbf{L}_n \rightarrow \mathbf{L}$ and $f_n \rightarrow f$ then for all the “classical” SFS Hamiltonians, we have by continuity: for all n large enough,

$$\forall x \in \overline{\Omega}, \quad \kappa_x^n - \left| {}^t A_x^{n-1} \mathbf{w}_x^n \right| > \frac{\delta}{2}$$

4.3 Application to the “classical” Shape from Shading problem¹⁷⁷

so, the functions H_n are coercive in p uniformly with respect to $x \in \overline{\Omega}$ and $n \in \mathbb{N}$. In particular, the hypothesis (4.25) holds.

- (c) For all $x \in \overline{\Omega}$ and $p \in S^2$ (the unit sphere in \mathbb{R}^2), let us consider $g : \Omega \times \mathbb{R}^+ \rightarrow \mathbb{R}$ defined by

$$g(x, r) = H(x, \nabla\psi + rp)$$

and g_n the approximation of g designed from H_n (instead of H). Clearly, there exist $a(x, p)$, $b(x, p)$, $c(x, p)$, $\mu(x, p)$ and $\nu(x, p)$ in \mathbb{R} such that

$$g(x, r) = \kappa_x \sqrt{a(x, p)r^2 + b(x, p)r + c(x, p)} + \mu(x, p)r + \nu(x, p).$$

Obviously, we have the same rewriting of g_n with a_n , b_n , c_n , μ_n and ν_n which are the appropriate approximations. The uniform coercivity of the functions H_n and function H involves that there exists $\delta > 0$ such that $\forall x \in \overline{\Omega}, p \in S^N, n \in \mathbb{N}$,

$$(\kappa_x^n)^2 a_n(x, p) - \mu_n(x, p)^2 > \delta \quad \text{and} \quad \kappa_x^2 a(x, p) - \mu(x, p)^2 > \delta.$$

Since $\psi = 0$ is a subsolution, we have

$$(\kappa_x^n)^2 c_n(x, p) - \nu_n(x, p)^2 \leq 0 \quad \text{and} \quad \kappa_x^2 c(x, p) - \nu(x, p)^2 \leq 0$$

with a strict inequality outside of \mathcal{S} (note that since $I_n = I$ then $\mathcal{S}_n = \mathcal{S}$).

Note that ν and ν_n are non positive.

So, by using the appendix C.4, we can claim that the equation $g(x, r) = 0$ has an unique solution in \mathbb{R}^+ ⁷. It is given by:

$$r(x, p) = \frac{-\left(\kappa_x^2 b(x, p) - 2\mu(x, p)\nu(x, p)\right) + \sqrt{\Delta(x, p)}}{2\left(\kappa_x^2 a(x, p) - \mu(x, p)^2\right)}$$

where

$$\begin{aligned} \Delta(x, p) &= \left(\kappa_x^2 b(x, p) - 2\mu(x, p)\nu(x, p)\right)^2 \\ &\quad - 4\left(\kappa_x^2 c(x, p) - \nu(x, p)^2\right)\left(\kappa_x^2 a(x, p) - \mu(x, p)^2\right). \end{aligned} \quad (4.32)$$

Of course, the same result holds for the equation $g_n(x, r) = 0$. We denote $r_n(x, p)$ its solution. By using the adequate approximations, we obtain the same expression as $r(x, p)$.

⁷Let us fix x in $\overline{\Omega} \setminus \mathcal{S}$. For all our SFS Hamiltonians we have $\psi(x) = \operatorname{argmin}_p H(x, p)$ and $H(x, \nabla\psi(x)) < 0$. So, by continuity, coercivity and convexity of H , for all $p \neq 0$, the equation (in $r \in \mathbb{R}$) $H(x, \nabla\psi + rp) = 0$ has two solutions: a positive one and a negative one. The positive solution is the largest...

(d) For all $x \in \overline{\Omega} \setminus \mathcal{S}$ and $p \in S^2$, let us denote

$$\theta_n(x, p) = \frac{r_n(x, p)}{r(x, p)}.$$

If (x, p) is fixed in $\overline{\Omega} \setminus \mathcal{S} \times S^2$, then we have $\theta_n(x, p) \rightarrow 1$, when $n \rightarrow +\infty$. As we explain in the sequel, the conclusion follows as soon as we have proved that this convergence is uniform. In the following example, we show that, with a few additional regularity hypotheses (for example, $I \in C^1(\overline{\Omega})$), this step can be done by considering some precise SFS Hamiltonians. But this step is not obvious because $r(x, p)$ and $r_n(x, p)$ vanishes on \mathcal{S} . Also, we do not have find a generic proof.

(e) Now let us prove that the conclusion follows as soon as $\theta_n(x, p) \rightarrow 1$ uniformly when $n \rightarrow +\infty$.

Let us denote

$$\underline{\theta}_n = \min_{(x,p) \in \overline{\Omega} \setminus \mathcal{S} \times S^N} \theta_n(x, p),$$

we have $\underline{\theta}_n \rightarrow 1$ when $n \rightarrow +\infty$. In other respects, by hypothesis (H23), we have:

$$\forall x \in \overline{\Omega}, \forall q \in \tilde{\mathcal{Z}}(x), \quad \exists \mu \geq 1 \text{ such that } \mu q \in \partial \tilde{\mathcal{Z}}(x).$$

By definition of $\theta_n(x, p)$, we have

$$\theta_n \left(x, \frac{q}{|q|} \right) (\mu q) \in \partial \tilde{\mathcal{Z}}_n(x).$$

Since $0 \leq \underline{\theta}_n \leq \mu \theta_n \left(x, \frac{q}{|q|} \right)$, the hypothesis (H23) involves

$$\underline{\theta}_n q \in \tilde{\mathcal{Z}}_n(x).$$

Thus, we have proved $\forall x \in \overline{\Omega}$,

$$\underline{\theta}_n \tilde{\mathcal{Z}}(x) \subset \tilde{\mathcal{Z}}_n(x).$$

So,

$$\underline{\theta}_n \mathcal{Z}(x) + (1 - \underline{\theta}_n) \nabla \psi \subset \mathcal{Z}_n(x).$$

So the hypothesis (4.26) holds.

Let us remind that above, we have shown that in general the hypotheses (4.25) also holds with the SFS equations (when the focal length, the light source direction (...) are corrupted and when errors vanish). (4.27) clearly holds. Therefore, theorem 4.5 applies. The stability is then proved.

4.3 Application to the “classical” Shape from Shading problem 179

Example : Let us consider the example of the Hamiltonian $H_{D/O}^{orth}$ with $\mathbf{L}_n \rightarrow \mathbf{L}$. So

$$H(x, p) = I(x) \sqrt{1 + |p|^2} - 2p \cdot \mathbf{l} + p \cdot \mathbf{l} - 1$$

and

$$H_n(x, p) = I(x) \sqrt{1 + |p|^2} - 2p \cdot \mathbf{l}_n + p \cdot \mathbf{l}_n - 1.$$

Easily, one can verify that

$$r(x, p) = \sqrt{1 - I(x)^2} \frac{I(x) \sqrt{1 - (p \cdot \mathbf{l})^2} - (p \cdot \mathbf{l}) \sqrt{1 - I(x)^2}}{I(x)^2 - (p \cdot \mathbf{l})^2},$$

and that $\forall x \in \overline{\Omega}, \forall p \in S^N$,

$$\theta_n(x, p) = \frac{I(x) \sqrt{1 - (p \cdot \mathbf{l}_n)^2} - (p \cdot \mathbf{l}_n) \sqrt{1 - I(x)^2}}{I(x) \sqrt{1 - (p \cdot \mathbf{l})^2} - (p \cdot \mathbf{l}) \sqrt{1 - I(x)^2}} \cdot \frac{I(x)^2 - (p \cdot \mathbf{l})^2}{I(x)^2 - (p \cdot \mathbf{l}_n)^2}.$$

If the brightness image I is differentiable and if ∇I is bounded on $\overline{\Omega}$ ⁸ then, $\partial_x \theta_n(x, p)$ is bounded independantly of $x \in \overline{\Omega}$, $n \in \mathbb{N}$ and p on a neighborhood of S^N .

Proof. Let us denote $s_n = p \cdot \mathbf{l}_n$ and $s = p \cdot \mathbf{l}$.

Note that $s_n \rightarrow s$ uniformly with respect to p in a neighborhood of S^N .

Let us consider the function

$$\begin{aligned} T : \mathbb{R} &\rightarrow \mathbb{R} \\ X &\mapsto \frac{\sqrt{1 - s_n X} - s_n \sqrt{1 - X^2}}{\sqrt{1 - s X} - s \sqrt{1 - X^2}}. \end{aligned} \quad (4.33)$$

$\forall \delta > 0$ (and small enough), we have for all n large enough, $|s_n| < |s| + \delta \leq 1$, T is continuously derivable on $[s + \delta, 1]$ and T' is bounded independantly of s_n ⁹.

By the uniform coercivity assumption, there exists $\delta > 0$ such that for all p in a neighborhood of S^N and for all n large enough,

$$|s_n| < |s| + \delta < \min_{x \in \overline{\Omega}} I(x) \leq 1.$$

Since,

$$\nabla_x (T \circ I)(x) = T'(I(x)) \nabla_x I(x),$$

⁸for example, since Ω is bounded, ∇I is bounded as soon as $I \in C^1(\overline{\Omega})$.

⁹so independantly of n and p in a neighborhood of S^N .

therefore $\nabla_x(T \circ I)$ is bounded independently of x, p and n . We can conclude by using the fact that the function

$$x \mapsto \frac{I(x)^2 - (p \cdot \mathbf{1})^2}{I(x)^2 - (p \cdot \mathbf{1}_n)^2}$$

and its gradian are bounded independently of x in $\overline{\Omega}$, n in \mathbb{N} and p in a neighborhood of S^N . \square

In a same way, we prove that $\partial_p \theta_n(x, p)$ is uniformly bounded. Let us denote $X = (x, p)$. So we have $\nabla_X \theta_n(X)$ uniformly bounded. Moreover,

$$\forall X, Y \in \overline{\Omega} \times S^N, \quad |\theta_n(X) - \theta_n(Y)| \leq |\nabla_X \theta_n|_\infty L(X, Y),$$

where $L(X, Y)$ is the Euclidean geodesic distance in $\Omega \times S^N$. Also, it is well known [95] that for any fixed $X \in \overline{\Omega}$, $Y \mapsto L(X, Y)$ is *Lipschitz continuous* in $\overline{\Omega} \times S^N$ and that the Lipschitz constant does not depend on X . Thus the functions θ_n are uniformly Lipschitz continuous. Therefore the convergence of the sequence θ_n is uniform.

Remark 38. In a general way, the above development is not systematically applicable when the images are noised and the corrupted images I_n converge toward I . For example, let us consider the Hamiltonian $H_{D/O}^{orth}$ with $I_n \rightarrow I$ and $\mathbf{L} = (0, 0, 1)$. So

$$H(x, p) = I(x) \sqrt{1 + |p|^2} - 1$$

and

$$H_n(x, p) = I_n(x) \sqrt{1 + |p|^2} - 1.$$

$\forall x \in \overline{\Omega} \setminus \mathcal{S}, \forall p \in S^N$, we have

$$\theta_n(x, p) = \frac{I(x)}{I_n(x)} \frac{\sqrt{1 - I_n(x)^2}}{\sqrt{1 - I(x)^2}}.$$

4.4 A general framework for the “classical” Shape from Shading problem

In this section, we explain *why the notion of state constraints is relevant* when we do not know the values of the solution and we describe this boundary condition in a more intuitive way. Moreover, we show that *the notion of SDVS*

provides a general mathematical framework unifying the previous mathematical frameworks based on viscosity solution theory proposed in the SFS literature.

The main contribution of the notion of SDVS lies in the possibility to impose the heights of the solution at the singular points when we know them¹⁰ and on the possibility to “send to infinity” the boundary conditions when we do not know them. This possibility also holds for all the points located on the boundary of the image $\partial\Omega$. Let us recall that in previous work [134, 127, 120, 119, 24, 55, 56], the various notions of viscosity solutions [continuous, discontinuous or singular] are used with (finite) Dirichlet conditions on the boundary of the images. Note that, in [96], Lions et al. have already used the notion of states constraints, but they used it only to deal with apparent contours and in the eikonal setup. More precisely, they use it only at the points $x \in \partial\Omega$ such that $I(x) = 0$ and “ $\frac{\partial u}{\partial n} = -\infty$ ”. Here, we use the state constraints at each point of $\partial\Omega \cup \mathcal{S}$, where we do not know the value of the solution.

Let us focus on the points on the boundary $\partial\Omega$ of the image. For simplicity, let us assume that we know the values of the solution at all the singular points. First, in contrast with the Dirichlet and Neumann boundary conditions, the state constraints are interesting because they do not require any data. Let us recall that the Dirichlet (respectively, Neumann) boundary conditions require the knowledge of the values of the solution (respectively, the values of $\nabla u(x) \cdot n(x)$, where $n(x)$ is the unit inward normal vector to $\partial\Omega$ at the point x) on the boundary of the domain. Also, we rarely have such data at our disposal. Second, the notion of state constraints is also interesting because it provides a relevant solution as soon as the image is the one of a “surface” u which verifies the supersolution constraint on $\partial\Omega$. Also, as we explain below, this constraint is very weak and it is commonly verified with real observable surface. Recall that an equivalent way to define the viscosity supersolution constraint at a point $x \in \partial\Omega$ is to require that

$$H(x, \xi) \geq 0, \quad \forall \xi \in D^-u(x) \tag{4.34}$$

where

$$D^-u(x) = \left\{ \xi \in \mathbb{R}^N \mid \liminf_{y \rightarrow x, y \in \bar{\Omega}} \frac{u(y) - u(x) - (\xi, y - x)}{|y - x|} \geq 0 \right\}$$

(see for example [7, 5, 29]). This constraint can be roughly interpreted as following: *For all plane P subtangent to u at x , the gradient ∇P verifies $H(x, u(x), \nabla P) \geq 0$.* To better understand the constraint (4.34) for x in $\partial\Omega$, let us consider the particular case of a differentiable solution.

¹⁰This is impossible with discontinuous viscosity solutions; see the second part of section 2.2.6.3. It is possible with continuous viscosity solutions but compatibility conditions are required. In [24, 55, 56], Falcone et al. “send” systematically the singular points “at the infinity”.

Proposition 4.6 *Let u be a solution differentiable on $\overline{\Omega}$ of the HJB equation associated with the Hamiltonian*

$$H(x, p) = \sup_{a \in A} \{-f(x, a) \cdot p - l(x, a)\}. \quad (4.35)$$

and denote by $a_0(u, x)$ the optimal control of (4.35) associated to u at the point x (i.e. $a_0(u, x)$ is the control $a \in A$ maximizing $-f(x, a) \cdot \nabla u(x) - l(x, a)$). If for $x \in \partial\Omega$,

$$f(x, a_0(u, x)) \cdot n(x) > 0, \quad (4.36)$$

where $n(x)$ is the unit inward normal vector to $\partial\Omega$ at the point x , then (4.34) is satisfied.

In other words, the surface u is a supersolution on $\partial\Omega$ (i.e. u verifies the state constraints on $\partial\Omega$) as soon as the *dynamic of the optimal control* (associated with u) *points inward of Ω* at all points x on the boundary $\partial\Omega$. In the classical example of the Eikonal equation, the optimal control associated to a differentiable function u is

$$f(x, a_0(u, x)) = -a_0(u, x) = -\frac{\nabla u(x)}{|\nabla u(x)|}.$$

So in this example, u is a supersolution on $\partial\Omega$ as soon as for all x on $\partial\Omega$, the gradient $\nabla u(x)$ points outward of Ω , i.e. roughly speaking, when $u(x)$ “increases” when x come up to $\partial\Omega$. More generally, (4.36) can be globally interpreted as “ $u(x) - \psi(x)$ increases when x come up to $\partial\Omega$ ”.

In other respects, let us note that proposition 4.6 shows that the notion of state constraints coincides with the constraint formulated by Dupuis and Oliensis in assumption 2.1 of [47] and introduced in the case of C^1 solutions.

Proof of Proposition 4.6. Let $x \in \partial\Omega$ be such that (4.36) is satisfied. We have for $c \leq 0$

$$\begin{aligned} H(x, \nabla u(x) + cn(x)) &= H(x, \nabla u(x) + cn(x)) - H(x, \nabla u(x)) \\ &\geq -f(x, a_0(x, u)) \cdot (\nabla u(x) + cn(x)) - l(x, a_0(x, u)) \\ &\quad - (-f(x, a_0(x, u)) \cdot \nabla u(x) - l(x, a_0(x, u))) \\ &= -f(x, a_0(x, u)) \cdot cn(x) \geq 0 \end{aligned}$$

Moreover, since u is differentiable on $\overline{\Omega}$, we have

$$D^-u(x) = \{\xi \mid \xi = \nabla u(x) + cn(x), \ c \leq 0\}.$$

Thus, for any $\xi \in D^-u(x)$,

$$H(x, \xi) \geq 0.$$

So the constraint (4.34) holds. □

Now, let us focus on the singular points. In section 4.2.5, we have denoted by Π_u the set of points in Ω such that a constant function cannot be S -subtangent to $u - \psi$ at x . Let us remind that if $x \notin \mathcal{S}$ or $B_S(x) = \{x\}$, this means that x cannot be a local minimum point for $u - \psi$. For this reason we have called Π_u the set of minimum points of $u - \psi$. We have also set

$$\Gamma_u = \{x \in \Omega \mid \exists y \in B_S(x) \text{ verifying } u(x) \geq \varphi(y) + \psi(x) - \psi(y)\}$$

and demonstrated

Theorem 4.6 *Let u be a (discontinuous) viscosity solution of (4.2)-(4.5) such that $u(x) \leq \varphi(x)$ for any $x \in \mathcal{S}$. If $\Pi_u \subset \Gamma_u$ then u is the SDVS of (4.2)-(4.5).*

In other words, the SDVS is the unique (discontinuous) viscosity solution u of (4.2)-(4.5) (verifying $\forall x \in \mathcal{S}, u(x) \leq \varphi(x)$) without local minima on $\Omega - \Gamma_u$. Of course, the reciprocal statement of theorem 4.6 holds. As we explain in section 4.2.5, an important interpretation and consequence of theorem 4.6 is the following:

The (discontinuous) viscosity solutions of (4.2)-(4.5) can be characterized only by their minima

(see section 4.2.5). **Thus this result extends consistently the work of Dupuis and Oliensis [47]. In [47], the authors characterize the C^1 solutions by their values at the local minimum points. Here, we have extended this characterization to the (discontinuous) viscosity solutions.**

Finally, let us emphasize that the notion of SDVS allows to *unify* the various theories based on viscosity solutions used for solving the SFS problem. Indeed,

- in the case where the Dirichlet Boundary Conditions (DBC) are finite on $\partial\Omega \cup \mathcal{S}$ and the compatibility condition (see [95]) holds, then the SDVS of (4.2)-(4.5) is the continuous viscosity solution used by [134, 96, 127, 120];
- in the case where the DBC are finite on $\partial\Omega$ and where there do not exist singular points, then the SDVS of (4.2)-(4.5) coincides with the discontinuous viscosity solution used by [120, 119, 123] (the compatibility conditions are no more required);
- when the DBC are finite on the boundary of the image and state constraints are imposed at the singular points, the SDVS of (4.2)-(4.5) corresponds

to the Camilli and Siconolfi’s singular viscosity solutions [26, 23, 27] used by Falcone et al. [24, 55, 56];

- as we have demonstrated above the SDVSs coincide with the C^1 solutions of (4.2) verifying the assumption 2.1 of Dupuis and Oliensis (when smooth solutions exist). Therefore, when there does not exist C^1 solutions¹¹, the notion of SDVS allows to extend consistently the work of Dupuis and Oliensis [47] to the notion of viscosity solutions. Also, the SDVS coincides with the value function (of the associated optimal control problem) considered in [47].

Lastly, let us note that in [47], the authors introduce the SFS Hamiltonian $H_{D/O}^{orth}$ (instead of dealing with $H_{R/T}^{orth}$) in order to obtain a Hamiltonian with a nonnegative Legendre transform. Also, most of their proofs are based on this hypothesis ($H^*(x, q) \geq 0$). Here, we also relax this constraining assumption: we can deal with all the classical SFS Hamiltonians, in particular with $H_{R/T}^{orth}$.

As a consequence, all the theoretical results of Falcone et al. [24, 55, 56]¹², Rouy et al. [134, 96]¹³, Prados et al. [127, 120]¹⁴ and Dupuis et al. [47]¹⁵ are *automatically extended to the “perspective SFS”* (use H_F^{pers} and $H_{P/F}^{pers}$).

Finally, one can conjecture that by using the work of [78, 112, 146, 28], the notion of SDVS can be extended to solve SFS problem with discontinuous images. This would be very difficult without the tool of viscosity solutions.

4.5 Minimal and global viscosity solutions

The SDVS allows to send the boundary conditions at $+\infty$, thereby obtaining the “maximal” solution. So for obtaining the “minimal” solution, it can seem natural to send them at $-\infty$. Nevertheless with such boundary conditions there do not exist solutions. In other respects, the viscosity solutions of the equation $H(x, \nabla u) = 0$ are different from the viscosity solutions of $-H(x, \nabla u) = 0$. For example, the opposite two equations on $]0, 1[$ associated with $H_1(x, p) = |p| - 1$ constrained by $u(0) = u(1) = 0$ have a unique viscosity solution given by figure 4.3. By schematizing, the solution of $H(x, \nabla u) = 0$ allows upward kinks when $-H(x, \nabla u) = 0$ allows downward kinks. Moreover, it is well known that:

¹¹Let us recall that, because of noise, of errors on parameters (focal length, light position, etc) and of incorrect modeling (interreflections, nonpunctual light source, nonlambertian reflectance...) there never exists such smooth solutions in practice.

¹²Who only deal with “orthographic Shape from Shading”.

¹³Who only deal with “orthographic SFS” by using $H_{R/T}^{orth}$.

¹⁴Who deal with $H_{R/T}^{orth}$ and $H_{P/F}^{pers}$.

¹⁵Who deal with “orthographic SFS” by using $H_{D/O}^{orth}$. Nevertheless let us note that their work deals more generally with convex Hamiltonians with nonnegative Legendre transform.

$$[u \text{ solution of } -H(x, p)] \iff [-u \text{ solution of } H(x, -p)].$$

Thus it is natural to define the “minimal” solution of $H(x, p)$ by the opposite of the SDVS of $H(x, -p)$. Obviously, the Hamiltonians $H(x, -p)$ associated with all the SFS Hamiltonians are particular cases of the generic SFS Hamiltonian. Therefore all the previous theoretical and algorithmic results hold for the “minimal” SFS solutions.

The interest of the notion of the “minimal” solution is twofolds: first it allows to recover surfaces which are “globally” concave (whereas SDVSs are “globally” convex). The second interest of these “minimal” solutions lies on a possible extension of the “global algorithm” of Oliensis [108, 47].

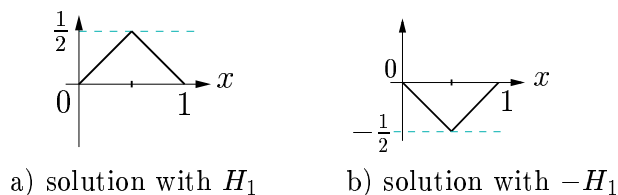


Figure 4.3: solutions of H versus $-H$; minimal solutions

4.6 Numerical approximation of the SDVS of the “classical” Shape from Shading problem

This section explains how to compute a numerical approximation of the SDVS of the generic SFS equation. This requires four steps. First we deal with the state constraints. Second, we “regularize” the equation. Third, we approximate the “regularized” SFS equation by approximation schemes. Finally, from the approximation schemes, we design numerical algorithms.

4.6.1 Management of the state constraints

In this section, we explain how to deal with the state constraints *in practice*. In particular, we show that, in this setup, the state constraints can always be rewritten as Dirichlet boundary conditions.

Let u be the SDVS of equation (4.2)-(4.5):

$$\begin{cases} H(x, \nabla u) = 0 & \forall x \in \Omega, \\ u(x) = \varphi(x) & \forall x \in \partial\Omega \cup \mathcal{S} \end{cases}$$

In section 4.2, we have seen that u is Lipschitz continuous and then bounded on Ω . Let $M \in \mathbb{R}$ an upper bound of u on Ω such that

$$\forall x \in \Omega, \quad u(x) < M - 1.$$

Now, let us consider $\tilde{\varphi}$ the real function defined on $\partial\Omega \cup \mathcal{S}$ by

$$\tilde{\varphi}(x) = \min(M, \varphi(x)),$$

and let \tilde{u} be the SDVS of equation

$$\begin{cases} H(x, \nabla u) = 0 & \forall x \in \Omega, \\ u(x) = \tilde{\varphi}(x) & \forall x \in \partial\Omega \cup \mathcal{S}. \end{cases}$$

Following these notations, we have

Proposition 4.7 *\tilde{u} and u coincide on Ω , i.e.*

$$\forall x \in \Omega, \quad \tilde{u}(x) = u(x).$$

Proof. Thank to the strong uniqueness of the SDVS (theorem 4.3), it is sufficient to prove that \tilde{u} is an SDVS of (4.2)-(4.5). Let us recall that the uniqueness of the SDVS only holds on Ω but not on $\overline{\Omega}$. Also, \tilde{u} and u can take different values at some points of $\partial\Omega$.

First, since $\tilde{\varphi} \leq \varphi$, by the maximum principle (theorem 4.2) we have,

$$\forall x \in \Omega, \quad \tilde{u}(x) \leq u(x).$$

- \tilde{u}^* is a subsolution of (4.2)-(4.5):
 - \tilde{u}^* is a subsolution of (4.2) on $\Omega - \mathcal{S}$;
 - for all x_0 in $\partial\Omega \cup \mathcal{S}$ such that $\tilde{u}^*(x_0) \leq \tilde{\varphi}(x_0)$ we have trivially $\tilde{u}^*(x_0) \leq \varphi(x_0)$.
 - for all x_0 in $\partial\Omega$ such that $\tilde{u}^*(x_0) > \tilde{\varphi}(x_0)$, \tilde{u}^* verifies the subsolution property.
- \tilde{u}_* is a supersolution of (4.2)-(4.5):
 - \tilde{u}_* is a supersolution of (4.2) on $\Omega - \mathcal{S}$;
 - Let $y \in \partial\Omega \cup \mathcal{S}$ be a point such that $\tilde{u}_*(y) \geq \tilde{\varphi}(y) = \min(\varphi(y), M)$.
 So $\tilde{u}_*(y) \geq M$ or $\tilde{u}_*(y) \geq \varphi(y)$. But $\tilde{u}_*(y) \geq M$ is impossible (because, for all $z \in \Omega$, $\tilde{u}(z) \leq u(z) < M - 1$, then for all $y \in \overline{\Omega}$ $\tilde{u}_*(y) \leq M - 1 < M$). Therefore $\tilde{u}_*(y) \geq \varphi(y)$.

- Let $x_0 \in \partial\Omega \cup \mathcal{S}$. If there exist $y \in B_S(x_0)$ such that $\tilde{u}_*(y) \geq \tilde{\varphi}(y)$. then by the previous item, $\tilde{u}_*(y) \geq \varphi(y)$. Else, the singular viscosity property holds for \tilde{u}_* at x_0 .
Therefore \tilde{u}_* is a supersolution of (4.2)-(4.5) for all points $x_0 \in \partial\Omega \cup \mathcal{S}$.

□

Therefore, equations (4.2)-(4.5) with some state constraints (i.e. such that for some $x \in \partial\Omega \cup \mathcal{S}$ $\varphi(x) = +\infty$) can be rewritten as equations without state constraints; i.e. with (finite) Dirichlet boundary conditions on the whole set $\partial\Omega \cup \mathcal{S}$. So in practice, we always consider (finite) Dirichlet boundary conditions: when we know the values of the solution on $\partial\Omega$ we can transfer these informations in φ ; when we do not have these data and we want to compute the solution of with state constraints, we impose φ to be a “great” *constant*. In our (C++) code, this constant is fixed as the value of `FLT_MAX`. Let us emphasize that by modifying φ in such a way, we do not change the solution of (4.2)-(4.5) neither the approximation computed by our algorithm.

4.6.2 Regularization of the generic SFS equation

For an intensity image I and $\varepsilon > 0$, let us consider the truncated image I_ε defined by $I_\varepsilon(x) = \min(I(x), 1 - \varepsilon)$. By using the stability result of theorem (4.5), we have proved in section 4.3.2 that for all SFS Hamiltonians, the classical discontinuous viscosity solution¹⁶ associated with the image I_ε converges uniformly toward the singular viscosity solution associated with the image I , when $\varepsilon \rightarrow 0$. Thus for approximating this equation, we can use the tools we have developed in chapter 3.

4.6.3 Approximation schemes for the nondegenerate SFS equations

Let us consider the “regularized” generic SFS equation. In chapter 3, we design SFS monotonous approximation schemes which are always stable (existence of a solution). Moreover, we also prove that (as soon as the intensity image is Lipschitz continuous and the Hamiltonian is coercive) the solutions of these schemes converge toward the unique (classical) discontinuous viscosity solution of the adequate *nondegenerate* SFS equation when the mesh size vanishes.

¹⁶equation associated with I_ε is *no more degenerate*.

4.6.4 Numerical algorithms for the generic SFS problem

In chapter 3, we design algorithms that compute some numerical approximations of the solutions of the considered schemes. Moreover, we prove that the computed numerical approximations converge toward the solution of the considered schemes.

4.6.5 Examples of SFS results obtained from synthetic images

Let us recall that our method does not necessarily require boundary data (except at least at one point¹⁷ in $\partial\Omega \cup \mathcal{S}$). Figure 4.4 shows some reconstructions of the Mozart face when using the exact boundary data on the boundary of the image and at all singular points (Fig.4.4-c), when using the exact boundary data at all the singular points and state constraints on the boundary of the image (Fig.4.4-d), and with no boundary data, except for the tip of the nose (Fig.4.4-e). Let us remark that, as the theory predicted, our algorithms show an exceptional robustness to noise and errors on the parameters; This robustness is even bigger when we send the boundary to infinity (apply the state constraints). Figure 4.5 displays a reconstruction of Mozart’s face from an image perturbed by additive uniformly distributed white noise (SNR $\simeq 5$) by using the implicit algorithm (see [119]) with the wrong parameters $\mathbf{l}_\varepsilon = (0.2, -0.1)$ and $f_\varepsilon = 10.5$ (focal length) and without any boundary data. The original image Fig.4.5-a) has been synthesized with $\mathbf{l} = (0.1, -0.3)$ and $f = 3.5$. The angle between the initial light vector \mathbf{L} and the corrupted light vector \mathbf{L}_ε is around 13° .

4.7 Toward applications of Shape from Shading

Now that we have removed the requirement of the knowledge¹⁸ of the data on the boundary of the image $\partial\Omega$, we can apply our method to real images. Also, we can suggest some *applications* of our SFS method. Note that, here, we do not provide complete descriptions, but we hope that the results will convince the reader of the *applicability of our SFS method to real problems*. Let us emphasize that all the results we present in this section are obtained from real images:

Note: When we apply SFS methods to real images we assume that the camera is geometrically and photometrically calibrated. In our experiments of sections 4.7.1 and 4.7.2 we know the focal length (5.8 mm) and approximately the pixel size (0.0045 mm; CCD size = 1/2.7”) of our cheap digital camera

¹⁷Let us remind the reader that the boundary condition φ must verify $\varphi \neq \infty$.

¹⁸Let us emphasize that we must at least choose the pixel (a singular point) which will have the minimal depth...

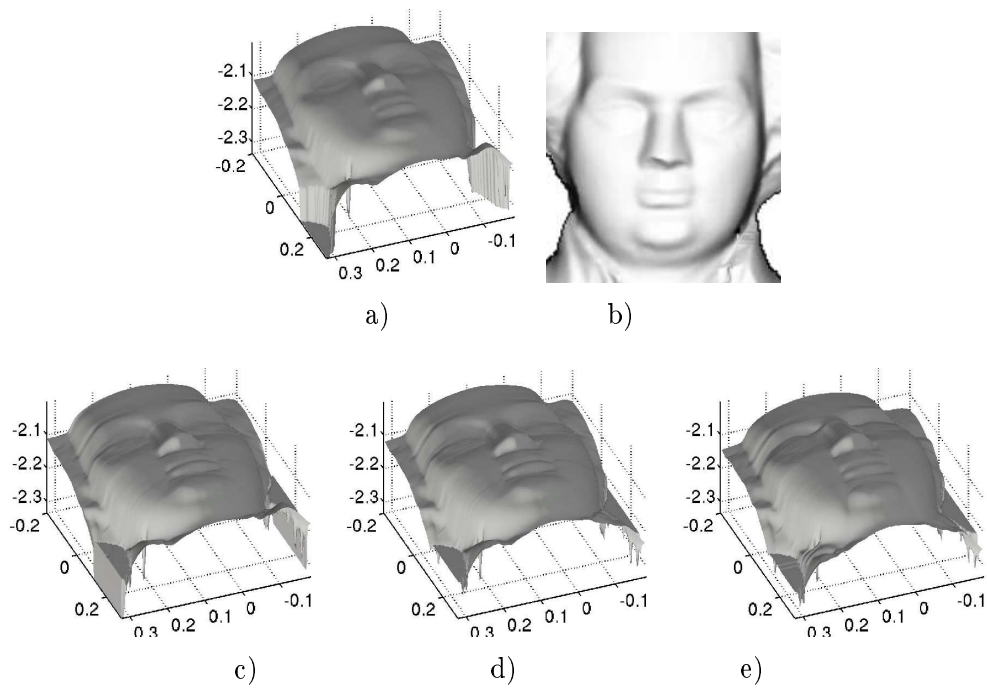


Figure 4.4: Reconstruction of Mozart's face *with and without* boundary data. a) original surface; b) image generated from a) [size $\simeq 200 \times 200$]; c) reconstructed surface from b) with the implicit algorithm (IA) after only 3 iterations, using the exact boundary data on the boundary of the image and at all singular points; d) reconstructed surface by the IA (after 3 iterations) with state constraints on the boundary of the image; e) reconstructed surface by the IA (after 3 iterations) with state constraints on the boundary of the image and at all the singular points except at the one on the nose.

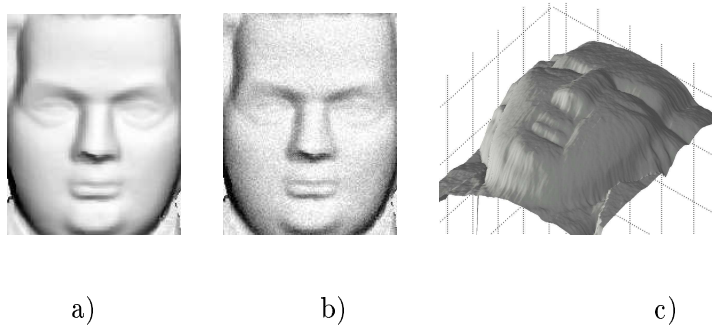


Figure 4.5: Reconstruction of Mozart’s face from a noisy image with the wrong parameters $\mathbf{l}_\varepsilon = (0.2, -0.1)$ and $f_\varepsilon = 10.5$.

a) Image generated from Mozart’s face represented in Fig.4.4-a) with $\mathbf{l} = (0.1, -0.3)$ and $f = 3.5$ [size $\simeq 200 \times 200$]; b) noisy image (SNR $\simeq 5$); c) reconstructed surface from b) after 4 iterations of the implicit algorithm, using the incorrect parameters $\mathbf{l}_\varepsilon = (0.2, -0.1)$ and $f_\varepsilon = 10.5$, and with state constraints on the boundary of the image and at all the singular points except at the singular point on the nose.

(Pentax Optio 330GS). In section 4.7.3, we choose some arbitrary reasonable parameters. Also, note that there exists classical methods to calibrate photometrically a camera [98, 99]. In our tests, we do not use them, but we make some educated guesses for gamma correction (when the photometric properties of the images seem incorrect).

4.7.1 Document restoration using SFS

In this section, we propose a *reprographic system*¹⁹ to remove the geometric and photometric distortions generated by the classical photocopy of a bulky book. A first solution has been proposed by Wada and coworkers [163] who deal with *scanner* images involving a complex optical system (with a moving light). Here, the acquisition process we use is a classical camera²⁰. The book is illuminated by a single light source located at infinity or close to the optical center (following the models we describe in section 2.1.3). Note that Cho et al. [31] propose a similar system but they use two light sources²¹. The acquired images are then processed using our SFS method to obtain the shape of the photographed

¹⁹Suggested to us by Durou (private communication); see [36].

²⁰Note that a camera snapshot is practically instantaneous, whereas a scan takes several seconds.

²¹We can also note that the numerical method proposed by [31] requires that global variations of depth only exist along one direction. Our method does not require this hypothesis.

page. Let us emphasize that, for obtaining a compact experimental system, the camera must be located relatively close to the book. Therefore the *perspective model is especially relevant* for this application. Also, the distortion due to the perspective clearly appears in the image a) of figure 4.8.

In our SFS method we assume that the albedo is constant. In this application, this does not hold because of the printed parts. Before recovering the surface of the page, we therefore localize the printed parts by using image statistic (similar to Cho's [31])²² and we erase them automatically by using e.g. the inpainting algorithm of Tschumperlé and Deriche [160]. This step can produce an important pixel noise. Nevertheless, this is not a problem for us because, as figure 4.7-b) shows, *our SFS method is extremely robust to pixel noise*: figure 4.7-b) displays the result produced by our algorithm (after 10 iterations) using the image of a text page with its pigmented parts, Fig.4.7-a). In this test, characters are considered as noise. Note that one could say that such a restoration system (based on SFS) is flawed because it does not use the information provided by the *rows* of characters. This is partially true but nevertheless, for pages containing few rows of characters but a lot of graphics and pictures (separated by large white bands²³), such a SFS method could provide a simple and efficient solution.

Once we have recovered the three-dimensional shape of the page, we can flatten the surface by using e.g. the algorithm of Brown and Seales²⁴ [20]. Note that at each step of this restoration process (3D reconstruction and flattening) we keep the correspondences with the pixels in the image. Thus, at the final step, we can restore the printed parts.

To prove the applicability of this method, we have tested it on a page mapped on a cylindrical surface²⁵ (we have used our cheap camera and flash in an approximately dark room). Figure 4.8 shows the original image in a), the reconstructed surface (after 10 iterations) (textured by the ink parts of a) in b) and an orthographic projection of the reconstructed surface, in c). Figure 4.8-c) indicates that our method allows to remove the perspective and photometric distortions.

4.7.2 Face reconstruction from SFS

The interest of the SFS methods for some applications dealing with faces has been demonstrated in e.g. the work of Zhao and Chellappa [173] (who use symmetric SFS for illumination-insensitive face recognition), by Smith and Hancock [143] (who use SFS needle map for face recognition), and by Choi and coworkers

²²Most probably, we can also achieve this step by using the excellent work of Bell and Freeman [12] who propose a learning-based approach.

²³This is often the case for scientific documents.

²⁴Not yet implemented, because of time.

²⁵For emphasizing the perspective effect.

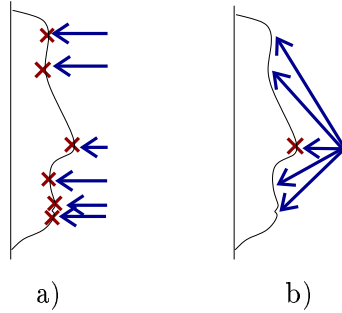


Figure 4.6: Singular points of the profile of a face. a) Singular points (6) for a homogeneous horizontal light; b) Singular point for a point light source at the optical center.

[33] (who use SFS for determining the face pose). In this section we propose a very simple protocol based on SFS for face reconstruction. We use one camera equipped with a basic flash in an approximately dark place. As shown in figure 4.6, the interest of this method lies in the fact that, with such a protocol, the generated image should contain a unique singular point (if the distance of the face to the camera and the focal length are sufficiently small). Therefore, the propagation of the height information starts from this unique singular point.

We have tested our generic algorithm on a real image of a face²⁶ located at ≈ 700 mm of the camera in an approximately dark place (see Fig.4.9-a)). Figure 4.9-b) shows the surfaces recovered by our generic algorithm (after 5 iterations) with the perspective SFS model with a point light source at the optical center. As in the previous application, the albedo is not constant over the whole image. Therefore we removed the eyes and the eyebrows in the image by using e.g. the inpainting algorithm of Tschumperlé and Deriche [160]. Moreover, note that this step can be automated by matching the image²⁷ to a model image already segmented. Figure 4.9 shows in c) the surface recovered from the image obtained after the inpainting process.

4.7.3 Potential applications to medical images

In this section, we are interested in applying our SFS method to some medical images. Our interest is motivated by the work of Craine et al. [38], Okatani and Deguchi [103], Forster and Tozzi [58], Smithwick and Seibel [144], Yeung et al. [169], Gillies et al. [149, 86] and Yamany et al. [168]. For illustrating the relevance of the “perspective SFS” modeling with the light source located at

²⁶Slightly made-up to be more Lambertian.

²⁷We can use for example the very robust multi-modal and non-rigid matching method proposed by Hermosillo and Faugeras in [62].

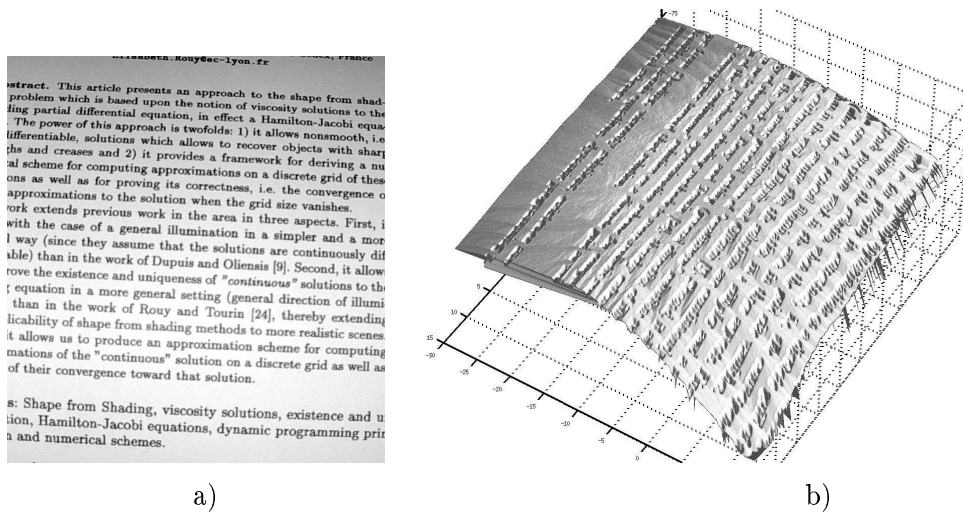


Figure 4.7: a) Real image of a page of text [size $\simeq 800 \times 800$]; b) Surface recovered from a) by our generic algorithm (without removing the printed parts of a)).

infinity, we apply our algorithm to an endoscopic image of a normal stomach²⁸ (see figure 4.10-a)). In fact, for producing such an image, the light source must be very close to the camera, because of space constraints. In figure 4.10-b), we show the result obtained (after 3 iterations) by our generic algorithm in the perspective case with the light source at the optical center. In figure 4.10-b), the surface is visualized with a light source located at the optical center. This reconstruction looks quite good. To further show the quality of the reconstruction, we display in c), the surface b) with a different illumination. Finally, notice that the stomach wall is not perfectly Lambertian (see Fig.4.10-a)). This suggests the robustness of our SFS method to departures from the Lambertian hypothesis.

²⁸Suggested by Tankus and Sochen (private communication) and downloaded from <http://www.gastrolab.net/>.

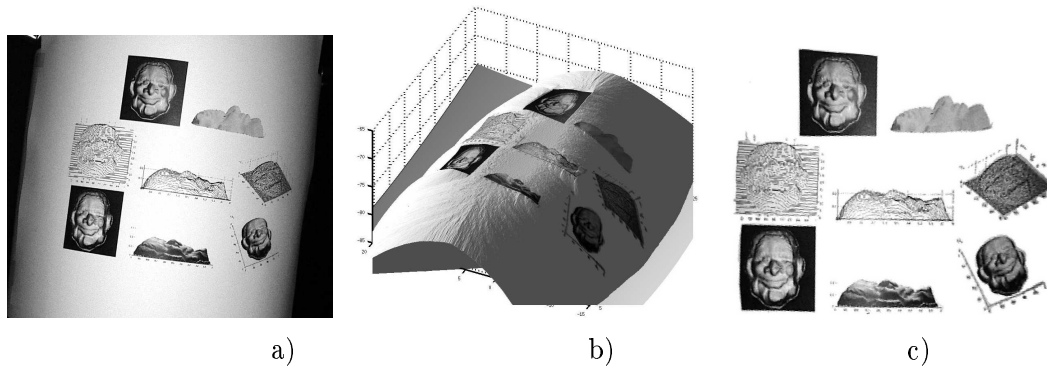


Figure 4.8: a) real image of a page containing pictures and graphics [size $\simeq 2000 \times 1500$], b) surface (textured by the printed parts of a)) recovered from a) by our generic algorithm (after having removed and inpainted the ink parts of a)). c) An orthographic projection of the surface b): the geometric (and photometric) distortions are significantly reduced.

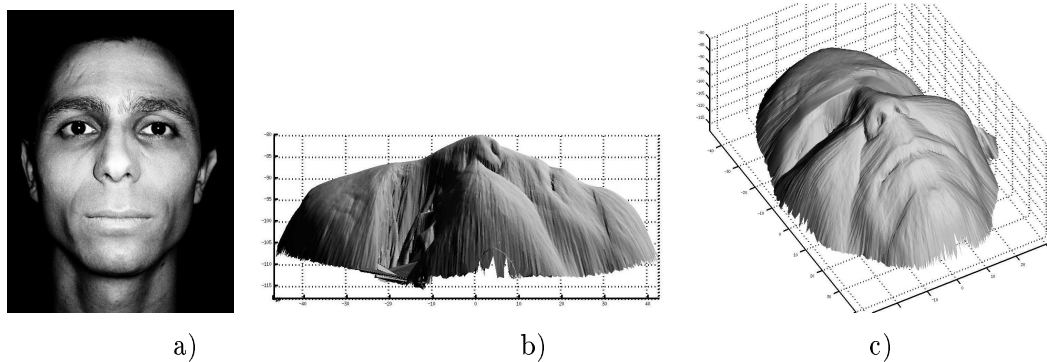


Figure 4.9: Face reconstruction from SFS: a) Real face image [size $\simeq 450 \times 600$]; b) surface recovered from a) by our generic algorithm with the perspective model with the light source located at the optical center; c) surface recovered by our generic algorithm with the same modeling hypotheses after the inpainting process.

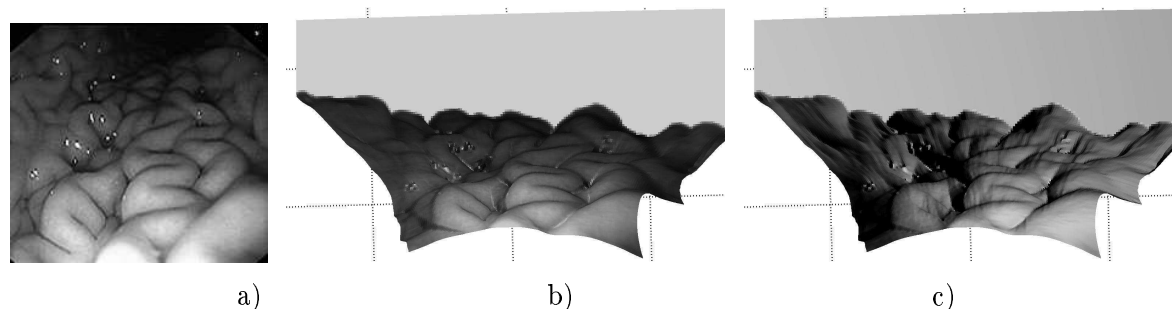


Figure 4.10: Reconstruction of a normal stomach: a) Original image of a normal stomach [size $\simeq 200 \times 200$]; b) surface recovered from a) by our generic algorithm with the perspective model and with the light source located at the optical center; c) surface b) visualized with a different illumination.

4.8 Conclusion and contributions of chapter 4

- In the first part of this chapter, we have slightly modified the notion of singular viscosity solutions developed in [77, 26, 23, 27] in order to obtain a **discontinuous** viscosity solution on a domain Ω containing some singular points **without necessarily requiring data on the boundary** $\partial\Omega$. Thereby we have defined the notion of **SDVS**. We have demonstrated the **existence** and the **uniqueness** of the SDVS for a wide class of convex Hamilton-Jacobi equations $H(x, \nabla u) = 0$. Some **stability results** have been proved. In other respects, we have shown that this new framework allows to **characterize the classical discontinuous viscosity solutions by their “minima”**.
- In the second part of this chapter, we have shown that the notion of SDVS allows to **unify** the various theoretical results proposed in the Shape from Shading literature. More precisely, it unifies the work of Lions et al. [96, 134], of Dupuis and Oliensis [47], of Falcone et al. [24, 55, 56] and of Prados and Faugeras [127, 120]. Thus, it also allows to **generalize** this previous work to all the “classical” SFS Hamiltonians, in particular to the “perspective SFS” ones.

Moreover, let us point out that the notion of SDVS is **really more adapted to the SFS specifications** than the other classical notions of weak solutions used in chapter 2 and in [96, 134, 24, 55, 56, 127, 120]. In particular, it **does not necessarily require data on the boundary of the image and at all the critical points**. Nevertheless, let us note that for characterizing and computing a solution we need to fix at least one point²⁹. Also, when the image contains **several singular points**, to

²⁹Since the boundary condition φ must verify $\varphi \neq \infty$.

be able to compute an approximation of the original surface, **we need to know the depth of all its points of local “minima”**.

Finally, using a stability result, we have shown **how to approximate numerically the SDVS** of the “classical” SFS equations. Also, we have proved the convergence of the computed approximations toward the SDVS.

- We have successfully applied our SFS method to **real images** and we have suggested that it may be useful in a number of **real-life applications**.
- **Note:** our ECCV'04 paper [124] is extracted from this chapter. Several other communications have been based on its content; let us cite for example [126, 125]. Some journal articles are in preparation.

Chapter 5

Toward more realistic modelizations.

Shape from Shading: a well-posed problem?

Before starting the main parts of this chapter, let us emphasize on the ill-posedness of the “classical” formulation of the Shape from Shading problem. As we have underlined in the introduction (chapter 1), the resolving of the Shape from Shading problem is confronted with some ambiguities. In particular, when the lighting and the reflectance of the scene are unknown, its exact 3D structure cannot be recovered. This difficulty is well illustrated by the concave/convex ambiguity displayed in figure 1.2 and by the “Bas-relief Ambiguity” demonstrated by Belhumeur and his coworkers [11]; see figure 1.3. Also, it is reasonable to assume that we know all the parameters of the light source, the surface reflectance and the camera. Nevertheless this knowledge is not sufficient to get rid of some concave/convex ambiguities. In effect, even though we assume complete control of the experimental setup, we are hampered by this kind of difficulty. For example, let us focus on the “Eikonal” framework; i.e. we assume that the camera performs an orthographic projection of the scene, that the surface is Lambertian and that the light source direction¹ is the same as that of the axis of the camera. In this setup, a concave/convex duality clearly appears, see Figures 5.1 and 5.2. The surfaces represented in Figure 5.1-a) and in Figure 5.1-b) yield the same image. This also holds for the more complex surfaces represented in Figures 5.2-a), 5.2-b), 5.2-c) and 5.2-d). In these figures, the

¹We consider here that the light source is at infinity.

various surfaces have been obtained from the surfaces a) by applying horizontal symmetries. Today, this concave/convex ambiguity is completely understood.

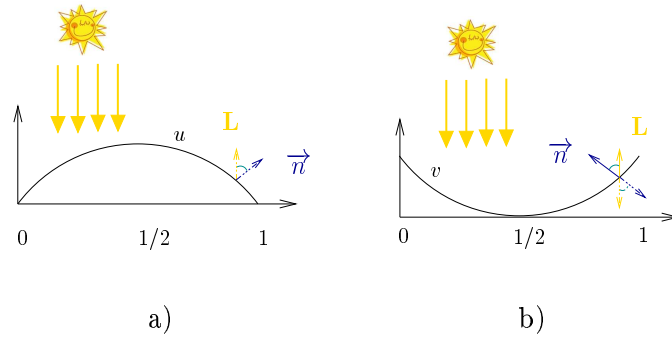


Figure 5.1: Concave/convex duality in the Eikonal framework: The surfaces a) and b) yield the same image.

It is due to the existence of the singular points that we have described in section 2.2.6. Let us remind that these points are the pixels of the image corresponding to points of the surface such that the surface normal coincides with the light direction. These points x have maximal brightness: $I(x) = 1$. In effect, the presence of the singular points is due to the modeling. In particular it is due to the fact that the authors assume that the scene is illuminated by a single point light source located at infinity (or to the fact that they neglect the $1/r^2$ attenuation term in the brightness equation, see section 5.1). Also, this kind of ambiguity holds for all the “classical” SFS modelings. In particular, it holds for the orthographic SFS (see section 2.1.1) as well as for the perspective SFS (see sections 2.1.2 and 2.1.3) problem. In particular, it holds even when the light source direction does not coincide with the camera axis. Nevertheless, *in contradiction with all these results, we are going to prove now that the Shape from Shading problem can be well-posed*. Not surprisingly, this new result is obtained by considering a more realistic image formation model.

These last ten years, various authors have attempted to improve the applicability of the Shape from shading methods by modeling the physics of the problem, in particular the illumination process, in a more realistic manner. In a similar vein, Bakshi, or Lee and Kuo [4, 92] propose a solution for some non-Lambertian Shape from Shading problems. Some authors take into account the interreflections [147, 59]. Other authors deal with multiple light sources [155]. Finally, various solutions have been proposed for taking into account the perspective effect [114, 91, 61, 165, 171, 120, 152, 124, 37, 153]. Looking at some recent Shape from Shading surveys², one may have the feeling that the work of [4, 92, 147, 59, 155, 114, 91, 61, 165, 171, 120, 152, 124, 37, 153] has appeared

²For example [172, 49].

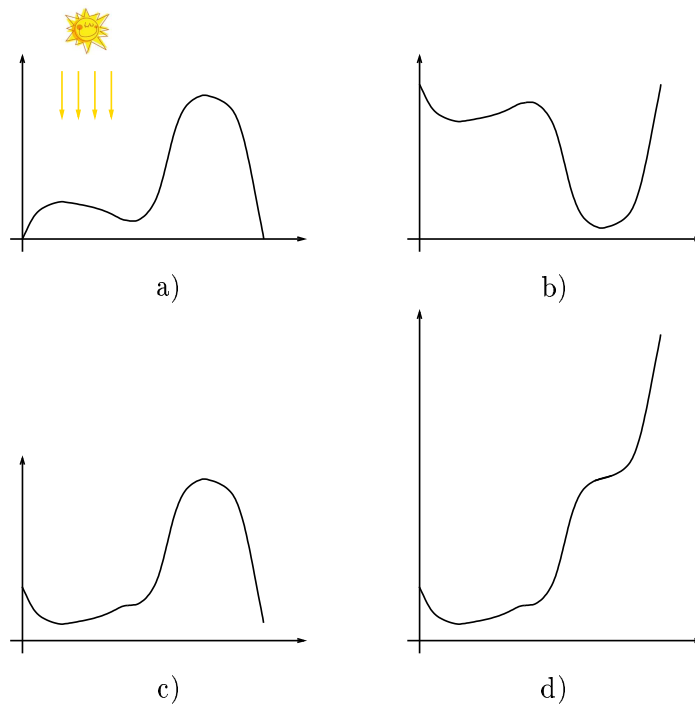


Figure 5.2: Consequences of the concave/convex duality in the Eikonal framework. Examples of more complex surfaces. The surfaces a), b), c) and d) yield the same image...

too early, insofar as the existing Shape from Shading methods dealing with the traditional framework, i.e. Lambertian surface + light source at infinity + orthographic projection, are quite unsatisfactory³ even with very simple synthetic images verifying the modeling hypotheses. Also, since we are not able to solve the simplest version of the SFS problem, it seems unreasonable to attempt to solve this problem by modeling it in a more complex way. *Here, we hope to remove this feeling.*

One of the reasons why SFS is ill-posed is the over-simplification in the modeling. Now, we are going to prove that by using more realistic hypotheses than the classical ones, the Shape from Shading becomes well-posed (modulo some weak a priori on the creases of the solution near the boundary). As a consequence it becomes easier to solve. In detail, we assume that the camera is a pinhole and that the light source is located at the optical center. Nevertheless, contrary to the modeling of section 2.1.3 (which is also the modeling associated to the report [122]), now, we do not neglect the $1/r^2$ attenuation term (see section 5.1). As proved in section 5.3, this “new” term makes the problem better posed. In particular, the notion of singular points does not make sense anymore and the concave/convex duality disappears.

This chapter first describes a *complete theoretical study* of the Shape from Shading problem in this particular setup (section 5.3). Second, it proposes an *original and rigorous numerical method* allowing to approximate numerically the solutions of the problem. We detail a stable and consistent approximation scheme and we describe a provably convergent numerical algorithm (section 5.4). Finally, we demonstrate the practical relevance of our method by displaying some experimental results (section 5.5).

5.1 More realistic modeling of the SFS problem

In order to obtain a more realistic modeling of the SFS problem, we are going to recall the image formation process. To do this, we will upstream the light ray from the optical system to the light source. For more details we refer to [65].

- We start with the relationship between the image brightness and the surface radiance. This relationship is well-known, see for example [65]:

$$E_i = L_s \frac{\pi}{4} \left(\frac{d}{f} \right)^2 \cos^4 \alpha , \quad (5.1)$$

where E_i is image irradiance, which is assumed to be equal to the image brightness. L_s denotes the surface radiance⁴. d is the diameter of the

³See the results shown in [172, 49].

⁴I.e. the radiance of the surface in the direction of the viewer (the optical center).

lens, f is the focal length and α is the angle between optical axis and the line of sight to a surface point of a corresponding image point. Because the term $\cos^4 \alpha$ is easily derived from the image coordinates and can be compensated for, image brightness is substantially proportional to surface irradiance.

- Next we assume that the scene is illuminated by a single point light source and that there are not interreflections. In this case, the relationship between the radiance L_s of a point of the surface (in the view direction) with the surface normal (at this point) and the light source direction is generally described by the Bi-directional Reflectance Distribution Function (BRDF):

$$L_s = F(\theta_i, \theta_r, \phi_r) E_s, \quad (5.2)$$

where E_s is the irradiance of the surface and the angles θ_i , θ_r and ϕ_r are described in Figure 5.3. In this figure N is the object surface normal, L is the direction to the light source, and V is the direction to the viewer. θ_i is the angle between L and N , and θ_r is the angle between V and N , respectively. ϕ_r is the azimuthal angle between L and V with respect to the surface normal N .

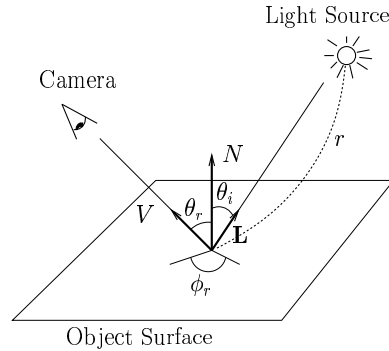


Figure 5.3: The surface local coordinate system (see [103, 65]).

A fundamental example: An ideal *Lambertian* surface is one that appears equally bright from all viewing directions and reflects all incident light, absorbing none. Its BRDF is then a constant ($\frac{1}{\pi}$, see [65]) and we have:

$$L_s = \frac{1}{\pi} E_s. \quad (5.3)$$

- Finally, we describe the irradiance E_s of the surface point. We have (see [65]):

$$E_s = I_0 \frac{\cos \theta_i}{r^2} \quad (5.4)$$

where I_0 is the intensity of the light source and r is the distance between the light source and the considered surface point.

In summary, combining (5.1),(5.2) and (5.4), the brightness image is given by:

$$E_i = \sigma_1 F(\theta_i, \theta_r, \phi_r) \frac{\cos \theta_i}{r^2}, \quad (5.5)$$

where σ_1 is a constant coefficient related to the parameters of imaging system and the intensity of the light source.

For a *Lambertian surface*, the brightness image is then:

$$E_i = \sigma_2 \frac{\cos \theta_i}{r^2}, \quad (5.6)$$

σ_2 being a constant coefficient.

Remark 39. In the case where the light source is located far from the surface⁵, the variations of the brightness of the image is essentially due to those of $\cos \theta_i$ and we can assume that r is constant. In this case the brightness image is given by:

$$E_i = \sigma_3 F(\theta_i, \theta_r, \phi_r) \cos \theta_i, \quad (5.7)$$

where σ_3 is a constant coefficient. For a Lambertian surface, the brightness image is even simpler:

$$E_i = \sigma_4 \cos \theta_i \quad (5.8)$$

(σ_4 being a constant coefficient).

In effect, *this setup corresponds exactly to the one of the “classical” Shape from Shading problem* we have considered in chapter 2.

Let us recall that in the Shape from Shading literature, the surface is always assumed Lambertian (except, to our knowledge, for very few papers [4, 102, 92]) and the light source is unique, reduced to a point and located at infinity (except for an extremely small number of papers [102, 163, 31]). To simplify even more the problem, the authors usually assume that the camera performs an orthographic projection of the scene. As Okatani and Deguchi [102] and as in section 2.1.3, in this chapter we model the camera as a *pinhole* (therefore we assume that the camera performs a perspective projection of the scene) and we assume that the scene is illuminated by a single point light source *located at the optical center* (hence not at infinity). Let us remind that this modeling is

⁵i.e. the normal vector $N(x)$ (or $\cos \theta_i(x)$) “varies more than” the distance $r(x)$, when the point x parameterizes the surface.

quite relevant for many applications. In particular, we show in section 4.7 that it nicely corresponds to the situation encountered in some medical protocols like endoscopy and to the situation encountered when we use a simple camera equipped with a flash; see section 4.7, for more details. Finally, let us emphasize that, contrary to the “classical” modeling of the SFS problem, *in the sequel we do not neglect the $\frac{1}{r^2}$ term.*

5.2 New mathematical formulation of the SFS problem

In this section, we formulate the problem as that of solving a Partial Differential Equation (PDE). More precisely, we describe some Hamilton-Jacobi equations arising from equation (5.6) and we detail the associated Hamiltonians.

Exactly as in section 2.1, let us pose Ω be an open subset of \mathbb{R}^2 . Let us remind that Ω represents the image domain, e.g., the rectangle $]0, X[\times]0, Y[$. The surface \mathfrak{S} is parameterized by the function $S : \overline{\Omega} \rightarrow \mathbb{R}^3$:

$$S(x) = \frac{f u(x)}{\sqrt{|x|^2 + f^2}} (x, -f),$$

as in section 2.1.3. Let us recall that $f > 0$ denotes the focal length, see Figure 2.2.

As in section 2.1.3, we show that for such a surface \mathfrak{S} , a normal vector $\mathbf{n}(x)$ at the point $S(x)$ is given by:

$$\mathbf{n}(x) = \left(f \nabla u(x) - \frac{f u(x)}{|x|^2 + f^2} x, \nabla u(x) \cdot x + \frac{f u(x)}{|x|^2 + f^2} f \right).$$

Remark 40. It is possible to parameterize differently the surface \mathfrak{S} ; for example, we can define

$$S(x) = u(x)(x, -f), \quad \forall x \in \overline{\Omega}.$$

In this case, we have

$$\mathbf{n}(x) = (f \nabla u(x), u(x) + x \cdot \nabla u(x)).$$

For $y \in \mathbb{R}^3$, we denote $\mathbf{L}(y)$ the unit vector representing the light source direction at the point y . Since we assume that the light source is located at the optical center, the vector $\mathbf{L}(S(x))$ is equal to⁶:

$$\mathbf{L}(S(x)) = 1/\sqrt{|x|^2 + f^2} (-x, f).$$

⁶We choose $\mathbf{L}(S(x))$ such that its third coordinate is positive.

Now, let us assume that the surface is *Lambertian*. If we denote $I(x) = \frac{E_i(x)}{\sigma_2}$, the brightness equation (5.6) becomes⁷:

$$I(x) = \frac{\cos \theta_i}{r^2}. \quad (5.9)$$

Since $\cos \theta_i$ is the dot product

$$\cos \theta_i = \mathbf{L}(S(x)) \cdot \frac{\mathbf{n}(x)}{|\mathbf{n}(x)|}$$

and

$$r = f u(x),$$

we obtain from (5.9) the following PDE:

$$I(x) = \frac{u(x)}{\sqrt{[f^2|\nabla u(x)|^2 + (\nabla u(x) \cdot x)^2]/Q(x)^2 + u(x)^2}} \frac{1}{f^2 u(x)^2}, \quad (5.10)$$

where $Q(x) = \sqrt{f^2/(|x|^2 + f^2)}$. For convenience we rewrite Equation (5.10) as:

$$-u(x)^{-2} + I(x) f^2 \frac{\sqrt{[f^2|\nabla u(x)|^2 + (\nabla u(x) \cdot x)^2]/Q(x)^2 + u(x)^2}}{u(x)} = 0. \quad (5.11)$$

If we assume that the surface \mathfrak{S} is visible, i.e. in front of the optical center, u is strictly positive, see Figure 2.2. This allows us to simplify equation (5.11) by using the *change of variables* $v = \ln(u)$:

$$-e^{-2v(x)} + J(x) \sqrt{f^2|\nabla v(x)|^2 + (\nabla v(x) \cdot x)^2 + Q(x)^2} = 0, \quad (5.12)$$

where $J(x) = \frac{I(x) f^2}{Q(x)}$ is a positive function. To this equation, we associate the *Hamiltonian*

$$H_F(x, u, p) = -e^{-2u} + J(x) \sqrt{f^2|p|^2 + (p \cdot x)^2 + Q(x)^2}.$$

Remark 41. In the case where we parameterize \mathfrak{S} by $S(x) = u(x)(x, -f)$, we obtain the equation

$$-e^{-2v(x)} + J(x) \sqrt{f^2|\nabla v(x)|^2 + (\nabla v(x) \cdot x + 1)^2} = 0, \quad (5.13)$$

instead of (5.12), and the Hamiltonian

$$H'_F(x, u, p) = -e^{-2u} + J(x) \sqrt{f^2|p|^2 + (p \cdot x + 1)^2}$$

⁷We assume that all the parameters of the camera (diameter of lens, focal length...), of the light source and of the surface (albedo) are known. Therefore σ_2 and hence $I(x)$ are known.

instead of H_F . All the results presented in this chapter can be obtained with either equation (5.12) or (5.13) and the associated Hamiltonians. Since the Hamiltonian H_F is mathematically simpler than H'_F ⁸ therefore in the sequel, we work only with the first one and its associated equation.

In [102, 103], Okatani and Deguchi do not formalize the problem with PDEs (in particular equation (5.12)), and the associated Hamiltonians H_F . Let us emphasize that stating the problem as that of solving PDEs is a fundamental preliminary step for a theoretical study, for example for proving the uniqueness of the solution.

5.3 Shape From Shading can be a completely well-posed problem!

5.3.1 Related work

To our knowledge, only Okatani and Deguchi [102] deal with the model considered here (pinhole camera and light source at the optical center).

In [102], Okatani and Deguchi do not address at all the theoretical question of existence and uniqueness of a solution. Also, they do not write the adequate Hamilton-Jacobi equation (as we do in section 5.2). They only propose a numerical method based on the propagation of the iso-distance contours, turning the static equation (5.5) into an evolution equation.

In the previous chapters, we have yet considered this modeling (pinhole camera and light source at the optical center), but in effect, we have dealt with equation (5.8) but not with equation (5.6). We have neglected the $1/r^2$ term. By simplifying the modeling, one can think simplify the problem. On the contrary, we make it more complex. In effect, as explained in chapter 2 by ignoring the $1/r^2$ attenuation term the problem becomes ill-posed: the uniqueness of the solution does not hold. To obtain a unique solution (more exactly, a characterization) one needs to specify Dirichlet boundary conditions on the boundary of the image and at all the singular points (as in the case of a distant point light source), see section 2.2.6.

To get around this difficulty⁹ in chapter 4, we have obtained the uniqueness of a maximal solution by using sophisticated mathematical tools. In particu-

⁸For example, For some fixed (x, u) , $H_F(x, u, p)$ reaches its minimum at $p = 0$. Also, the application $\lambda \mapsto H_F(x, u, \lambda p)$ is nondecreasing for $\lambda \in \mathbb{R}^+$. These properties do not hold for the Hamiltonian H'_F .

⁹In the SFS problem, we rarely know the values of the solution on the boundary of the image.

lar, the tools we have developed in chapter 4 allow to “send to infinity” the boundary conditions (at the singular points and at the boundary of the image) when we do not know them. Even if we obtain excellent numerical results with real images with a unique singular point (see section 4.7) this method presents some difficulties when there exist several singular points. Aware of the major role played by the singular points, Oliensis and Dupuis [108] and Kimmel and Bruckstein [79] propose some “global” methods (based on the nature of these particular points) allowing to recover some (very) smooth and constrained surfaces¹⁰ (in the case where these surfaces exist). Okatani and Deguchi, in [104, 105], use the isophotes of the image for classifying part of the singular points. They also suggest how to use the informations they obtain for improving the global methods of Dupuis and Oliensis [108] and of Kimmel and Bruckstein [79].

Note that although the papers [108, 79, 104, 105] are based on an orthographic camera and a single distant light source, this work can be easily extended to the more realistic modelings described in chapter 2 by using the tools developed in chapter 4. Nevertheless, despite their advantages, these global methods [108, 79, 104, 105] have an important weakness. In effect, in practice, because of noise, of errors on the parameters (focal length, light position, etc. . .) and of incorrect modeling (interreflections, spatially extended light source, non-lambertian reflectance. . .) the SFS equations (such as those described in [108, 79, 122]) do not have smooth solutions! Also, the global methods proposed in [108, 79, 104] are quite disappointing when applied to real images. These global methods tend to return satisfying results only with simple synthetic images.

Opposite to all the previous work [108, 79, 104, 105] and the study of chapters 2 and 4, let us stress that *the notion of singular points does not make any sense as soon as we do not neglect the $1/r^2$ attenuation term*. This is particularly relevant in the framework considered here, i.e. a pinhole camera with a single light source located at the optical center. As a result of a more realistic modeling, the difficulties described above completely disappear.

The results presented in the next section are based on the classical notion of viscosity solutions of the Hamilton-Jacobi PDEs [95, 41, 40, 5, 7].

¹⁰They consider C^2 surfaces with second order derivatives satisfying some properties: for example, Kimmel and Bruckstein [79] consider surfaces represented by Morse functions (with non-degenerate Hessians).

5.3.2 Well-posedness of the SFS problem

Let us assume that Ω is *bounded*, a very reasonable assumption since the CCD sensors have finite size. In this case, it is well known that Hamilton-Jacobi equations, in particular the SFS equation

$$-e^{-2u(x)} + J(x)\sqrt{f^2|\nabla u(x)|^2 + (\nabla u(x) \cdot x)^2 + Q(x)^2} = 0, \quad \forall x \in \Omega, \quad (5.14)$$

do not have a unique (discontinuous) viscosity solution [95, 7, 5]. To overcome this difficulty we need to add some a priori. In the viscosity framework, the authors generally add boundary conditions. The main classical boundary conditions are Dirichlet's, Neumann's [95, 7, 5] or Soner's state constraints [145, 29]. For the Shape from Shading problem, the authors generally consider *Dirichlet boundary conditions* [134, 55, 56, 127, 120, 123, 119]. With such boundary conditions, equation (5.14) becomes

$$\begin{cases} -e^{-2u(x)} + J(x)\sqrt{f^2|\nabla u(x)|^2 + (\nabla u(x) \cdot x)^2 + Q(x)^2} = 0, & \forall x \in \Omega, \\ u(x) = \varphi(x), & \forall x \in \partial\Omega, \end{cases} \quad (5.15)$$

where φ is a real continuous function defined on $\partial\Omega$. In this case, the following theorem ensures the uniqueness of the (discontinuous) viscosity solution.

Theorem 5.1 ¹¹ *Let Ω be bounded and smooth enough¹², and $H : \Omega \times \mathbb{R} \times \mathbb{R}^2 \mapsto \mathbb{R}$, continuous. If φ is continuous and if the hypotheses (H25)-(H9') and the boundary hypotheses (H12')-(H13')-(H14') (described below) hold, then we have a strong uniqueness property for equation*

$$\begin{cases} H(x, u(x), \nabla u(x)) = 0, & \forall x \in \Omega, \\ u(x) = \varphi(x), & \forall x \in \partial\Omega \end{cases} \quad (5.16)$$

(in the discontinuous viscosity sense) on Ω .

Let us recall that the *strong uniqueness* property (on a subset D of Ω) is the following:

If u and v are a (discontinuous) viscosity subsolution and supersolution, respectively, then

$$u \leq v \text{ on } D$$

Let us remind that the strong uniqueness property involves the uniqueness of the (discontinuous) viscosity solution. Also, since the set of classical solutions is a subset of the (discontinuous) viscosity solutions, therefore the uniqueness

¹¹See theorem 4.5 and corollary 4.1 of Barles' book [7].

¹² $\Omega \in W^{2,\infty}$.

of the (discontinuous) viscosity solution implies the uniqueness of the solution in the classical sense. Let us also recall that the strong uniqueness property involves the continuity of the (discontinuous) viscosity solution. Finally, note that in theorem 5.1, the strong uniqueness holds on Ω and not on $\overline{\Omega}$.

The hypotheses (H25) and (H9') are:

$$(H25) \quad H(x, u, p) - H(x, v, p) \geq \gamma_R(u - v), (\gamma_R > 0)$$

for all $x \in \Omega$, $-R \leq v \leq u \leq R$, and $p \in \mathbb{R}^2$ ($\forall 0 < R < +\infty$).

$$(H9') \quad |H(x, u, p) - H(y, u, p)| \leq m_R(|x - y|(1 + |p|))$$

for all $x, y \in \Omega$, $-R \leq u \leq R$ and $p \in \mathbb{R}^2$,
where $m_R(t) \rightarrow 0$ when $t \rightarrow 0$.

The boundary hypotheses (H12'), (H13') and (H14') are the following:
There exists a subset Γ of \mathbb{R}^2 which is a neighborhood of $\partial\Omega$ such that

(H12') for all $0 < R < +\infty$, there exists $m_R(t) \rightarrow 0$ when $t \rightarrow 0$ such that

$$|H(x, u, p) - H(x, u, q)| \leq m_R(|p - q|)$$

for all $x \in \Gamma$, $-R \leq u \leq R$ and $p, q \in \mathbb{R}^2$.

(H13') for all $0 < R < +\infty$, there exists $C_R > 0$ such that

$$H(x, u, p + \lambda\eta(x)) \leq 0 \implies \lambda \leq C_R(1 + |p|),$$

for all $(x, u, p) \in \Gamma \times [-R, R] \times \mathbb{R}^2$.

(H14') $\forall R_1, R_2 \in \mathbb{R}^{+*}$,

$$H(x, u, p - \lambda\eta(x)) \rightarrow +\infty \quad \text{when } \lambda \rightarrow +\infty,$$

uniformly for (x, u, p) in $\Gamma \times [-R_1, R_1] \times B(0, R_2)$.

In hypotheses (H13') and (H14'), $\eta(x)$ is the unit outward pointing normal vector to $\partial\Omega$.

Application of theorem 5.1 to the SFS Hamiltonian H_F :

We have the

Proposition 5.1 i) *The hypothesis (H25) holds for H_F , for all brightness image I ;*

ii) *if the intensity image I is differentiable and I and ∇I are bounded on Ω , then (H9') holds for H_F ;*

iii) if the intensity image I is upper bounded on a bounded neighborhood Γ of $\partial\Omega$, then the hypothesis (H12') holds for H_F ;

iv) if there exists a neighborhood Γ of $\partial\Omega$ and $\delta > 0$ such that

$$\forall x \in \Gamma, \quad \delta \leq I(x)$$

then hypotheses (H13') and (H14') are verified with H_F .

Proof. See section 5.6 at page 258. □

So as soon as I is differentiable and such that there exist $\delta > 0$ and M verifying $\delta \leq I(x) \leq M$ and $|\nabla I(x)| \leq M$ (for all x in a bounded neighborhood of Ω), therefore by proposition 5.1, the Shape From Shading equation (5.15) has a unique (discontinuous) viscosity solution. In other words, if we know on the boundary of the image the depth of the surface which has produced the image, we are able to recover uniquely this surface. This surface corresponds to the viscosity solution of (5.15). Let us emphasize that this result holds independently of the local properties of the original surface. More precisely, this result holds even if the function u representing the original surface has local minima and maxima on Ω . This is in contrast with the difficulties encountered with all the other “classical” SFS equations presented in chapter 2. In effect, for the other “classical” SFS equations, the local minima and maxima¹³ of u create singular points. So, even though we know the values of the solution on $\partial\Omega$, the problem is still ill-posed. In particular some concave/convex ambiguities can appear. In order to recover a “global solution” [108, 79] we need to introduce some extra regularity hypotheses (we must consider at least C^2 solutions with nondegenerate Hessians, but let us recall that in practice such smooth solutions never exist) and to come up with a (very difficult) classification of the singular points [104]. Finally, if we want to characterize or compute a viscosity solution of such degenerate equations, we require the knowledge of the solution at the points of the local minima, see theorem 4.6 and its corollary in chapter 4 (at page 170). With the new modeling this kind of difficulty completely disappears.

In chapter 4 we have shown that the idea of *state constraints* provides a more convenient notion of boundary conditions than Dirichlet's or Neumann's¹⁴. Let

¹³In fact, we must consider the local minima and maxima of $u - \psi$, where ψ is an adequate subsolution; see chapter 4. For most of the SFS Hamiltonians, an adequate subsolution ψ is the null function.

¹⁴Let us recall that, already in [47], Dupuis and Oliensis have introduced some similar tools in the case of the C^1 solutions. Also in [96], Lions, Rouy and Tourin used the notion of state constraint for dealing with occluding contours.

us recall that the “state constraint” is a boundary condition which is reduced to

$$H(x, u(x), \nabla u(x)) \geq 0 \quad \text{on } \partial\Omega,$$

in the viscosity sense (see for example [7, 29]) and that this constraint corresponds to the Dirichlet’s conditions

$$\forall x \in \partial\Omega, \quad u(x) = \varphi(x) \quad \text{with } \varphi(x) = +\infty$$

in the viscosity sense. In the sequel we will write this constraint as

$$u(x) = +\infty, \quad \forall x \in \partial\Omega.$$

As we explain in chapter 4, the interest of the notion of state constraints is twofolds. 1) In contrast with the Dirichlet and Neumann boundary conditions, the state constraints do not require any data. Let us recall that the Dirichlet (respectively, Neumann) boundary conditions require the knowledge of the exact values of the solution (respectively, the exact values of $\nabla u(x) \cdot n(x)$, where $n(x)$ is the unit inward normal vector to $\partial\Omega$ at the point x) on the boundary of the image. This is quite unrealistic because in the Shape from Shading problem, we rarely have such data at our disposal. 2) The notion of state constraints provides a relevant solution as soon as the image is obtained from a surface represented by u verifying that for all $x \in \partial\Omega$,

$$H(x, u, \xi) \geq 0, \quad \forall \xi \in D^-u(x), \tag{5.17}$$

see chapter 4, for more details and the proof of the fact that a function u verifies the constraint (5.17) as soon as

$$\nabla_p H(x, u, \nabla u(x)) \cdot n(x) < 0.$$

For the Hamiltonian H_F , a function u verifies the constraint (5.17) as soon as $-f_c(x, \nabla u(x)) \cdot n(x) < 0$ (where f_c is defined below in section 5.4.1), i.e. as soon as

$$\nabla u(x) \cdot [{}^t \text{Dil}_x n(x)] < 0. \tag{5.18}$$

Since in this case the eigen values of Dil_x are strictly positive, the previous assumption holds roughly when $u(x)$ “increases when x comes up to $\partial\Omega$ ”.

Remark 42. The reader may wonder at this stage how constraining this condition really is. It is in fact not a strong constraint since for example, as soon as the image to be processed contains an object of interest in front of a background, the condition is satisfied in a neighbourhood of the object where $u(x)$ increases rapidly.

In order to prove the uniqueness of the solution in the case of state constraints, we have the theorem¹⁵

Theorem 5.2 *Let Ω be bounded and smooth enough¹⁶, and $H : \Omega \times \mathbb{R} \times \mathbb{R}^2 \mapsto \mathbb{R}$, continuous. If the hypotheses (H25)-(H9') hold and the boundary hypotheses (H12')-(H13') hold, then we have a strong uniqueness result for equation*

$$\begin{cases} H(x, u(x), \nabla u(x)) = 0, & \forall x \in \Omega, \\ u(x) = +\infty, & \forall x \in \partial\Omega \end{cases}$$

(in the discontinuous viscosity sense) on Ω .

By using theorem 5.2, we prove (as we have done for theorem 5.1) that the Shape From Shading equation

$$\begin{cases} -e^{-2u(x)} + J(x) \sqrt{f^2 |\nabla u(x)|^2 + (\nabla u(x) \cdot x)^2 + Q(x)^2} = 0, & \forall x \in \Omega, \\ u(x) = +\infty, & \forall x \in \partial\Omega \end{cases} \quad (5.19)$$

has a unique (discontinuous) viscosity solution, as soon as $\delta < I(x) < M$ and $|\nabla I(x)| \leq M$. Thus we have a unique solution of (5.14) without requiring boundary data (as must be done with classical Neumann or Dirichlet boundary conditions). This solution corresponds to the actual surface producing the image as soon as this surface roughly increases when x gets close to the boundary of the image¹⁷. If this condition does not hold the resulting solution corresponds to the actual surface on the largest subset Θ of Ω for which (5.18) holds on $\partial\Theta$. As in the case of Dirichlet boundary conditions (theorem 5.1), let us emphasize that this uniqueness result and the correspondence of the solution with the actual surface hold even when the actual surface has local minima and maxima on Ω . In particular, we do not need to impose constraints at the singular points¹⁸. In other words the concave/convex ambiguities linked to the presence of the singularities completely disappear. Finally, if we know a priori that the original surface “increases” toward $\partial\Omega$ then the SFS problem is completely well-posed and there are no ambiguities. Of course, this conclusion does not hold for all the other “classical” SFS equations.

Remarks 43.

R43.1 - We have discussed the uniqueness of the solution of the SFS equations (5.15) and (5.19) but we have not considered the problem of the *existence*

¹⁵Theorem 4.6 of Barles' book [7].

¹⁶ $\Omega \in W^{2,\infty}$.

¹⁷The exact condition is the condition (5.18).

¹⁸Let us recall that the notion of singular points does not have sense in this setup!

of a solution. In fact, using some stability results, we prove below that equations (5.15) and (5.19) always have a solution. In particular, thanks to the strong uniqueness result, we prove in section 5.4.3 that the solutions of the schemes we propose in section 5.4.3 converge toward a function which is a (discontinuous) viscosity solution of (5.15) (or (5.19), see section 5.4.2).

R43.2 - In large segments of the Shape from Shading literature, the authors state that the Shape from Shading problem is ill-posed and suggest that in order to solve it (numerically and/or theoretically) one has to resort to regularization. For example,

- 1.the minimization approaches [66, 42] add regularization terms in the SFS equations.
- 2.Oliensis and Dupuis [108, 47] need regularity hypotheses for characterizing a “global solution”. They work in a set of constrained C^2 solutions.

Contrary to this previous work, we prove here that regularization is not required for ensuring the well-posedness of the SFS problem and for computing a numerical approximation of its solution. In particular, we can characterize nonsmooth solutions and we do not need to add regularization terms in the equations.

5.4 A provably convergent numerical method

In [102, 103], Okatani and Deguchi describe a numerical method based on the propagation of the equal-distance contours. As Bruckstein and Kimmel [21, 80] for the Eikonal equation, they design an evolution equation and propose to solve it by using a level-set method [111, 110, 140]. Although the method of Okatani and Deguchi is rigorous, it suffers from an important drawback because it requires an *initial equal-distance contour* and uses the *distance function of this contour*. The consequences are twofolds. First, it decreases the applicability of the method since such data (initial equal-distance contour and distance function of this contour) is usually not available. Second because these data, when available, are noisy they in fact may perturb the reconstruction! In effect, as we show in section 5.3, in the modeling framework of this chapter (pinhole camera and light source located at the optical center, considering the attenuation term in $1/r^2$) the Shape from Shading problem is well posed¹⁹. Also, the characterization of the solution (and therefore its computation) does not require additional data. Let us note that when the initial equal-distance contour and

¹⁹Here, we consider the SFS problem with state constraints on the boundary of the image.

distance function of this contour are exact, the numerical solution returned by the algorithm of Okatani and Deguchi is an approximation of the solution of equation (5.19) (equation completed with the state constraints). Nevertheless, when the imposed initial data contain errors, the reconstructed surface does not correspond with the solution of (5.19), neither with a solution of (5.15), for some φ . This kind of difficulties shows the interest of the theoretical analyses such as those presented in section 5.3.

We next propose a new numerical method. Contrary to [102, 103] it does not require an initial equal-distance contour. Moreover, our method is provably convergent: We prove that our numerical schemes are *stable, consistent* and that *their solutions converge toward the unique viscosity solution* of the problem. Let us note that Okatani and Deguchi do not even consider such questions whose practical importance should not be underestimated because, for example, they allow to certify algorithms, to guarantee their robustness and to describe their limitations. . .

From another point of view (although we have not implemented their method and hence have not made comparison tests), our numerical method *based on control theory* (and computing directly the solution of the *stationary equation*) is most probably much more efficient than theirs that solves an *evolution equation* by a *level-sets method*.

In the following we first describe a control formulation of the Hamiltonian H_F (section 5.4.1) and we explain how to deal with the boundary conditions (section 5.4.2). From this control formulation of H_F we design two monotonous approximation schemes and we prove their stability, consistence and convergence (section 5.4.3). Finally, we propose numerical algorithms which compute numerical approximations of the solutions of our new schemes (section 5.4.4).

5.4.1 Control formulation of the Hamiltonian H_F

Let us consider the function $H_C : \Omega \times \mathbb{R}^2 \mapsto \mathbb{R}^2$ given by:

$$H_C(x, p) = J(x) \sqrt{r^2 |p|^2 + (p \cdot x)^2 + Q(x)^2}.$$

We therefore have

$$H_F(x, u, p) = -e^{-2u} + H_C(x, p).$$

In section 2.2.3 (page 67), we have described a “generic” SFS Hamiltonian H_g we recall here:

$$H_g(x, p) = \tilde{H}_g(x, A_x p + \mathbf{v}_x) + \mathbf{w}_x \cdot p + c_x,$$

with $\tilde{H}_g(x, q) = \kappa_x \sqrt{|q|^2 + K_x^2}$,

- $\kappa_x > 0$ and $K_x \geq 0$,
- $A_x = D_x R_x$, where
 - $D_x = \begin{pmatrix} \mu_x & 0 \\ 0 & \nu_x \end{pmatrix}$, $\mu_x, \nu_x \neq 0$,
 - if $x \neq 0$, R_x is the rotation matrix $R_x = \begin{pmatrix} \cos \theta & \sin \theta \\ -\sin \theta & \cos \theta \end{pmatrix}$;
 where $\cos \theta = \frac{x_2}{|x|}$ and $\sin \theta = -\frac{x_1}{|x|}$,
 - if $x = 0$, $R_x = Id_{2 \times 2}$;
- $\mathbf{v}_x, \mathbf{w}_x \in \mathbb{R}^2$,
- $c_x \in \mathbb{R}$.

As in appendix B.1 (at page 277), we prove that H_C is the particular case of H_g corresponding to:

$$\begin{aligned} \mu_x &= f & \nu_x &= \sqrt{f^2 + |x|^2} \\ \kappa_x &= J(x) & K_x &= \sqrt{\frac{f^2}{f^2 + |x|^2}} \quad (= Q(x)) \\ \mathbf{w}_x &= 0 & \mathbf{v}_x &= 0 \\ c_x &= 0. \end{aligned}$$

Therefore we can use the control formulation of H_g detailed in section 2.2.3 (at page 67):

$$H_g(x, p) = \sup_{a \in \overline{B}_2(0,1)} \{ -f_g(x, a) \cdot p - l_g(x, a) \},$$

with

$$\begin{aligned} f_g(x, a) &= - [Dil_x a + \mathbf{w}_x], \\ l_g(x, a) &= - [K_x \kappa_x \sqrt{1 - |a|^2} + \kappa_x ({}^t R_x \mathbf{v}_x) \cdot a + c_x], \end{aligned}$$

where $Dil_x = \kappa_x {}^t R_x D_x R_x$.

If we denote f_c and l_c the functions f_g and l_g associated with H_C , we have

$$H_F(x, u, p) = -e^{-2u} + \sup_{a \in \overline{B}_2(0,1)} \{ -f_c(x, a) \cdot p - l_c(x, a) \} \quad (5.20)$$

where

$$\begin{aligned} f_c(x, a) &= -Dil_x a, \\ l_c(x, a) &= -I(x) f^2 \sqrt{1 - |a|^2}. \end{aligned} \quad (5.21)$$

5.4.2 Management of the boundary conditions

Exactly as in section 4.6.1 (at page 185), we prove that the state constraints can always be rewritten as Dirichlet boundary conditions. The main argument of the proof is based on the fact that all the viscosity solutions of (5.19) are bounded by the same constant (see lemma 5.3 of section 5.6 at page 260). More precisely, we prove that the discontinuous viscosity solution of (5.19) (equation with state constraints) coincides with the discontinuous viscosity solution of (5.15) (equation with Dirichlet's conditions) with $\varphi(x) = M$ ($\forall x \in \partial\Omega$). In practice we therefore always consider Dirichlet boundary conditions. If we happen to know the values of the solution on $\partial\Omega$ we constrain φ accordingly otherwise we choose φ to be a “large” constant.

5.4.3 Two new approximation schemes

In this section, we propose two finite difference approximation schemes on a regular mesh. Note that as in chapter 3, the schemes we describe here can be easily extended to irregular meshes.

Let us just recall that an approximation scheme is a functional equation of the form

$$T(\rho, x, u) = 0 \quad \forall x \in \overline{\Omega};$$

where $T : \mathcal{M} \times \overline{\Omega} \times B(\overline{\Omega}) \rightarrow \mathbb{R}$, $\mathcal{M} = \mathbb{R}^+ \times \mathbb{R}^+$ and $B(D)$ is the space of bounded functions defined on a set D . $\rho = (h_1, h_2) \in \mathcal{M}$ defines the size of the mesh that is used in the corresponding numerical algorithms. Moreover, as in chapter 3, we use the representations S of a scheme T as

$$S(\rho, x, u(x), u) = 0 \quad \forall x \in \overline{\Omega},$$

where

$$\begin{aligned} S : \mathcal{M} \times \overline{\Omega} \times \mathbb{R} \times B(\overline{\Omega}) &\longrightarrow \mathbb{R} \\ (\rho, x, t, u) &\longmapsto S(\rho, x, t, u). \end{aligned}$$

and we consider “schemes with Dirichlet boundary conditions”, i.e. schemes such that:

$$S(\rho, x, t, u) = \begin{cases} \tilde{S}(\rho, x, t, u) & \text{if } x \in \Omega_\rho, \\ t - \varphi(x) & \text{if } x \in \mathfrak{b}\Omega_\rho, \end{cases} \quad (5.22)$$

where

$$\Omega_\rho = \{x \in \Omega \mid \forall i \in \{1, 2\}, x \pm h_i \vec{e}_i \in \overline{\Omega}\} \quad \text{and} \quad \mathfrak{b}\Omega_\rho = \overline{\Omega} - \Omega_\rho.$$

Note that we assume in (5.22) that we have extended φ continuously to $\mathfrak{b}\Omega_\rho$.

Design of the approximation schemes

Let us recall that there exists more or less a standard method ensuring the convergence of the solutions of schemes toward viscosity solutions, i.e. the one presented by Barles and Souganidis in [9]. This method requires the monotonicity of the scheme; this is why, as in chapter 3, we design a monotonous scheme in the sequel. We recall the definition:

Definition 3.1 (monotonicity) *The scheme $S(\rho, x, u(x), u) = 0$ defined on $\overline{\Omega}$ is monotonous if $\forall \rho, \forall x \in \overline{\Omega}, \forall t \in \mathbb{R}$ and $\forall u, v \in B(\overline{\Omega})$,*

$$u \leq v \implies S(\rho, x, t, u) \geq S(\rho, x, t, v)$$

(that is to say: the scheme is nonincreasing with respect to u).

For proving the stability of our scheme, we apply the general theorem 3.1 given at page 101. This requires that the function $t \mapsto S(\rho, x, t, u)$ is nondecreasing.

As in chapter 3, we approximate $H_C(x, \nabla u(x))$ by:

$$\begin{aligned} H_C(x, \nabla u(x)) &\approx \sup_{a \in A} \left\{ \sum_{i=1}^2 (-f_i(x, a)) \frac{u(x) - u(x + s_i(x, a)h_i \vec{e}_i)}{-s_i(x, a)h_i} - l_c(x, a) \right\} \\ &= \sup_{a \in A} \left\{ \left(\sum_{i=1}^2 \frac{|f_i(x, a)|}{h_i} \right) u(x) - \sum_{i=1}^2 \frac{|f_i(x, a)|}{h_i} u(x + s_i(x, a)h_i \vec{e}_i) - l_c(x, a) \right\}, \end{aligned} \quad (5.23)$$

where here, $f_i(x, a)$ is the i^{th} component of $f_c(x, a)$, where $s_i(x, a)$ is its sign and where A is the closed unit ball $\overline{B}(0, 1)$.

We can therefore approximate $H_F(x, u(x), \nabla u(x))$ by:

$$\begin{aligned} H_F(x, u(x), \nabla u(x)) &\approx -e^{-2} u(x) \\ &+ \sup_{a \in A} \left\{ \left(\sum_{i=1}^2 \frac{|f_i(x, a)|}{h_i} \right) u(x) - \sum_{i=1}^2 \frac{|f_i(x, a)|}{h_i} u(x + s_i(x, a)h_i \vec{e}_i) - l_c(x, a) \right\}. \end{aligned} \quad (5.24)$$

So, we can formulate a first representation (with Dirichlet boundary conditions) S_{impl} based on the function:

$$\begin{aligned} &\tilde{S}_{impl}(\rho, x, t, u) \\ &= -e^{-2} t + \sup_{a \in A} \left\{ \left(\sum_{i=1}^2 \frac{|f_i(x, a)|}{h_i} \right) t - \sum_{i=1}^2 \frac{|f_i(x, a)|}{h_i} u(x + s_i(x, a)h_i \vec{e}_i) - l_c(x, a) \right\} \\ &= -e^{-2} t + \sup_{a \in A} \left\{ \sum_{i=1}^2 (-f_i(x, a)) \frac{t - u(x + s_i(x, a)h_i \vec{e}_i)}{-s_i(x, a)h_i} - l_c(x, a) \right\}. \end{aligned} \quad (5.25)$$

Remarks 44.

r44.1 - The function $t \mapsto S_{impl}(\rho, x, t, u)$ is obviously nondecreasing. The representation S_{impl} is also clearly monotonous.

r44.2 - This first representation should provide a very fast algorithm.

As in chapter 3 for HJB equations, here we can provide another (more explicit) representation. We multiply (5.25) by a fictitious time increment $\Delta\tau$ ($\Delta\tau > 0$ can depend on x , $\Delta\tau = \Delta\tau(x)$), add $u(x)$ and $-u(x)$ and obtain:

$$\begin{aligned} \hat{S}(\rho, x, u(x), u) &= u(x) - \Delta\tau e^{-2u(x)} \\ + \sup_{a \in A} &\left\{ - \left(1 - \Delta\tau \sum_{i=1}^2 \frac{|f_i(x, a)|}{h_i} \right) u(x) - \Delta\tau \sum_{i=1}^2 \frac{|f_i(x, a)|}{h_i} u(x + s_i(x, a) h_i \vec{e}_i) - \Delta\tau l_c(x, a) \right\}. \end{aligned} \quad (5.26)$$

We can also choose a second representation (with Dirichlet boundary conditions) S_{semi} based on the function:

$$\begin{aligned} \tilde{S}_{semi}(\rho, x, t, u) &= t - \Delta\tau e^{-2t} \\ + \sup_{a \in A} &\left\{ - \left(1 - \Delta\tau \sum_{i=1}^2 \frac{|f_i(x, a)|}{h_i} \right) u(x) - \Delta\tau \sum_{i=1}^2 \frac{|f_i(x, a)|}{h_i} u(x + s_i(x, a) h_i \vec{e}_i) - \Delta\tau l_c(x, a) \right\} \\ &= t - \Delta\tau e^{-2t} - u(x) + \Delta\tau \sup_{a \in A} \left\{ \sum_{i=1}^2 (-f_i(x, a)) \frac{u(x) - u(x + s_i(x, a) h_i \vec{e}_i)}{-s_i(x, a) h_i} - l_c(x, a) \right\}. \end{aligned} \quad (5.27)$$

Remark 45. The function $t \mapsto S_{semi}(\rho, x, t, u)$ is obviously nondecreasing. But the representation S_{semi} is not always monotonous.

Let us denote now a_0 the optimal control²⁰ of (5.23). For all x such that $a_0 \neq 0$, let us introduce

$$\Delta\tau_{opt} = \left(\sum_{i=1}^2 \frac{|f_i(x, a_0)|}{h_i} \right)^{-1}.$$

Remark 46. a_0 and the optimal $\Delta\tau_{opt}$ depend on x .

The reader will easily verify that the scheme $S_{semi}(\rho, x, u(x), u) = 0$ is

²⁰The a in A for which the maximum of (5.23) is reached

monotonous iff $\Delta\tau \leq \Delta\tau_{opt}$. Let us mention that the larger the “parameter” $\Delta\tau$, the faster the convergence. When we choose $\Delta\tau = \Delta\tau_{opt}$, \tilde{S}_{semi} can be rewritten²¹:

$$\begin{aligned} \tilde{S}_{semi}^{opt}(\rho, x, t, u) &= t - \frac{1}{\sum_{j=1}^N |f_j(x, a_0)|/h_j} e^{-2t} \\ &- \sum_{i=1}^2 \frac{|f_i(x, a_0)|/h_i}{\sum_{j=1}^2 |f_j(x, a_0)|/h_j} u(x + s_i h_i \vec{e}_i) - \frac{1}{\sum_{j=1}^2 |f_j(x, a_0)|/h_j} l_c(x, a_0). \end{aligned} \quad (5.28)$$

In summary the representation S_{impl} is always monotonous, the representation S_{semi} is monotonous iff $\Delta\tau \leq \Delta\tau_{opt}$, the representation S_{semi}^{opt} is always monotonous and it is the most effective monotonous representation of the form S_{semi} .

Remark 47. The reader will verify that the numerical method we describe here can be applied to all equations of the form:

$$G(u(x)) + H(x, \nabla u(x)) = 0,$$

where G is a nondecreasing function and H is a convex Hamiltonian (with respect to p).

Stability of our approximation schemes

Thanks to the monotonicity properties we can apply theorem 3.1 which proves the stability of our new schemes. Here, let us just recall that an approximation scheme is “(uniformly) stable” when it has (uniformly) bounded solutions; (see page 100 for the definition of the stability).

Remark 48. By construction $S_{semi}(\rho, x, u(x), u) = \Delta\tau S_{impl}(\rho, x, u(x), u)$. So the schemes S_{semi} and S_{impl} have exactly the same subsolutions, supersolutions and solutions. Therefore, S_{semi} is (uniformly) stable iff S_{impl} is (uniformly) stable.

The following proposition ensures the stability of our schemes.

Proposition 5.2 *If there exist δ and M such that $\forall x \in \overline{\Omega}$, $M \geq I(x) \geq \delta > 0$, then all the hypotheses of theorem 3.1 ((H15), (H16), (H17), (H18), (H19), (H20)) hold. Therefore the schemes S_{impl} and S_{semi} are uniformly stable.*

²¹ a_0 does not depend on $\Delta\tau$.

Proof. See section 5.6 at page 261. \square

Moreover, let us note that we have also

Proposition 5.3 *If the hypotheses of proposition 5.2 are verified then the hypotheses (H16'), (H19') and (H20') hold.*

Proof. See section 5.6 at page 262. \square

Therefore the schemes S_{impl} and S_{semi} are also *stable* when *starting from a supersolution* (see remark R15.3, page 104). This remark is very important because it ensures the convergence of the associated algorithm when starting from a supersolution. In practice we have noticed that *the numerical algorithm converges much faster toward the solution of the scheme when we start from a supersolution than when we start from a subsolution.*

Remark 49. The (uniform) stability of the schemes S_{impl} and S_{semi} does not require regularity of the brightness image I .

Convergence toward the viscosity solutions

In the previous section we have proved that the schemes S_{impl} and S_{semi} are uniformly stability. That is to say, for all fixed mesh size ρ , the schemes have solutions (i.e there exists of a function u s.t. $\forall x \in \overline{\Omega}$, $S(\rho, x, u(x), u) = 0$) and all the solutions are bounded independently of ρ . In this section we prove furthermore that the solutions of these schemes converge toward the unique (discontinuous) viscosity solution of the considered equation ((5.15) or (5.19)), when the size of the mesh ρ vanishes.

First, by using proposition 3.4 (at page 115), the schemes S_{impl} and S_{semi} are consistent (following Barles and Souganidis's definition [9]; see definition 3.5 at page 112) as soon as f_c and l_c are continuous on $A \times \overline{\Omega}$ and Lipschitz continuous with respect to $x \in \overline{\Omega}$ and l_c is bounded. More precisely, it is consistent as soon as the *brightness image I is Lipschitz continuous* (the expressions of f_c and l_c are detailed on page 214).

Now let us assume that Ω is bounded, that the brightness image I is Lipschitz continuous (hence upper bounded) and that there exists δ such that $\forall x \in \overline{\Omega}, I(x) \geq \delta > 0$, then by proposition 5.2, the schemes S_{impl} and S_{semi} are uniformly stable. By construction, these schemes are monotonous. Moreover

we have just seen that they are consistent with the SFS equations (5.15) and (5.19). Finally, in section 5.3 we have proved that the strong uniqueness property holds on Ω . Therefore, we can apply theorem 3.3 (given at the page 113), we remind here:

Theorem 3.3 (Convergence toward the viscosity solution)

Let S be a monotonous, uniformly stable and consistent²² approximation scheme. Let us suppose that the strong uniqueness property is verified on a subset D of $\overline{\Omega}$. Then the solutions of the scheme S converge on D toward the viscosity solution of the considered equation when $\rho \rightarrow 0$.

The solutions of the schemes S_{impl} and S_{semi} hence converge on Ω toward the unique viscosity solution of considered equation ((5.15) or (5.19)) when the mesh size vanishes.

Remark 50. It is worth noting that this result (theorem 3.3) also proves the existence of the viscosity solution of equation (5.15). More precisely, this theorem shows that, when the mesh size vanishes, the solutions of our schemes converge toward a function which is a (discontinuous) viscosity solution of equation (5.15) (equation with Dirichlet Boundary Conditions). Similarly combining section 5.4.2 with theorem 3.3 allows to prove the existence of a (discontinuous) viscosity solution of equation (5.19) (equation with state constraints).

5.4.4 A numerical algorithm

Let rho be a canonical mesh.

We now describe an algorithm that computes an approximation of the solutions of the scheme (5.27) for all $\rho > 0$. We also prove its convergence. It is important to keep in mind that the approximations computed by our algorithm converge toward solutions of the scheme but not toward the viscosity solution.

For a fixed $\rho > 0$, let us denote

- $x_k = (k_1 h_1, k_2 h_2)$ for k in \mathbb{Z}^2 , $x_{ij} = (i h_1, j h_2)$ for $i, j \in \mathbb{Z}$,
- $Q := \{k \in \mathbb{Z}^2 \text{ such that } x_k \in \overline{\Omega}\}$.

We call “pixel” a point x_k in $\overline{\Omega}$. Since $\overline{\Omega}$ is bounded; therefore the number of pixels is finite. The following algorithm computes for all $k \in Q$ a sequence of approximations U_k^n of $u(x_k)$:

²²Consistent with the considered equation.

Algorithm 5.1

1. *Initialisation* ($n = 0$):

$$\forall k \in Q, \quad U_k^0 = u_0(x_k),$$

where u_0 is a subsolution or a supersolution of the considered scheme.

2. *Choice of a pixel x_k and modification* (step $n + 1$) of U_k^n :

Choose

$$U^{n+1} = \sup \{ V = (V_l)_{l \in Q} \text{ such that } \forall l \neq k, \quad V_l = U_l^n \text{ and } S(\rho, x_k, V_k, V) = 0 \}.$$

In other words, we choose U^{n+1} such that

$$\begin{cases} U_l^{n+1} = U_l^n & \text{if } l \neq k, \\ U_k^{n+1} = \max \{ t \mid S(\rho, x_k, t, U^n) = 0 \}. \end{cases}$$

3. Choose the next pixel x_k in such a way that all pixels are regularly visited and go back to 2.

This algorithm is exactly the same as algorithm 3.1 described at page 119. Therefore all the remarks of sections 3.1.5 and 3.2 about paths and speed of convergence still hold for this new method (the schemes described in the previous section are monotonous schemes of the form $S(p, x, u^p(x), u^p) = 0$). For example, in practice, for an optimal velocity, we should start from a supersolution. Also, since all the hypotheses of theorem 3.1 (as well as the equivalent hypotheses adapted to supersolutions) hold for our two representations S_{impl} and S_{semi} , theorem 3.5 ensures that the approximations converge toward the solutions of our new schemes. Moreover, let us remind that, when the intensity image is discontinuous, the viscosity solutions theory does not apply yet, but we can prove that the numerical approximation computed by our algorithms converge.

Details of the step 2 for the semi-implicit algorithm

Step 2 requires two stages. We suppose that we work with pixel x_{ij} and for simplicity we drop the upper index n , i.e. write U_{ij} instead of U_{ij}^n .

1. First we need to compute:

$$M = \sup_{a \in A} \left\{ -f_c(x_{ij}, a) \cdot P_{U_{i,j}}^{s_1(x_{ij}, a), s_2(x_{ij}, a)} - l_c(x_{ij}, a) \right\},$$

with

$$P_{U_{i,j}}^{s_1, s_2} = \begin{pmatrix} \frac{U_{i,j} - U_{i+s_1,j}}{-s_1 \Delta x_1 1} \\ \frac{U_{i,j} - U_{i,j+s_2}}{-s_2 \Delta x_1 2} \end{pmatrix},$$

and where $s_i(x, a)$ is the sign of $f_i(x, a)$. To this end, we divide the set A into four subsets $A_{s_1, s_2} = \{a \in A \mid (s_1(x_{ij}, a), s_2(x_{ij}, a)) = (s_1, s_2)\}$, $s_1, s_2 \in \{\pm 1\}$

$$A = \bigcup_{s_1, s_2 = \pm 1} A_{s_1, s_2}$$

and we compute the optimal control $a_0^{s_1, s_2}$ for each subset:

$$a_0^{s_1, s_2} = \arg \sup_{a \in A_{s_1, s_2}} \left\{ -f_c(x_{ij}, a) \cdot P_{U, i, j}^{s_1, s_2} - l_c(x_{ij}, a) \right\}.$$

This must be done carefully. In particular, we must separate the cases where $a_0^{s_1, s_2}$ verifies $f_i(x_{ij}, a_0^{s_1, s_2}) = 0$ for some $i \in \{1, 2\}$ (i.e $a_0^{s_1, s_2} \in \partial A_{s_1, s_2}$) and the cases where $a_0^{s_1, s_2} \in \text{Int} A_{s_1, s_2}$. To simplify this step, we use convexity arguments and differential calculus.

Moreover, if we write

$$M_{s_1, s_2} = -f_c(x_{ij}, a_0^{s_1, s_2}) \cdot P_{U, i, j}^{s_1(x_{ij}, a_0^{s_1, s_2}), s_2(x_{ij}, a_0^{s_1, s_2})} - l_c(x_{ij}, a_0^{s_1, s_2}),$$

it follows that $M = \max_{s_1, s_2 \in \{\pm 1\}} M_{s_1, s_2}$.

Remark 51. Various simple tricks (for example based on the fact that the intersection $\bigcap_{s_1, s_2 \in \{\pm 1\}} A_{s_1, s_2}$ is not empty) allow to decrease the computational complexity of this step, but because of space we do not detail them here. The interested reader will most probably discover very easily most of them...

2. Second, we need to solve with respect to t the equation

$$t - \Delta\tau e^{-2t} + c = 0, \quad (5.29)$$

where c is the constant coefficient:

$$c = -U_{i, j} + \Delta\tau \sup_{a \in A} \left\{ -f_c(x_{ij}, a) \cdot P_{U, i, j}^{s_1(x_{ij}, a), s_2(x_{ij}, a)} - l_c(x_{ij}, a) \right\} \quad (5.30)$$

$$= -U_{i, j} - \Delta\tau f_c(x_{ij}, a_0) \cdot P_{U, i, j}^{s_1(x_{ij}, a_0), s_2(x_{ij}, a_0)} - \Delta\tau l_c(x_{ij}, a_0) \quad (5.31)$$

(which is also equal to

$$c = -\Delta\tau_{opt} [f_c(x_{ij}, a_0) \cdot Q_{U, i, j}^{s_1(x_{ij}, a_0), s_2(x_{ij}, a_0)} + l_c(x_{ij}, a_0)]$$

with $Q_{U, i, j}^{s_1, s_2} = (s_1 U_{i+s_1, j} / \Delta x_1, s_2 U_{i, j+s_2} / \Delta x_2)$, when $\Delta\tau = \Delta\tau_{opt}$).

For solving equation (5.29), we use Newton's method. This method can be easily improved by using some acceleration technique (see for example [15]). Let $g : \mathbb{R} \rightarrow \mathbb{R}$ be the C^∞ function defined by

$$g(t) = t - \Delta\tau e^{-2t} + c$$

and let $(t^k)_{k \in \mathbb{N}}$ be the sequence defined by:

$$\begin{aligned} t^0 &= U_{i,j}, \\ t^{k+1} &= t^k - \frac{g(t^k)}{g'(t^k)}. \end{aligned} \quad (5.32)$$

Proposition 5.4 *For all $\Delta\tau > 0$ and c in \mathbb{R} , equation (5.29) has a unique solution \bar{t} . Also, the sequence designed by (5.32) converges toward this solution.*

Proof. g is continuous, $\lim_{t \rightarrow -\infty} g(t) = -\infty$ and $\lim_{t \rightarrow +\infty} g(t) = +\infty$. So equation (5.29) has always a solution. For all t in \mathbb{R} , we have

$$g'(t) = 1 + 2\Delta\tau e^{-2t} > 1. \quad (5.33)$$

g is therefore strictly increasing and the solution of (5.29) is unique. Let us denote \bar{t} this solution.

Lemma 5.1 $\forall k > 1, t^k \leq t^{k+1} \leq \bar{t}$.

By lemma 5.1, $(t^k)_{k > 1}$ is an increasing and bounded sequence, hence convergent. By continuity of $h : r \mapsto r - \frac{g(r)}{g'(r)}$ the limit of $(t^k)_{k > 1}$ is a fixed point of h , so it is equal to \bar{t} .

Proof of Lemma 5.1. First let us assume that $t^1 \leq \bar{t}$.

Proof by recursion:

(a) $t^1 \leq \bar{t}$.

(b) let us assume that $t^k \leq \bar{t}$. Since g is a nondecreasing function we have $g(t^k) \leq 0$. By (5.33), $-\frac{g(t^k)}{g'(t^k)} \geq 0$. Therefore $t^{k+1} \geq t^k$.

Graphically, $(t^{k+1}, 0)$ is on the tangent to the graph of g at $(t^k, g(t^k))$. Since g is strictly concave²³, $(t^{k+1}, 0)$ is above the graph of g and so above $(t^{k+1}, g(t^{k+1}))$. Hence $g(t^{k+1}) \leq 0$ and therefore $t^{k+1} \leq \bar{t}$ (because g is strictly increasing).

In short: $t^k \leq t^{k+1} \leq \bar{t}$.

The proof that $t^1 \leq \bar{t}$ is based on the same ideas. □

□

²³ $g''(t) = -4\Delta\tau e^{-2t} < 0$.

Examples of supersolutions of our schemes

In this section, we describe two examples of supersolutions of the schemes presented in section 5.4.3.

Let us recall that the implicit scheme (5.25) and the semi-implicit scheme (5.27) (and of course (5.28)) have exactly the same solutions, subsolutions and supersolutions.

We have the

Proposition 5.5 *The constant function $u_0 : \overline{\Omega} \rightarrow \mathbb{R}$ defined by*

$$u_0(x) = -\frac{1}{2} \ln(\delta \, f^2)$$

where $\delta = \min(I(x)) > 0$, and the function $v_0 : \overline{\Omega} \rightarrow \mathbb{R}$ defined by

$$v_0(x) = -\frac{1}{2} \ln(I(x) \, f^2) = -\left(\frac{1}{2} \ln I(x) + \ln f\right)$$

are two supersolutions of the implicit scheme (5.25).

Proof. Let us consider the case of v_0 . For all $x \in \overline{\Omega}$, we have

$$\tilde{S}_{impl}(\rho, x, v_0(x), v_0) = -e^{-2 v_0(x)} + \sup_{a \in A} \left\{ \sum_{i=1}^2 (-f_i(x, a)) \frac{v_0(x) - v_0(x + s_i(x, a) h_i \vec{e}_i)}{-s_i(x, a) h_i} - l_c(x, a) \right\},$$

where $A = \overline{B}(0, 1)$. Since $0 \in A$, $f(x, 0) = 0$ and $l(x, 0) = -I(x) \, f^2$, we have

$$\tilde{S}_{impl}(\rho, x, v_0(x), v_0) \geq -e^{-2 v_0(x)} + I(x) \, f^2 = 0.$$

So v_0 is a supersolution of the scheme (5.25).

In the same way, we prove that u_0 is a supersolution of the scheme (5.25). \square

5.5 Experimental results

Let us emphasize that in all the experiments that follow, *we have only imposed state constraints on the boundary of the images $\partial\Omega$* . In particular, we do *not* have imposed Dirichlet boundary conditions on $\partial\Omega$. Of course, we have not imposed Dirichlet boundary conditions at the singular points. Let us recall that in our framework, the notion of singular points does not make sense anymore! In other words, in these experiments *we have not used any boundary data*.

We have implemented the algorithm associated with the *optimal semi-implicit* approximation scheme. The reader familiar with the numerical methods presented in chapter 3 will easily see that the implementation of this new semi-implicit algorithm is almost a direct extension of the implementation of the “generic” semi-implicit algorithm described in chapter 3. We only have to implement Newton’s method detailed in subsection 5.4.4 in order to solve equation (5.29) and we need to slightly change the update step... We have not implemented yet the algorithm associated to the implicit scheme.

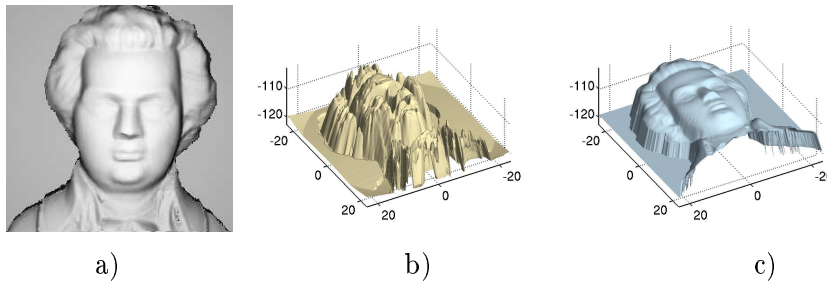
Since our new semi-implicit algorithm is *iterative*, to start the process we need an *initial surface* U_0 . Of course, as usual, the choice of this initial surface is very important. As we show in section 5.4.4, starting from a supersolution ensures the convergence of the computed numerical approximations toward the solution of the associated scheme. In section 5.4.4, we have given two examples of supersolutions: the constant function

$$u_0(x) = -\frac{1}{2} \ln(\delta f^2),$$

where $\delta = \min(I(x)) > 0$, and the function

$$v_0(x) = -\left(\frac{1}{2} \ln I(x) + \ln f\right).$$

Figure 5.4 displays the supersolution v_0 associated to image of the classical



a) Image; b) supersolution v_0 associated to the image a); c) solution (groundtruth).

Figure 5.4: Example of initial supersolution for the image of Mozart’s Face.

Mozart’s face²⁴. We have tested our algorithm with the two supersolutions. As the theory predicts, in both cases, we obtain the same numerical solutions (i.e two extremely close solutions, with the same order of errors; the difference between the surfaces is invisible). But the number of iterations required for obtaining the convergence is very different. Indeed, starting from the supersolution v_0 is significantly faster than starting from the constant supersolution

²⁴See Zhang et al. [172] (Computer Vision Lab. of the university of Central Florida).

u_0 . On average, if we start from u_0 , the convergence is reached after around 500 iterations, when if we start from v_0 , less than 60 iterations are sufficient (the number of iterations is reduced by one order of magnitude!). This result could be easily anticipated since the supersolution v_0 is very much closer to the solution than the supersolution u_0 , as figure 5.4 shows. Figures 5.10 and 5.11 illustrate the difference of the evolutions in the two cases: when the algorithm starts from u_0 and when it starts from v_0 . In other respects, let us note that exactly as for the algorithms presented in chapter 3, it is clear that the implicit version of this algorithm will allow to reduce again the number of iterations by one order of magnitude (on average, the implicit algorithm should converge in less than 10 iterations). In the results displayed in the sequel, *n corresponds to the number of iterations*. Our algorithms being iterative, they also require a *stopping criterion*. We choose to stop the iterations when the difference between the successive reconstructions is negligible. In practice, we have fixed a thresholds of $s = 10^{-10}$ and we stop the process when

$$\frac{1}{NM} \sum_{i,j} |U^{k+1}(i,j) - U^k(i,j)| \leq s,$$

where NM is the number of pixels.

Let us also note the *very high efficiency* of *Newton's method* (summarized by equation (5.32) of section 5.4.4) for solving the equation (5.29). On average, the numerical solution of equation (5.29) is computed in 5 iterations; our stopping criterion is $|t^{k+1} - t^k| \leq 10^{-20}$.

5.5.1 Experiments with synthetic images

We have tested our semi-implicit algorithm on several *synthetic images* provided by various types of surfaces. In such tests, we can compare the reconstructed surfaces with the groundtruth. In all the examples, the errors noted ε_1 , ε_2 and ε_∞ are the mean absolute errors between the reference and reconstructed surfaces measured according to the L_1 , L_2 and L_∞ norms, respectively. They are measured with the logarithm of the depth modulation in the coordinate system of the camera, i.e. the approximations of the solution v of equation (5.12). Let us remind that the parameter f corresponds to the focal length.

Experiments on various synthetic images

In this first series of results, we show the original object (i.e. the groundtruth) from two points of view (in a) and b)), the input image obtained from the original object (in c)), the reconstructed surface from the same two points of view as the original object (in d) and e)). In f), we display the superposition of

the reconstructed surface and the original object in the same point of view as e) . The groundtruth is always displayed in blue and the color of the reconstructed solution is gold (this holds for all the experiments with synthetic images). Let us recall that one of the most significant improvements of our method is that it can recover surfaces containing *several local mimima* (and maxima) *without any additional data*²⁵.

We have first tested our algorithm with images synthetized from such surfaces: in particular the “hills surface” displayed in Figure 5.5-ab) and the field of bumps displayed in figure 5.6-ab). The second rows of these figures show the surfaces returned by our algorithm (starting from the supersolution v_0) after convergence. The results are visually excellent and the computed errors $\varepsilon_1, \varepsilon_2, \varepsilon_\infty$ are very small. Let us emphasize that these solutions have been computed without *any boundary data* and that in this case, *none of the classical propagation/PDE's methods* ([67, 134, 47, 80, 81, 123, 124] among others can return a satisfying solution. At this stage, let us remind the reader that to be able to recover the original surface, this surface must verify the state constraints (described in section 5.3.2, page 210) on the boundary of the image. The hills surface and the field of bumps verify this constraint. In particular, the example of the hills surface shows how weak this constraint is.

The classical Mozart's face associated to the paper by Zhang et al. [172] (Computer Vision Lab. of the university of Central Florida) is today an unavoidable test. We have also applied our algorithm to this surface, see Figure 5.7. In [124] we needed to fix the height of the singular point on the nose for obtaining a relatively satisfying solution. Here we do not need this information. Note that the reconstruction errors of Mozart's face are mainly located in the part of the image corresponding to the background of the scene. These errors are due to the large discontinuity of the groundtruth along the apparent contours of the face. Indeed, since we compute some approximations of the viscosity solution which is continuous (due to the strong uniqueness), we are not able to recover discontinuous surfaces. Let us note that the theory we have developed assumes that the intensity image is *continuous*. Also, the surfaces and the images of Figure 5.5 and Figure 5.6 are continuous and smooth.

In order to test the ability of our algorithm to deal with discontinuous images we have applied it to synthetic images generated by shapes containing edges. First, we use a surface containing (decreasing and increasing) edges such that all its maxima²⁶ are smooth, see Figure 5.8. In this case, the reconstruction is perfect. Second, we use a more complex surface containing (decreasing and increasing) edges with nonsmooth (local and global) maxima²⁶, see Figure 5.9.

²⁵We only use the image.

²⁶ More precisely, we should consider the local *minima of the depth modulation*. The minima of depth modulation are approximately the maxima of the visualized surface.

iteration (n)	ε_1 error	ε_2 error	ε_∞ error
0	3.58725	3.58753	3.68509
60	0.554503	0.558744	0.8996
120	0.205832	0.218589	0.683311
180	0.097647	0.111971	0.625567
240	0.0436155	0.0544579	0.593743
300	0.023504	0.029243	0.578646
360	0.0211661	0.0328685	0.576906
420	0.0213052	0.03496	0.576906
540	0.0213343	0.0350149	0.576906
600	0.0213343	0.0350149	0.576906
660	0.0213343	0.0350149	0.576906
720	0.0213343	0.0350149	0.576906

Table 5.1: Evolution of the errors associated to Figure 5.10: (Mozart’s face) with the number of iterations, starting from the supersolution u_0 .

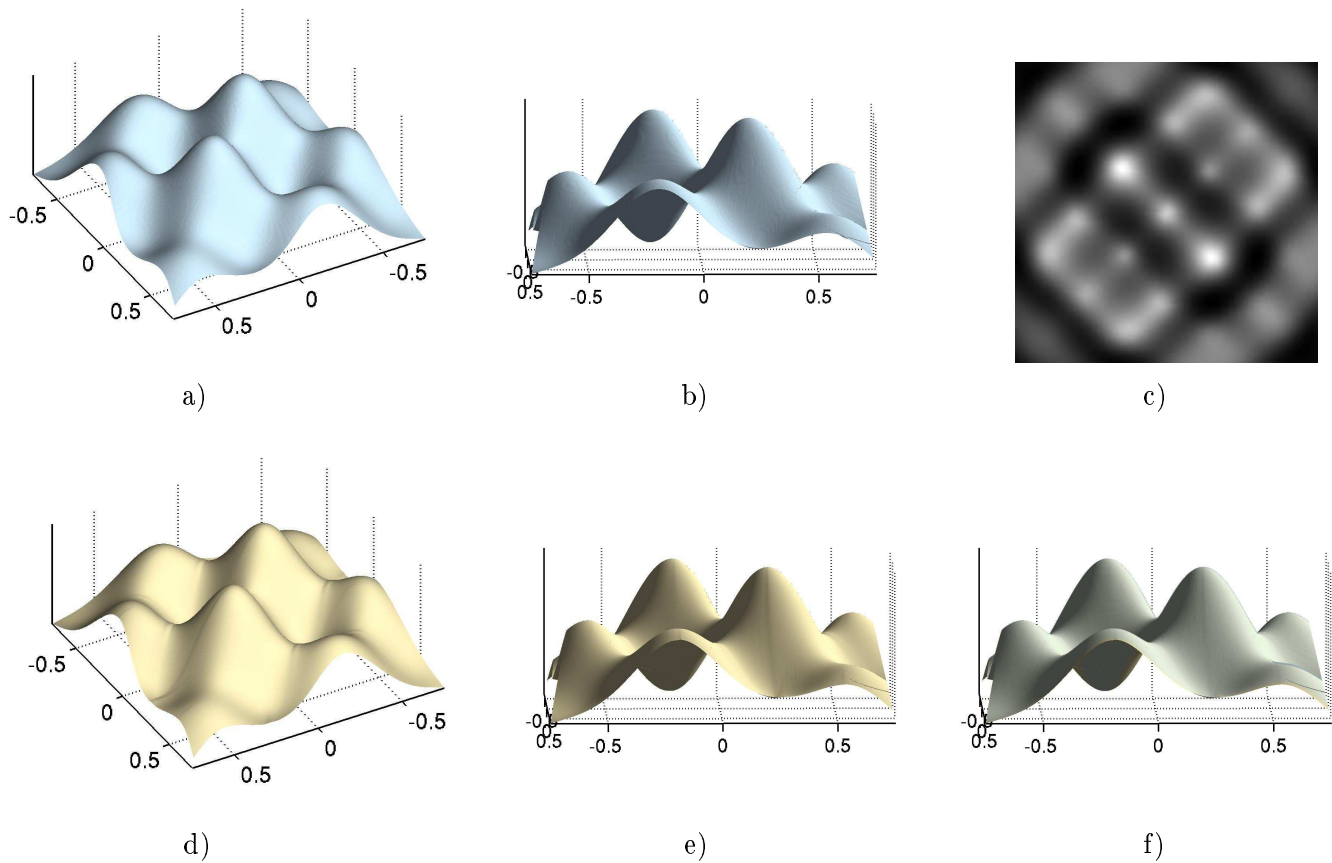
In this second case, the reconstructed surface is satisfying but not perfect. The size of the images of the hills, of the field of bumps, of the Mozart’s face and of surfaces containing edges are respectively: 300×300 , 400×400 , 250×250 , 250×250 , 250×250 .

Robustness of our method

The second part of the experiments is aimed at demonstrating the robustness of our method to various errors on the parameters. For these tests, we have used Mozart’s face image.

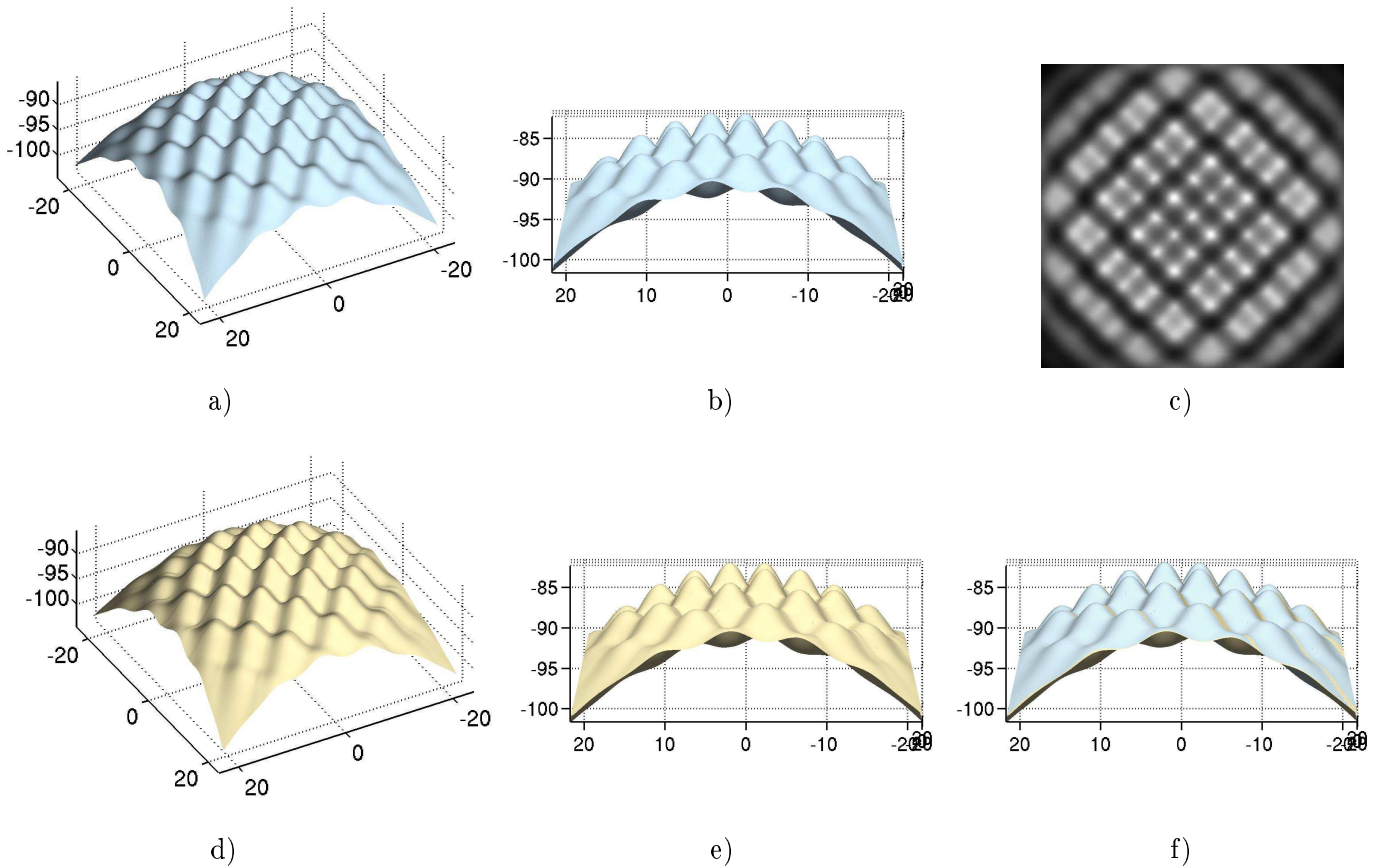
In the series of figures associated to these experiments (Figures 5.13, 5.14, 5.15, 5.16, 5.17), we show:

- in the first row, the reconstruction obtained without noise and with the exact input parameters, as a reference;
- in the other rows, some reconstructions obtained with corrupted images and/or with errors on some parameters;
- in the first column, the input images when they have been corrupted;
- in the second and third column, the reconstructed surfaces from two points of view.



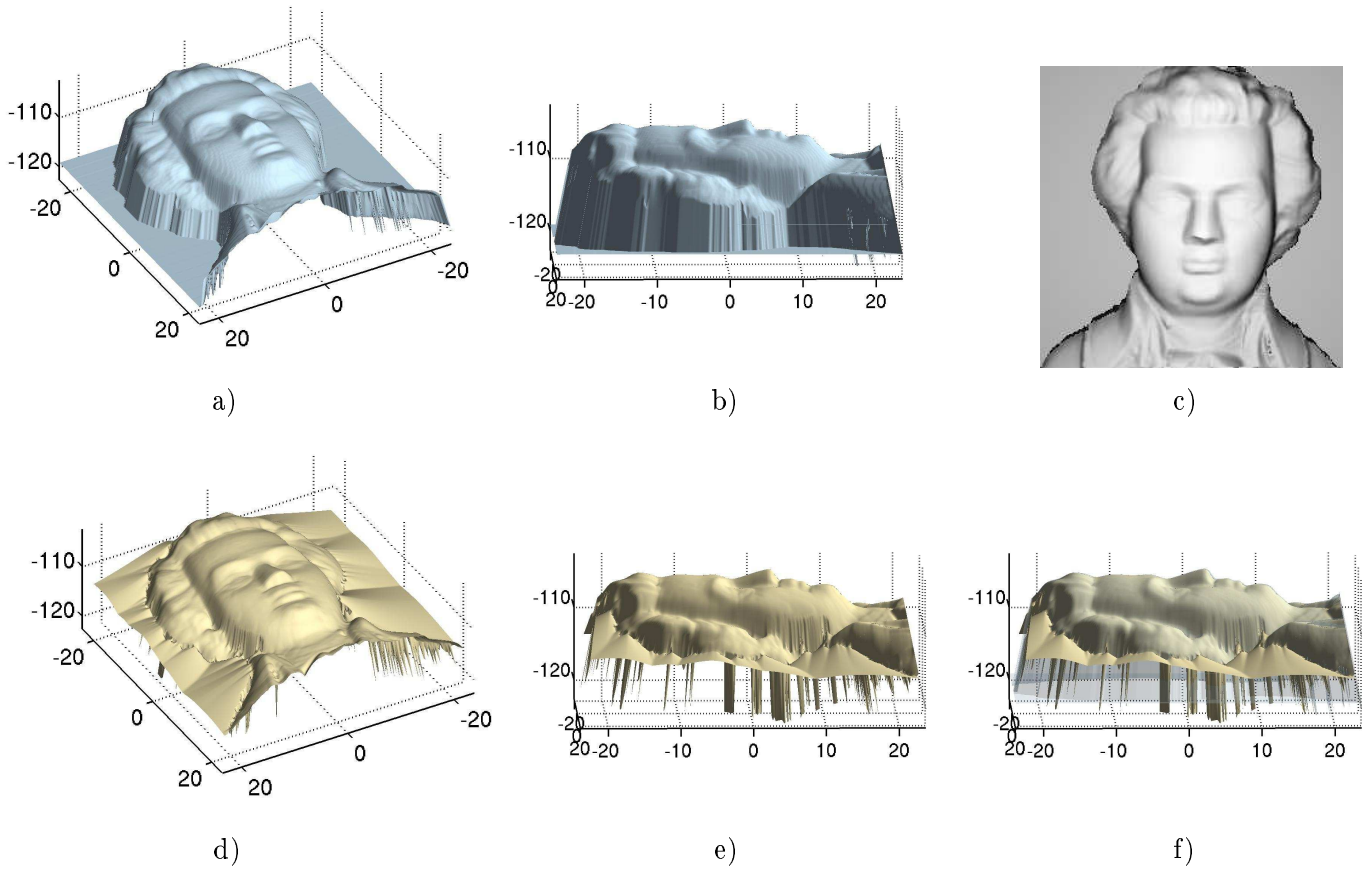
a) and b) original surface (groundtruth);
 c) image obtained from the original surface a): $f = 20mm$, $\text{size} = 300 \times 300$;
 d) and e) surface reconstructed from the image c): $n \simeq 65$, $\varepsilon_1 \simeq 0.00152397$,
 $\varepsilon_2 \simeq 0.0019405$, $\varepsilon_\infty \simeq 0.00655214$;
 f) superposition of the original surface (groundtruth) with the reconstructed surface (displayed in d) and e)).

Figure 5.5: Example of results for an image of a surface with several local minima: the “hill surface”.



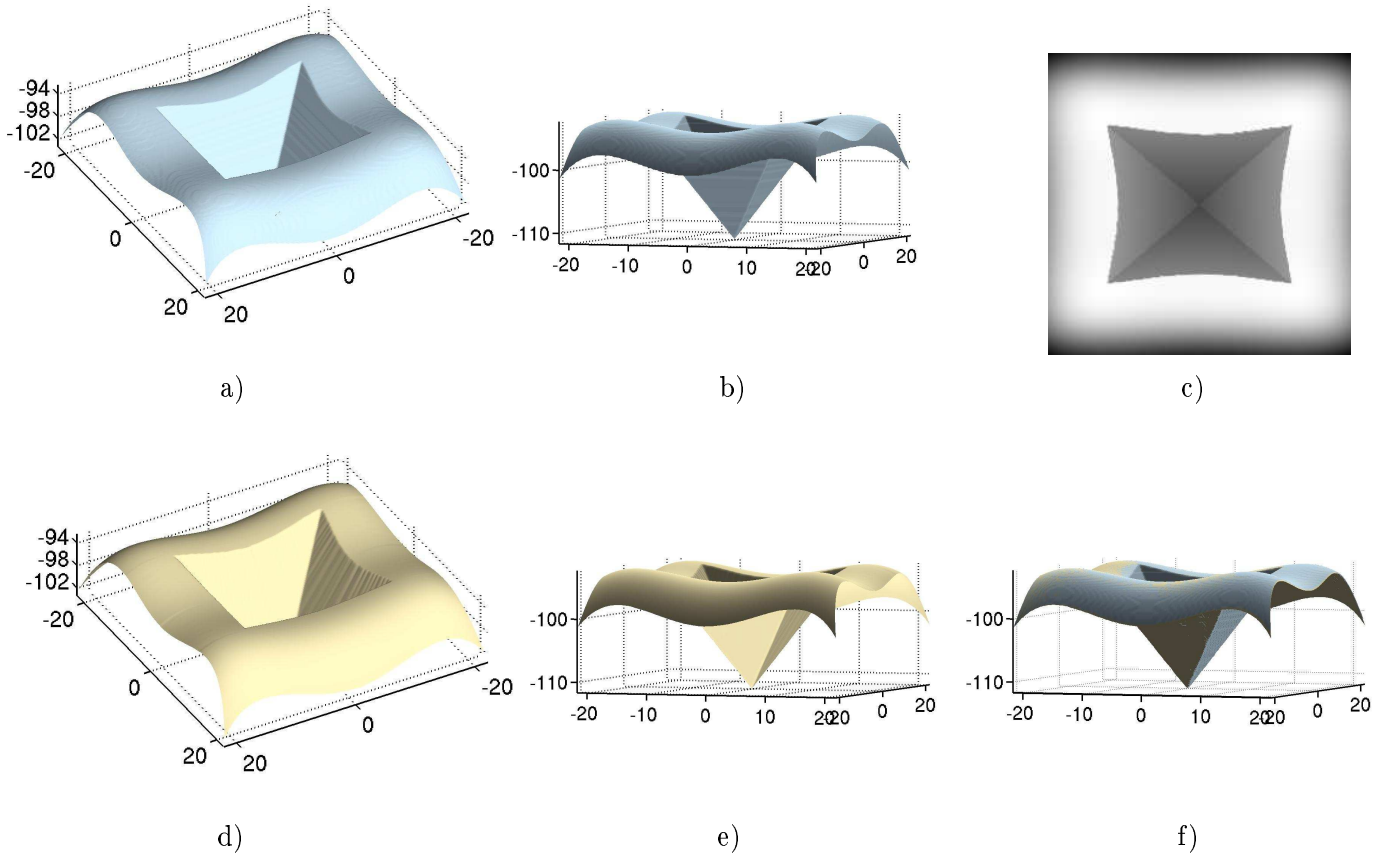
a) and b) original surface (groundtruth);
 c) image obtained from the original surface a): $f = 23mm$, size= 400×400 ;
 d) and e) surface reconstructed from the image c): $n \simeq 70$, $\varepsilon_1 \simeq 0.00136196$,
 $\varepsilon_2 \simeq 0.00170217$, $\varepsilon_\infty \simeq 0.00579273$;
 f) superposition of the original surface (groundtruth) with the reconstructed surface (displayed in d) and e)).

Figure 5.6: Example of results for the “field of bumps” image.



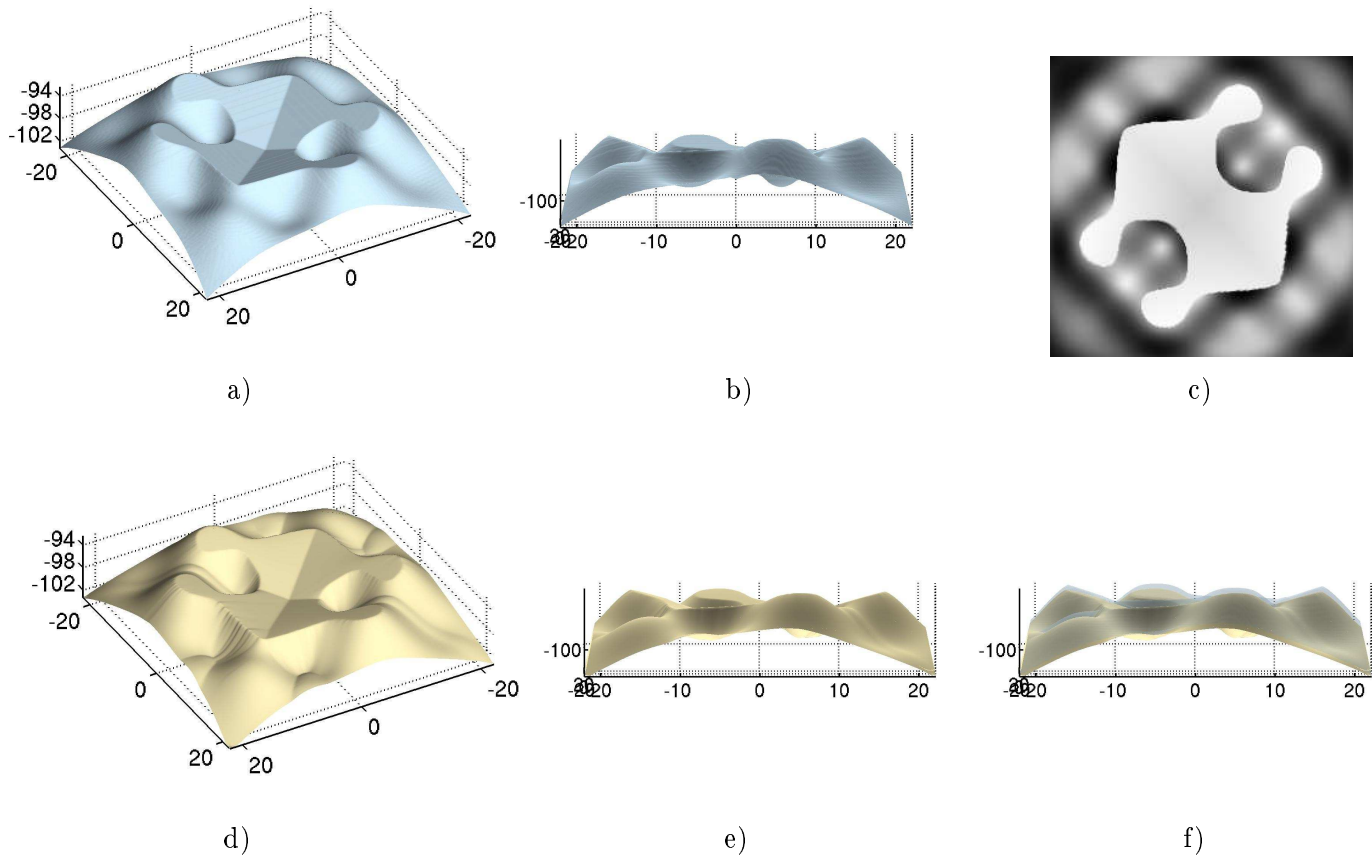
a) and b) original surface;
 c) image obtained from the original surface a): $f = 25mm$, $\text{size} = 250 \times 250$;
 d) and e) surface reconstructed from the image c): $n \simeq 50$, $\varepsilon_1 \simeq 0.0201287$,
 $\varepsilon_2 \simeq 0.0332239$, $\varepsilon_\infty \simeq 0.109705$;
 f) superposition of the original surface (groundtruth) with the reconstructed surface (displayed in d) and e)).

Figure 5.7: Result for the image of Mozart's face.



a) and b) original surface;
 c) image obtained from the original surface a): $f = 23mm$, size = 250×250 ;
 d) and e) surface reconstructed from the image c): $n \simeq 60$, $\varepsilon_1 \simeq 0.00098814$,
 $\varepsilon_2 \simeq 0.00139067$, $\varepsilon_\infty \simeq 0.0094318$;
 f) superposition of the original surface (groundtruth) with the reconstructed surface (displayed in d) and e)).

Figure 5.8: Result for an image containing discontinuities.



a) and b) original surface (groundtruth);
 c) image obtained from the original surface a): $f = 23mm$, $\text{size} = 250 \times 250$;
 d) and e) surface reconstructed from the image c): $n \simeq 85$, $\varepsilon_1 \simeq 0.00356152$,
 $\varepsilon_2 \simeq 0.00407986$, $\varepsilon_\infty \simeq 0.0265672$;
 f) superposition of the original surface (groundtruth) with the reconstructed surface (displayed in d) and e)).

Figure 5.9: Results for another image containing discontinuities.

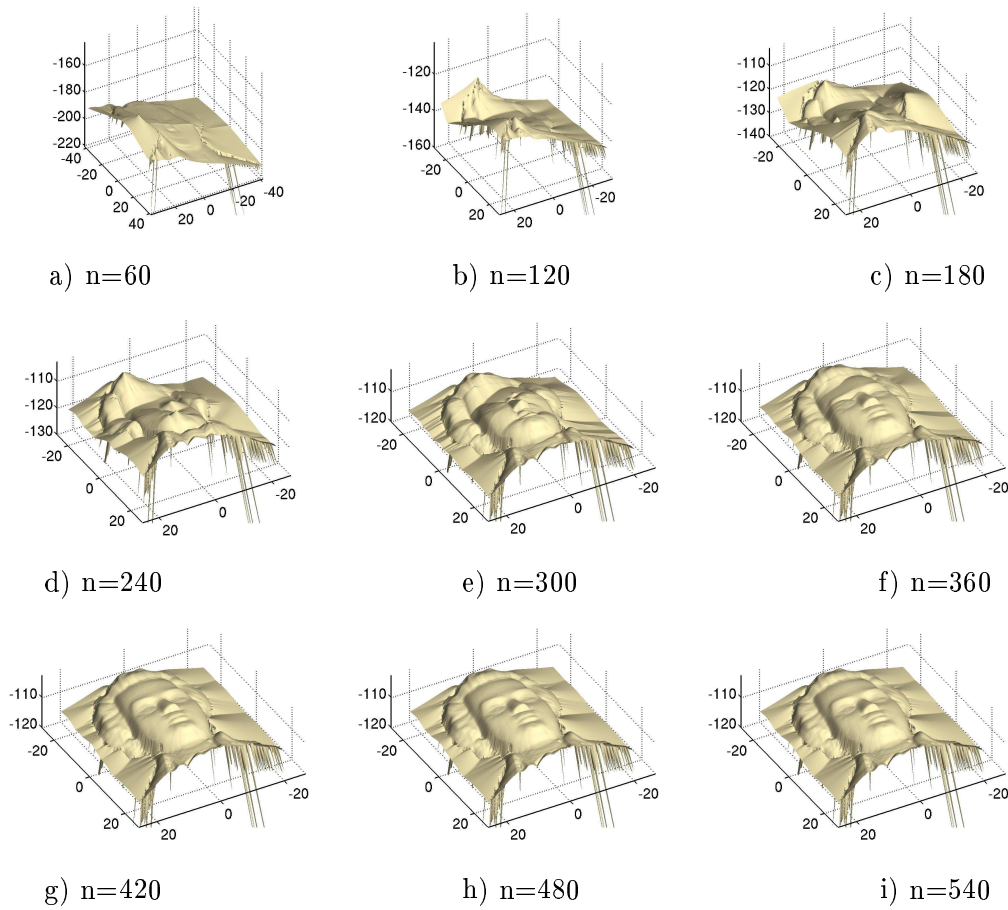


Figure 5.10: Evolution of the reconstructed surface for the image of Mozart's face, starting from the supersolution u_0 (for errors, see Table 5.1)

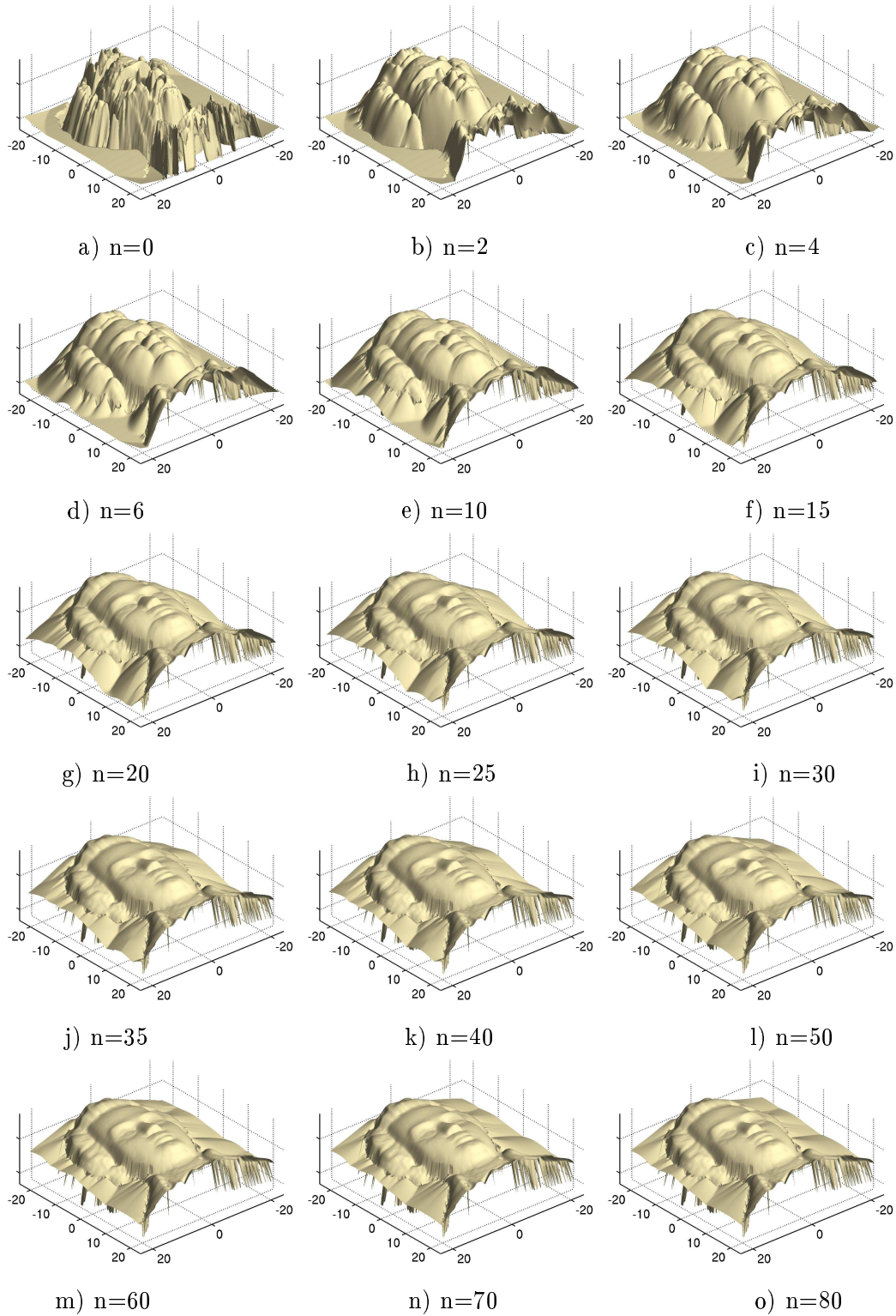


Figure 5.11: Evolution of the reconstructed surface for the image of Mozart's face, starting from the supersolution v_0 (for errors, see Table 5.2).

iteration (n)	ε_1 error	ε_2 error	ε_∞ error
0	0.0302943	0.0460551	0.180416
2	0.0220833	0.0312264	0.137289
4	0.0158622	0.0215666	0.124512
6	0.0133733	0.0177039	0.120779
10	0.0126053	0.0183098	0.111928
15	0.0133472	0.0213313	0.106305
20	0.0147987	0.0247051	0.108798
25	0.0165059	0.0277196	0.109686
30	0.0174543	0.0292335	0.109704
35	0.0185734	0.0309366	0.109705
40	0.0188836	0.0313961	0.109705
50	0.0201287	0.0332239	0.109705
60	0.0206475	0.0339851	0.109705
70	0.0208931	0.0343325	0.109705
80	0.0209713	0.0344363	0.109705

Table 5.2: Evolution of the errors associated to Figure 5.11: (Mozart's face) with the number of iterations, starting from the supersolution v_0 .

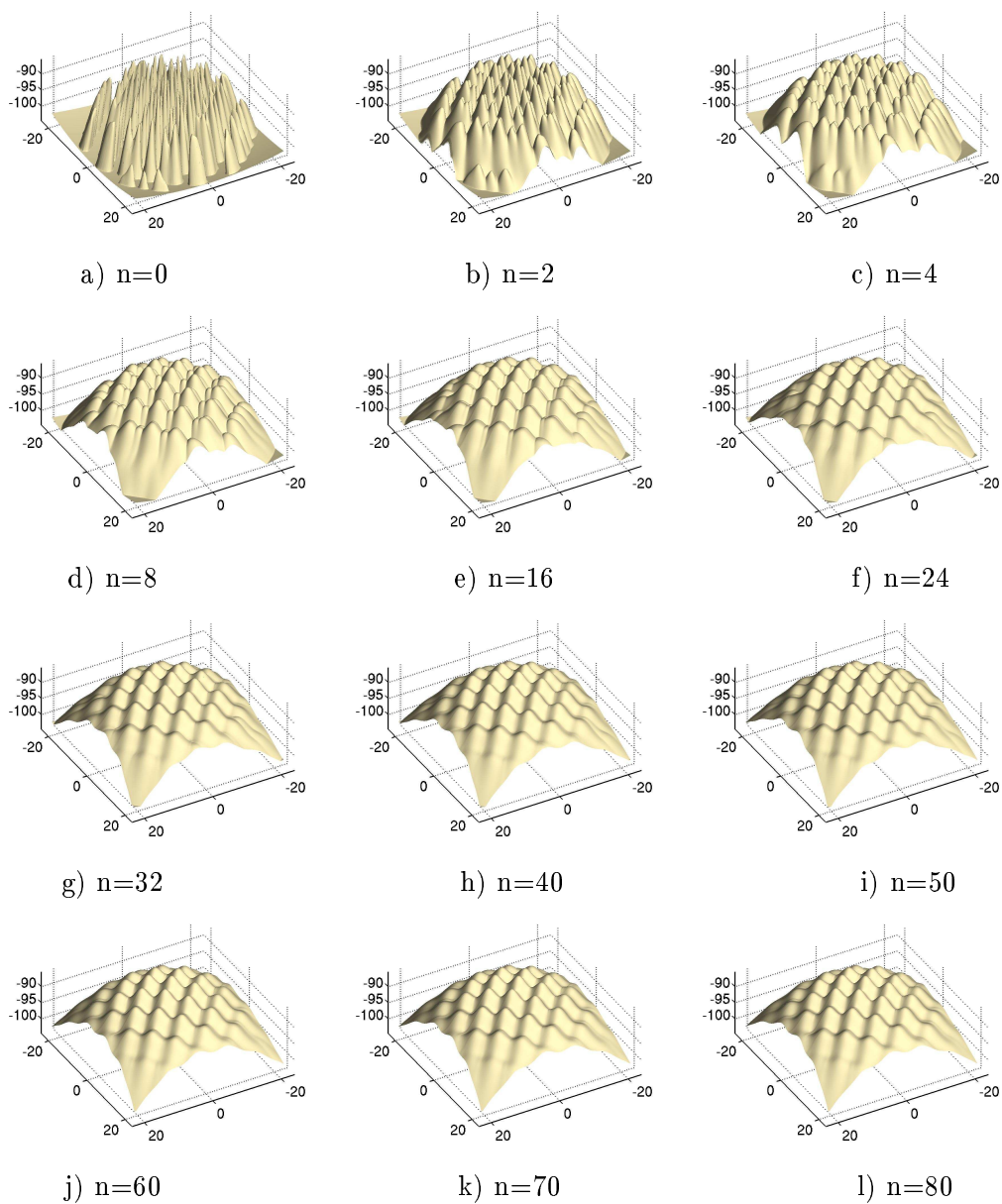


Figure 5.12: Evolution of the reconstructed surface from the image of the “field of bumps”, starting from the supersolution v_0 (for errors, see Table 5.3).

iteration (n)	ε_1 error	ε_2 error	ε_∞ error
0	0.00134159	0.00167079	0.00474082
2	0.042826	0.0488785	0.117484
4	0.0276274	0.033543	0.10354
8	0.0147751	0.0197772	0.0751836
16	0.00667883	0.0105963	0.0485785
24	0.0039321	0.00657979	0.0332412
32	0.00273465	0.00440412	0.0225997
40	0.00205176	0.00310148	0.0152853
50	0.00160707	0.00222596	0.0116531
60	0.00142766	0.00183524	0.00877063
70	0.00136196	0.00170217	0.00579273
80	0.00134347	0.00167312	0.00474082
90	0.00134163	0.00167086	0.00474082
100	0.00134159	0.00167079	0.00474082

Table 5.3: Evolution of the errors associated to Figure 5.12: (“field of bumps”) with the number of iterations, starting from the supersolution v_0 .

- in the last column, the superpositions of the reconstructed surface with the groundtruth.

We show the stability of our method with respect to five types of errors:

1. *image intensity errors due to noise.* Uniformly distributed white noise has been added to all pixels of the input images and the corresponding reconstructed surfaces are shown, see Figure 5.13. The Signal to Noise Ratio (SNR) is equal to 10.63, 5.32 and 2.65 in images Fig.5.13-e), Fig.5.13-i), and Fig.5.13-m), respectively. As seen from this figure, our algorithm is quite robust to intensity noise.
2. *gamma factor.* Most of the usual image acquisition devices do not have a linear intensity response. The actual response is usually well approximated by a power law, whose exponent is the gamma factor. If $\gamma = 1$ the response is linear. Typical values of γ range between 0.5 and 2.5. Figure 5.14 shows the reconstruction results when the algorithm is run on the original image raised to the power 0.5 and 2. The result corresponding to $\gamma = 0.5$ is flatter than the real surface whereas the form of the surface

reconstructed with $\gamma = 2$ if amplified. Let us note that even if quantitatively the numerical errors are important (due to the global and large deformation of the surface), these results are qualitatively very good.

3. *errors made on the parameters of the imaging system, on the calibration of the intensity of the light source and on the albedo of the surface.* As explained in section 5.1, these parameters are contained in the constant coefficient σ_2 of equation (5.6)

$$E_i = \sigma_2 \frac{\cos \theta_i}{r^2}.$$

Thus, for simulating errors on these parameters we distort the image by a linear transformation.

From the theoretical point of view, if we make an error on the σ_2 parameter, the input image is therefore $I_\lambda = \lambda I$ instead of I (where $\lambda = \frac{\sigma_2}{\sigma_\varepsilon} > 0$ and where σ_ε is the distorted parameter). Also, the algorithms compute some approximations of the solution of equation

$$-u(x)^{-2} + I_\lambda(x) f^2 \frac{\sqrt{[f^2 |\nabla u(x)|^2 + (\nabla u(x) \cdot x)^2]/Q(x)^2 + u(x)^2}}{u(x)} = 0 \quad (5.34)$$

instead of equation (5.11).

Let u the viscosity solution of (5.11) (with state constraints). Clearly, u is the solution of equation (with state constraints)

$$-\lambda u(x)^{-2} + \lambda I f^2 \frac{\sqrt{[f^2 |\frac{\nabla u(x)}{\sqrt{\lambda}}|^2 + (\frac{\nabla u(x)}{\sqrt{\lambda}} \cdot x)^2]/Q(x)^2 + \left(\frac{u(x)}{\sqrt{\lambda}}\right)^2}}{\frac{u(x)}{\sqrt{\lambda}}} = 0;$$

so it is the solution of equation (with state constraints)

$$-\left(\frac{u(x)}{\sqrt{\lambda}}\right)^{-2} + I_\lambda f^2 \frac{\sqrt{[f^2 |\frac{\nabla u(x)}{\sqrt{\lambda}}|^2 + (\frac{\nabla u(x)}{\sqrt{\lambda}} \cdot x)^2]/Q(x)^2 + \left(\frac{u(x)}{\sqrt{\lambda}}\right)^2}}{\frac{u(x)}{\sqrt{\lambda}}} = 0.$$

By proposition 2.1 (change of unknown), $u_\lambda = \frac{u(x)}{\sqrt{\lambda}}$ is the viscosity solution of equation²⁷ (5.34). In other words, errors on the σ_2 parameter just involve changes of scale.

In practice, the experiments confirm this theoretical remark. Figure 5.15 shows two examples of reconstructions with such distortions. The intensities I_λ of the images Fig.5.15-e) and Fig.5.15-i) correspond to $1.2I$ and $0.8I$, where I is the intensity of the original image Fig.5.15-a). Of course, due to these changes of scale, the absolute errors $\varepsilon_1, \varepsilon_2, \varepsilon_\infty$.

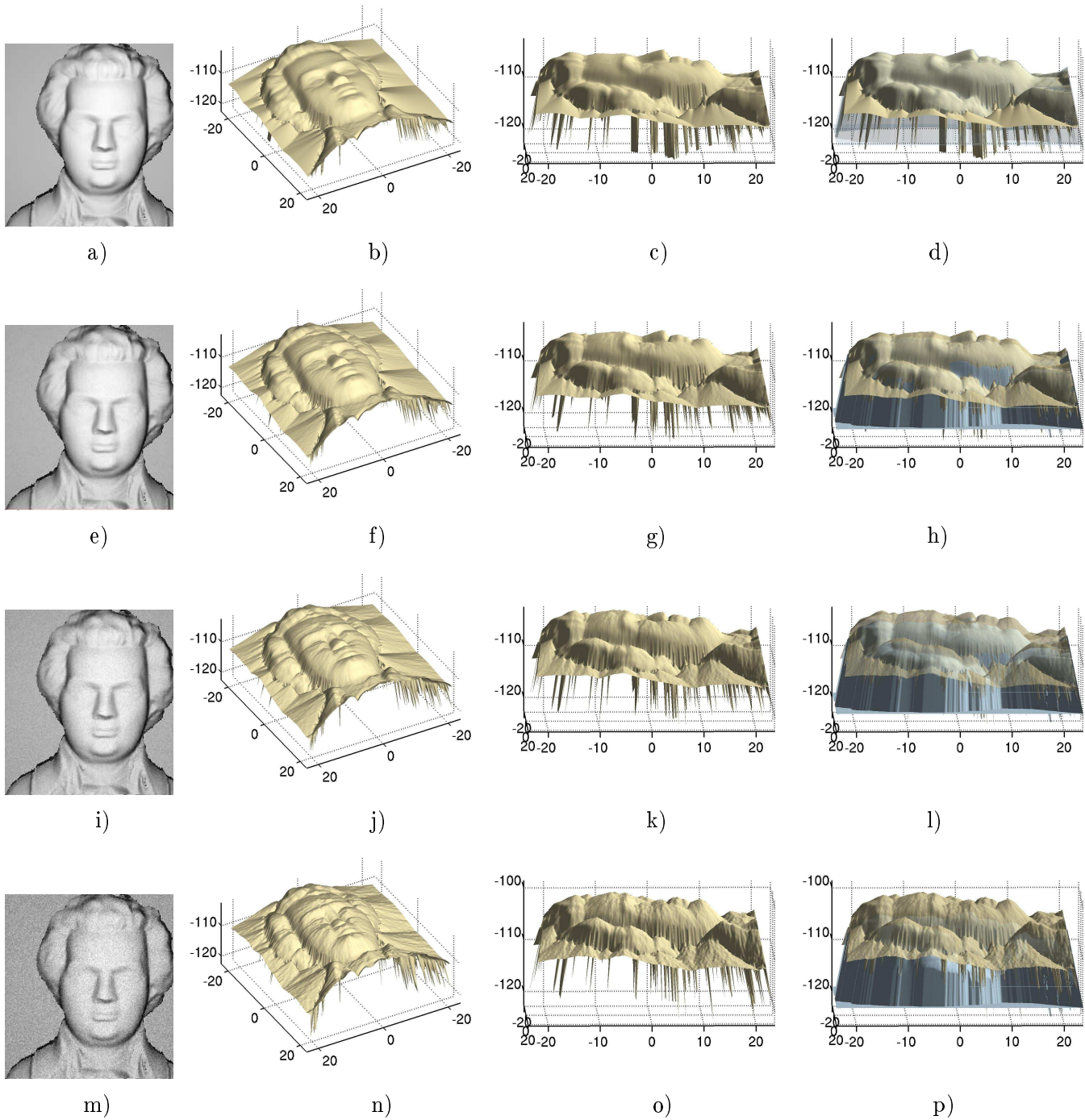
²⁷With state constraints.

image	noise/SNR	iteration	ε_1 error	ε_2 error	ε_∞ error
Fig.5.13-e)	10.63	$\simeq 50$	0.0266365	0.0386745	0.574023
Fig.5.13-i)	5.32	$\simeq 50$	0.0358871	0.0450536	0.569604
Fig.5.13-m)	2.65	$\simeq 50$	0.0554078	0.0612147	0.560532

Table 5.4: Errors associated to Figure 5.13 for the noisy images of Mozart's face.

4. *incorrect estimation of the focal length f* of the camera. We show in Figure 5.16 that errors of $10mm$ (40%) on the focal length parameter f do not affect much the reconstructed surface. The image used in these experiments is the image Fig.5.7-c). The focal length used for synthesizing this image is $f = 25mm$. The last two rows of Figure 5.16, show the reconstructions for $f_\varepsilon = 15mm$ and $f_\varepsilon = 35mm$.
5. *modeling errors*. In practice with real images, the *light source is never located exactly at the optical center*. For example when we use a camera equipped with a flash (situation corresponding quite nicely to the modeling hypotheses), the light source is generally located at several centimeters from the optical center. Note nevertheless that the distance between the flash and the optical center is usually inferior to $10cm$. For testing the robustness of our method to this kind of errors, we have synthesized a series of images of Mozart's face with the light source located at $10cm$ and $20cm$, above, under, to the right and to the left of the optical center, see Figure 5.18. In Figures 5.19 and 5.20, we show the reconstructions obtained from these images. In Fig.5.19 we display the reconstructed surfaces from a frontal point of view; in Fig.5.20 we display the same surfaces from the side. As the reader can see, in all cases, the reconstructed surfaces are very good when the the light source is located at $10 cm$. When the light source is located at $20 cm$, the distortions are more important, but the results are still quite good. In Figures 5.18, 5.19 and 5.20 \mathbf{P}_L is the position of the light source in the coordinate system of the scene. Let us recall that the optical center is located at $O = (0, 0, 0)$.

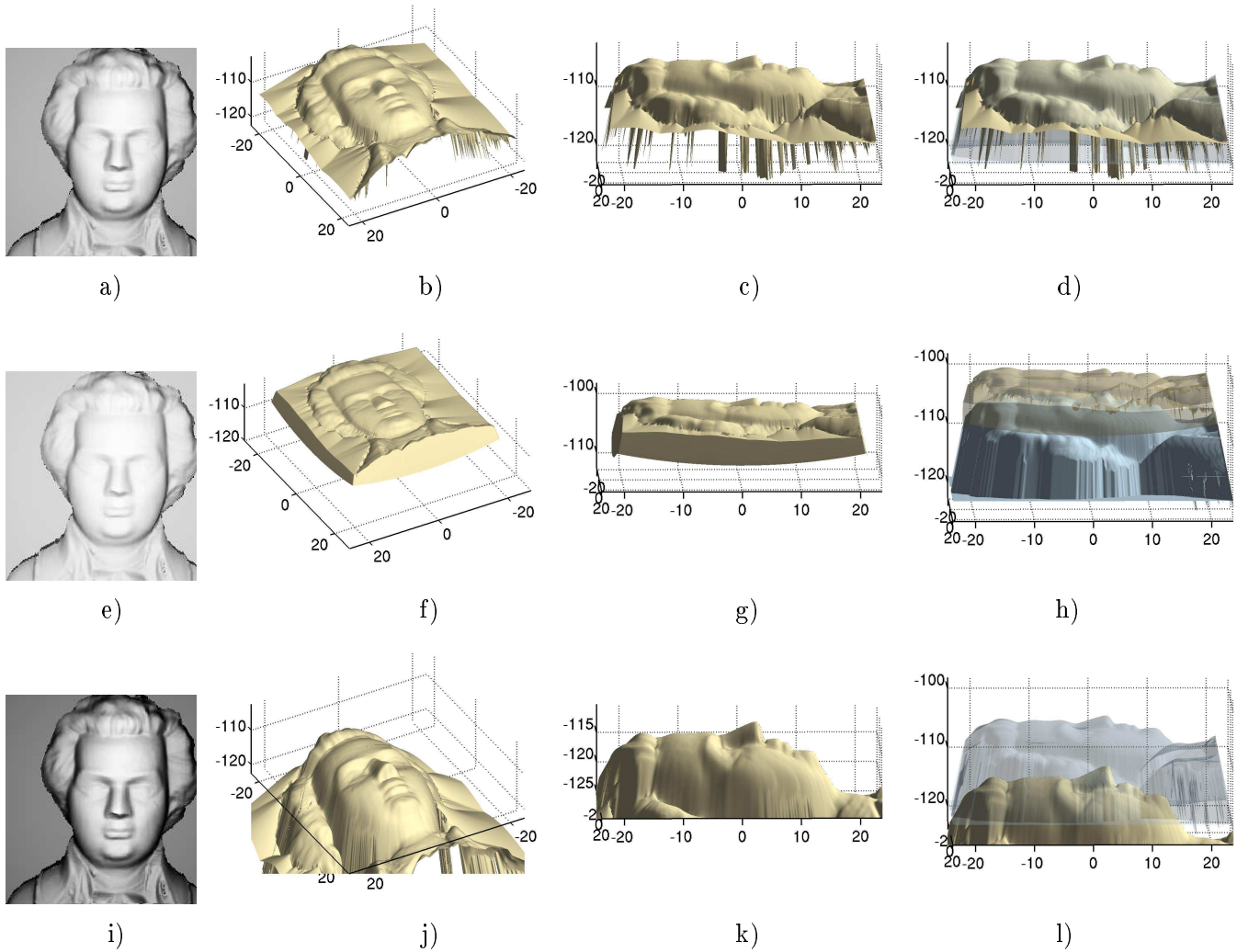
In Figure 5.17, we display the results for some images of Mozart's face corrupted by *pixel noise*, *gamma corrections*, *albedo errors*, and obtained with the *wrong focal length f* . In addition to the accumulation effect, let us note that the errors imposed are quite important. Surprisingly, the algorithm produces relatively satisfying results given the large difference between the original image and the input images.



a) original image; b) and c) surface reconstructed from image a);
 e) noisy image with a $SNR = 10.63$; f) and g) surface reconstructed from image e);
 i) noisy image with a $SNR = 5.32$; j) and k) surface reconstructed from image i);
 m) noisy image with a $SNR = 2.65$; n) and o) surface reconstructed from image m);
 In the last column, we display the superpositions of the reconstructed surfaces with
 the groundtruth.

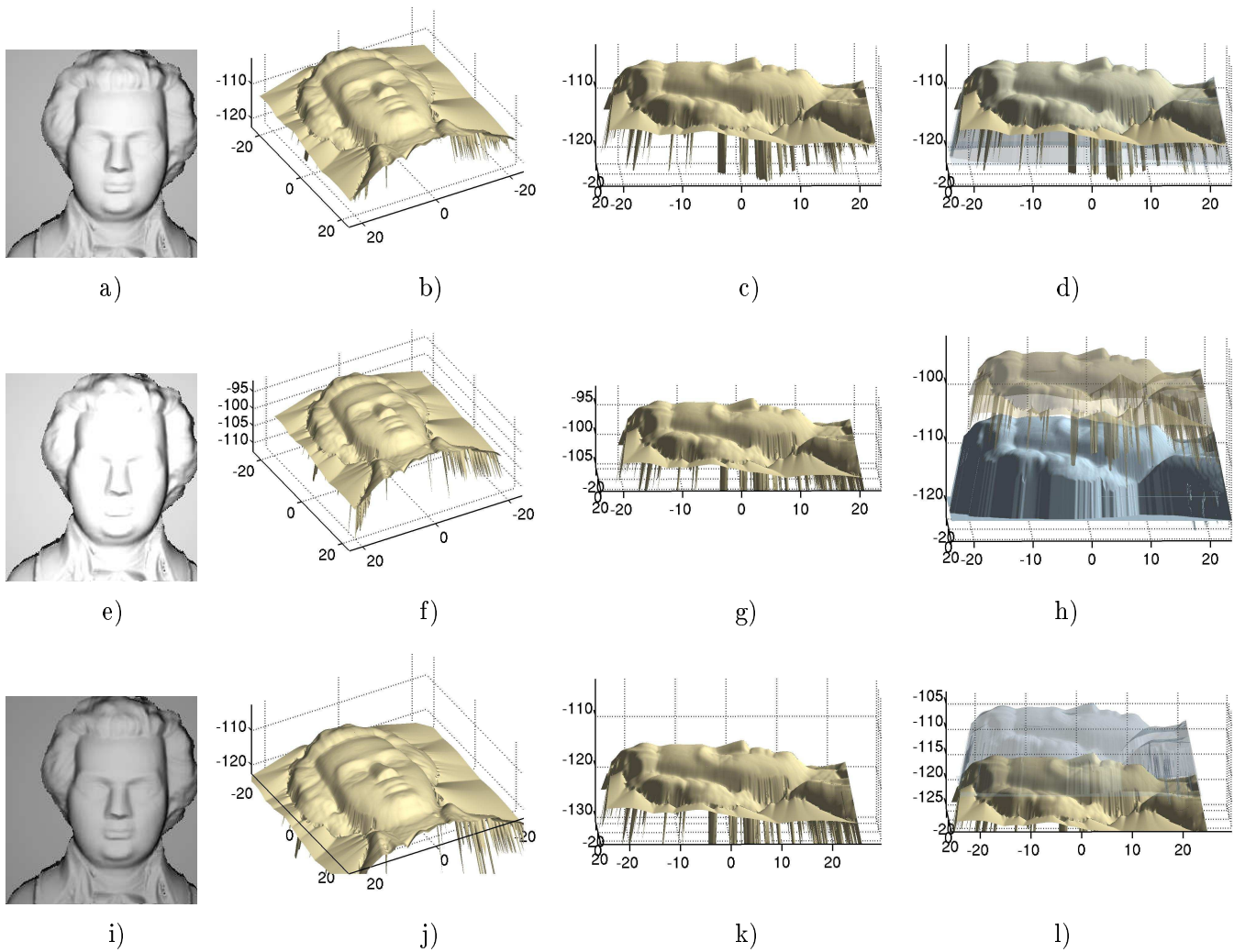
For errors, see Table 5.4.

Figure 5.13: Results for the noisy images of Mozart's face.



a) original image; b) and c) surface reconstructed from image a);
 e) image distorted with $\gamma = 0.5$ ($I_\varepsilon = \sqrt{I}$);
 f) and g) surface reconstructed from image e): $n \simeq 45$, $\varepsilon_1 \simeq 0.0559719$,
 $\varepsilon_2 \simeq 0.0568014$, $\varepsilon_\infty \simeq 0.079711$;
 i) image distorted with $\gamma = 2$ ($I_\varepsilon = I^2$);
 j) and k) surface reconstructed from image i): $n \simeq 50$, $\varepsilon_1 \simeq 0.126682$,
 $\varepsilon_2 \simeq 0.146416$, $\varepsilon_\infty \simeq 3.60861$;
 In the last column, we display the superpositions of the reconstructed surfaces
 with the groundtruth.

Figure 5.14: Results for the images of Mozart face distorted by *gamma distortions* $\gamma = 0.5$ and $\gamma = 2$, i.e. instead of the real image I we used \sqrt{I} and I^2 .



a) original image; b) and c) surface reconstructed from image a) with the correct constant coefficient σ ;

e) distorted image $I_\varepsilon = 1.2I$; f) and g) surface reconstructed from image e);

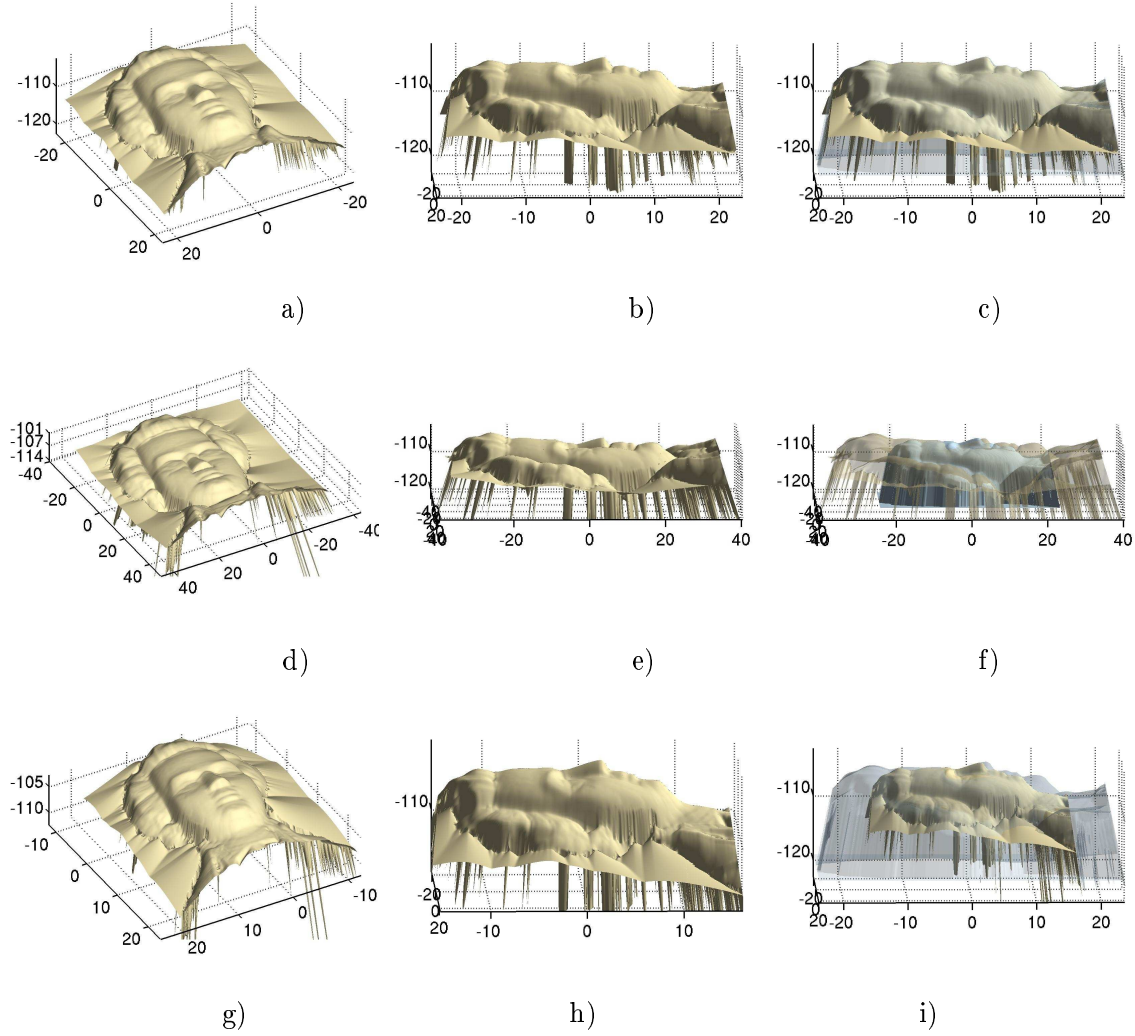
$n \simeq 40$, $\varepsilon_1 \simeq 0.0719292$, $\varepsilon_2 \simeq 0.077584$, $\varepsilon_\infty \simeq 0.668079$;

i) distorted image $I_\varepsilon = 0.8I$; j) and k) surface reconstructed from image i);

$n \simeq 50$, $\varepsilon_1 \simeq 0.130974$, $\varepsilon_2 \simeq 0.134119$, $\varepsilon_\infty \simeq 0.46533$;

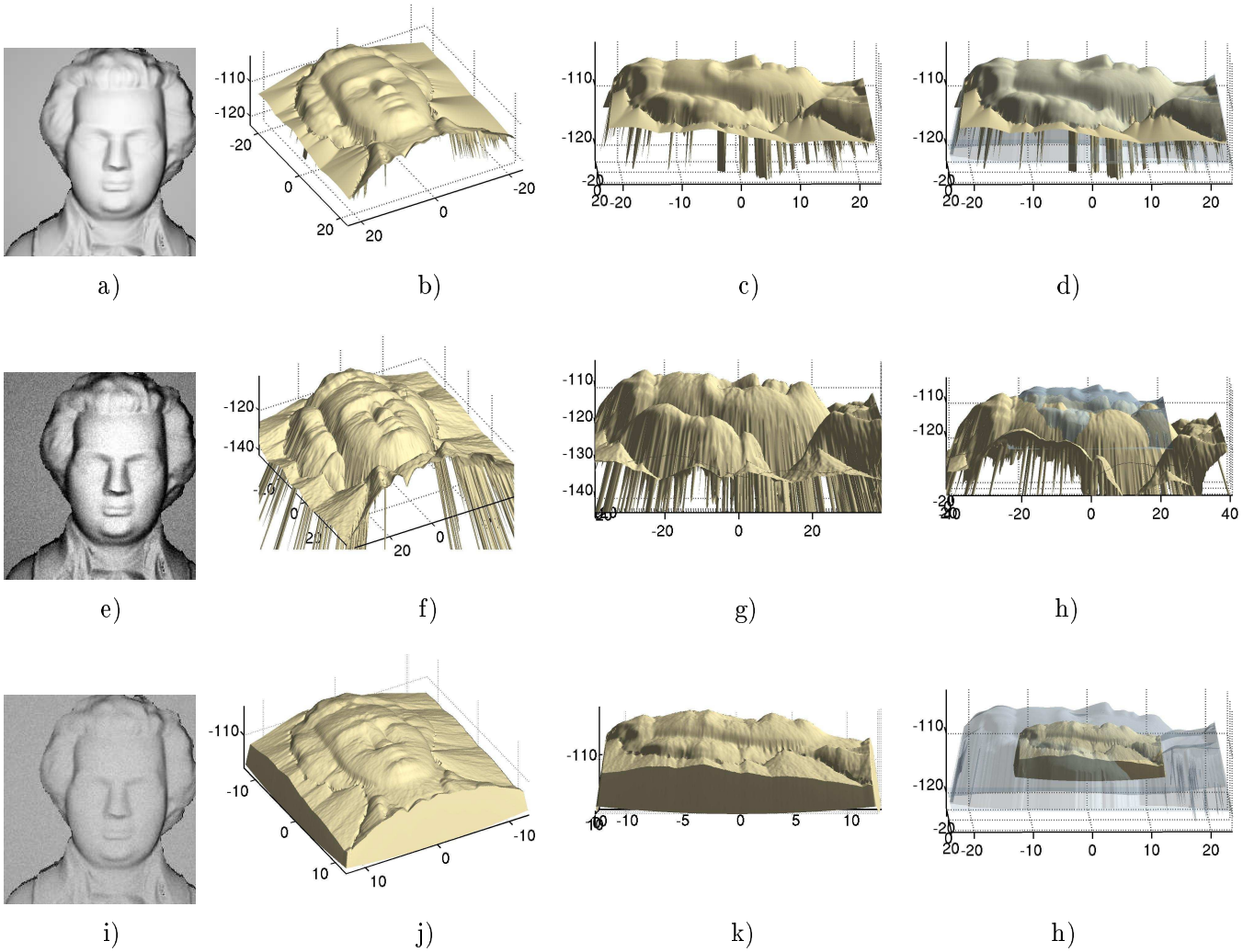
In the last column, we display the superpositions of the reconstructed surfaces with the ground truth.

Figure 5.15: Results for the images of Mozart's face distorted by some *intensity scaling* corresponding to a *distortion of the constant coefficient σ* (this contains the *albedo* distortion).



a) and b) surface reconstructed from image Fig.5.7-c) with the correct focal length parameter $f = 25mm$;
 $n \simeq 54$, $\varepsilon_1 \simeq 0.0213$, $\varepsilon_2 \simeq 0.0350$, $\varepsilon_\infty \simeq 0.577$;
 c) and d) surface reconstructed from image Fig.5.7-c) with the distorted focal length parameter $f_\varepsilon = 15mm$;
 $n \simeq 45$, $\varepsilon_1 \simeq 0.507348$, $\varepsilon_2 \simeq 0.507873$, $\varepsilon_\infty \simeq 1.22922$;
 e) and f) surface reconstructed from image Fig.5.7-c) with the distorted focal length parameter $f_\varepsilon = 35mm$;
 $n \simeq 60$, $\varepsilon_1 \simeq 0.369157$, $\varepsilon_2 \simeq 0.370821$, $\varepsilon_\infty \simeq 0.457924$;
 In the last column, we display the superposition of the reconstructed surface with the groundtruth.

Figure 5.16: Results obtained from Mozart's face image with *distorted focal length parameter* f .



a) original image; b) to d) surface reconstructed from image a) with all the correct parameters;

e) image a) distorted by noise with a SNR equal to 4.04, by a gamma distortion $\gamma = 2$ and by an albedo distortion $\sigma_\epsilon = 1.2\sigma$;

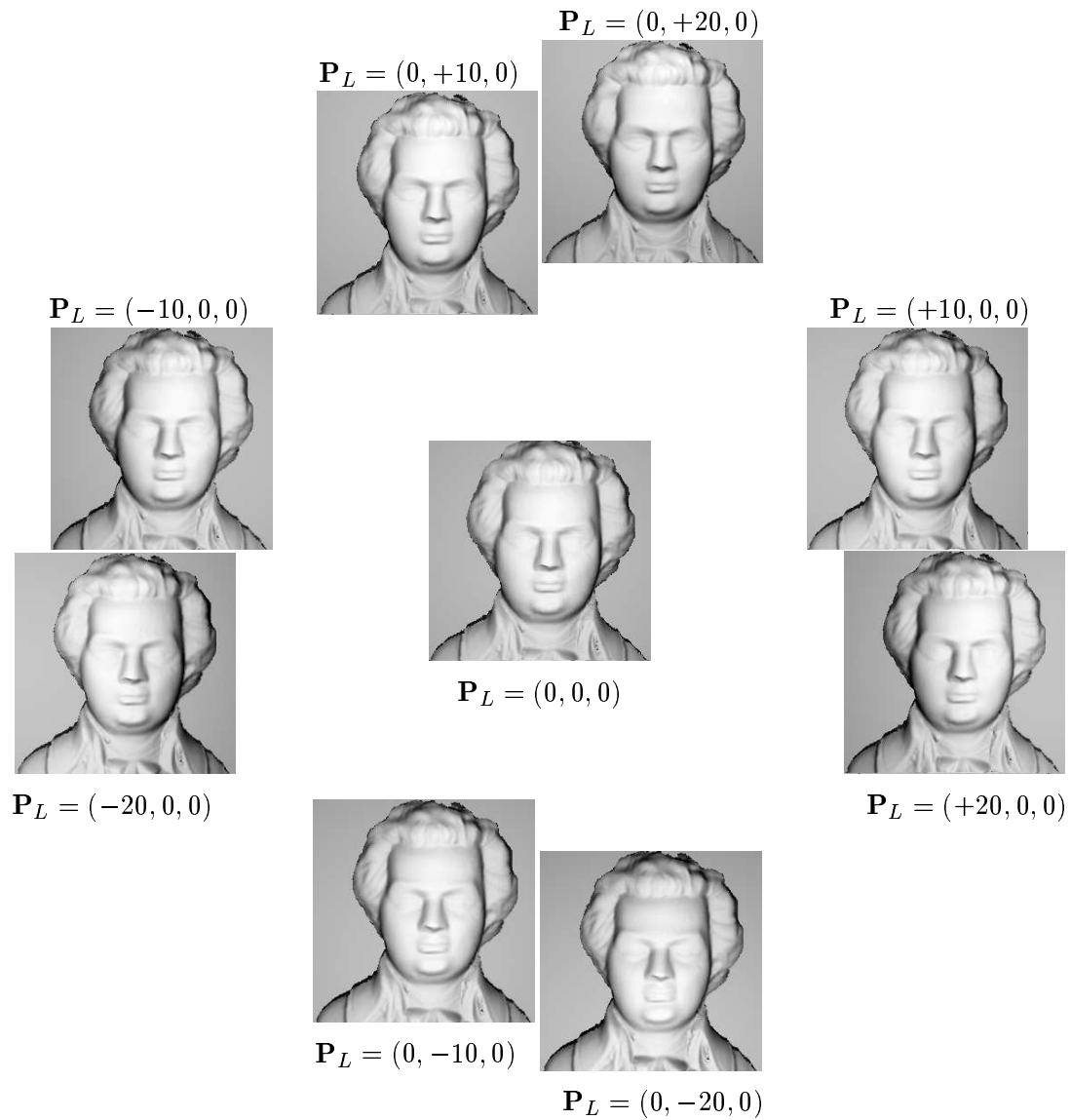
f) to h) surface reconstructed from image e) with a wrong focal length parameter $f_\epsilon = 15mm$ (the correct parameter is $f = 25mm$): $n \simeq 40$, $\epsilon_1 \simeq 0.610511$, $\epsilon_2 \simeq 0.61432$, $\epsilon_\infty \simeq 4.2899$;

i) image a) corrupted by noise with a SNR equal to 3.36, by a gamma distortion $\gamma = 0.5$ and by an albedo distortion $\sigma_\epsilon = 0.8\sigma$;

j) to l) surface reconstructed from image i) with a wrong focal length parameter $f_\epsilon = 45mm$: $n \simeq 50$, $\epsilon_1 \simeq 0.5105$, $\epsilon_2 \simeq 0.5432$, $\epsilon_\infty \simeq 2.2899$.

In the last column, we display the superpositions of the reconstructed surfaces with the groundtruth.

Figure 5.17: Results for the image of Mozart's face distorted by *pixel noise*, by *gamma γ distortions*, by *albedo σ errors*, and with a *wrong focal length f* .



\mathbf{P}_L is the position of the light source in the coordinate system of the scene. The optical center is located at $O = (0, 0, 0)$.

Figure 5.18: Images of Mozart's face with the light source located at 10cm or 20cm, above, under, to the right or to the left of the optical center.

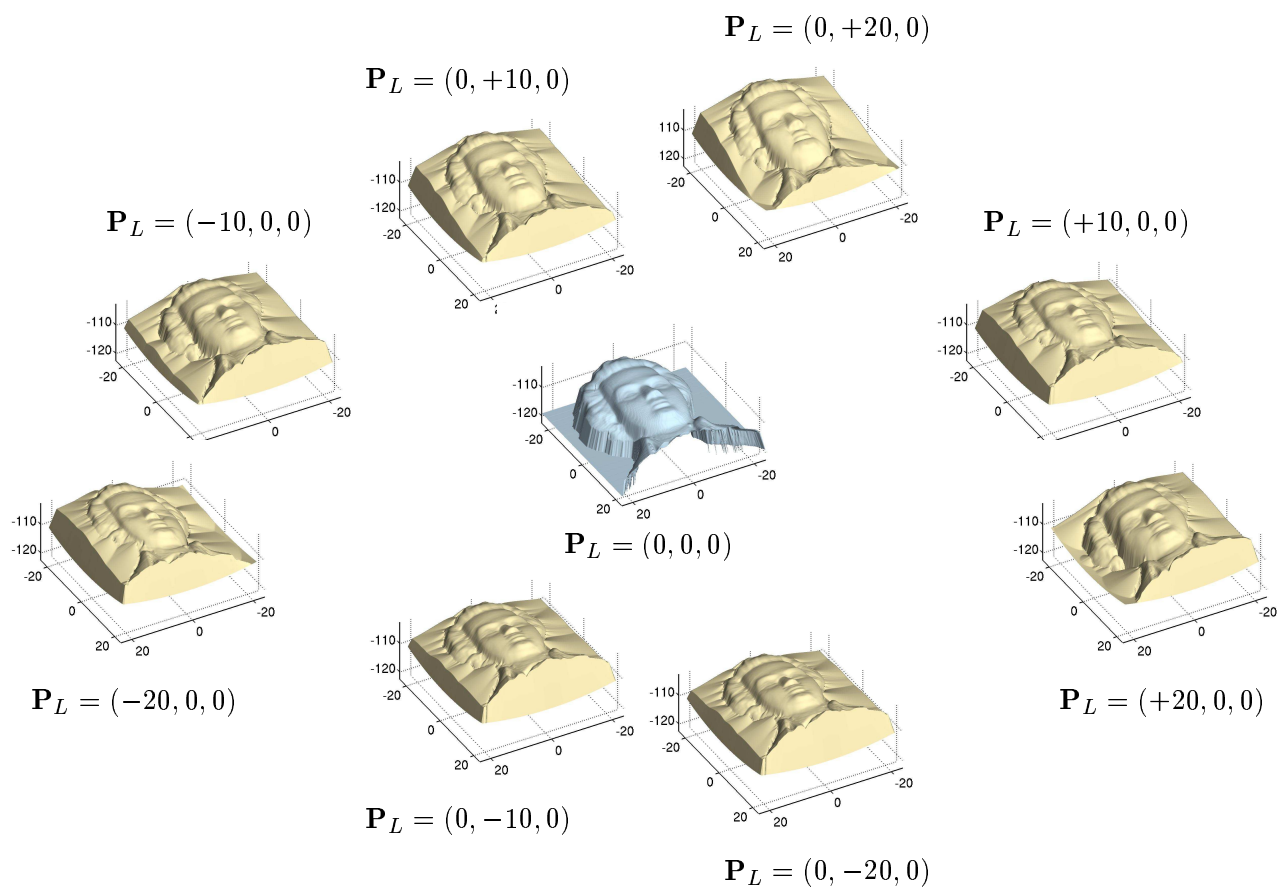


Figure 5.19: Reconstructed surfaces from the images of Mozart's face with the light source located at 10cm or 20cm, above, under, to the right or to the left of the optical center; these images are displayed in figure 5.18.

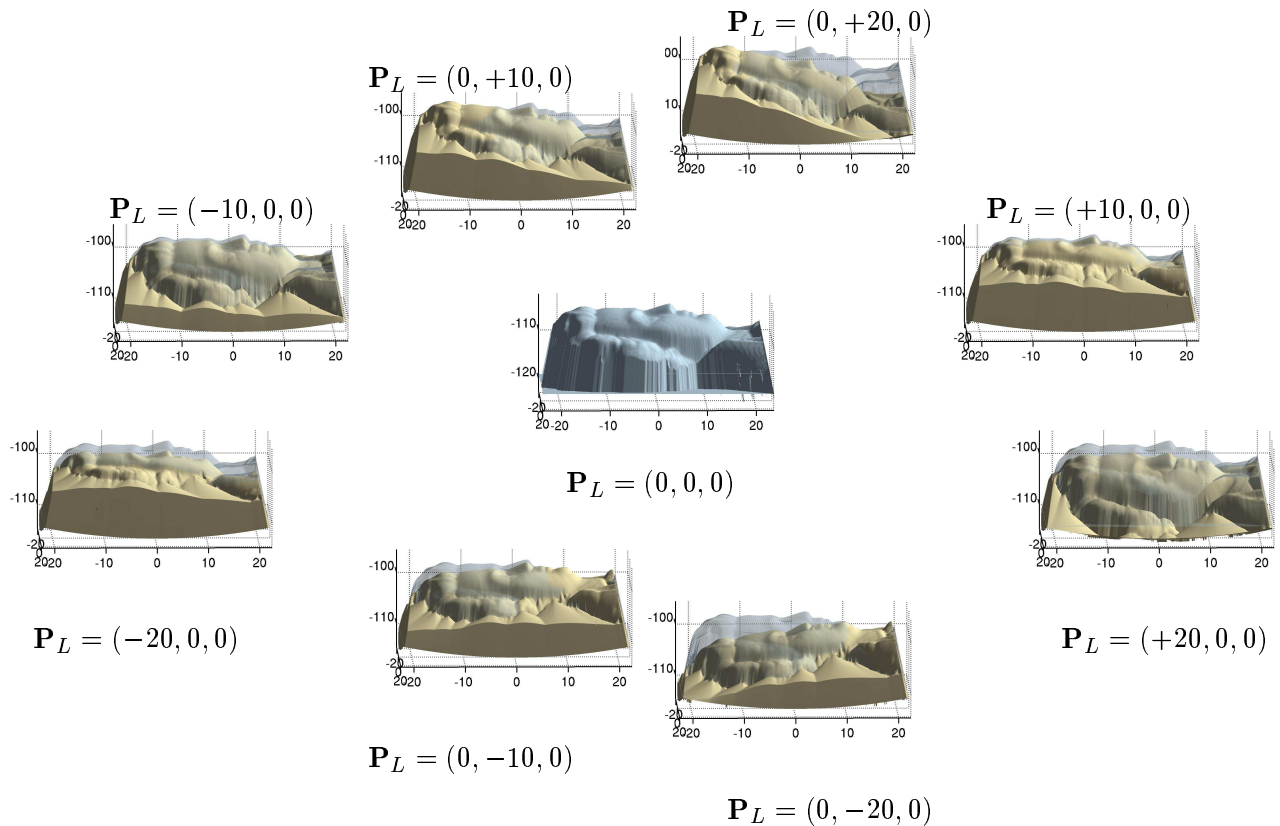


Figure 5.20: Reconstructed surfaces from the images of Mozart's face (side view) with the light source located at 10cm or 20cm, above, under, to the right or to the left of the optical center; these images are displayed in figure 5.18.

5.5.2 Experimental results on real images

In this section we show some examples of reconstructions with *real images*. We have constructed a small database of real images of faces verifying approximately our modeling assumptions. A sample of this database is shown in Figure 5.25. This database is available online from:

<http://www-sop.inria.fr/odyssee/team/Emmanuel.Prados/index.en.html>

For generating this data base, we have used the same cheap digital camera as for the experiments of section 4.7 (the Pentax Optio 330GS). So the size of the pixels of the images provided by the camera is approximately $0.0045 \times 0.0045 \text{ mm}^2$ (CCD size = $1/2.7''$). For reducing the pixel noise and the computation time, we have resized the images. The original images contain 2048×1536 pixels. The reduced images contain 512×384 pixels. After resizing, the size of the pixels is estimated to $0.018 \times 0.018 \text{ mm}^2$. For all these images, the focal length was fixed to 5.8 mm. The photos have been taken in an approximately dark place.

In our experiments, we need to fix the parameter σ_2 introduced in equation (5.6)

$$E_i = \sigma_2 \frac{\cos \theta_i}{r^2}$$

(see page 202). In these tests we have chosen to fix $\sigma_2 = 1000$. In the previous section, we have proved that a modification of the constant σ_2 involves a change of scale in the reconstruction. Figure 5.24 illustrates this. In this figure, to the right of each reconstructed surface, we show (in blue) the value of the σ_2 constant used. Note that the values on the axes of the figures are in centimeters. Contrary to section 4.7 (or [122, 117]), we do not have modified the gamma parameter of the image (we have fixed $\gamma = 1$).

Our modeling of the problem assumes that the scene is lambertian and the albedo is constant. Here, these hypotheses do not hold. For example, the albedo of the eyes is not the same as the albedo of the skin. Moreover it is not constant. Since the iris is very dark, they do not cause difficulties (they only have local effects). At the opposite, the white parts of the eyes can produce important peaks in the reconstruction (mathematically, we see that the surface is pulled up by the pixels with high intensity). To remove this problem, we have painted manually²⁸ the eyes, see Figure 5.21, for an example of reconstructions from an image with or without eye inpainting. Figures 5.22 and 5.23 show the same surface as Figure 5.21-d) from various points of view and with two

²⁸This step can be done automatically for example by matching the image to a model image already segmented. An example of a matching method is the robust multi-modal and non-rigid technique proposed by Hermosillo and Faugeras in [62].

different illuminations. Figure 5.26 displays the reconstructed surfaces from the images of Figure 5.25 (after having inpainted eyes); the photos and the associated reconstructions are ordered the same way. Figure 5.27 focuses on the results returned from the images Fig.5.26-k) and Fig.5.26-l). Note that these two images are very difficult to deal with. To our knowledge, none of the other SFS methods is able to return such results as ours...

In many of the reconstructions, one can see the appearance of peaks on the lips and on the forehead. These peaks are due to the highlights (the surfaces are clearly not Lambertian): contrary to the methods we have presented in the previous chapters (see section 4.7), this one seems fairly sensitive to highlights. Note methods allowing to automatically remove the highlights are available in the literature, e.g. the work of Ragheb and Hancock [129] and that of Tan et al. [151] (We have not tested these methods). We have also noticed that our new method can be fairly sensitive to salt and pepper noise. More precisely to “salt pixels” (but not to “pepper pixels”). In order to decrease this effect, we have first reduced the size of the images ($2048 \times 1536 \rightarrow 512 \times 384$ pixels) and processed it with a simple filter reducing the “salt” effects.

In spite of these small defects, the results are quite satisfying and, to our knowledge, much better than those obtained by any of the previous SFS methods.

Let us mention that for all the images of Figure 5.25, the number of iterations required for recovering the surfaces of Figure 5.26 is inferior to 80.

To close this section, let us emphasize again that contrary to the experiments of section 4.7 which were also performed on a real image of a face, we do not need to fix the height of the singular point²⁹ on the nose anymore. In section 4.7 is not a height datum; it is position datum. In effect, in section 4.7, we need to know the very important prior that the tip of the nose is the point of the surface which is the closest to the optical center of camera. In the experiments of this chapter, besides the intensity image, we do not use additional data except the intrinsic parameters of the camera (focal length and size of pixels) and photometric calibration (σ_2 constant).

²⁹Let us recall that at the opposite of the framework of section 4.7, in our new and more realistic framework, the notion of singular points does not have sense anymore.

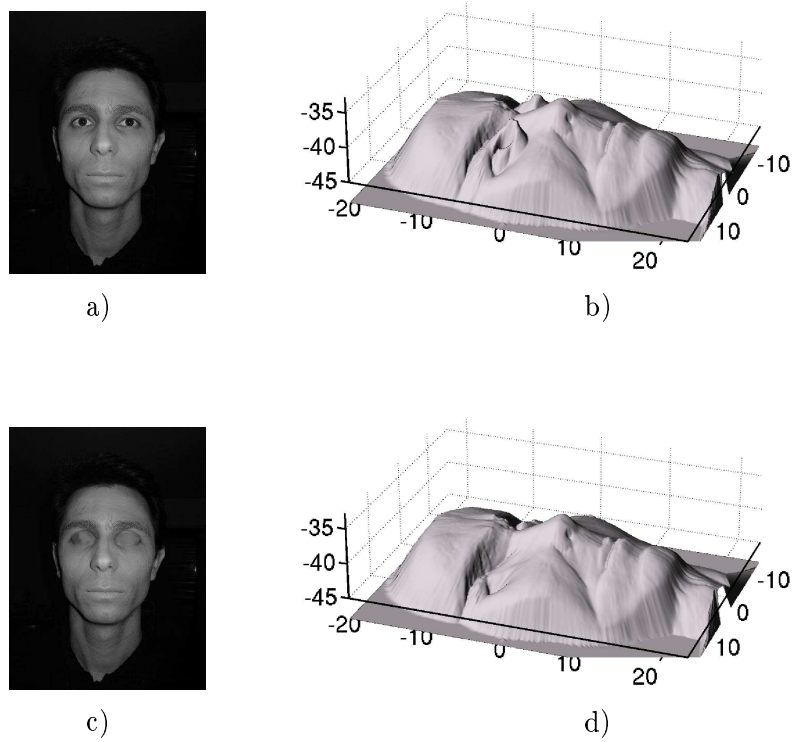


Figure 5.21: Example of reconstructions with or without eyes.

- a) Original photo (512×384), b) surface reconstructed from a);
c) photo a) after we have painted the eyes, d) surface reconstructed from c).

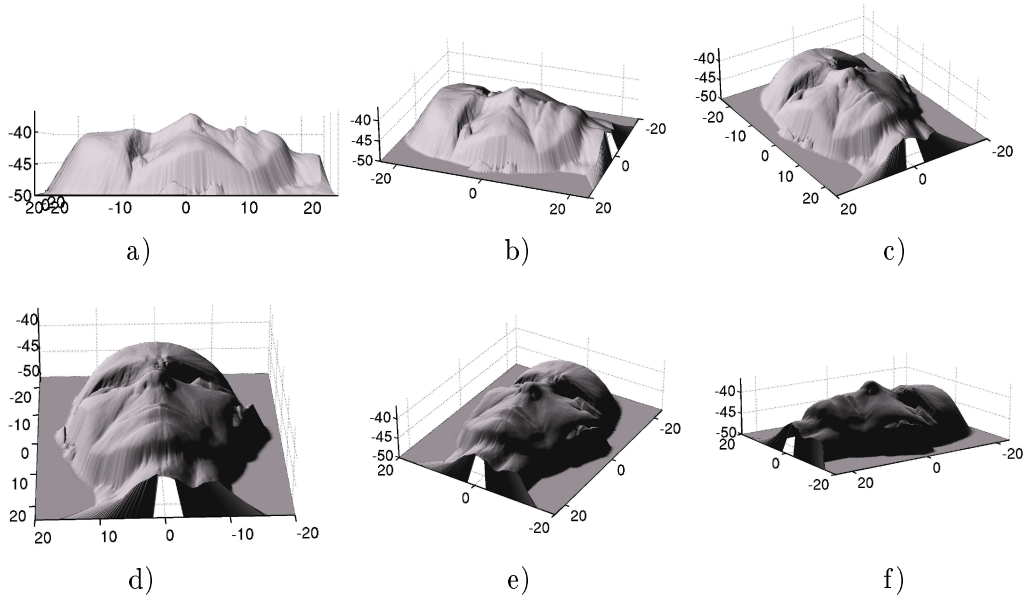


Figure 5.22: Surface reconstructed from the photo Fig.5.21-c) viewed from several points of view and illuminated by a single light source located at infinite. The light source direction is $(-49.00, 109, 100)$.

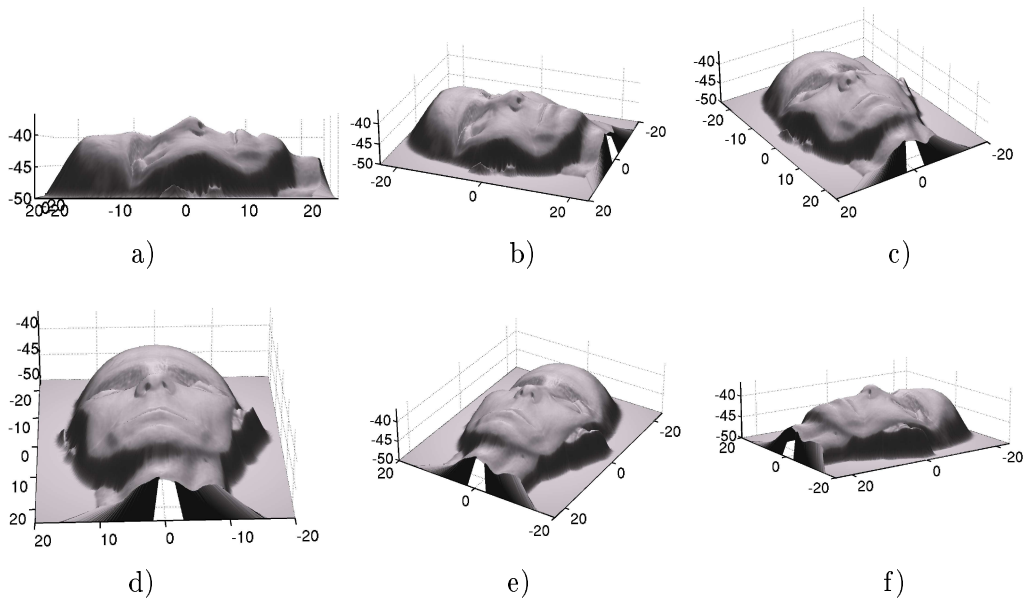


Figure 5.23: Same surface as Figure 5.22 illuminated by a single point light source located at the optical center, that is to say at $(0,0,0)$.

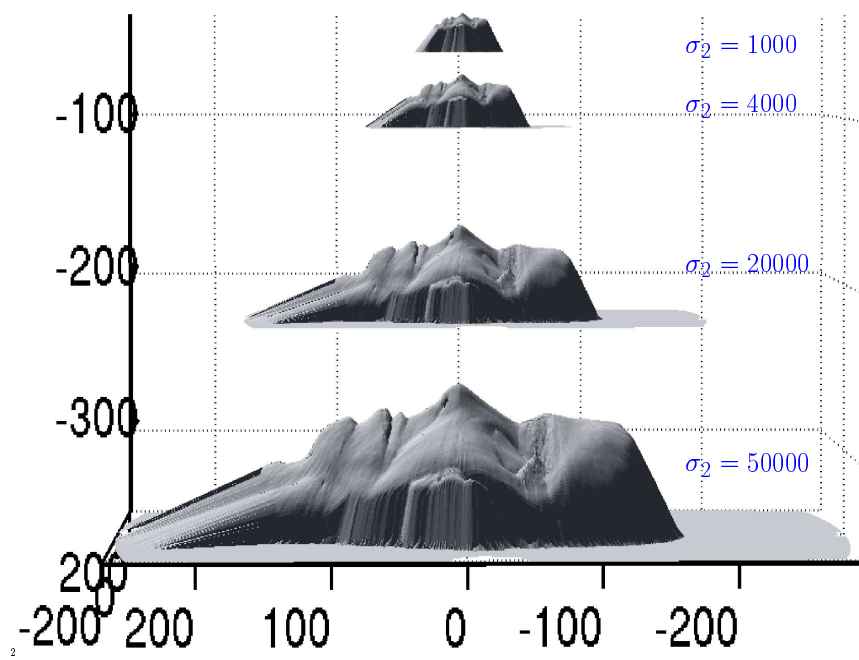


Figure 5.24: Influence of the errors on the σ_2 parameter (albedo of the surface).

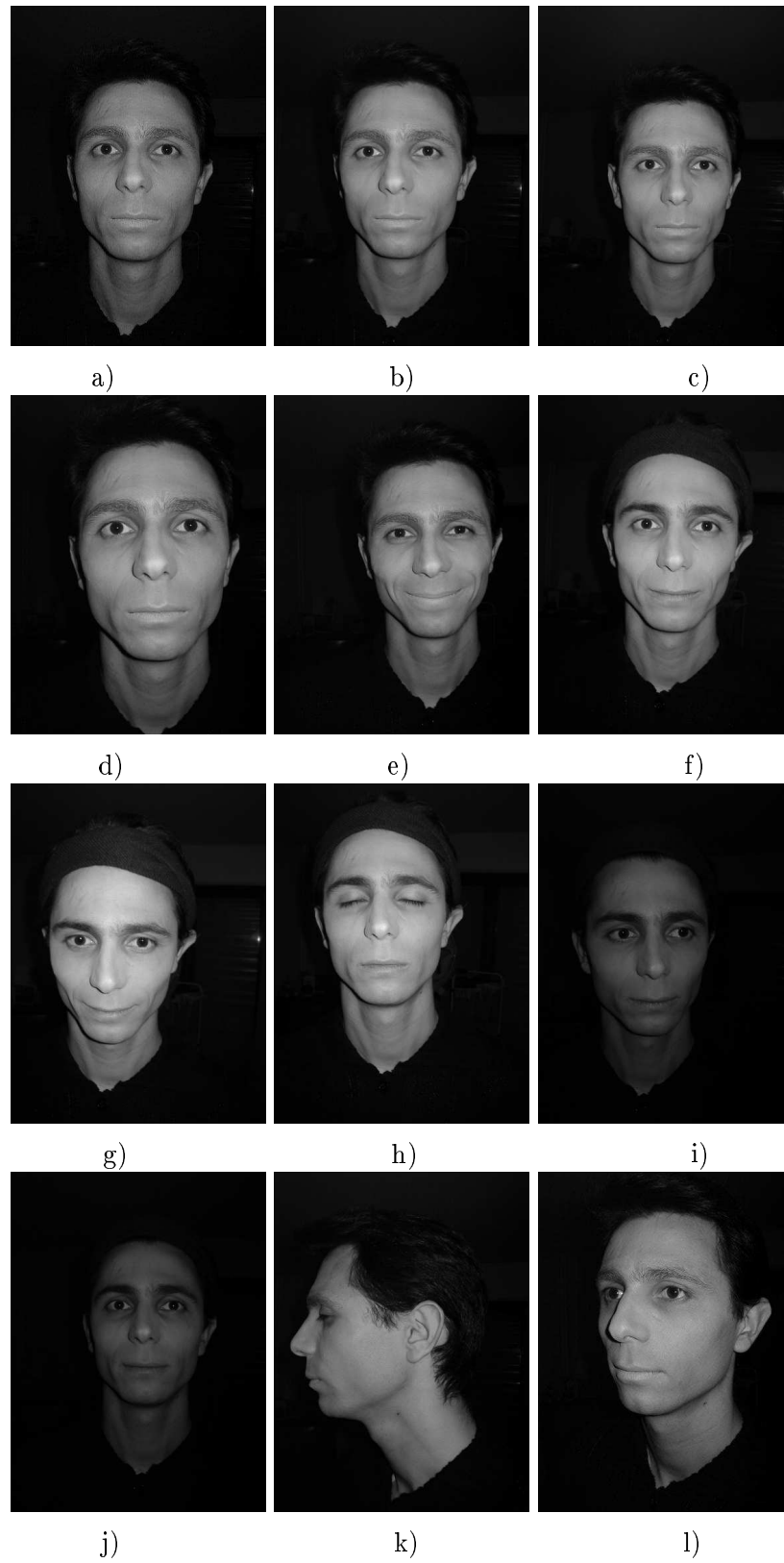


Figure 5.25: A sample of our database of real images of faces verifying approximately our modeling assumptions.

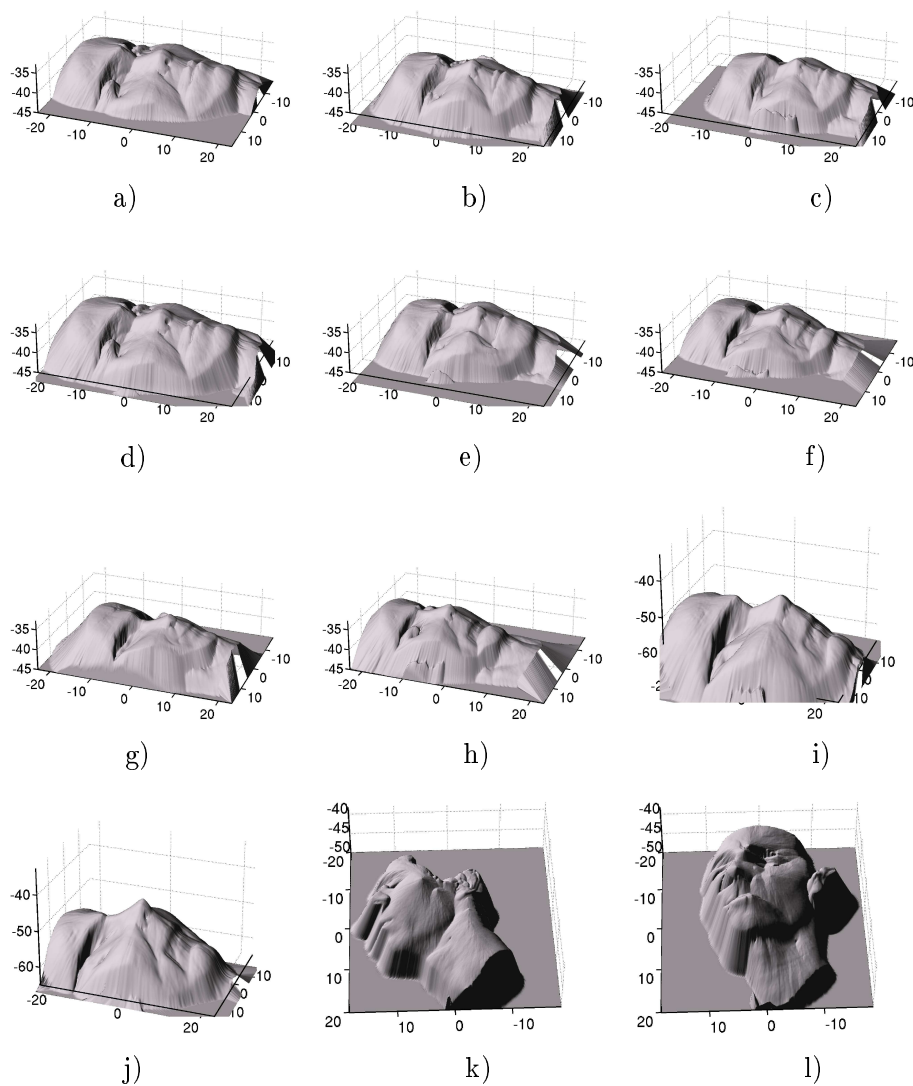


Figure 5.26: Surfaces reconstructed from the real images of Figure 5.25 (after having inpainted the eyes).

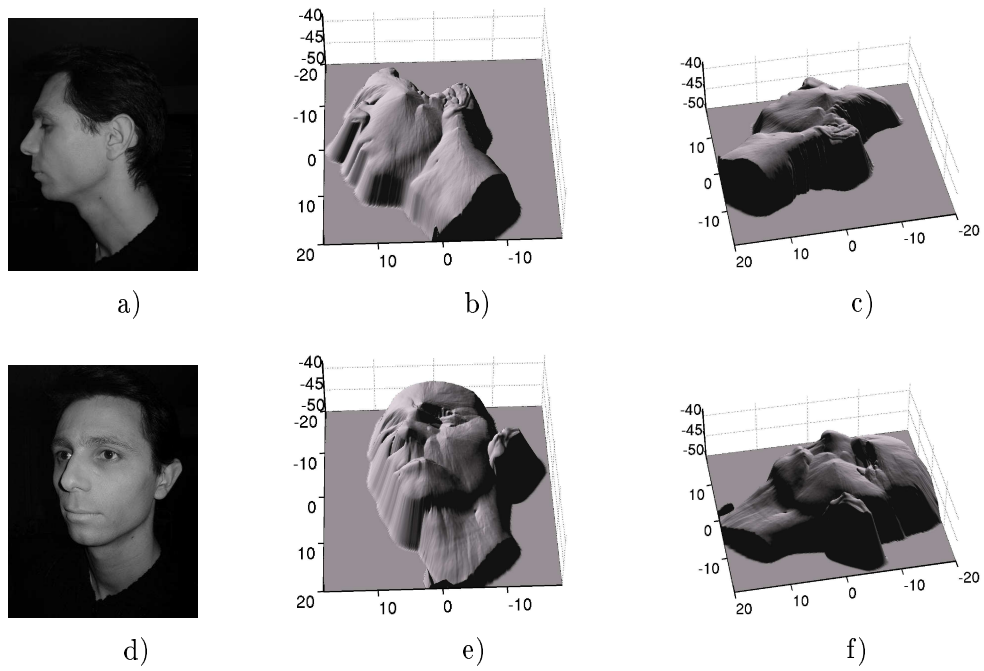


Figure 5.27: Surfaces reconstructed from the images Fig.5.26-k) and Fig.5.26-l).

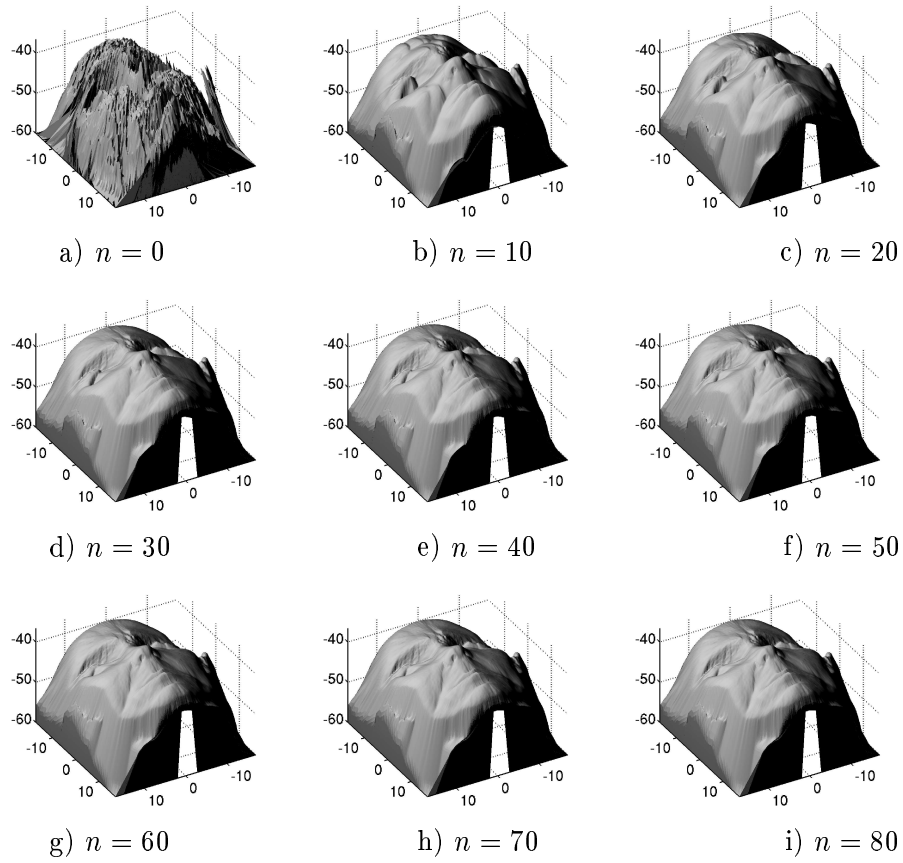


Figure 5.28: Evolution of the reconstructed surfaces in the course of the iterations (n =number of iterations).

5.6 Proof of lemmas and propositions of chapter 5

Proposition 5.1

- i) The hypothesis (H25) holds for H_F , for all brightness image I ;
- ii) if the intensity image I is differentiable and I and ∇I are bounded on Ω , then (H9') holds for H_F ;
- iii) if the intensity image I is upper bounded on a bounded neighborhood Γ of $\partial\Omega$, then the hypothesis (H12') holds for H_F ;
- iv) if there exists a neighborhood Γ of $\partial\Omega$ and $\delta > 0$ such that

$$\forall x \in \Gamma, \quad \delta \leq I(x)$$

then hypotheses (H13') and (H14') are verified with H_F .

Proof of Proposition 5.1.

- i) The hypothesis (H25) holds for H_F , for all brightness image I . In effect, for $-R \leq v \leq u \leq R$ we have:

$$\begin{aligned} H_F(x, u, p) - H_F(x, v, p) &= -e^{-2u} + e^{-2v} \\ &= 2(u - v)e^{-2c} \quad (\text{for some } c \in [v, u]; \text{ by Taylor's} \\ &\quad \text{expansion with remainder)} \\ &\geq 2(u - v)e^{-2R} \\ &\geq \gamma_R(u - v); \end{aligned}$$

where $\gamma_R = 2e^{-2R} > 0$.

- ii) About hypothesis (H9'), we write:

$$|H_F(x, u, p) - H_F(y, u, p)| = |H_C(x, p) - H_C(y, p)|.$$

Let us denote T_p the function defined by $T_p : \Omega \rightarrow \mathbb{R} : x \mapsto H_C(x, p)$.

- o As soon as for all x of Ω , $|\nabla J(x)|$ and $J(x)$ are bounded, lemma 5.2 (see below) involves that for all x and y in Ω , for all u s.t. $-R \leq u \leq R$ and for all p in \mathbb{R}^2 , we have

$$|H_F(x, u, p) - H_F(y, u, p)| \leq \alpha|x - y|(1 + |p|).$$

That is to say (H9') holds with $m_R(t) = \alpha t$.

- Since Ω is bounded (this involves in particular that $\forall x \in \Omega, Q(x) \geq \delta > 0$), one can verify easily that if the intensity image I is differentiable and I and ∇I are bounded on Ω , then $|\nabla J(x)|$ and $J(x)$ are bounded and so (H9') holds.
- iii) For all x in Γ , let us consider the function $R^x : \mathbb{R}^2 \rightarrow \mathbb{R}$ defined by $p \mapsto J(x)\sqrt{f^2|p|^2 + (x \cdot p)^2 + Q(x)^2}$. One can verify that for all $p \in \mathbb{R}^2$, $|\nabla R^x(p)| \leq J(x)\sqrt{f^2 + |x|^2}$. If the intensity image

I is upper bounded on a bounded neighborhood Γ of $\partial\Omega$,

then $J(x)$ and so $J(x)\sqrt{f^2 + |x|^2}$ are also upper bounded on Γ . Therefore $|\nabla R^x(p)|$ is bounded independently of x and p . The reader will conclude easily that, as soon as the intensity image I is upper bounded, the hypothesis (H12') holds.

- iv) Let us assume that there exists a neighborhood Γ of $\partial\Omega$ and $\delta > 0$ such that

$$\forall x \in \Gamma, \quad \delta \leq I(x).$$

For all $R > 0$ and for all (x, u, p) in $\Gamma \times [-R, R] \times \mathbb{R}^2$, we have

$$H_F(x, u, p) \geq -e^{2R} + \delta \epsilon^3 |p|.$$

Therefore $H_F(x, u, p)$ is coercive³⁰ in p uniformly with respect to $x \in \Gamma$ and $u \in [-R, R]$. Therefore hypotheses (H13') and (H14') are verified.

□

Lemma 5.2 *If J is differentiable on the smooth³¹ and bounded set Ω and if for all x in Ω , $|\nabla J(x)|$ and $J(x)$ are upper bounded, then for all $p \in \mathbb{R}^2$, the function T_p (defined at the page 258) is Lipschitz continuous with a Lipschitz' constant of the form $\alpha(1 + |p|)$ (α does not depend on p).*

Proof of Lemma 5.2. Let us denote R_p the function defined by

$$R_p : x \mapsto \sqrt{f^2|p|^2 + (x \cdot p)^2 + Q(x)^2}.$$

³⁰i.e. $\lim_{p \rightarrow +\infty} H_F(x, u, p) = +\infty$ uniformly with respect to $x \in \Gamma$ and $u \in [-R, R]$.

³¹i.e. if Ω is a locally Lipschitz continuous set.

◦ Since Ω is bounded, one can verify that for all x in Ω ,

$$R_p(x) \leq \alpha_2(1 + |p|)$$

$$\text{and } |\nabla R_p(x)| \leq \alpha_3(1 + |p|).$$

◦ Also, we have for all x in Ω ,

$$\begin{aligned} |\nabla T_p(x)| &\leq |\nabla J(x)| R_p(x) + |J(x)| |\nabla R_p(x)| \\ &\leq \alpha(1 + |p|). \end{aligned} \tag{5.35}$$

If Ω is convex, the conclusion follows by using the Mean value theorem. Else, we have

$$\forall x, y \in \overline{\Omega}, \quad |T_p(x) - T_p(y)| \leq |\nabla T_p|_{\infty} L(x, y),$$

where $L(x, y)$ is the Euclidean geodesic distance in Ω , i.e.

$$L(x, y) = \inf \left\{ \int_0^1 |\xi'(t)| dt \mid \xi(t) \in W^{1,\infty}([0, 1], \overline{\Omega}) \text{ s.t. } \xi(0) = x \text{ and } \xi(1) = y \right\}.$$

It is known, [95], that for any fixed $x \in \overline{\Omega}$, $y \mapsto L(x, y)$ is *Lipschitz continuous* in $\overline{\Omega}$ and that the Lipschitz constant does not depend upon x .

□

Lemma 5.3 *If the intensity image I verifies $\forall x \in \Omega$, $I(x) \geq \delta > 0$ then the solutions of (5.15) and (5.19) are bounded independently of φ .*

Proof of Lemma 5.3. Let us define $M = -\frac{1}{2} \ln(\delta f^2)$.

We have:

$$H(x, M, 0) = -e^{-2M} + J(x)Q(x).$$

Since $Q(x) = \frac{I(x) f^2}{J(x)}$, we have

$$H(x, M, 0) = -e^{-2M} + I(x)f^2.$$

So by definition of M ,

$$H(x, M, 0) \geq 0.$$

Therefore, the constant function M is a supersolution of (5.14) on Ω . Also, $\forall x \in \partial\Omega$ and $\forall \xi \in \mathbb{R}^2$, we have

$$H(x, M, \xi) = -e^{-2M} + J(x) \sqrt{f^2 |\xi|^2 + (x \cdot \xi)^2 + Q(x)^2} \geq -e^{-2M} + J(x)Q(x) \geq 0.$$

So for all boundary conditions φ , the constant function M is a supersolution of (5.15) on $\bar{\Omega}$. It is also a supersolution of (5.19). Thus, by the strong uniqueness result (theorems 5.1 and 5.2), for all φ , the solution of (5.15) and (5.19) are upper bounded by M on Ω . \square

Proposition 5.2 *If there exist δ and M such that $\forall x \in \bar{\Omega}$, $M \geq I(x) \geq \delta > 0$, then the schemes S_{impl} and S_{semi} are uniformly stable.*

Proof of Proposition 5.2.

- The hypotheses (H15), (H16) and (H17) are clearly satisfied.
- The proof that hypothesis (H18) holds is the same as the proof detailed in section 3.1.3 ensuring that (H18) holds for the implicit scheme associated to the HJB equations (see in particular proposition 3.1 at page 106).
- Let us assume that $I(x)$ is bounded by M on $\bar{\Omega}$. This implies that

$$\sup_{a \in A, x \in \bar{\Omega}} \{-l_c(x, a)\} \leq M \, \epsilon^2.$$

Considering equation (5.27) or (5.25), we see that, for all constant function u , we have:

$$\tilde{S}_{semi}(\rho, x, u(x), u) = \Delta\tau \tilde{S}_{impl}(\rho, x, u(x), u) = \Delta\tau \left(-e^{-2 \, u(x)} + \sup_{a \in A} \{-l_c(x, a)\} \right).$$

Since $\lim_{u \rightarrow -\infty} -e^{-2 \, u} = -\infty$, we can choose a constant function u such that

$$\forall x \in \bar{\Omega}, \quad -e^{-2 \, u(x)} \leq -M \, \epsilon^2.$$

For such a function u , we clearly have $\forall x \in \bar{\Omega}$

$$\tilde{S}_{semi}(\rho, x, u(x), u) \leq 0.$$

(of course, we also have, $\tilde{S}_{impl}(\rho, x, u(x), u) \leq 0$).

Modulo the subtraction of $\min \varphi(x)$ from u , we conclude that u is a subsolution of S_{semi} and S_{impl} . Therefore hypothesis (H19) holds for S_{semi} and S_{impl} , as soon as $I(x)$ is upper bounded by M on $\bar{\Omega}$.

- We now show that all the subsolutions of our schemes are uniformly bounded. Let u be a subsolution of S_{impl} and S_{semi} . For all $x \in b\Omega_\rho$,

$$u(x) \leq \varphi(x) \leq \max_{y \in \bar{\Omega}} \varphi(y).$$

Moreover, for all $x \in \Omega_\rho$, we have

$$-e^{-2u(x)} + \sup_{a \in A} \left\{ \sum_{i=1}^2 (-f_i(x, a)) \frac{u(x) - u(x + s_i(x, a)h_i \vec{e}_i)}{-s_i(x, a)h_i} - l_c(x, a) \right\} \leq 0.$$

In particular (for $a = 0$)

$$-e^{-2u(x)} + \sum_{i=1}^2 (-f_i(x, 0)) \frac{u(x) - u(x + s_i(x, 0)h_i \vec{e}_i)}{-s_i(x, 0)h_i} - l_c(x, 0) \leq 0.$$

Since $-l_c(x, 0) = I(x) f^2$ and $f_c(x, 0) = 0$, we have

$$-e^{-2u(x)} \leq -I(x) f^2.$$

If we assume $\forall x \in \bar{\Omega}$, $I(x) \geq \delta > 0$, then for all x in $\bar{\Omega}$,

$$-e^{-2u(x)} \leq -\delta f^2.$$

Thus, as soon as $\forall x \in \bar{\Omega}$, $I(x) \geq \delta > 0$, we conclude that all the sub-solutions of the scheme S_{impl} and S_{semi} are uniformly upper bounded by

$$\max\left\{-\frac{1}{2} \ln(\delta f^2), \max_{y \in \bar{\Omega}} \varphi(y)\right\}$$

and so the hypothesis (H20) holds.

- We have proved that all the hypotheses of theorem 3.1 hold for our new schemes S_{impl} and S_{semi} . This allows us to conclude that they are uniformly stable.

□

Proposition 5.3 *If the hypotheses of proposition 5.2 are verified then the hypotheses (H16'), (H19') and (H20') hold.*

Proof of proposition 5.3. Using the fact that $I(x) \geq \delta > 0$ and $\lim_{u \rightarrow +\infty} -e^{-2u} = 0$, the reader will verify easily that all “large enough” constant functions are *supersolutions* of S_{impl} and S_{semi} . Therefore *hypothesis (H19') holds*. The proof that all supersolutions are uniformly lower bounded (hypothesis (H20')) is slightly more difficult:

Let u be a supersolution. For each point $x \in \bar{\Omega}$, we can associated the grid \mathcal{X}_x :

$$\mathcal{X}_x := \left\{ x + \sum_{i=1..2} k_i h_i \vec{e}_i \mid (k_1, k_2) \in \mathbb{Z}^2 \right\} \cap \bar{\Omega}.$$

Since we have assumed that $\bar{\Omega}$ is bounded then \mathcal{X}_x is a finite set. Therefore $u|_{\mathcal{X}_x}$ has a minimum. Let us denote

$$y_x = \operatorname{argmin}_{y \in \mathcal{X}_x} u(y).$$

Thus for all $i = 1..2$, we have $u(y_x) - u(y_x + s_i(y_x, a)h_i \vec{e}_i) \leq 0$; so

$$\sup_{a \in A} \left\{ \sum_{i=1}^2 |f_i(y_x, a)| \frac{u(y_x) - u(y_x + s_i(y_x, a)h_i \vec{e}_i)}{h_i} - l_c(y_x, a) \right\} \leq \sup_{a \in A} \{-l_c(y_x, a)\} \leq I(y_x) \mathfrak{f}^2.$$

Since we have assumed that u is a supersolution, we have

$$S(\rho, y_x, u(y_x), u) \geq 0.$$

1. If $y_x \in \mathfrak{b}\Omega_\rho$ then

$$u(y_x) \geq \varphi(y_x) \geq \min_{y \in \bar{\Omega}} \varphi(y).$$

2. If $y_x \in \Omega_\rho$

$$\tilde{S}(\rho, y_x, u(y_x), u) \geq 0$$

then

$$-e^{-2} u(y_x) \geq -\sup_{a \in A} \left\{ \sum_{i=1}^2 |f_i(y_x, a)| \frac{u(y_x) - u(y_x + s_i(y_x, a)h_i \vec{e}_i)}{h_i} - l_c(y_x, a) \right\}.$$

Hence

$$-e^{-2} u(y_x) \geq -I(y_x) \mathfrak{f}^2.$$

If $\forall x \in \bar{\Omega}$, $I(x) < M$, then

$$u(y_x) \geq -\frac{1}{2} \ln(M \mathfrak{f}^2).$$

Let us denote $B := \min\{-\frac{1}{2} \ln(M \mathfrak{f}^2), \min_{y \in \bar{\Omega}} \varphi(y)\}$. Since $u(x) \geq u(y_x)$ (because $u(y_x)$ is the minimum of $u|_{\mathcal{X}_x}$) therefore $u(x) \geq B$. B being independent of x , we have $\forall x \in \bar{\Omega}$, $u(x) \geq B$. B being also independent of ρ , we conclude that the supersolutions are uniformly lower bounded. Therefore *hypothesis (H20') holds*.

Finally, the reader can verify easily that hypothesis (H16') also holds. \square

5.7 Conclusion and contributions of chapter 5

The main difficulties encountered in chapters 2 and 4 where we deal with the “classical” SFS problems, are due to the (unavoidable) presence of singular points. In this chapter, we have shown that these difficulties disappear completely when we model the SFS problem in a more realistic way than it is usually done. In effect, the notion of singular points does not make sense anymore when we do not neglect the $1/r^2$ attenuation term of the lighting. In other words, we have shown that the “classical” SFS problem is ill-posed because of an oversimplification in the modeling! Also, we have proved that generally in practice the SFS problem is well posed.

More precisely we have:

- detailed the appropriate **equations and Hamiltonians** to the “perspective SFS” problem for Lambertian scenes illuminated by single point light source located at the optical center, in the case where **we do not neglect the $1/r^2$ lighting attenuation term**.
- developed a **complete mathematical study** of the obtained equations. We have proved the **existence** and the **uniqueness** of the discontinuous viscosity solutions of the new equations with Dirichlet boundary conditions or state constraints.
- designed **monotonous schemes** for approximating the new PDEs. We have proved that our schemes are **stable** and **consistent** and that their solutions **converge toward the viscosity solution** when the mesh vanishes. We have proposed two **numerical algorithms** (an implicit one and a semi-implicit one). Also, we have proved that the computed solutions converge toward the solutions of the schemes.
- implemented and tested experimentally the semi-implicit algorithm.

As by the predicted theory, **in practice** our method allows to **recover any surface** which verifies hypothesis (5.17) **from its image only**. **We do not need any additional data or regularity assumptions**. Let us stress the fact that our method works even when the surface has **several local minima** and maxima. There are not ambiguities anymore. To our knowledge none of the previous SFS methods is able to produce such results. In that sense, we are the first to provide a SFS solution which is really satisfying!

Let us emphasize the fact that the hypothesis (5.17) is actually quite weak. For example, as soon as the image to be processed contains an object of interest in front of a background, the condition is satisfied in a neighbourhood of the object where u increases.

Finally, we have shown that our method is **robust** to pixel noise, to errors on the parameters and to modeling errors. Also, we have obtained quite good results with **real images**.

Chapter 6

Conclusion

When I started my PhD thesis in 2001, a quick study of the state of the art clearly showed that the interest in the Shape from Shading problem had decreased after the mid 90s. The reasons for this loss of interest were mostly connected to the fact that the results obtained with real images, but also with synthetic images (verifying all the modeling hypotheses and corresponding to the simplest version of the problem), were very disappointing. The problem was considered ill-posed and several researchers, e.g. Zhang et al. in 1999 [172], acknowledged failure.

Attempting to solve the Shape from Shading problem is an ambitious challenge. Indeed in this problem, the data are minimal. Contrary for example to photometric stereo and multiview reconstruction, in Shape from Shading one can only use one image. From this restriction follow important difficulties, theoretical and practical. This is why I think that the solution of the Shape from Shading problem lies in a tight interaction between Mathematics, Algorithmic and Modeling; this is what I have attempted to do in this work. Also, I hope to have convinced the reader of the interest of Mathematics in the Shape from Shading problem. For example, I hope to have shown that

- Mathematics allows to fully understand the difficulties of the “classical” Shape from Shading problem, why the previous Shape from Shading methods produce unsatisfying results and why our new method (presented in the last chapter) is intrinsically better than previous ones.
Moreover when there do not exist classical solutions (i.e. smooth solutions), Mathematics allows to understand what we compute, in our case approximations of the viscosity solutions...
- Mathematics is a very helpful guide in the design of the numerical methods and algorithms. It also allows to certify the algorithms, to guarantee their

robustness and to describe their limitations...

As a side-effect, we also hope to have made the notion of viscosity solutions more accessible and to have convinced the reader of the usability of these tools.

More precisely, in this manuscript we have first studied in detail the “classical” Shape from Shading problem. After having shown how to take into account the perspective, we have unified various modelings of the problem by introducing a “generic” Hamiltonian. Thanks to a complete mathematical study, we have shown the difficulties of the problem (basically, it is ill-posed). In order to alleviate them as much as possible, we have designed a new mathematical framework based on the notion of the viscosity solutions. This viscosity framework does not necessarily require data on the boundary of the image¹ and unifies the main theoretical results proved in the SFS literature [96, 134, 47, 24, 55, 56, 127, 120].

In the second part of our work, we have modeled the SFS problem in a more realistic way than is usually done. In particular, we do not neglect the attenuation effect of the lighting due to distance. With such a modeling the SFS problem becomes well posed. Thus, we have come up with a Shape from Shading method allowing to accurately recover a surface from one image only, without using any additional data or smoothness assumptions, thereby obtaining results never obtained previously. To get a better feel for the advances presented in this manuscript, we invite the reader to compare the results we display in the last chapter with, for example, those shown by the review articles of Zhang et al. in [172] and Durou et al. [49, 48].

¹But it still requires data at the local “minima” of the surface.

Conclusion (en français)

Lorsque j'ai commencé ma thèse, en avril 2001, un rapide état de l'art m'a permis de constater une diminution importante de l'intérêt porté au problème du "Shape From Shading" depuis le milieu des années 90. Les raisons de cette baisse d'intérêt sont très probablement liées au fait que jusqu'à présent, les résultats obtenus avec des images réelles, mais également avec des images synthétiques (vérifiant toutes les hypothèses de la modélisation et correspondant à la version la plus simple du problème) restaient très décevants. De plus, le problème était considéré comme un problème mal posé. Ainsi, par exemple en 1999, Zhang et al. aboutissent à un constat d'échec [172].

Tenter de résoudre le problème du "Shape From Shading" est un défi ambitieux. En effet, contrairement aux autres problèmes de vision tridimensionnelle, ici les données sont minimales. Dans le problème du "Shape From Shading", nous n'utilisons qu'une seule image! De cette restriction suit d'importantes difficultés, théoriques et pratiques. C'est pourquoi je pense que pour faire progresser ce domaine, nous devons impérativement faire interagir les mathématiques, l'algorithmique et la modélisation. Aussi, c'est ce que j'ai essayé de faire dans ce travail. Par ailleurs, j'espère aussi avoir convaincu le lecteur de l'intérêt des mathématiques dans le problème du "Shape From Shading".

Plus précisément, dans un premier temps, nous avons étudié en détail le problème "classique" du "Shape From Shading". Nous avons montré ses limites (le problème est naturellement mal posé) puis nous avons essayé d'exploiter son potentiel au maximum en proposant un nouveau cadre

mathématique mieux adapté que les précédents.

Dans une deuxième partie de notre travail, nous avons modélisé le problème du SFS de manière plus réaliste que ce qui est fait habituellement. En particulier, nous n'avons pas négligé l'effet d'atténuation de l'éclairage dû à la distance. Aussi, avec une telle modélisation, le problème du SFS devient bien posé. Ainsi, nous avons obtenu une méthode de "Shape From Shading" permettant de retrouver avec précision une surface à partir d'une seule image, sans utiliser de données additionnelles ou d'hypothèses de régularité. De cette façon, nous arrivons à obtenir des résultats jamais obtenus auparavant. Pour se rendre compte clairement des contributions présentées dans ce manuscrit, nous invitons le lecteur à comparer les résultats exposés dans notre dernier chapitre, avec, par exemple, les résultats donnés dans les états de l'art de Zhang et al. dans [172] et dans celui de Durou et al. [49, 48].

Appendix A

How to transform a convex Hamiltonian into a HJB Hamiltonian; Legendre Transform

In this section, we propose a method for transforming a convex Hamiltonian $H(x, \nabla u)$ into a HJB Hamiltonian.

In general, the Hamiltonian H is not given in the form

$$H(x, p) = \sup_{a \in A} \{-f(x, a) \cdot p - l(x, a)\}$$

but explicitly. In the case where $H(x, p)$ is a convex continuous function with respect to p (and Lipschitz continuous at least locally in x), it is possible to write $H(x, p)$ as a supremum of affine functions: We note H^* the dual convex function of H (also called the “Legendre transform” of H):

$$H^*(x, a) = \sup_{p \in \mathbb{R}^N} \{p \cdot a - H(x, p)\} \leq +\infty.$$

We know that

$$H(x, p) = \sup_{a \in \text{Dom}(H^*(x, \cdot))} \{p \cdot a - H^*(x, a)\},$$

see for example [52]. We notice that in general $D_x := \text{Dom}(H^*(x, \cdot))$ depends on x . To remove this dependency we change variables (see below).

In the case where the Hamiltonian is C^1 with respect to p , we can compute H^* explicitly through differential calculus. The method consists in computing

the gradient $\overrightarrow{\nabla_p H}$, solving equation $\overrightarrow{\nabla_p H}(p_0) = 0$ (p_0 depends on x), and calculating $H(x, p_0)$.

Example : for the Hamiltonian

$$H_{R/T}^{orth}(x, p) = I(x)\sqrt{1 + |p|^2} + p \cdot \mathbf{1} - \gamma,$$

we find

$$H_{R/T}^{orth*}(x, a) = \begin{cases} -\sqrt{I(x)^2 - |a - \mathbf{1}|^2} + \gamma & \text{if } x \in \overline{B}(\mathbf{1}, I(x)) \\ +\infty & \text{otherwise.} \end{cases}$$

Therefore we have

$$H_{R/T}^{orth}(x, p) = \sup_{a \in \overline{B}(\mathbf{1}, I(x))} \{p \cdot a + \sqrt{I(x)^2 - |a - \mathbf{1}|^2} - \gamma\}.$$

In this example, $D_x = \overline{B}(\mathbf{1}, I(x))$ depends of x . The change of variables $b = (a - \mathbf{1})/I(x)$ removes this dependency. Thus

$$H_{R/T}^{orth}(x, p) = \sup_{b \in \overline{B}(0,1)} \left\{ \underbrace{-(-I(x)b - \mathbf{1}) \cdot p}_{f_{R/T}^{orth}(x,b)} - \underbrace{(\gamma - I(x)\sqrt{1 - |b|^2})}_{l_{R/T}^{orth}(x,b)} \right\},$$

and $H_{R/T}^{orth}$ has the desired form.

Remarks 52.

R52.1 - With this method based on the Legendre transform, the set A of the controls has the same dimension as p (the second variable of $H(x, p)$). There exist other methods for rewriting H as a supremum. For example, for

$$H_{R/T}^{orth}(x, p) = I(x)\sqrt{1 + |p|^2} + p \cdot \mathbf{1} - \gamma,$$

with $p \in \mathbb{R}^2$, Falcone [56] uses the identity

$$\forall X \in \mathbb{R}^3, |X| = \sup_{a \in B_3(0,1)} \{a \cdot X\},$$

where $B_3(0, 1)$ is the unit ball of center 0 in \mathbb{R}^3 . Thus, for $X = \begin{pmatrix} p \\ 1 \end{pmatrix}$:

$$\sqrt{1 + |p|^2} = \sup_{(a_1, a_2, a_3) \in B_3(0,1)} \left\{ p \cdot \begin{pmatrix} a_1 \\ a_2 \end{pmatrix} + a_3 \right\}.$$

Therefore, we also have:

$$H_{R/T}^{orth}(x, p) = \sup_{a \in B_3(0,1)} \left\{ [I(x) \begin{pmatrix} a_1 \\ a_2 \end{pmatrix} + \mathbf{1}] \cdot p + I(x) a_3 - \gamma \right\}.$$

Let us note that in this case the control dimension is equal to 3 when the dimension of p is equal to 2.

r52.2 - The above method may be automated through a symbolic computation program such as Maple.

Appendix B

The “classical” SFS Hamiltonians and the generic Hamiltonian H_g

B.1 The Hamiltonians H_*^{orth} and H_*^{pers} are special cases of H_g

In this section, we detail the functions $\mu_x, \nu_x, \kappa_x, K_x, \mathbf{w}_x, \mathbf{v}_x$, and c_x for the SFS Hamiltonians H_*^{orth} and H_*^{pers} .

- For the “Rouy/Tourin Hamiltonian” [134]:

$$H_{R/T}^{orth}(x, p) = I(x)\sqrt{1 + |p|^2} + p \cdot \mathbf{1} - \gamma;$$

$$\begin{aligned}\mu_x &= 1 & \nu_x &= 1 \\ \kappa_x &= I(x) & K_x &= 1 \\ \mathbf{w}_x &= \mathbf{1} & \mathbf{v}_x &= \mathbf{0} \\ c_x &= -\gamma\end{aligned}$$

- For the “Dupuis/Oliensis Hamiltonian” [47]:

$$H_{D/O}^{orth}(x, p) = I(x)\sqrt{|p - \mathbf{1}|^2 + \gamma^2} + p \cdot \mathbf{1} - 1;$$

$$\begin{aligned}\mu_x &= 1 & \nu_x &= 1 \\ \kappa_x &= I(x) & K_x &= \gamma \\ \mathbf{w}_x &= \mathbf{1} & \mathbf{v}_x &= -R_x \mathbf{1} \\ c_x &= -1\end{aligned}$$

Let us remind the reader that R_x is the rotation

$$R_x = \begin{pmatrix} \frac{x_2}{|x|} & \frac{-x_1}{|x|} \\ \frac{x_1}{|x|} & \frac{x_2}{|x|} \end{pmatrix}.$$

- For the “Eikonal Hamiltonian”:

$$H_{Eik}^{orth}(x, p) = |p| - \sqrt{\frac{1}{I(x)^2} - 1};$$

$$\mu_x = 1 \quad \nu_x = 1$$

$$\kappa_x = 1 \quad K_x = 0$$

$$\mathbf{w}_x = 0 \quad \mathbf{v}_x = 0$$

$$c_x = -\sqrt{\frac{1}{I(x)^2} - 1}$$

Lemma B.1 *We have*

$$\left| \begin{pmatrix} f_1 & 0 \\ 0 & \sqrt{f_1^2 + f_2^2|x|^2} \end{pmatrix} R_x p \right|^2 = f_1^2 |p|^2 + f_2^2 (x \cdot p)^2.$$

Therefore

$$f^2 |p|^2 + (p \cdot x)^2 = |D_x R_x p|^2,$$

with $\mu_x = f$ and $\nu_x = \sqrt{f^2 + |x|^2}$.

Proof. Let us denote $x^\perp := \begin{pmatrix} x_2 \\ -x_1 \end{pmatrix}$.

We have

$$R_x p = \frac{1}{|x|} \begin{pmatrix} x^\perp \cdot p \\ x \cdot p \end{pmatrix},$$

therefore

$$\begin{pmatrix} f_1 & 0 \\ 0 & \sqrt{f_1^2 + f_2^2|x|^2} \end{pmatrix} R_x p = \frac{1}{|x|} \begin{pmatrix} f_1 x^\perp \cdot p \\ \sqrt{f_1^2 + f_2^2|x|^2} x \cdot p \end{pmatrix}.$$

Thus the square of the norm of the previous expression is equal to

$$\begin{aligned} & f_1^2 \left(\frac{x^\perp}{|x|} \cdot p \right)^2 + [f_1^2 + f_2^2|x|^2] \left(\frac{x}{|x|} \cdot p \right)^2 \\ &= f_1^2 \left[\left(\frac{x^\perp}{|x|} \cdot p \right)^2 + \left(\frac{x}{|x|} \cdot p \right)^2 \right] + f_2^2 (x \cdot p)^2 \\ &= f_1^2 |p|^2 + f_2^2 (x \cdot p)^2. \end{aligned}$$

□

- For the “Perspective SFS” with a point light source located at the focal center:

$$H_F^{pers}(x, p) = I(x) \sqrt{f^2 |p|^2 + (p \cdot x)^2 + \frac{f^2}{f^2 + |x|^2}} - \sqrt{\frac{f^2}{f^2 + |x|^2}},$$

Using lemma B.1, we have

$$\begin{aligned} \mu_x &= f & \nu_x &= \sqrt{f^2 + |x|^2} \\ \kappa_x &= I(x) & K_x &= \sqrt{\frac{f^2}{f^2 + |x|^2}} \\ \mathbf{w}_x &= 0 & \mathbf{v}_x &= 0 \\ c_x &= -\sqrt{\frac{f^2}{f^2 + |x|^2}} & & (= -K_x) \end{aligned}$$

- For the “Perspective SFS” with a point light source at infinity:

$$H_1^{pers}(x, p) = I(x) \sqrt{f^2 |p|^2 + (x \cdot p + 1)^2} - (f \mathbf{1} + \gamma x) \cdot p - \gamma,$$

therefore we have

$$\begin{aligned} \mu_x &= f & \nu_x &= \sqrt{f^2 + |x|^2} \\ \kappa_x &= I(x) & K_x &= \sqrt{\frac{f^2}{f^2 + |x|^2}} \\ \mathbf{w}_x &= -(f \mathbf{1} + \gamma x) & \mathbf{v}_x &= D_x^{-1} R_x x = \left(0, \frac{|x|}{\sqrt{f^2 + |x|^2}}\right) \\ c_x &= -\gamma. \end{aligned}$$

Proof. By using lemma B.1, we have

$$f^2 |p|^2 + (x \cdot p + 1)^2 = |D_x R_x p|^2 + 2 x \cdot p + 1$$

with $\mu_x = f$ and $\nu_x = \sqrt{f^2 + |x|^2}$.

If we denote $q := D_x R_x p$, we have

$$\begin{aligned} f^2 |p|^2 + (x \cdot p + 1)^2 &= |D_x R_x p|^2 + 2x \cdot (R_x^{-1} D_x^{-1} D_x R_x p) + 1 \\ &= |q|^2 + 2 [{}^t(R_x^{-1} D_x^{-1}) x] \cdot q + 1 \\ &= |q|^2 + 2 [D_x^{-1} R_x x] \cdot q + 1. \end{aligned}$$

Since

$$|q|^2 + 2\mathbf{v} \cdot q = |q + \mathbf{v}|^2 - |\mathbf{v}|^2,$$

then

$$f^2|p|^2 + (x \cdot p + 1)^2 = |D_x R_x p + [D_x^{-1} R_x x]|^2 - |D_x^{-1} R_x x|^2 + 1.$$

Let us note that: $D_x^{-1} R_x x = (0, \frac{|x|}{\sqrt{f^2 + |x|^2}})$. □

B.2 HJB formulation of H_g

In this section we show how to compute the HJB formulation of H_g .

$$H_g(x, p) = \tilde{H}_g(x, A_x p + \mathbf{v}_x) + \mathbf{w}_x \cdot p + c_x, \tag{B.1}$$

with $A_x \in GL^N(\mathbb{R})$, $\mathbf{v}_x, \mathbf{w}_x \in \mathbb{R}^2$, $c_x \in \mathbb{R}$, and $\tilde{H}_g(x, q) : \Omega \times A \rightarrow \mathbb{R} : (x, q) \mapsto \tilde{H}_g(x, q)$, convex with respect to q .

We do not use the method presented in the previous section. We have

$$\tilde{H}_g(x, q) = \sup_{a \in \text{Dom}(\tilde{H}_g^*(x, \cdot))} \{q \cdot a - (\tilde{H}_g)^*(x, a)\}. \tag{B.2}$$

By replacing \tilde{H}_g by the supremum of (B.2) in the identity (B.1), we obtain:

$$H_g(x, p) = \sup_{a \in \text{Dom}(\tilde{H}_g^*(x, \cdot))} \{ [{}^t A_x a + \vec{w}_x] \cdot p - [\tilde{H}_g^*(x, a) - \vec{v}_x \cdot a - c_x] \}.$$

Let us emphasize that for computing the HJB formulation of H_g , we do not need to compute the Legendre transform H_g^* of H_g ; we only need to compute the Legendre transform $(\tilde{H}_g)^*$ of \tilde{H}_g .

Appendix C

Maxi(Mini)mization of various functions

In this section, we details some necessary results for coding the algorithms associated to the implicit and semi-implicit decentered schemes.

C.1 Maximisation of $\delta\sqrt{1-|a|^2} + w \cdot a + c$

Let us consider the function Ψ_1 defined by:

$$\Psi_1 : \overline{B}_2(0, 1) \rightarrow \mathbb{R} : a \mapsto \delta\sqrt{1-|a|^2} + w \cdot a + c$$

with $w \in \mathbb{R}^2$ and $\delta, c \in \mathbb{R}$, $\delta > 0$.

The maximum of Ψ_1 is reached at

$$a_0 = \frac{1}{\sqrt{\delta^2 + |w|^2}} w.$$

The value of Ψ_1 at a_0 is:

$$\Psi_1(a_0) = \sqrt{\delta^2 + |w|^2} + c.$$

C.2 Maximisation of $\delta\sqrt{c-br-ar^2} + \mu r + \nu$

Let us consider the function Ψ_2 defined by:

$$\Psi_2 : I \subset \mathbb{R} \rightarrow \mathbb{R} : r \mapsto \delta\sqrt{c-br-ar^2} + \mu r + \nu$$

with $\delta, a, b, c, \mu, \nu \in \mathbb{R}$, $\delta > 0$ and $a > 0$.

We distinguish two cases:

1. $b^2 + 4ac < 0$:

The definition set of Ψ_2 is the empty set ($I = \emptyset$).

2. $b^2 + 4ac \geq 0$:

The maximum of Ψ_2 is reached at

$$r_0 = \frac{1}{2a} \left[\mu \sqrt{\frac{b^2 + 4ac}{a\delta^2 + \mu^2}} - b \right]$$

The value of Ψ_2 at r_0 is:

$$\Psi_2(r_0) = \frac{1}{2a} \sqrt{a\delta^2 + \mu^2} \sqrt{b^2 + 4ac} - \frac{\mu b}{2a} + \nu.$$

C.3 Minimization $\delta\sqrt{c + br + ar^2} + \mu r + \nu$

Let us consider the function Ψ_3 defined by:

$$\Psi_3 : J \subset \mathbb{R} \rightarrow \mathbb{R} : r \mapsto \delta\sqrt{c + br + ar^2} + \mu r + \nu$$

with $\delta, a, b, c, \mu, \nu \in \mathbb{R}$, $\delta > 0$ and $a > 0$.

1. **If $a\delta^2 - \mu^2 \leq 0$, there are no minima.**

To have a minimum, the function Ψ_3 needs to be coercive.

We have:

Ψ_3 is coercive

$$\text{iff } \lim_{r \rightarrow \pm\infty} \delta\sqrt{a}|r| + \mu r = +\infty$$

$$\text{iff } \delta\sqrt{a} \geq |\mu|$$

$$\text{iff } a\delta^2 - \mu^2 \geq 0.$$

2. **If $4ac - b^2 \leq 0$, there are no minima.**

Let us suppose that $a\delta^2 - \mu^2 \geq 0$.

If $4ac - b^2 \leq 0$, there are no minima in the set of definition of Ψ_3 .

If $4ac - b^2 \geq 0$, then Ψ_3 reaches his minimum at

$$r_0 = -\frac{b}{2a} - \frac{\mu}{2a} \sqrt{\frac{4ac - b^2}{a\delta^2 - \mu^2}}.$$

The value of this minimum is:

$$\Psi_3(r_0) = \frac{1}{2a} \sqrt{a\delta^2 - \mu^2} \sqrt{4ac - b^2} - \frac{\mu b}{2a} + \nu.$$

C.4 Solving $\sqrt{c + br + ar^2} + \mu r + \nu = 0$ with respect to r

Let us consider the following function Ψ_4 :

$$\Psi_4 : J \subset \mathbb{R} \rightarrow \mathbb{R} : r \mapsto \sqrt{c + br + ar^2} + \mu r + \nu$$

with $a, b, c, \mu, \nu \in \mathbb{R}$, $a > 0$ (Ψ_4 is the above function Ψ_3 with $\delta = 1$).

We have :

$$\Psi_4(r) = 0 \quad \Longleftrightarrow \quad \begin{cases} \mu r + \nu \leq 0, \\ c + br + ar^2 - (\mu r + \nu)^2 = 0. \end{cases}$$

The discriminant of

$$c - \nu^2 + (b - 2\mu\nu)r + (a - \mu^2)r^2 = 0$$

is:

$$\Delta = (b - 2\mu\nu)^2 - 4(c - \nu^2)(a - \mu^2).$$

- If $\Delta < 0$, then equation

$$c + br + ar^2 - (\mu r + \nu)^2 = 0$$

has no solutions.

- If $\Delta \geq 0$, then it has two solutions (which can be equal):

$$r_{\pm} := \frac{-(b - 2\mu\nu) \pm \sqrt{\Delta}}{2(a - \mu^2)}.$$

Therefore, $\Psi_4(r) = 0$ can have two solutions: r_{\pm}

- if $\mu r_+ + \nu \leq 0$, then r_+ is solution,
- if $\mu r_- + \nu \leq 0$, then r_- is solution.

Appendix D

List of all hypotheses

- (H1) H is convex with respect to p for all x in $\overline{\Omega}$. (page 60)
- (H2) $H(x, p) \rightarrow +\infty$ when $|p| \rightarrow +\infty$ uniformly with respect to $x \in \overline{\Omega}$. (page 60)
- (H2') $\liminf_{|p| \rightarrow +\infty} H(x, p) = +\infty$, for any $x \in \overline{\Omega}$. (page 154)
- (H3) $\inf_{p \in \mathbb{R}^2} H(x, p) \leq 0$ in $\overline{\Omega}$. (page 61)
- (H3') There exists a subsolution $\psi \in C^1(\Omega) \cap W^{1, \infty}(\Omega)$ of (4.2) (i.e: $\forall x \in \Omega, H(x, \nabla \psi(x)) \leq 0$). (page 155)
- (H4) $H \in C(\overline{\Omega} \times \mathbb{R}^N)$. (page 61)
- (H5) $\forall x, y \in \partial\Omega, \varphi(x) - \varphi(y) \leq L(x, y)$. (page 61)
- (H6) A is a compact topological space and Ω is a bounded open subset of \mathbb{R}^N . (page 64)
- (H6') A is a compact topological space. (page 106)
- (H7) $f : \overline{\Omega} \times A \rightarrow \mathbb{R}^N$ is continuous;
 $l : \overline{\Omega} \times A \rightarrow \mathbb{R}$ is continuous and bounded. (page 65)
- (H7') $f : A \rightarrow \mathbb{R}^N$ is continuous;
 $l : A \rightarrow \mathbb{R}$ is continuous and bounded. (page 106)
- (H8) f and l are Lipschitz continuous in $x \in \overline{\Omega}$ uniformly in $a \in A$. (page 65)

(H9) *There exists a nondecreasing function ω which goes to zero at zero, such that $\forall x, y \in \Omega, \forall p \in \mathbb{R}^N$,*

$$|H(x, p) - H(y, p)| \leq \omega(|x - y|(1 + |p|)). \quad (\text{page 77})$$

(H9') $|H(x, u, p) - H(y, u, p)| \leq m_R(|x - y|(1 + |p|))$

for all $x, y \in \Omega, -R \leq u \leq R$ and $p \in \mathbb{R}^2$,

where $m_R(t) \rightarrow 0$ when $t \rightarrow 0$. (page 208)

(H10) *there exists a strict subsolution $\underline{u} \in C^1(\Omega) \cap C(\overline{\Omega})$ of (2.36) (i.e. such that $H(x, \nabla \underline{u}(x)) < 0$ for all x in Ω).* (page 77)

(H10') *there exist $\underline{u} \in C^1(\Omega) \cap C(\overline{\Omega})$ and $\delta < 0$ such that for all x in Ω ,*

$$H(x, \nabla \underline{u}(x)) < \delta. \quad (\text{page 80})$$

(H11) Ω is a bounded open subset of \mathbb{R}^N of class $W^{2,\infty}$. (page 80)

(H12) *There exists a function ω which goes to zero at zero, such that*

$$\forall x \in \Gamma, \forall p, q \in \mathbb{R}^N, |H(x, p) - H(x, q)| \leq \omega(|p - q|).$$

(page 80)

(H12') *for all $0 < R < +\infty$, there exists $m_R(t) \rightarrow 0$ when $t \rightarrow 0$ such that*

$$|H(x, u, p) - H(x, u, q)| \leq m_R(|p - q|)$$

for all $x \in \Gamma, -R \leq u \leq R$ and $p, q \in \mathbb{R}^2$. (page 208)

(H12'') $|H(x, p) - H(x, q)| \leq \lambda|p - q| \quad \forall x \in A, \quad \forall p, q \in \mathbb{R}^N$. (page 166)

(H13) $\forall x \in \Gamma, \forall p \in \mathbb{R}^N, \quad H(x, p + \lambda\eta(x)) \leq 0 \implies \lambda \leq C(1 + |p|)$.

(page 80)

(H13') *for all $0 < R < +\infty$, there exists $C_R > 0$ such that*

$$H(x, u, p + \lambda\eta(x)) \leq 0 \implies \lambda \leq C_R(1 + |p|),$$

for all $(x, u, p) \in \Gamma \times [-R, R] \times \mathbb{R}^2$. (page 208)

(H14) $\forall p \in \mathbb{R}^N, \quad H(x, p - \lambda\eta(x)) \rightarrow +\infty$ uniformly with respect to x in Γ , when $\lambda \rightarrow +\infty$. (page 80)

(H14') $\forall R_1, R_2 \in \mathbb{R}^{+*},$

$$H(x, u, p - \lambda\eta(x)) \rightarrow +\infty \quad \text{when } \lambda \rightarrow +\infty,$$

uniformly for (x, u, p) in $\Gamma \times [-R_1, R_1] \times B(0, R_2)$. (page 208)

- (H15) *Let ν be a fixed mesh. For all x, t in $\bar{\Omega} \times \mathbb{R}$, the value of $S_{\nu, x, t}(u) := S(\nu, x, t, u)$ does not depend on all the values of the function u but only on the values it takes on the neighborhood \mathcal{V}_x of x (i.e. at points $y \in \mathcal{V}_x$). In other words, we can rewrite $S(\nu, x, t, u)$ as $\check{S}(\nu, x, t, (u(y))_{y \in \mathcal{V}_x})$. (page 93)*
- (H16) *$\forall \rho > 0, x \in \bar{\Omega}, u \in B(\bar{\Omega})$, the function $S_{\rho, x, u} : t \mapsto S(\rho, x, t, u)$ is continuous, nondecreasing and $\lim_{t \rightarrow +\infty} S_{\rho, x, u}(t) \geq 0$. (page 101)*
- (H16') *$\forall \nu \in \mathcal{M}, x \in \bar{\Omega}, u \in B(\bar{\Omega})$, the function $S_{\nu, x, u} : t \mapsto S(\nu, x, t, u)$ is continuous, nondecreasing and $\lim_{t \rightarrow -\infty} S_{\nu, x, u}(t) \leq 0$. (page 104)*
- (H17) *The scheme is monotonous (see definition 3.1). (page 101)*
- (H18) *$\forall \nu \in \mathcal{M}, x \in \bar{\Omega}$, the function $\check{S}_{\nu, x}$ is continuous with respect to $(t, (u(y))_{y \in \mathcal{V}_x})$ (we denote $\check{S}_{\nu, x}(\cdot, \cdot) := \check{S}(\nu, x, \cdot, \cdot)$ where \check{S} is defined in the hypothesis (H15)). (page 101)*
- (H19) *$\forall \nu \in \mathcal{M}$, there exists a subsolution of the scheme (3.9). (page 101)*
- (H19') *$\forall \nu \in \mathcal{M}$, there exists a supersolution of the scheme (3.9) (v is a supersolution of the scheme $S(\nu, x, u(x), u) = 0$ if $\forall x \in \bar{\Omega}, S(\nu, x, v(x), v) \geq 0$). (page 104)*
- (H20) *$\forall \nu \in \mathcal{M}$, there exists $M^\nu \in \mathbb{R}$ such that for all subsolutions v^ν of (3.9), $\forall x \in \bar{\Omega}, v^\nu(x) \leq M^\nu$. (page 101)*
- (H20') *$\forall \nu \in \mathcal{M}$, there exists $M^\nu \in \mathbb{R}$ such that for all supersolutions v^ν of (3.9), $\forall x \in \bar{\Omega}, v^\nu(x) \geq M^\nu$. (page 104)*
- (H21) *There exists $M \in \mathbb{R}$ such that for all $\nu \in \mathcal{M}$, all subsolutions of (3.9) are upper bounded by M . (page 103)*
- (H22) *For all $x \in \Omega$, we have:
there exists $a_x \in A$ such that $f(x, a_x) \neq 0$. (page 106)*
- (H23) *For any $\lambda \in (0, 1), p \in \mathbb{R}^N$ s.t $H(x, p) \leq 0$ then
$$H(x, \lambda p + (1 - \lambda)\nabla\psi(x)) < 0. \quad (\text{page 155})$$*
- (H24) *$\forall x \in \mathcal{S}, \mathcal{Z}(x) = \{\nabla\psi(x)\}$. (page 158)*
- (H25) *$$H(x, u, p) - H(x, v, p) \geq \gamma_R(u - v), (\gamma_R > 0)$$

for all $x \in \Omega, -R \leq v \leq u \leq R$, and $p \in \mathbb{R}^2$ ($\forall 0 < R < +\infty$).
(page 208)*

Appendix E

Publications of the author

Book Chapters :

1. **“Shape From Shading”** (Emmanuel Prados and Olivier Faugeras). **Mathematical Models of Computer Vision: The Handbook**; N. Paragios, Y. Chen and O. Faugeras (eds), in preparation, 2005.

International Journal :

1. **A rigorous method for the Lambertian Shape From Shading problem with orthographic and pinhole camera** (Emmanuel Prados and Olivier Faugeras). **Submitted to the International Journal of Computer Vision**, 2004.

Main International Computer Vision Conferences :

1. **Shape from Shading: a well-posed problem?** (Emmanuel Prados, Olivier Faugeras and Fabio Camilli). Submitted to **CVPR’2005**, International Conference on Computer Vision and Pattern Recognition , San Diego, CA, USA, June 2005.
2. **Unifying approaches and removing unrealistic assumptions in Shape From Shading: Mathematics can help** (Emmanuel Prados and Olivier Faugeras). **ECCV’2004**, European Conference on Computer Vision, Prague, Czech Republic, May 2004.
3. **Perspective Shape from shading and viscosity solutions** (Emmanuel Prados and Olivier Faugeras). **ICCV’2003**, International Conference on Computer Vision, Nice, France, October 2003.

4. **Shape from shading and viscosity solutions** (Emmanuel Prados, Olivier Faugeras, Elisabeth Rouy). **ECCV'2002**, European Conference on Computer Vision, Copenhagen, Denmark, June 2002.

Other Conferences and Research Reports :

1. **A mathematical framework unifying various Shape from Shading approaches** (Emmanuel Prados, Olivier Faugeras and Fabio Camilli). Mathematics and Image Analysis - **MIA 2004**, Paris, France, September 2004.
2. **Viscosity solutions for realistic Shape-From-Shading** (Emmanuel Prados and Olivier Faugeras). **Workshop on Numerical Methods for Viscosity Solutions and Applications**, Rome, Italy, September 2004.
3. **De nouvelles solutions au problème du Shape from Shading** (Emmanuel Prados, Fabio Camilli and Olivier Faugeras). **CANUM'2004**, 36ème Congrès national d'Analyse NUMérique, Obernai, France, May 2004.
4. **Reconstruction photogrammétrique des formes 3D; nouveaux résultats théoriques et nouveaux algorithmes pour des projections orthographiques et en perspective** (Emmanuel Prados and Olivier Faugeras). **RFIA'2004**, 14th AFRIF-AFIA French-speaking Congress: Object Recognition and Artificial Intelligence, Toulouse, France, January 2004.
5. **Shape from Shading: a well-posed problem?** (Emmanuel Prados, Olivier Faugeras and Fabio Camilli) **INRIA Research Report**, No RR-5297, August 2004.
6. **A viscosity method for Shape From Shading without boundary data** (Emmanuel Prados, Fabio Camilli and Olivier Faugeras) **INRIA Research Report**, No RR-5296, August 2004.
7. **A rigorous and realistic Shape From Shading method and some of its applications** (Emmanuel Prados and Olivier Faugeras) **INRIA Research Report** No RR-5133, March 2004.
8. **A mathematical and algorithmic study of the Lambertian SFS problem for orthographic and pinhole cameras** (Emmanuel Prados and Olivier Faugeras). **INRIA Research Report** No RR-5005, September 2003.
9. **Approximations numériques des solutions de viscosité de divers EDPs provenant du Shape from Shading** (Emmanuel Prados and

Olivier Faugeras). **CANUM'2003**, 35th French Congress of Numerical Analysis, La Grande Motte, France, june 2003.

10. **Shape from Shading and viscosity solutions** (Emmanuel Prados, Olivier Faugeras, Elisabeth Rouy). **INRIA Research Report** No RR-4638, November 2002.

Dissertations :

1. **PhD Thesis:** (Emmanuel Prados). University of Nice-Sophia Antipolis, France, To appear in October 2004.
2. **Masters Thesis:** “Une approche du Shape from shading par solutions de viscosité” (Emmanuel Prados). University of Nice-Sophia Antipolis, France, September 2001.

Invited Talks

1. Mathematics and Image Analysis 2004 (MIA'04), Paris, France, September 6-9, 2004. Organizer: Laurent Cohen (Ceremade).
2. Seminary “Probabilité, Optimisation, Contrôle”, Paris, France, October 28, 2004. Organizer: Maxplus Lab. (INRIA).

And many other papers are in preparation...

Bibliography

- [1] *17th International Conference on Pattern Recognition*, Cambridge, UK, August 2004. Computer Society Press.
- [2] J.J. Atick, P.A. Griffin, and N.A. Redlich. Statistical approach to shape from shading: reconstruction of three-dimensional face surfaces from single two-dimensional. *Neural Comput.*, 8(6):1321–1340, 1996.
- [3] S. Bakshi and Y.H. Yang. Shape from shading for non-lambertian surfaces. In *Proceedings of the International Conference on Image Processing*, volume 94, pages 130–134, 1994.
- [4] S.M. Bakshi. Shape from shading for non-lambertian surfaces. Master's thesis, University of Saskatchewan, July 1994.
- [5] M. Bardi and I. Capuzzo-Dolcetta. *Optimal control and viscosity solutions of Hamilton-Jacobi-Bellman equations*. Birkhauser, 1997.
- [6] G. Barles. An approach of deterministic control problems with unbounded data. *Ann. Ist. Henri Poincaré*, 7(4):235–258, 1990.
- [7] G. Barles. *Solutions de Viscosité des Equations de Hamilton-Jacobi*. Springer-Verlag, 1994.
- [8] G. Barles and B. Perthame. Comparison principle for dirichlet-type hamilton-jacobi equations and singular perturbations of degenerated elliptic equations. *Applied Mathematics and Optimization*, 21:21–44, 1990.
- [9] G. Barles and P.E. Souganidis. Convergence of approximation schemes for fully nonlinear second order equations. *Asymptotic Analysis*, 4:271–283, 1991.
- [10] I. Barnes and K. Zhang. Instability of the eikonal equation and shape from shading. *ESAIM: Mathematical Modelling and Numerical Analysis (M2AN)*, 34(1):127–138, 2000.

- [11] P. N. Belhumeur, D. J. Kriegman, and A. L. Yuille. The bas-relief ambiguity. *The International Journal of Computer Vision*, 35(1):33–44, November 1999.
- [12] M. Bell and W.T. Freeman. Learning local evidence for shading and reflectance. In *Proceedings of the International Conference on Computer Vision (ICCV)*, volume 1, pages 670–677, Vancouver, Canada, July 2001. IEEE Computer Society, IEEE Computer Society Press.
- [13] V. Blanz and T. Vetter. A morphable model for the synthesis of 3d faces. In *SIGGRAPH 1999*, pages 187–194, 1999.
- [14] J.F. Bonnans, J.C. Gilbert, C. Lemarechal, and C.A. Sagastizabal. *Numerical Optimization: Theoretical and Practical Aspects*. Springer-Verlag, 2002.
- [15] C. Brezinski. Convergence acceleration during the 20th century. *J. Comput. Appl. Math.*, 122:1–21, 2000.
- [16] M.J. Brooks. Two results concerning ambiguity in shape from shading. In *AAAI-83*, pages 36–39, 1983.
- [17] M.J. Brooks, W. Chojnacki, and R. Kozera. Circularly symmetric eikonal equations and non-uniqueness in computer vision. *J. Mathematical Analysis Applications*, 165:192–215, 1992.
- [18] M.J. Brooks, W. Chojnacki, and R. Kozera. Impossible and ambiguous shading patterns. *ijcv*, 7(2):119–126, January 1992.
- [19] M.J. Brooks, W. Chojnacki, and R. Kozera. Shading without shape. *Quarterly of Applied Mathematics*, 50(1):27–38, 1992.
- [20] M. S. Brown and W. B. Seales. Document restoration using 3D shape. In *Proceedings of ICCV'01*, July 2001.
- [21] A. M. Bruckstein. On shape from shading. *Computer. Vision Graphics Image Process*, 44:139–154, 1988.
- [22] A.R. Bruss. The eikonal equation: Some results applicable to computer vision. *Journal of Mathematical Physics*, 23(5):890–896, May 1982.
- [23] F. Camilli. *A characterization of the value function for a class of degenerate control problems*, chapter 3, pages 47–58. Volume 59 of Falcone and Makridakis [54], 2001.

- [24] F. Camilli and M. Falcone. An approximation scheme for the maximal solution of the shape-from-shading model. *International Conference on Image Processing*, pages 49–52, 1996.
- [25] F. Camilli and L. Grune. Numerical approximation of the maximal solutions for a class of degenerate hamilton-jacobi equations. *SIAM Journal of Numerical Analysis*, 38(5):1540–1560, 2000.
- [26] F. Camilli and A. Siconolfi. Maximal subsolutions for a class of degenerate hamilton-jacobi problems. *Indiana Univ. Math. J.*, 48(3):1111–1132, 1999.
- [27] F. Camilli and A. Siconolfi. Nonconvex degenerate Hamilton-Jacobi equations. *Mathematische Zeitschrift*, 242:1–21, 2002.
- [28] F. Camilli and A. Siconolfi. Hamilton-jacobi equations with measurable dependence on the state variable. *Adv. Differential Equations*, 8(6):733–768, June 2003.
- [29] I. Capuzzo-Dolcetta and P.-L. Lions. Hamilton-jacobi equations with state constraints. *Trans. Amer. Math. Soc.*, 318(2):643–68, 1990.
- [30] J.Y. Chang, K. Lee, and S.U. Lee. Shape from shading using graph cuts. In *Proceedings of the International Conference on Image Processing*, pages 421–424. IEEE Signal Processing Society, 2003.
- [31] S.I. Cho and H. Saito. A Divide-and-Conquer Strategy in Shape from Shading problem. In *Proceedings of CVRP'97*, June 1997.
- [32] S.Y. Cho and T.W.S Chow. A new color 3d sfs methodology using neural-based color reflectance models and iterative recursive method. *Neural Computation*, 14(11):2751–2789, November 2002.
- [33] K.N. Choi, P. Worthington, and E.R. Hancock. Facial pose using shape-from-shading. In *Proceedings of BMVC'99*, pages 402–411, 1999.
- [34] F. H. Clarke. *Optimization and Nonsmooth Analysis*. SIAM, Classics in Applied Mathematics 5, 1990.
- [35] S. Collings, R. Kozera, and L. Noakes. A piecewise quadratic approach to single image shape from shading. In *Proceedings of the International Conference on Pattern Recognition*, volume IV, pages 126–129, Qubec City, Canada, August 2002. Computer Society Press.
- [36] F. Courteille, A. Crouzil, J.-D. Durou, and P. Gurdjos. Shape from Shading en conditions réalistes d'acquisition photographique. In *Proceedings of RFIA '04*, 2004.

- [37] F. Courteille, A. Crouzil, J.-D. Durou, and P. Gurdjos. Towards shape from shading under realistic photographic conditions. In *Proceedings of the International Conference on Pattern Recognition* [1].
- [38] B.L. Craine, Craine E.R., C.J. O'Toole, and Q. Ji. Digital imaging colposcopy: Corrected area measurements using Shape-from-Shading. *IEEE Transactions on Medical Imaging*, 17(6):1003–1010, December 1998.
- [39] M.G. Crandall. Viscosity solutions of Hamilton–Jacobi equations. In *Nonlinear Problems: Present and Future, Proc. 1st Los Alamos Conf., 1981*, volume 61, pages 117–125. North-Holland Math. Stud., 1982.
- [40] M.G. Crandall, H. Ishii, and P.-L. Lions. User's guide to viscosity solutions of second order partial differential equations. *Bull. Amer. Soc.*, 27:1–67, 1992.
- [41] M.G. Crandall and P.-L. Lions. Viscosity solutions of Hamilton–Jacobi equations. *Trans. AMS*, 277:1–43, 1983.
- [42] A. Crouzil, X. Descombes, and J.-D. Durou. A multiresolution approach for shape from shading coupling deterministic and stochastic optimization. *IEEE Transactions on Pattern Analysis and Machine Intelligence*, 25(11):1416–1421, November 2003.
- [43] A. Crouzil, X. Descombes, and J.-D. Durou. A multiresolution approach for shape from shading coupling deterministic and stochastic optimization. Technical Report 2003-19-R, IRIT, September 2003.
- [44] P. Daniel. *Peut-on extraire le relief d'une seule image ?* PhD thesis, Universit Paul Sabatier, Toulouse, January 2000.
- [45] P. Daniel and J.-D. Durou. From deterministic to stochastic methods for shape from shading. In *Proceedings of the 4th Asian Conference on Computer Vision*, pages 187–192, Taipei, Taiwan, January 2000. IEEE.
- [46] R. Dovgand and R. Basri. Statistical symmetric shape from shading for 3d structure recovery of faces. In Pajdla and Matas [113].
- [47] P. Dupuis and J. Oliensis. An optimal control formulation and related numerical methods for a problem in shape reconstruction. *The Annals of Applied Probability*, 4(2):287–346, 1994.
- [48] J.-D. Durou, M. Falcone, and M. Sagona. Numerical methods for shape from shading: A survey with benchmarrks. *Submitted to Elsevier Science*, 2004.

- [49] J.-D. Durou, M. Falcone, and M. Sagona. A survey of numerical methods for shape from shading. Research report 2004-2-R, IRIT, January 2004.
- [50] J.-D. Durou and H. Maître. On convergence in the methods of Strat and Smith for shape from shading. *The International Journal of Computer Vision*, 17(3):273–289, 1996.
- [51] J.-D. Durou and D. Piau. Ambiguous shape from shading with critical points. *Journal of Mathematical Imaging and Vision*, 12(2):99–108, 2000.
- [52] I. Ekeland and R. Temam. *Analyse Convexe et Problèmes Variationnels*. Etudes mathématiques. Dunod; Gauthier-Villars, Paris, Bruxelles, Montreal, 1974.
- [53] L.C. Evans and P.E. Souganidis. Differential games and representation formulas for solutions of hamilton-jacobi-isaacs equations. *Indiana Univ. Math. J.*, 33:773–797, 1984.
- [54] M. Falcone and C. Makridakis, editors. *numerical methods for viscosity solutions and applications*, volume 59 of *Series on advances in mathematics for applied sciences*. World Scientific, 2001.
- [55] M. Falcone and M. Sagona. An algorithm for the global solution of the shape-from-shading model. *International Conference on Image Analysis and Processing*, 1:596–603, 1997. LNCS 1310.
- [56] M. Falcone, M. Sagona, and A. Seghini. A scheme for the shape-from-shading model with "black shadows". In *Proceedings of ENUMATH 2001*, 2001.
- [57] P. Favaro, A. Mennucci, and S. Soatto. Observing shape from defocused images. *The International Journal of Computer Vision*, 52(1):25–43, April 2003.
- [58] C.H.Q. Forster and C.L. Tozzi. Towards 3d reconstruction of endoscope images using shape from shading. In *13th Brazilian Symposium on Computer Graphics and Image Processing (SIBGRAPI)*. IEEE Computer Society, October 2000.
- [59] D. Forsyth and A Zisserman. Reflections on shading. *IEEE Transactions on Pattern Analysis and Machine Intelligence*, 13(7):671–679, July 1991.
- [60] R.T. Frankot and R. Chellappa. A method for enforcing integrability in shape from shading algorithms. *pami*, 10(4):439–451, July 1988.

- [61] J.K. Hasegawa and C.L. Tozzi. Shape from shading with perspective projection and camera calibration. *Computers and Graphics*, 20(3):351–364, May 1996.
- [62] G. Hermosillo and O. Faugeras. Dense image matching with global and local statistical criteria: a variational approach. In *Proceedings of CVPR'01*, 2001.
- [63] A. Heyden, G. Sparr, M. Nielsen, and P. Johansen, editors. *Proceedings of the 7th European Conference on Computer Vision*, Copenhagen, Denmark, May 2002. Springer-Verlag.
- [64] B. K.P. Horn. Height and Gradient from Shading. *The International Journal of Computer Vision*, 5(1):37–75, August 1990.
- [65] B.K. Horn. *Robot Vision*. MIT Press, 1986.
- [66] B.K. Horn and M.J. Brooks, editors. *Shape from Shading*. The MIT Press, 1989.
- [67] B.K.P. Horn. Obtaining shape from shading information. In P.H. Winston, editor, *The Psychology of Computer Vision*. McGraw-Hill, New York, 1975.
- [68] B.K.P. Horn. Relative orientation. *The International Journal of Computer Vision*, 4(1):59–78, January 1990.
- [69] B.K.P. Horn and M.J. Brooks. The variational approach to shape from shading. *Computer Vision Graphics and Image Processing*, 33(2):174–208, February 1986.
- [70] B.K.P. Horn, R.S. Szeliski, and A.L. Yuille. Impossible shaded images. *IEEE Transactions on Pattern Analysis and Machine Intelligence*, 15(2):166–170, 1993.
- [71] IEEE Computer Society. *Proceedings of the 9th International Conference on Computer Vision*, Nice, France, 2003. IEEE Computer Society Press.
- [72] O. Ikeda. A robust iterative shape-from-shading algorithm with modified transforming matrix. In *British Machine Vision Conference, BMVC'03*, 2003.
- [73] K. Ikeuchi and B.K.P. Horn. Numerical shape from shading and occluding boundaries. *Artificial Intelligence Journal*, 17:181–184, 1981.

- [74] A. Ishii. A simple, direct proof of uniqueness for solutions of the hamilton-jacobi equations of eikonal type. *Proceedings of the American Mathematical Society*, pages 247–251, 1987.
- [75] H. Ishii. Hamilton-Jacobi equations with discontinuous hamiltonians on arbitrary open subsets. *Bull. Fac. Sci. Engrg. Chuo Univ.*, 28:33–77, 1985.
- [76] H. Ishii. a boundary value problem of the dirichlet type for hamilton-jacobi equations. *Ann. Sci. Ecole Norm. Sup.*, 4(16):105–135, 1989.
- [77] H. Ishii and M. Ramaswamy. Uniqueness results for a class of Hamilton-Jacobi equations with singular coefficients. *Comm. Par. Diff. Eq.*, 20:2187–2213, 1995.
- [78] J. Kain and D.N. Ostrov. Numerical shape-from-shading for discontinuous photographic images. *The International Journal of Computer Vision*, 44(3):163–173, 2001.
- [79] R. Kimmel and A.M. Bruckstein. “Global shape-from-shading”. *CVGIP: Image Understanding*, pages 360–369, 1995.
- [80] R. Kimmel and A.M. Bruckstein. Tracking level sets by level sets : A method for solving the shape from shading problem. *Computer Vision and Image Understanding*, 62(2):47–58, July 1995.
- [81] R. Kimmel and J.A. Sethian. Optimal algorithm for shape from shading and path planning. *Journal of Mathematical Imaging and Vision*, 14(2):237–244, May 2001.
- [82] R. Klette, R. Kozera, and K. Schlüns. Shape from shading and photometric stereo methods. Technical Report CITR-TR-20, CITR, University of Auckland, New Zealand, 1998.
- [83] L. L. Kontsevich, A. P. Petrov, and I. S. Vergelskaya. Reconstruction of shape from shading in color images. *J. Opt. Soc. Am. A*, 11(3):1047–1052, March 1994.
- [84] R. Kozera and R. Klette. Finite difference based algorithms in linear shape from shading. *Machine Graphics and Vision*, 6(2):157–201, 1997.
- [85] R. Kozera and R. Klette. Well-posedness of linear shape-from-shading problem. In *Proceedings of Computer Analysis of Images and Patterns, CAIP'97*, volume 1296 of *Lecture Notes in Computer Science*, pages 130–137. Springer, September 1997.

- [86] C.K. Kwoh, G.N. Khan, and D.F. Gillies. Automated endoscope navigation and advisory system from medical imaging. In *Proceedings of SPIE'99*, volume 3660, 1999.
- [87] Y.G. Leclerc and A.F. Bobick. The direct computation of height from shading. In *CVPR:91*, volume 91, pages 552–558, 1991.
- [88] C.H. Lee and A. Rosenfeld. Improved methods of estimating shape from shading using the light source coordinate system. *Artificial Intelligence*, 26(2):125–143, May 1985.
- [89] D. Lee. A provably convergent algorithm for shape from shading. In *Proceedings of the DARPA Image Understanding Workshop*, pages 489–496, 1985.
- [90] K.M. Lee and C.C. Kuo. Shape from shading with a linear triangular element surface model. *pami*, 15(8):815–822, August 1993.
- [91] K.M. Lee and C.C.J. Kuo. Shape from shading with perspective projection. *CVGIP: Image Understanding*, 59(2):202–212, 1994.
- [92] K.M. Lee and C.C.J. Kuo. Shape from shading with a generalized reflectance map model. *Computer Vision and Image Understanding*, 67(2):143–160, August 1997.
- [93] C. Lenglet, R. Deriche, and O. Faugeras. Inferring white matter geometry from diffusion tensor MRI: Application to connectivity mapping. In Pajdla and Matas [113].
- [94] Christophe Lenglet, Rachid Deriche, and Olivier Faugeras. Diffusion tensor magnetic resonance imaging: Brain connectivity mapping. Technical Report RR-4983, INRIA, November 2003.
- [95] P.-L. Lions. *Generalized Solutions of Hamilton–Jacobi Equations*. Number 69 in Research Notes in Mathematics. Pitman Advanced Publishing Program, 1982.
- [96] P.-L. Lions, E. Rouy, and A. Tourin. Shape-from-shading, viscosity solutions and edges. *Numer. Math.*, 64:323–353, 1993.
- [97] J. Malik and D.E. Maydan. Recovering three-dimensional shape from a single image of curved objects. *IEEE Transactions on Pattern Analysis and Machine Intelligence*, 11(6):555–566, 1989.
- [98] C.S. McCamy, H. Marcus, and J.G. Davidson. A colorrendition chart. *J. App. Photog. Eng.*, 2:95–99, 1976.

- [99] G.W. Meyer. Wavelength selection for synthetic image generation. *Computer Vision, Graphics, and Image Processing*, 41:57–79, 1988.
- [100] M.G.H. Mostafa, S.M. Yamany, and A.A. Farag. Integrating shape from shading and range data using neural networks. In *Proceedings of the International Conference on Computer Vision and Pattern Recognition*, pages 2015–2020, Fort Collins, Colorado, June 1999. IEEE Computer Society.
- [101] S.K. Nayar, K. Ikeuchi, and T. Kanade. Shape from interreflections. pages 2–11, December 1990.
- [102] T. Okatani and K. Deguchi. Reconstructing Shape from Shading with a Point Light Source at the Projection Center: Shape Reconstruction from an Endoscope Image. In *Proceedings of ICPR'96*, pages 830–834, August 1996.
- [103] T. Okatani and K. Deguchi. Shape reconstruction from an endoscope image by shape from shading technique for a point light source at the projection center. *Computer Vision and Image Understanding*, 66(2):119–131, May 1997.
- [104] T. Okatani and K. Deguchi. On classification of singular points for global shape from shading. In *Proceedings of the 3rd Asian Conference on Computer Vision*, volume 1351, pages 48–55, Hong Kong, January 1998. springer-verlag.
- [105] T. Okatani and K. Deguchi. On identification of singular points using photometric invariants for global shape from shading problem. In *Proceedings of the International Conference on Pattern Recognition*, volume 2, pages 1787–1790, Brisbane, Australia, August 1998. Computer Society Press.
- [106] J. Oliensis. Shape from shading as a partially well-constrained problem. *CVGIP: Image Understanding*, 54(2):163–183, 1991.
- [107] J. Oliensis. Uniqueness in shape from shading. *The International Journal of Computer Vision*, 2(6):75–104, 1991.
- [108] J. Oliensis and P. Dupuis. A global algorithm for shape from shading. In *Proceedings of ICCV'93*, pages 692–701, 1993.
- [109] A.E. Ononye and P.W. Smith. Estimating the shape of a surface with non-constant reflectance from a single color image. In *British Machine Vision Conference, BMVC'02*, pages 163–172, 2002.

- [110] S. Osher. A level set formulation for the solution of the dirichlet problem for a hamilton-jacobi equations. *SIAM Journal on Mathematical Analysis*, 24(5):1145–1152, 1993.
- [111] S. Osher and J. Sethian. Fronts propagating with curvature dependent speed: algorithms based on the Hamilton–Jacobi formulation. *Journal of Computational Physics*, 79:12–49, 1988.
- [112] D.N. Ostrov. Extending viscosity solutions to eikonal equations with discontinuous spatial dependence. *Nonlinear Anal.*, 42(4):709–736, 2000.
- [113] T. Pajdla and J. Matas, editors. *Proceedings of the 8th European Conference on Computer Vision*, Prague, Czech Republic, 2004. Springer–Verlag.
- [114] M.A. Penna. Local and semi-local shape from shading for a single perspective image of a smooth object. *Computer Vision, Graphics, and Image Processing*, 46(3):346–366, 1989.
- [115] A. Pentland. Local shading analysis. *IEEE Transactions on Pattern Analysis and Machine Intelligence*, 6:170–187, 1984.
- [116] A.P. Pentland. Linear shape from shading. *The International Journal of Computer Vision*, 4(2):153–162, March 1990.
- [117] E. Prados, F. Camilli, and O. Faugeras. A viscosity method for shape-from-shading without boundary data. Technical report, INRIA, 2004.
- [118] E. Prados and O. Faugeras. Une approche du “Shape from Shading” par solutions de viscosité. Master’s thesis, Université de Nice Sophia-Antipolis, France, INRIA, September 2001.
- [119] E. Prados and O. Faugeras. A mathematical and algorithmic study of the lambertian SFS problem for orthographic and pinhole cameras. Technical Report RR-5005, INRIA, November 2003.
- [120] E. Prados and O. Faugeras. “Perspective Shape from Shading” and viscosity solutions. In *Proceedings of the 9th International Conference on Computer Vision* [71], pages 826–831.
- [121] E. Prados and O. Faugeras. Reconstruction photogramtrique des formes 3D; nouveaux rsultats thoriques et nouveaux algorithmes pour des projections orthographique et en perspective. In *Proceedings of RFIA’04*, January 2004.

- [122] E. Prados and O. Faugeras. A rigorous and realistic shape from shading method and some of its applications. Technical Report 5133, INRIA, March 2004.
- [123] E. Prados and O. Faugeras. A rigorous lambertian shape-from-shading method for orthographic and pinhole cameras. *Submitted to IJCV*, 2004.
- [124] E. Prados and O. Faugeras. Unifying approaches and removing unrealistic assumptions in Shape from Shading: Mathematics can help. In *Proceedings of ECCV'04*, 2004.
- [125] E. Prados and O. Faugeras. Viscosity solutions for realistic shape-from-shading. In *Workshop on Numerical Methods for Viscosity Solutions and Applications*, Rome, Italy, September 2004.
- [126] E. Prados, O. Faugeras, and F. Camilli. A mathematical framework unifying various shape from shading approaches. In *Mathematics and Image Analysis - MIA 2004*, Paris, France, September 2004.
- [127] E. Prados, O. Faugeras, and E. Rouy. Shape from shading and viscosity solutions. In Heyden et al. [63], pages 790–804.
- [128] E. Prados, O. Faugeras, and E. Rouy. Shape from shading and viscosity solutions. Technical Report 4638, INRIA, November 2002.
- [129] H. Ragheb and E.-R. Hancock. Highlight removal using shape-from-shading. In Heyden et al. [63], pages 626–641.
- [130] H. Ragheb and E.R. Hancock. A probabilistic framework for specular shape-from-shading. *Pattern Recog.*, 36:407–427, 2003.
- [131] T. Rindfleisch. Photometric method for lunar topography. *Photometric Engineering*, 32(2):262–277, March 1966.
- [132] A. Robles-Kelly and E. R. Hancock. A graph spectral approach to shape-from-shading. *IEEE Transactions on Image Processing*, 13(7), 2004.
- [133] S. Romdhani, V. Blanz, and T. Vetter. Face identification by fitting a 3d morphable model using linear shape and texture error functions. In Heyden et al. [63], pages 3–19.
- [134] E. Rouy and A. Tourin. A Viscosity Solutions Approach to Shape-from-Shading. *SIAM Journal of Numerical Analysis*, 29(3):867–884, June 1992.
- [135] M. Sagona and A. Seghini. *An Adaptive Scheme on Unstructured Grids for the Shape-From-Shading Problem*, chapter 11, pages 197–219. Volume 59 of Falcone and Makridakis [54], 2001.

- [136] D. Samaras, D. Metaxas, P.V. Fua, and Y.G. Leclerc. Variable albedo surface reconstruction from stereo and shape from shading. In *Proceedings of the International Conference on Computer Vision and Pattern Recognition*, volume I, pages 480–487, Hilton Head Island, South Carolina, June 2000. IEEE Computer Society.
- [137] D. Samaras and D.N. Metaxas. Coupled lighting direction and shape estimation from single images. In *Proceedings of the 7th International Conference on Computer Vision*, volume 2, pages 868–874, Kerkyra, Greece, September 1999. IEEE Computer Society, IEEE.
- [138] J.A. Sethian. A fast marching level set method for monotonically advancing fronts. In *Proceedings of the National Academy of Sciences*, volume 93, pages 1591–1694, 1996.
- [139] J.A. Sethian. *Level Set Methods*. Cambridge University Press, 1996.
- [140] J.A. Sethian and J. Strain. Crystal growth and dendritic solidification. *Journal of Computational Physics*, 98:231–253, 1992.
- [141] J.A. Sethian and A. Vladimirsky. Ordered upwind methods for static hamilton–jacobi equations: Theory and algorithms. *SIAM Journal on Numerical Analysis*, 41(1):325–363, 2003.
- [142] I. Shimshoni, Y. Moses, and M. Lindenbaum. Shape reconstruction of 3d bilaterally symmetric surfaces. *The International Journal of Computer Vision*, 39(2):97–110, September 2000.
- [143] W.A.P. Smith and E.R. Hancock. Face recognition using Shape-from-Shading. In *Proceedings of British Machine Vision Conference (BMVC)*, pages 597–606, September 2002.
- [144] Q.Y.L. Smithwick and E.J. Seibel. Depth enhancement using a scanning fiber optical endoscope. In *Proceedings of SPIE BiOS*, 2002.
- [145] H. M. Soner. Optimal control with state space constraints. *SIAM J. Contr. Optim.*, 24:Part I: 552–562, Part II: 1110–1122, 1986.
- [146] P. Soravia. Optimal control with discontinuous running cost: eikonal equation and shape from shading. In *39th IEEE Conference on Decision and Control*, pages 79–84, December 2000.
- [147] A.J. Stewart and M.S. Langer. Toward accurate recovery of shape from shading under diffuse lighting. *IEEE Transactions on Pattern Analysis and Machine Intelligence*, 19(9):1020–1025, September 1997.

- [148] T.M. Strat. A numerical method for shape from shading from a single image. Master's thesis, Artificial Intelligence Lab., Massachusetts Institute of Technology, Cambridge, 1979.
- [149] L. E. Sucar, D. F. Gillies, and H. Rashid. Integrating shape from shading in a gradient histogram and its application to endoscope navigation. In *Proceedings of 5th International Conference on Artificial Intelligence (ICAI-V)*, 1992.
- [150] R. Szeliski. Fast shape from shading. *Computer Vision Graphics and Image Processing: Image Understanding*, 53(2):129–153, March 1991.
- [151] P. Tan, S. Lin, L. Quan, and H.Y. Shum. Highlight removal by illumination-constrained inpainting. In *Proceedings of the 9th International Conference on Computer Vision* [71], pages 164–169.
- [152] A. Tankus, N. Sochen, and Y. Yeshurun. A new perspective [on] Shape-from-Shading. In *Proceedings of the 9th International Conference on Computer Vision* [71], pages 862–869.
- [153] A. Tankus, N. Sochen, and Y. Yeshurun. Perspective Shape-from-Shading by Fast Marching. In *IEEE Conference on Computer Vision and Pattern Recognition*, Washington, DC (United States), June 2004.
- [154] A. Tankus, N. Sochen, and Y. Yeshurun. Reconstruction of medical images by perspective Shape-from-Shading. In *Proceedings of the International Conference on Pattern Recognition* [1].
- [155] Y.L Tian, H.T. Tsui, S.Y. Yeung, and S. Ma. Shape from shading for multiple light sources. *Journal of the Optical Society of America A*, 16(1):36–52, January 1999.
- [156] J. R.A. Torreao. A green's function approach to shape from shading. *Pattern Recognition*, 34(12):2367–2382, December 2001.
- [157] P.S. Tsai and M. Shah. Shape from shading using linear-approximation. *Image and Vision Computing*, 12(8):487–498, October 1994.
- [158] P.S. Tsai and M. Shah. Shape from shading with variable albedo. *Optical Engineering*, 37(4):1212–1220, April 1998.
- [159] D. Tschumperlé. *PDE's Based Regularization of Multivalued Images and Applications*. PhD thesis, Universit de Nice-Sophia Antipolis, December 2002.

- [160] D. Tschumperlé and R. Deriche. Vector-valued image regularization with PDE's : A common framework for different applications. In *IEEE Conference on Computer Vision and Pattern Recognition*, Madison, Wisconsin (United States), June 2003.
- [161] G. Ulich. Provably convergent methods for the linear and nonlinear shape from shading problem. *Journal of Mathematical Imaging and Vision*, 9(1):69–82, July 1998.
- [162] J. Van Diggelen. A photometric investigation of the slopes and the heights of the ranges of hills in the maria of the moon. *Bulletin of the Astronomical Institute of the Netherlands*, 11(423):283–290, 1951.
- [163] T. Wada, H. Ukida, and T. Matsuyama. Shape from shading with interreflections under proximal light source-3D shape reconstruction of unfolded book surface from a scanner image. In *Proceedings of ICCV'95*, June 1995.
- [164] G.Q. Wei and G. Hirzinger. Learning shape-from-shading by a multilayer network. *IEEE Transactions on Neural Networks*, 7(4):985–995, 1996.
- [165] I. Weiss. A perspective 3D formalism for shape from shading. In *Proceedings of DARPA Image Understanding Workshop*, volume 2, pages 1393–1402, May 1997.
- [166] P.L. Worthington and E.R. Hancock. New constraints on data-closeness and needle map consistency for shape-from-shading. *pami*, 21(12):1250–1267, 1999.
- [167] P.L. Worthington and E.R. Hancock. Coarse view synthesis using shape-from-shading. *Pattern Recognition*, 36:439–449, 2003.
- [168] S.M. Yamany and A.A. Farag. A system for human jaw modeling using intra-oral images. In *IEEE-EMBS*, volume 20, pages 563–566, 1998.
- [169] S.Y. Yeung, H.T. Tsui, and A. Yim. Global shape from shading for an endoscope image. In Chris Taylor and Alan C. F. Colchester, editors, *Proceedings of Medical Image Computing and Computer-Assisted Intervention (MICCAI)*, volume 1679 of *Lecture Notes in Computer Science*, pages 318–327, September 1999.
- [170] A. Yilmaz and M. Shah. Estimation of arbitrary albedo and shape from shading for symmetric objects. In *Proceedings of British Machine Vision Conference, BMVC'02*, pages 728–736, 2002.

-
- [171] S.Y. Yuen, Y.Y. Tsui, Y.W. Leung, and R.M.M. Chen. Fast marching method for shape from shading under perspective projection. In *Proceedings of VIIP'02*, pages 584–589, September 2002.
- [172] R. Zhang, P.-S. Tsai, J.-E. Cryer, and M. Shah. Shape from Shading: A survey. *IEEE Transactions on Pattern Analysis and Machine Intelligence*, 21(8):690–706, August 1999.
- [173] W. Zhao and R. Chellappa. Illumination-insensitive face recognition using symmetric Shape-from-Shading. In *proceedings of CVPR'00*, pages 1286–1293, 2000.
- [174] W.Y. Zhao and R. Chellappa. Robust face recognition using symmetric shape-from-shading. Technical Report TR4036, University of Maryland, July 1999.

UNIVERSITE DE NICE-SOPHIA ANTIPOLIS

ECOLE DOCTORALE DES SCIENCES ET TECHNOLOGIES DE
L'INFORMATION ET DE LA COMMUNICATION

Rapport de soutenance

De doctorat de Monsieur PRADOS Emmanuel

Titre du mémoire : *application of the theory of the viscosity solution to the shape from shading problem*

	Pierre BERNHARD, <i>Président</i>	Rachid DERICHE
<u>Membres du jury</u> :	Luis ALVAREZ, <i>Rapporteur</i>	Luc ROBERT
	Christoph SCHNÖRR, <i>Rapporteur</i>	Invarié :
	Jean Denis DUROU	Olivier FAUGERAS

Émanuel Prados présente un travail qui constitue une véritable percée technologique dans un domaine, le "shape from shading", qui était largement considéré comme dans un cul de sac. Il s'agit d'un travail profond de réflexion et de modélisation, et d'un travail très technique de mathématiques sur les solutions de viscosité des équations de Hamilton Jacobi. L'écart entre les résultats pratiques obtenus avec sa méthode et ceux des plus récents surveys de la littérature est impressionnant.

Le mémoire de thèse est particulièrement —mais pas inutilement— copieux. Il présente une analyse critique extrêmement complète de treize années de littérature en termes nouveaux et unificateurs, avant de déduire de cette analyse les nouvelles modélisations qui mènent au résultat. Les mathématiques, difficiles, se lisent bien, sont rigoureuses et sans formalisme excessif inutile.

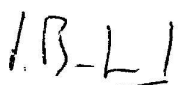
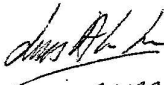
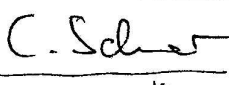

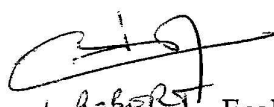

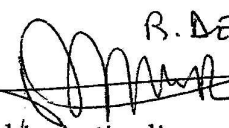
L'exposé oral, remarquablement préparé, a fait le choix, sans doute judicieux, d'insister sur les idées et les résultats, et d'esquisser, voire d'esquiver, les détails techniques. À ce prix, il a été parfaitement clair, vivant et informatif. Émanuel Prados fait ainsi preuve d'un grand talent pédagogique.

Une longue séance de questions du jury, et de réponses du candidat, a permis à Émanuel Prados de montrer le recul qu'il a su prendre par rapport à son travail, l'aisance qu'il a acquise dans les débats avec les meilleurs spécialistes internationaux du domaine, et sa grande honnêteté intellectuelle.

Aussi le jury lui décerne à l'unanimité le grade de docteur en *automatique, traitement du signal et des images* de l'Université de Nice-Sophia Antipolis.

Signature des membres du jury :

date : 22 octobre 2004

 P. BERNHARD	 Luis ALVAREZ	 C. SCHNÖRR	 O. FAUGERAS
 L. ROBERT	 J.-D. DUROU	 R. DERICHE	

Ecole Doctorale STIC de l'Université de Nice-Sophia Antipolis

